Chemo-enzymatic tools to elucidate glycan-mediated TRPV5 regulation

Liz Leunissen

The research presented in this thesis was conducted at the department of Physiology, Radboud university medical center (Radboudumc), the Netherlands and at the Synthetic Organic Chemistry group, Institute for Molecules and Materials (IMM), Radboud University, the Netherlands. This work was financially supported by a grant of the Radboud Institute for Molecular Life Sciences (RIMLS) to J.G.J. Hoenderop and F.L. van Delft.

ISBN/EAN: 9789462330870
Cover design: Armand Lahaije
Printed by: Gildeprint - www.gildeprint.nl
Vormgeving: Daan Driever & Liz Leunissen

Chemo-enzymatic tools to elucidate glycan-mediated TRPV5 regulation

Proefschrift

ter verkrijging van de graad van doctor
aan de Radboud Universiteit Nijmegen
op gezag van de rector magnificus prof. dr. Th.L.M. Engelen,
volgens besluit van het college van decanen
in het openbaar te verdedigen op woensdag 11 november 2015
om 12:30 uur precies

door

Elizabeth Hendrika Paulina Leunissen
geboren op 31 maart 1987
te Hilvarenbeek

Table of contents

Promotoren:
Prof. dr. J. G. J. Hoenderop
Prof. dr. F.L. van Delft

Copromotor:
Dr. J. van der Wijst

Manuscriptcommissie:
Prof. dr. U. Brandt
Prof. dr. ir. J.C.M. van Hest
Prof. dr. M. Merkx (TUE)

Paranimfen:
Ellen P. M. van Loon
Charlotte L. F. Leunissen

I

CHAPTER 1

General introduction

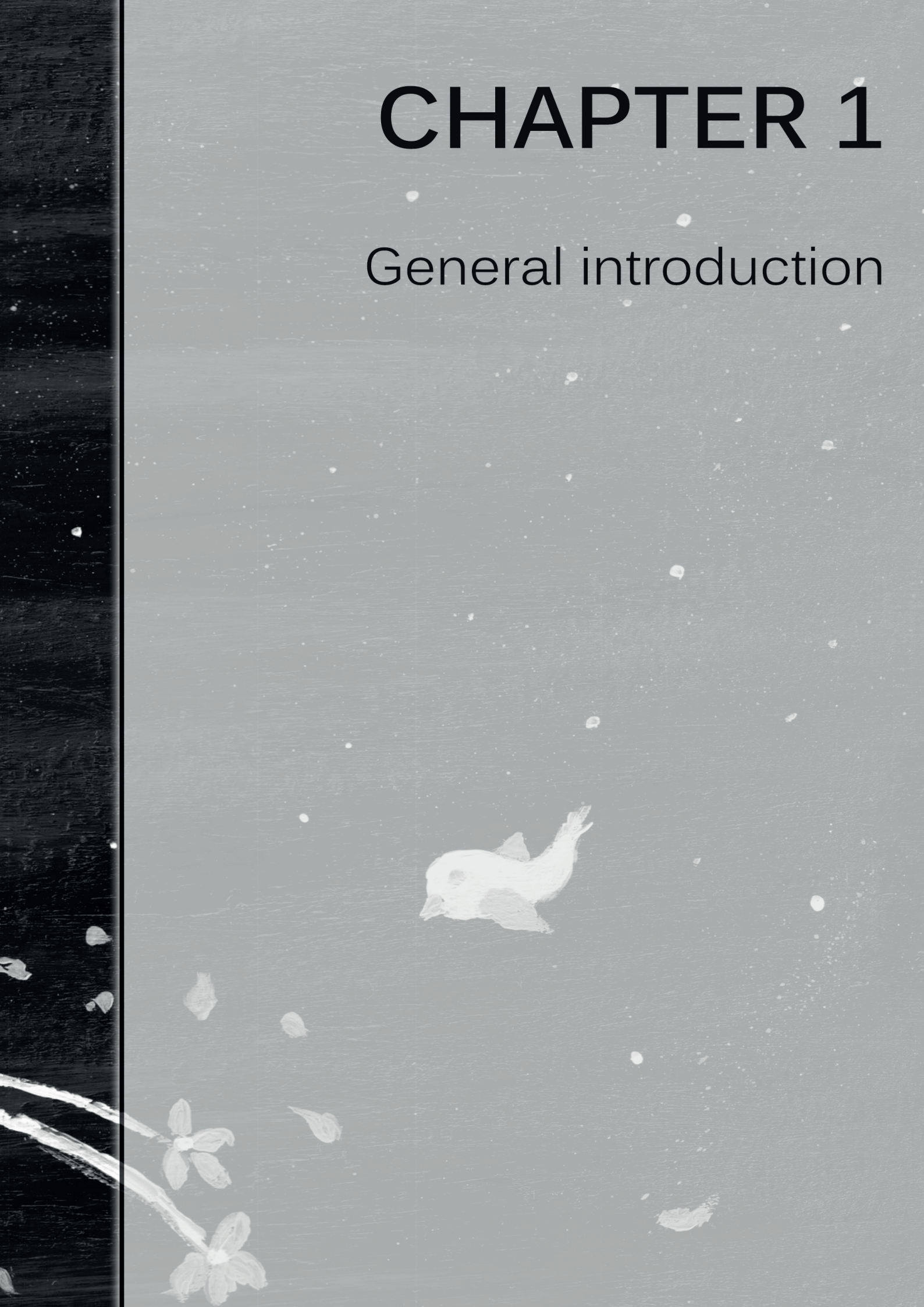

I

Glycobiology in cellular function

All living organisms in nature are composed of the same biological building blocks, *i.e.* nucleic acids (DNA/RNA), proteins, carbohydrates and lipids. Amongst these four classes, the central dogma dictates that biological information flows from DNA to RNA to protein. Even though DNA, RNA and proteins are needed for cellular function, it cannot explain the enormous complexity of life, as the number of genes is relatively small (~30,000). Two major major classes of biomolecules are not taken into account in the central dogma, namely lipids and carbohydrates. Both of which, are essential for cell function. While lipids play an important role in cell membrane composition, especially carbohydrates increase the complexity of proteins and lipids necessary for living organisms. The complete set of glycans and glycoconjugates that are produced by a cell or organism, known as the glycome, is involved in many regulatory processes such as cell-cell contacts, protein folding and protein trafficking (1,2). Glycosylation is the most complex form of post-translational protein and lipid modification in nature. The theoretical number of all possible hexamers (i.e. consisting of 6 building units) for glycans is 1.44×10^{15} as a result of the different monosaccharides, the glycosidic linkage options and the possible anomeric conformations. The complexity of the glycans is several orders of magnitude higher than for oligonucleotides (4096 options for an hexamer) or peptides (6.4×10^{6} options for an hexamer) (3). The enormous glycan diversity arises from the thirteen monosaccharide building blocks (Fig 1A, the seven most common saccharides are depicted). These monosaccharides can be connected via a range of glycosidic linkages, with one of the two possible anomeric configurations and additional chemical modifications (acetylation, sulfonation and phosphorylation) (4). Around 50% of the total cellular proteome and even >90% of the secreted proteome is glycosylated (5). Moreover, lipids, tRNA and many secondary metabolites can be glycosylated as well (6). Glycosylation of proteins leads to the generation of new binding sites, has crucial roles in recognition events and creates the diversity required to perform necessary physiological tasks. Malfunctions in the glycosylation pathway are often associated with diseases and a thorough understanding of the process of glycosylation has significant implications in the treatment of glycosylation-related diseases.

Glycosylation of proteins

The most prominent forms of eukaryotic glycosylation processes are O-linked and N-linked glycosylation. Other glycosylation forms such as proteoglycans, phosphoglycosylation, GPI-anchors or C-linked glycosylation are beyond the scope of this intorduction (6). This thesis focuses on the N-linked glycosylation, which has a multitude of biological functions including protection of the proteins against denaturation and proteolysis, enhance solubility, facilitate orientation of proteins on the cell plasma membrane, confer structural rigidity to proteins, regulate protein turnover, fine-tune the charge and iso-electric point of proteins and mediate interactions with pathogens (4,7). Structurally, N-glycans are covalently linked to the side-chain aminogroup of an asparagine, which typically resides within a defined N-X-S/T motif of the protein (or more rarely N-X-C, N-X-V, or N-G sequons), where X is any amino acid except proline (8).

The biosynthesis of glycoproteins commences when proteins entering the endoplasmic reticulum (ER) are covalently modified on the asparagine aminogroup with a pre-assembled oligosaccharide ($Glc_3Man_9GlcNAc_2$). This 14-mer glycan is transferred, as a whole, from a lipid donor (dolichol) onto the nascent protein by an enzyme named oligosaccharyltransferase. Next, the glycan is trimmed to $Man_9GlcNAc_2$ by a range of

enzymes, before the glycoprotein leaves the ER. If the protein is misfolded, trimming is compromised and a checkpoint protein called EDEM (ER degradation-enhancing α-mannosidase I-like protein) will target the glycoprotein for ER degradation (9). The hydrophilic character of the glycan increases the solubility and prevents cleavage by proteases. Moreover, addition of large polar groups can make the polypeptide chain more rigid, which increases the stability resulting in proper folding (10).

After passing the ER, a series of reactions further trim the glycan until $Man_5GlcNAc_2$ is formed in the *cis*-Golgi (7,9) and $GlcNAcMan_3GlcNAc_2$ in the *medial*-Golgi. Finally, maturation takes place in the *trans*-Golgi. Three different types of N-glycans are commonly present on proteins; high mannose, hybrid and complex type N-glycan. Especially complex type N-glycans can be very diverse, an example of each type is depicted in Fig 1B. Synthesis of complex and hybrid N-glycans is initiated in the *medial*-Golgi, and further processed in the *trans*-Golgi. Addition of fucose to the *N*-acetylglucosamine adjacent to the aminogroup in the core is a common modification in the *trans*-Golgi (7). Other important capping reactions are the addition of sialic acids (NeuAc), galactose, *N*-acetylgalactosamine and sulfate to the branches. These capping saccharides often facilitate the presentation of terminal sugars to glycan binding proteins and antibodies (7).

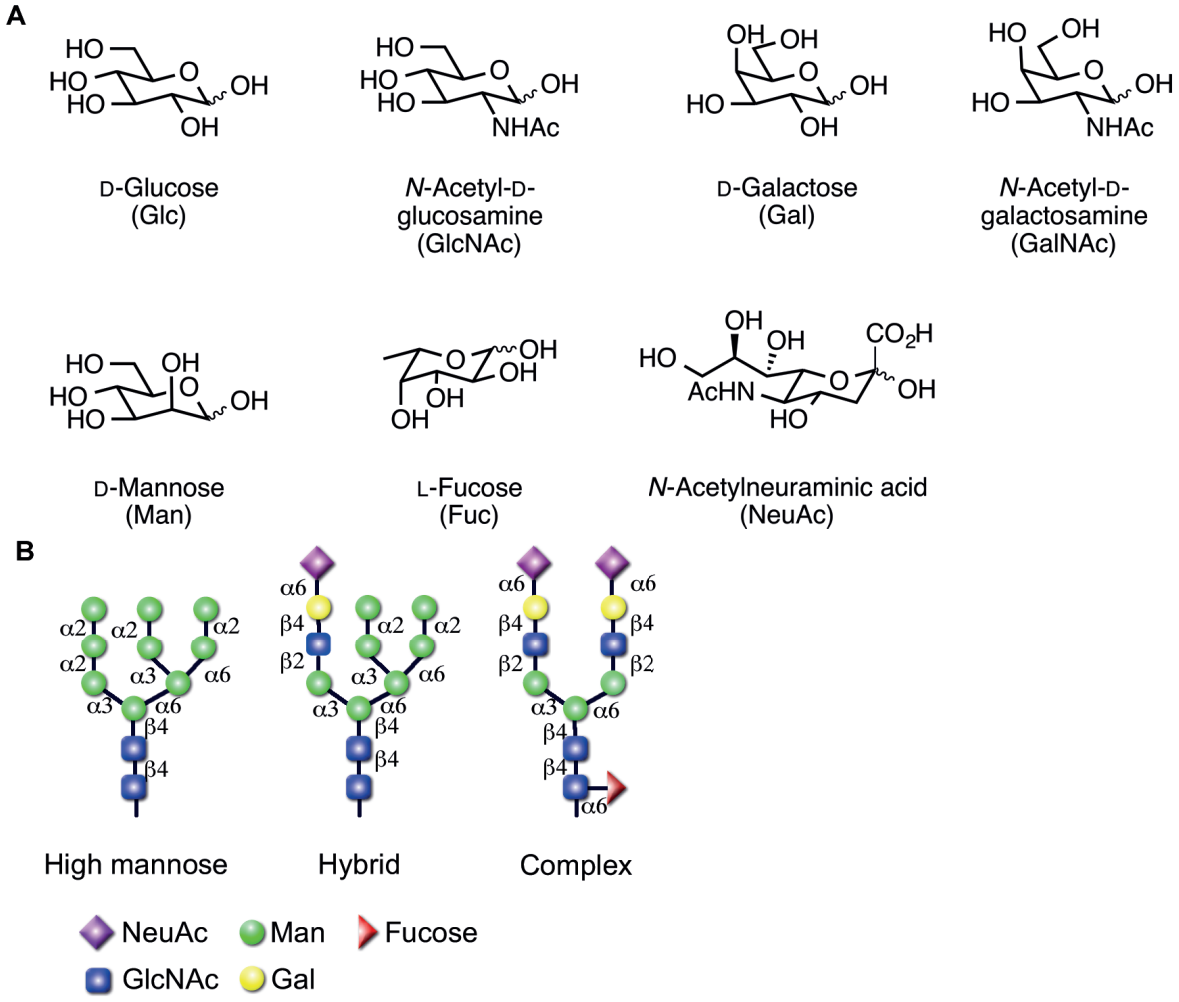

Figure 1. General structures of natural linked N-glycans.
A) Chemical structures of the most common saccharides expressed in N-glycans. **B)** Three examples of mature N-glycans. A high mannose, a hybrid and a complex type N-glycan is depicted from left to right. Figure is adapted from Varki *et al.* (7).

Once processed by the ER and Golgi, many glycoproteins are translocated towards the plasma membrane. Here, the glycans are exposed to the extracellular compartment as flexible, hydrofile branches that can reach 3 nm or more into the extracellular fluid. X-ray crystal structures of glycoproteins and NMR studies indicate that the majority of glycans have only minor contact with the protein surface (11). Within the extracellular space, the glycan can interact with various glycan-binding proteins, known as lectins. These proteins without enzymatic activity have a high degree of heterogeneity in structure and function. Lectin-glycan interactions are involved in many biological cellular processes such as apoptosis, differentiation and proliferation (12). Changes in these interactions are often associated with tumor formation and metastasis, but also with other diseases like nephritis or increased susceptibility to infections (13-16). Lectins are divided into 14 different families based on their folding properties and capacity to bind sugars (3,7). Most mammalian lectins can be classified into five major groups based on the folding of the carbohydrate binding module: I-type lectins, C-type lectins, P-type lectins, L-type lectins and galectins (7,12).

For the research performed in this thesis, only the interactions of galectins on specific glycoproteins were evaluated. Galectins are a family of glycan-binding proteins characterized by their affinity for β-galactose in a specific reoccurring sequence of N-acetyllactosamine (LacNAc, Gal-(β-1,4)-GlcNAc) on branched N-glycans. However, some galectins have a relatively weak binding affinity to LacNAc repeats and bind more specific to variants of this repeat (17).

Galectins

There are 15 galectins known, of which 11 are expressed in humans. The proteins can be classified into three main subgroups; the prototypical, the chimeric and the tandem-repeat galectins. Galectin-1 is part of the prototypical galectin group and acts as a homodimer with a single carbohydrate-recognition domain (CRD) in each subunit. Moreover, galectin-2, -7, -10, -13 and -14 are also human prototypical galectins. Galectin-3 is the only protein found in vertebrates belonging to the chimeric galectin group, characterized by a single CRD and a large amino-terminal domain. Finally, the tandem-repeat galectins, galectin-4, -8, -9 and -12, have two CRD's linked by a small peptide (7,18,19). The function of galectins is diverse and they can even counteract each other in some systems. For example, galectins can mediate cell-cell interactions, cell-matrix interactions, protein-protein interactions, cross-linking of proteins or initiate signaling cascades (20). In the kidney, only galectin-1, -3, -7, -8 and -9 are expressed (21,22). From these galectins, galectin-1, -3, -8, and -9 are located in lipid rafts, and only galectin-3 and -9 are involved in cell trafficking and endocytosis (20).

To enhance our knowledge on glycan structure and function, adequate labeling techniques are required, as the complexity of these glycans is enormous. The conventional toolbox to visualize and investigate glycans is relatively small. Lately, new techniques derived from various research fields enable glycan labeling.

Bioorthogonal glycan labeling reactions

Special chemical reactions are often used to study the glycosylation of cells *in vitro* and eventually in mammalians (23). Such reactions have to be suitable for application in biological systems, indicating they should proceed under aqueous, non-toxic conditions at physiological temperatures (4–37 °C). Another requirement is bioorthogonality, meaning that the chemical reaction must occur inside living cells or systems without interfering with native biochemical processes. Bioorthogonal reactions include amongst

others the so-called chemical reporter strategy which consists of the following two steps: 1) the introduction of a reactive component such as an azide, an alkyne, a ketone or an aldehyde into a biomolecule by metabolic incorporation and 2) bioorthogonal conjugation with a molecule of interest to impart a specific property onto the biomolecule, *e.g.* a fluorescent group or a radioisotope label (Fig 2A). A bioorthogonal reaction enabling glycan labeling implies that the mutually selective chemical reactivity of the two functional groups ensures specific targeting of the metabolically labeled glycans. To insert the reactive component the introduction of non-natural monosaccharides, such as *N*-azidoacetylmannosamine (ManNAz), with unique chemical moieties is necessary. Presently used bioorthogonal reactions can be divided into two major groups, the polar reactions (reactions in which a nucleophile adds to an electrophile, with the formation of a covalent bond) and the cycloadditions (a reaction in which two or more unsaturated molecules combine with the formation of a cyclic adduct) (24) (Fig 2 B,C).

i) Polar reactions

Aldehydes and ketones are susceptible to nucleophilic addition of amines, leading to a condensation reaction (formation of a new carbon-nitrogen bond with elimination of water). Ketones and aldehydes are not bioorthogonal, as they are present in hormones such as cortisone, progesterone and testosterone (25), in the citric acid cycle and in monosaccharides. Despite this, the carbonyl moiety is of sufficient uniqueness for extracellular labeling of glycans and proteins. Ketones and aldehydes displayed on the cell surface can react with hydrazide- and aminooxy-derivatized ligands (26). It has been demonstrated that an unnatural mannosamine derivative with a keto group, *N*-levulinoylmannosamine (ManLev), can compete with endogenous ManNAc (a natural NeuAc precursor). Subsequently, the saccharide derivative is implemented into the complex glycan and presented at the cell surface. At this stage, the ketone can react with a hydrazide to covalently attach a biotin tag (27). An alternative method to introduce an aldehyde in a glycan is via periodate oxidation of the diol present in endogenous sialic acids and galactose. Subsequently, via oxime ligation, aminooxy-biotin can form a covalent bond with the newly formed aldehyde on the sialic acids at the cell surface (28). The drawback of the ligation reactions between hydrazide or aminooxy with a carbonyl group is the need for acidic conditions (pH 5–6) and high reagent concentrations (2–5 mM) (26,29), a combination that is often toxic for the cells. In addition, the reaction products, hydrazones or oximes, respectively are susceptible to hydrolysis thereby giving the reverse reaction. One elegant solution to avoid the reversibility of the condensation is by using a Pictet-Spengler reaction between an aldehyde and a specific tryptamine derivative, which will give a hydrolytically stable product (30).

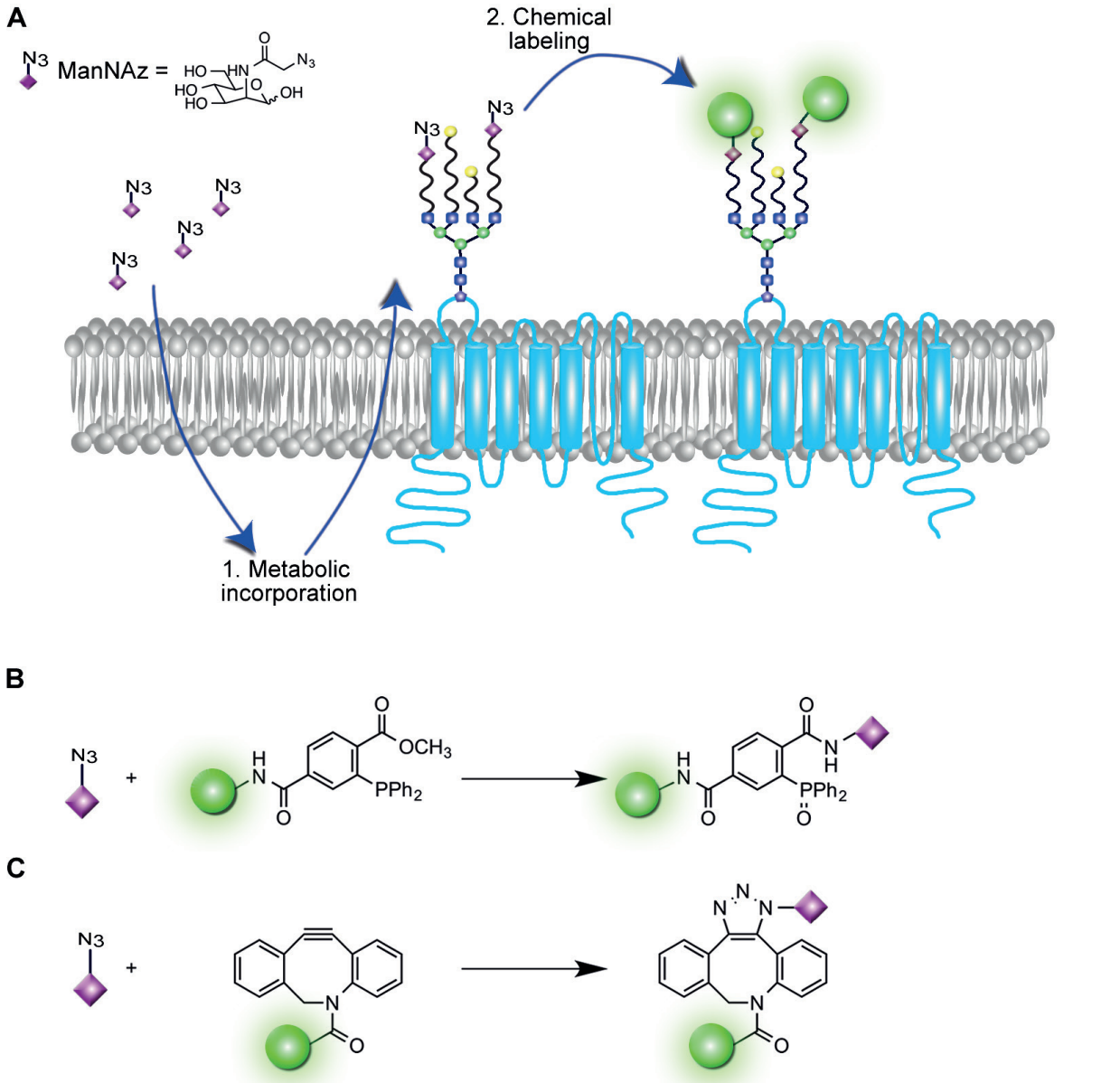

Figure 2. Metabolic incorporation of non-natural saccharide and examples of bioorthogonal reactions. **A)** 1. Cells incubated with an azido-saccharide such as ManNAz (purple) have this sugar incorporated into the N-glycan of membrane expressing proteins and into glycolipids. 2. This chemical handle is used to label the glycan with a tag (green). **B)** Example of a Staudinger-Bertozzi ligation to label azido-saccharides with a tag (31). **C)** SPAAC reaction between an azide and a strained alkyne (DIBAC), forming a stable triazole ring (32).

The Staudinger-Bertozzi reaction is another polar reaction frequently used for protein and glycan labeling (Fig 2B). The reaction between an azide moiety and a phosphine group adjacent to a methyl ester results in an amide linkage (31). Unlike aldehydes and ketones, azides are completely abiotic, small, stable in water and biocompatible, which makes them useful for bioorthogonal ligation reactions (33,34). Monosaccharide analogs functionalized with an azide moiety, such as ManNAz, SiaNAz, GalNAz, FucAz and GlcNAz, are often used for metabolic oligosaccharide engineering (23,35). However, monosaccharide analogs enter the cell inefficiently as a result of their hydrophilicity and the low level of adequate membrane transporters at the cell membrane. The incorporation of these modified monosaccharides can be improved by converting the alcohol-moieties into esters with short chain fatty acids, via acetylation for example, to increase the hydrophobicity. Peracetylation of sugar analogs increases the metabolic

incorporation efficiency by 600-fold. One disadvantage of the peracetylated sugar analogs is that they are 2-3 orders of magnitude more cytotoxic compared to the non-acetylated saccharide (36). The cellular uptake, incorporation and distribution of modified saccharides into glycoproteins are tissue-specific, as a result of the differences in protein and transferase expression levels (36). Moreover, the reaction kinetics of the Staudinger-Bertozzi ligation is rather low and the technique is hampered by oxidation of the phosphane (31). Yet the remarkable selectivity of this reaction and the compatibility with cells, tissues and animals make this reaction a popular choice for *in vivo* studies (37).

ii) Cycloadditions

Next to the polar reactions used for biochemical labeling, cycloadditions are often applied to label glycans. The previously described azide-moieties belong to the class of so-called 1,3-dipoles, which can be used for cycloaddition reactions. Previously, it was found that the reaction rate of azides with terminal alkynes is extremely enhanced by using copper(I) (Cu(I)) as a catalyst (38,39). Nowadays, the most commonly used cycloaddition in cellular systems is the copper(I)-catalyzed alkyne–azide 1,3-dipolar cycloaddition (CuAAC), also referred to as the 'click reaction', forming robust triazoles. Due to the high reaction rate and simplicity, this reaction is highly desirable for its use in biomolecular systems. The stable alkynes and azides are one of the smallest applicable groups with little interference in biological systems, which makes the click reaction suitable for *in vitro* glycan labeling. However, the required Cu(I) source used to catalyze this reaction is highly toxic, driving the need for elimination of Cu(I) in these cycloadditions. Two alternatives were developed, one of these was the application of a Cu(I) ligand (40). An example of a Cu(I) ligand is the water-soluble THPTA, which accelerates CuAAC and protects the cells from damage (41). The BTTES does not only prevent cytotoxicity of Cu(I), but also enhances the reaction rates in zebrafish (42). Furthermore, using BTTAA as a ligand increases labeling specificities both *in vitro* and *in vivo* (43).

Another method to circumvent the toxicity of Cu(I) is via the strain-promoted alkyne-azide cycloaddition (SPAAC), a reaction with good kinetics in the absence of the Cu(I) catalyst. A range of strained alkynes has been developed with improved specificity and reaction rates in the absence of Cu(I). By definition, SPAAC involves the reaction between an azide and a strained cyclooctyne, forming a stable triazole ring (Fig 2C). The most well known strained cyclooctynes are; difluorinated cyclooctyne (DIFO) (44), biarylazacyclooctynone (BARAC) (45), dibenzocyclooctyne (DIBO) (32), azadibenzocyclooctyne (DIBAC/DBCO) (46) and bicyclo[6.1.0]nonyne (BCN) (47) (Fig 1, chapter 2). All these strained alkynes have their advantages and disadvantages, which are extensively reviewed (34,48). SPAAC is a popular method to label glycans on living cells (32,47,49) and in living organisms (50-52). The reaction rates can be even further improved by using different SPAAC-like reactions such as the strain-promoted inverse-electron-demand Diels–Alder cycloaddition (SPIEDAC) between a *trans*-cyclooctyne and a tetrazine, or the similar reaction between a cyclooctene and a tetrazine (53,54). However, these reactions have not been used for glycan labeling thus far.

The role of glycosylation in the regulation of the calcium homeostasis

The activity of most proteins is regulated by glycosylation, as around 50% of the total cellular proteome and 90% of the secreted proteome are glycosylated (5). One of the cell membrane proteins that is regulated via its N-glycan, is the epithelial calcium (Ca^{2+}) channel transient receptor potential vanilloid type 5 (TRPV5). TRPV5, and its

orthologue TRPV6, are part of the large TRP ion channel family (55). These channels are highly selective for Ca^{2+} and share biophysical properties that are distinct from the other TRP channels (56,57). Moreover, they are known key players in the maintenance of the body's Ca^{2+} balance and expressed in the Ca^{2+} transporting organs; the kidney, the bone and the intestine. Regulation of the Ca^{2+} balance is a concerted action balancing Ca^{2+} absorption with Ca^{2+} excretion and storage. While the bone is mainly used for Ca^{2+} storage, the kidney and intestine are involved in Ca^{2+} (re)absorption (55). Subtle dysregulation in the balance causes alterations in plasma Ca^{2+} levels (hyper/hypocalcemia) that are associated with major diseases such as cardiac disease, osteoporosis, schizophrenia, bipolar disorder and Alzheimer's disease (58). TRPV5 is expressed at the resorptive surface of osteoclasts, facilitating the removal of bone matrix (59). In the kidney, TRPV5 is the gatekeeper of active Ca^{2+} transport (60,61).

Ca^{2+} reabsorption in the kidney

The kidney controls the excretion of Ca^{2+} and thereby allows the body to adapt to changes in Ca^{2+} demands and to fluctuations in dietary Ca^{2+} intake via a strictly regulated mechanism. The Ca^{2+} needs in the human body varies as a result of growth, pregnancy or aging (62). Ca^{2+} plays crucial roles in many processes such as the release of hormones or neurotransmitters, bone mineralization and muscle contraction (63).

Only 1-2% of the filtered Ca^{2+} is excreted by the kidney, therefore the largest fraction is reabsorbed along the different segments of the nephron (64,65) (Fig 3A). Ca^{2+} reabsorption is accomplished via two main mechanisms; passive paracellular and active transcellular transport. The majority of Ca^{2+} is absorbed paracellularly along the proximal tubule (PT) and the thick ascending limb (TAL), driven by the electrochemical gradient (55). Active transcellular transport (~10%) takes place in the distal convolutions (distal convoluted tubule (DCT) and connecting tubule (CNT)) and is responsible for the fine-tuning of the final urinary Ca^{2+} excretion (55,66) (Fig 3A). The active transcellular transport starts with apical (luminal) influx of Ca^{2+} from the pro-urine via TRPV5. To maintain a low cytosolic Ca^{2+} concentration, Ca^{2+} is bound by buffering proteins called calbindin-D_{28K} (kidney) or calbindin-D_{9K} (intestine). Finally, calbindin-bound Ca^{2+} is shuttled to the basolateral side and extruded into the bloodstream via a Na^{+}/Ca^{2+} exchanger (NCX1) and the plasma membrane Ca^{2+}-ATPase 1b or 4 (PMCA1b, PMCA4) (Fig 3B).

The importance of the renal transcellular Ca^{2+} reabsorption in the late DCT and CNT is illustrated by several knockout mouse models. The TRPV5 knockout ($TRPV5^{-/-}$) mice model shows the importance of TRPV5 as the gatekeeper of the Ca^{2+} balance in the kidney (68), as these mice exhibit several phenotypical deviations correlated to a diminished active Ca^{2+} reabsorption. $TRPV5^{-/-}$ mice display hypercalciuria, compensatory hyperabsorption of dietary Ca^{2+} and disturbances in bone structure such as reduced trabecular and cortical bone thickness (68). Recently, a mice strain generated using N-ethyl-N-nitrosourea, a chemical mutagen causing point mutations, displayed autosomal dominant hypercalciuria (69). Linkage studies identified a heterozygous S682P mutation in TRPV5 that affects channel trafficking, confirming the importance of TRPV5 in Ca^{2+} homeostasis (69).

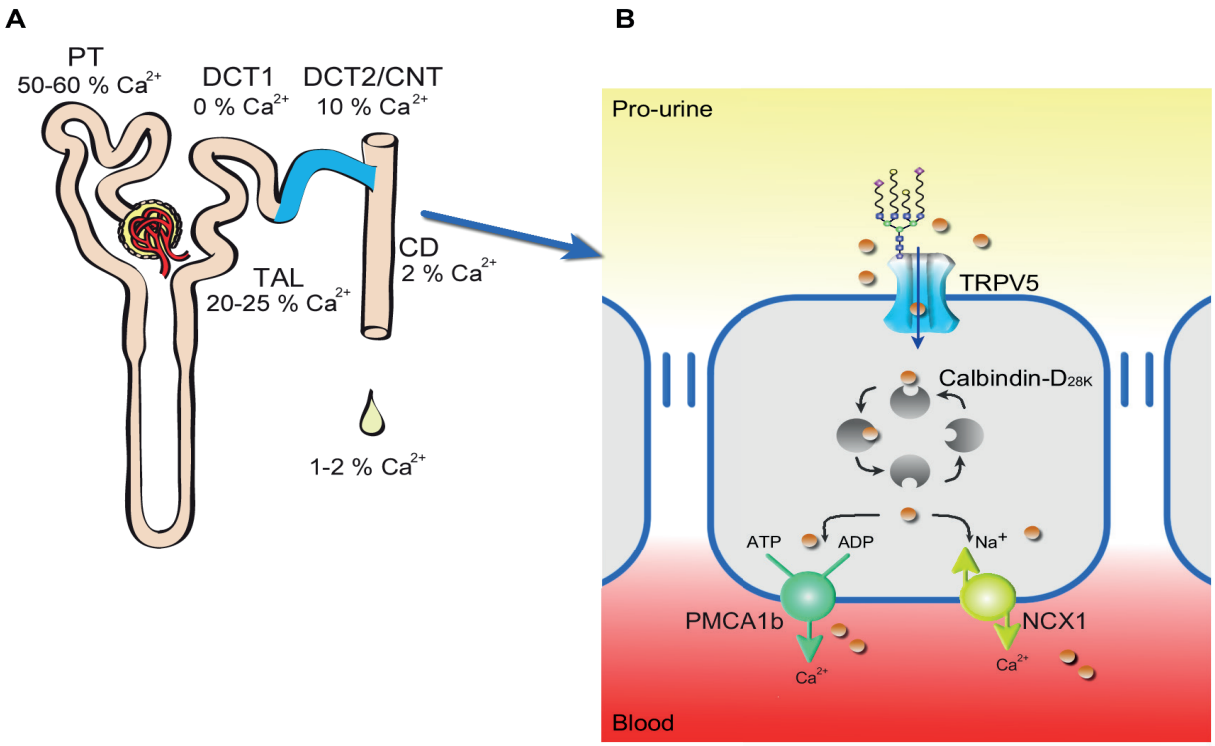

Figure 3. Ca^{2+} reabsorption along the nephron.
A) Paracellular transport takes place in the PT and TAL of the kidney. ~10% of the total Ca^{2+} reabsorption takes place in the DCT2/CNT where TRPV5 is expressed, illustrated in blue. This part of the kidney is responsible for the fine-tuning of Ca^{2+} excretion. Adapted from Glaudemans *et al.* (67). **B)** TRPV5 mediates the transcellular Ca^{2+} uptake from the pro-urine. In the cell, calbindin-D_{28K} transports Ca^{2+} to the basolateral side, where it is extruded by NCX1 and PMCA1b. Adapted from Dimke *et al.* (55).

The cytosolic Ca^{2+} levels (~ 100 nM) are low, whereas the extracellular Ca^{2+} levels are about 10.000 times higher, indicating the importance of calbindin-D_{28K} for Ca^{2+} buffering in the cell (56). Calbindin-$D_{28K}^{-/-}$ mice displayed normal plasma Ca^{2+} concentrations and urinary Ca^{2+} excretion. However, when placed on high Ca^{2+} diet, these mice had a two- to threefold increase in urinary Ca^{2+} (70). The modest effect on the mice phenotype is probably a result of the co-expression of calbindin-D_{9K} together with calbindin-D_{28K} in the kidney of mice, in contrast to humans that express calbindin-D_{9K} mainly in the intestine (71). Calbindin-D_{9K} might compensate for the calbindin-D_{28K} loss in mice. Double calbindin-$D_{28K/9K}^{-/-}$ mice display reduced transcellular Ca^{2+} transport, based on changes in the phenotype (decreased bone length and serum Ca^{2+} levels) and the expression of active Ca^{2+} transport genes (72). Moreover, the lack in transcellular Ca^{2+} reabsorption is compensated via paracellular Ca^{2+} reabsorption, as the level of tight junction related transcripts and proteins has been increased (73). Mice ablated of NCX1 in the distal part of the nephron are hypercalciuric, have a higher urine volume and lower urinary pH compared to the wild type (WT) mice. To compensate for chronic Ca^{2+} loss, the intestinal TRPV6-mediated Ca^{2+} absorption is increased (74). Homozygote PMCA1$^{-/-}$ mice are embryonic lethal, while heterozygous mutants show no apparent phenotype. PMCA4$^{-/-}$ mice appear normal, however the males are infertile (75).

I

Structure of TRPV5

The human *TRPV5* gene, located on chromosome 7 and encoding 15 exons, is expressed as a membrane bound protein of 729 amino acids with a molecular mass of 83 kDa (76). TRPV5 consists of 6 transmembrane (TM) segments with intracellular amino (N) and carboxyl (C) termini (56) (Fig 4A) and is thought to function as a constitutively active Ca^{2+} channel, as Ca^{2+} transport is also detected in absence of a ligand or stimulus (77).

The functional TRPV5 channel is assembled as a tetramer, with a highly Ca^{2+}-selective pore (78,79). The pore region is composed at the interface of the four subunits between TM 5 and 6. This was recently confirmed by Liao *et al.* who elucidated the tertiary structure of TRPV1, a related cation channel (80) (Fig 4B). The amino acid composition of the selectivity filters of TRPV5 and TRPV6 are distinct from other TRP channels, explaining the more pronounced selectivity for Ca^{2+} over monovalent cations (80). The D542 residue in the selectivity filter of TRPV5 and TRPV6 is essential for the Ca^{2+} selectivity of the channel (77) (Fig 4B). Mutating this residue into an alanine abolishes Ca^{2+} permeability without altering the permeability for monovalent cations. Interestingly, the positively charged H712 is highly important for constitutive internalization of TRPV5. Mutation of this histidine in a neutral or negatively charged amino acid stimulates TRPV5 activity by increasing the plasma membrane expression (81).

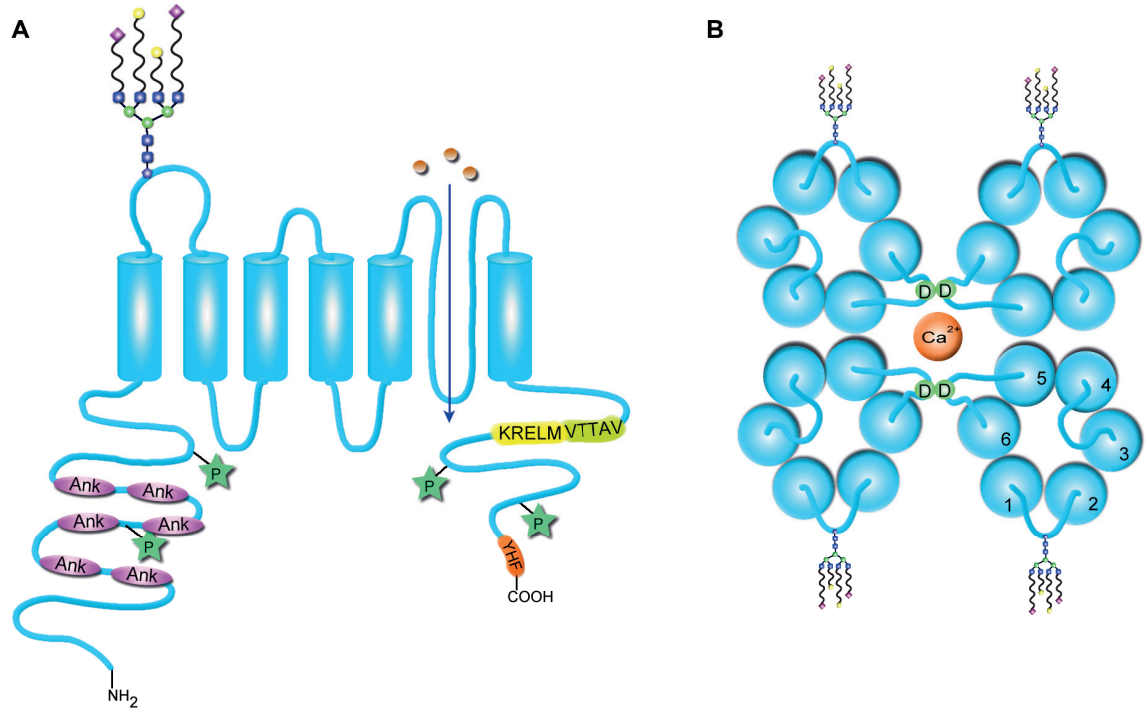

Figure 4. Monomeric and tetrameric topology of the TRPV5 channel.
A) TRPV5 spans the plasma membrane 6 times, and has an intracellular C- and N-terminal tail. The ANK repeating domains at the N-terminal region are highlighted in pink. Glycosylation of the channel takes place at N358 with a complex type N-glycan. The phosphorylation sites are indicated with green stars (S144, S299, S654, T709). The VATTV recognition site for S100A10/Annexin 2 is highlighted in green, while the MLERK recognition site (highlighted in yellow) is bound by NHERF2 and 80K-H. Finally, the recognition site for NHERF2 is located at the end of the C-terminal region (YHF, highlighted in orange). **B)** Top view of the tetrameric TRPV5 channel. The pore consists of TM 5, 6 and the pore forming region, with D542 (green) as a crucial residue to mediate the Ca^{2+} selectivity of the pore.

The N-terminal region of TRPV5 contains an ankyrin-repeat domain (ARD) consisting of 6 ankyrin (ANK) motives. These motives are involved in channel tetramerization (78,82,83), as they are frequently associated with protein-protein interactions. The

C-terminal region of TRPV5 can bind to different proteins including S100A10/annexin 2, Ras-related protein 11a (Rab11a), protein kinase C substrate 80K-H (80K-H) and Na^+/H^+ exchanger regulatory factor 2 (NHERF2) (84-87). S100A10/annexin 2 binds to the VATTV amino acid sequence in the C-terminal region of TRPV5. Mutation of this binding site reduces TRPV5 membrane trafficking in *Xenopus laevis* oocytes (84). S100A10/annexin 2 is involved in various intracellular protein trafficking processes, therefore it is likely that the complex is responsible for TRPV5 routing towards the plasma membrane. Rab11a binds to the MLERK motif and is involved in the recycling of endosomes. Direct binding of Rab11a translocates TRPV5 from the endosomes to the plasma membrane (85). The calcium-sensing protein, 80K-H, binds to the same motif as Rab11a, and is postulated to increase channel activity (86). Finally, NHERF2 binds to the YHF motif at the end of the C-terminus, thereby stabilizing TPRV5 at the plasma membrane, probably by linking the channel to cytoskeletal proteins (87) (Fig 4A). The TRPV5 channel is subjected to different posttranslational modifications. Phosphorylation of TRPV5 at S144, S299, S654 and/or T709 regulates the channel activity (88-90). In addition, the channel is glycosylated at N358, with most likely a tetra-antennary complex N-glycan (91) whose exact composition remains unknown. Regulation of TRPV5 function by this posttranslational modification will be extensively discussed in this thesis.

Regulation of TRPV5 by hormones, biochemical and biophysical factors

A variety of factors control TRPV5 function at three different levels *i*) gene/protein expression; *ii*) channel activity and *iii*) channel plasma membrane expression (Fig 5). The expression of TRPV5 channels is regulated by calciotropic hormones including parathyroid hormone (PTH), 1,25-dihyroxy vitamin D_3 ($1,25\text{-}(OH)_2D_3$), fibroblast growth factor 23 (FGF23) and estrogens (92-94).

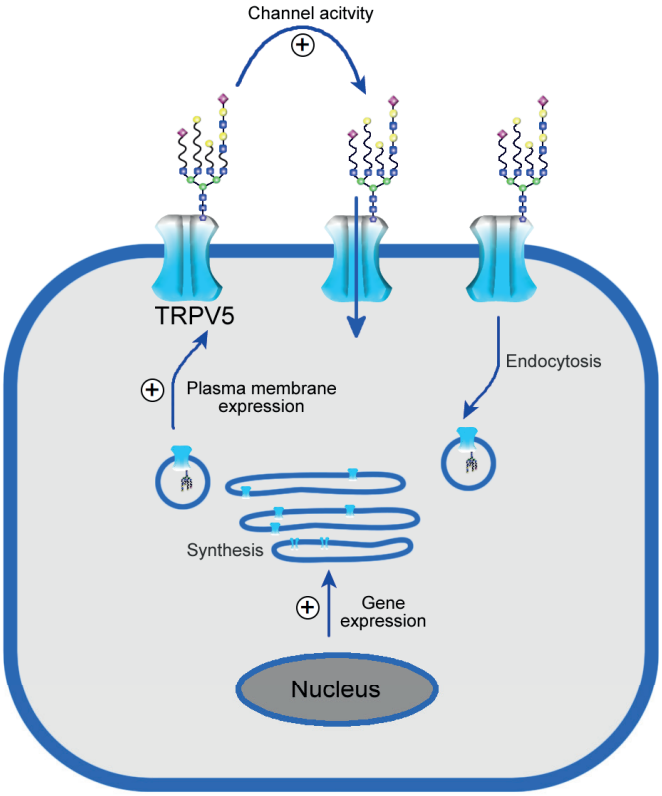

Figure 5. The TRPV5 channel can be regulated at three different levels.
TRPV5 function can be controlled at three different levels: gene/protein expression, channel plasma membrane expression and channel activity. Finally the protein is endocytosed and degraded.

In addition to TRPV5 protein expression, the Ca^{2+} reabsorption is dependent on TRPV5 single-channel activity. Conductance in combination with the open probability (P_o) determine TRPV5 single-channel activity. The probability of a channel being open is termed P_o, whereas conductance is the amount of electrical charge that is conducted during the open state (56). Factors influencing single-channel activity are intracellular Ca^{2+}, calmodulin (CaM), PTH, shear force and pH (95-100). Stabilization of TRPV5 at the plasma membrane is often regulated via glycosylation. Several factors stabilize TRPV5 on the plasma membrane, such as tissue transglutaminase (tTG), tissue kallikrein (TK), NHERF2, with-no-lysine kinase 4 (WNK4), pH, uromodulin (UMOD) and klotho (89,101-106).

Divalent ions regulate TRPV5 activity

A high intracellular Ca^{2+} level functions as a negative feedback mechanism and will inhibit TRPV5 channel activity (95). This inhibition is controlled by the concentration of Ca^{2+} in a micro-domain near the inner mouth of the channel. Recovery of TRPV5 activity follows after restoration of the basal Ca^{2+} levels (95), and depends on dissociation of Ca^{2+} from an internal Ca^{2+}-binding site in TRPV5. Since the half maximal inhibition (IC_{50}) value is in the range of the intracellular Ca^{2+} concentration, this effect is likely to be physiologically relevant. Intracellular Ca^{2+} sensing takes place at the C-terminal region of TRPV5. Removal of the last 30 amino acids desensitizes TRPV5 to intracellular Ca^{2+} concentrations (96). A second Ca^{2+}-sensing domain is present between amino acids 650-653 (96). Part of this Ca^{2+}-mediated negative feedback mechanism functions via the binding of CaM, a binding protein that is activated upon Ca^{2+} binding (107). The P_o of TRPV5 is reduced upon CaM binding (97). A high intracellular Ca^{2+} concentration enhances this CaM binding and inhibits Ca^{2+} uptake via TRPV5. Removal of the C-terminal fragment of TRPV5 (696-729) abolishes TRPV5 sensitivity by CaM (97).

The combined action of phosphatidylinositol 4,5-bisphosphate (PIP_2) and Mg^{2+} is an important factor involved in TRPV5 channel activity (108). Intracellular Mg^{2+} reduces TRPV5 channel activity by binding to D542, thereby blocking the pore filter, resulting in a voltage-dependent TRPV5 inhibition (109). In addition, Mg^{2+} binding to the same position impedes TRPV5 channel activity via a slow inactivation mechanism (109). It has been hypothesized that slow inhibition is caused by a conformational change in the channel structure. The membrane phospholipid PIP_2 reduces the slow inhibition by Mg^{2+} by preventing the Mg^{2+}-induced conformational change of TRPV5. Thereby TRPV5 is stabilized in the open conformation at the plasma membrane (109).

Dual function of PTH

The primary role of the PTH-vitamin D axis is to maintain the plasma Ca^{2+} levels within a narrow range. Minor variations in extracellular Ca^{2+} levels are sensed by the Ca^{2+}-sensing receptor (CaSR) located in the parathyroid gland (110,111) and the loop of Henle (112). A decline in the extracellular Ca^{2+} concentration triggers the release of PTH. Subsequently, PTH acts on several organs throughout the body to maintain the Ca^{2+} balance. Elevation of plasma PTH levels increases the mobilization of Ca^{2+} from hollow trabecular bones and at the same time stimulates the 1α-hydroxylase (1α-OHase) activity in the kidney (92). 1α-OHase is responsible for the conversion of 25-hydroxyvitamin D_3 into the active hormone 1,25-$(OH)_2D_3$. The active vitamin D hormone stimulates transcription of many proteins involved in renal active Ca^{2+} reabsorption, such as TRPV5 and calbindin-D_{28k} (93). 1,25-$(OH)_2D_3$ functions as a negative feedback mechanism and lowers plasma PTH levels (94). In contrast, low PTH

levels resulting from allosteric activation of the CaSR via calcimimetic drugs can alter the expression levels of TRPV5 and calbindin-D_{28k} independent of the 1,25-$(OH)_2D_3$ levels (113). This could imply that the expression of proteins involved in renal Ca^{2+} reabsorption is also directly associated with PTH levels, without the influence of 1,25-$(OH)_2D_3$ (113).

Intertwined in the PTH-vitamin D axis is the hormone FGF23 via the so-called FGF23-bone-kidney axis (92). FGF23 directly increases the PTH production, stimulating hormonal regulation by 1,25-$(OH)_2D_3$ and thereby stimulating Ca^{2+} reabsorption (114). In addition, renal Ca^{2+} reabsorption and membrane abundance of TRPV5 are reduced in FGF23$^{-/-}$ mice (115). Binding of the assumed glycosidase klotho to the FGF receptor (FGFR) increases the affinity for FGF23. Next, FGF23 binding results in activation of a signaling cascade involving the extracellular regulating kinase 1/2 (ERK1/2), serine/threonine kinase 1 (SGK1) and WNK4, thereby increasing renal TRPV5 transport to the plasma membrane (115).

Next to the long-term effect, PTH can also act directly on TRPV5 channel function. Binding of PTH to its receptor initiates an increase in TRPV5 plasma membrane retention via activation of the protein kinase C (PKC) signaling cascade (116). This will result in phosphorylation of the residues S229/S654 in the TRPV5 channel, which will increase the plasma membrane expression. Moreover, PTH mediates phosphorylation of TRPV5 T709 via protein kinase A (PKA). Phosphorylation at this position diminishes CaM binding and thereby increases P_o, stimulating TRPV5-mediated Ca^{2+} transport (97).

pH regulates TRPV5 activity

Shifts in the extracellular acid-base balance can regulate the Ca^{2+} balance by influencing TRPV5 transcription (117). Metabolic acidosis decreases the expression of the TRPV5 channel and leads to hypercalciuria. Moreover, metabolic acidosis in TRPV5$^{-/-}$ mice does not further influence the hypercalciuria, implying that TRPV5 is involved in hypercalciuria upon metabolic acidosis (117). Chronic metabolic alkalosis increases the expression of Ca^{2+} transport proteins such as TRPV5 and calbindin-D_{28K} in WT mice, which decreases the urinary Ca^{2+} excretion. However, this effect is not TRPV5 dependent, since this Ca^{2+} sparing effect is also present in TRPV5$^{-/-}$ mice. In addition, cell surface delivery of TRPV5 is dynamically controlled by the extracellular pH via TRPV5-containing vesicles. Upon extracellular acidification, vesicles are retrieved from the plasma membrane, which results in decreased TRPV5 activity, while alkylation has the opposite effect (104).

Single channel activity is also regulated by the pH. Two residues, E522 (located extracellular) and K607 (located intracellular), are involved in pH sensing (118,119). Protonation of either of these residues results in a change of the pore helix, reducing channel activity. E522 is important for extracellular pH sensing (119). Mutation of K607 into a non-charged residue ablates the intracellular pH sensitivity of the TRPV5 channel (100). Intracellular acidification results in conformational changes of the pore helix, thereby closing the channel (100). The exact mechanism causing the rotation of the pore helix remains elusive. However, mathematical models based on the experimental data suggest that pH-dependent changes in channel activity is only of minor importance for the *in vivo* Ca^{2+} regulation (120,121). These models imply that the changes in TRPV5 abundance upon acidification contribute more to the renal Ca^{2+} wasting observed in chronic metabolic acidosis than changes in TRPV5 activity (121).

TRPV5 activity is regulated by posttranslational modifications

The TRPV5 channel is subjected to different posttranslational modifications. Plasmin, a urokinase, stimulates TRPV5 phosphorylation at S144 (90). Thereby, the P_o of the

channel is decreased, inhibiting TRPV5-mediated Ca^{2+} reabsorption. Phosphorylation of S299 and S654 is stimulated by serine protease TK and PTH, delaying TRPV5 retrieval from the plasma membrane (89). PTH also stimulates the phosphorylation of TRPV5 T709, via the adenylyl cyclase-cAMP-protein kinase A pathway as described previously. Phosphorylation at this position increases the P_o of the channel (88).

As previously pointed out, TRPV5 is regulated posttranslationally via its N-glycan. The anti-aging protein klotho is a hormone that plays a key role in this type of TRPV5 regulation. In the kidney, klotho co-localizes with TRPV5 and calbindin-D_{28k} (91). Klotho is a single-pass transmembrane protein with the majority of amino acids located extracellularly. The extracellular part consists of two domains, KL1 and KL2, which shares homology to the family 1 glycosidases (122). Interestingly, two highly conserved residues essential for enzymatic activity and present in all glycosidases, are not conserved in klotho (122). The extracellular domain is cleaved by a disintegrin and metalloprotease (ADAM) 10 and 17, thereby enabling klotho to enter the pro-urine, a process that is stimulated by insulin (123). The secreted form of klotho increases the cell surface abundance of TRPV5. Since the N-glycan depleted $TRPV5^{N358Q}$ mutant does not respond to klotho stimulation, klotho is expected to function via the TRPV5 N-glycan (124). Initially, it was suggested that klotho has β-glucuronidase activity and acts through hydrolysis of glucuronic acids from the TRPV5 N-glycan (124). Later, Tohyama *et al*. detected that klotho-mediated β-glucuronidase activity is approximately 26 times lower than that of the original β-glucuronidase (125). This finding in combination with the fact that glucoronic acids are rarely present in N-glycans, makes it unlikely that klotho contains β-glucuronidase activity (126). Recently, Cha *et al.* proposed that klotho could cleave sialic acids from the TRPV5 N-glycan. Thereby galectins, specifically galectin-1, can bind and stabilize the tetrameric channel at the plasma membrane (106). Klotho does not regulate TRPV5 membrane expression in Chinese hamster ovarian (CHO) cells, which lack α2,6-sialyltransferase, a protein responsible for the synthesis of α2,6-linked glycosidic bonds between galactose and sialic acids. Cleavage of the sialic acids, results in exposure of a LacNAc region, consisting of a galactose and an *N*-acetylglucosamine. It is proposed that galectin-1 binds to this LacNAc region, preventing endocytosis, stabilizing the Ca^{2+} channel at the plasma membrane (106). The mutant CHO cell line depleted of the β1,6-*N*-acetylglucosamine branch and transfected with α2,6-sialyltransferase, is also not responsive to klotho (106).

tTG and shear stress also regulate TRPV5 dependent on the N-glycan of the channel. TRPV5 is inhibited by extracellular tTG treatment, as shown in Human embryonic kidney 293 (HEK293) cells over-expressing the channel (98). tTG is a Ca^{2+}-dependent protein that is responsible for the specific cross-linking of lysine and glutamine residues (127). It reduces the pore diameter of the channel in an N-glycan dependent manner. The exact mechanism and its dependence on the TRPV5 N-glycan has not been unraveled (98).

Shear force activates TRPV5 and TRPV6 channels, thereby increasing the intracellular Ca^{2+} concentration (99). The N-glycan-deficient TRPV5 mutant, however, shows reduced sensitivity to stimulation by fluid flow (99). The molecular mechanism underlying the glycosylation-dependent TRPV5 regulation via shear force has not been elucidated. Of note, various studies emphasize the importance of shear force, generated by fluid flow, and its influence on renal tubule proteins (128).

Purpose and line of this thesis

As outlined in the introduction, protein glycosylation is of significant importance for many regulatory processes in the cell. This is reflected by the large amount of proteins

subjected to different complex forms of glycosylation. TRPV5 is an example of a protein that is regulated via its N-glycan. Since it is essential that the channel is tightly controlled, the N-glycan-dependent regulation is likely to be strictly organized. As a result of the high complexity and the poor methods for proper glycan labeling, N-glycan-dependent TRPV5 regulation is not well understood. The general aim of this thesis was, therefore, to investigate the role of the N-glycan of TRPV5 in the physiological process of renal Ca^{2+}-reabsorption. **Chapter 2** describes a novel method for more specific *in vitro* glycan labeling via cycloadditions. Small changes in the chemical structure of the cyclooctyne greatly aid in the labeling specificity via SPAAC in HEK293 cells. Increasing the hydrophilicity of the cyclooctyne allows more specific TRPV5 detection via the sialic acids in its N-glycan. **Chapter 3** elucidates on the klotho-dependent TRPV5 stimulation. Klotho increases TRPV5 plasma membrane expression in a caveolae-independent manner, only in the presence of TRPV5 its N-glycan. Sialidase, on the other hand, stimulates TRPV5 membrane expression also in the absence of the TRPV5 N-glycan. TRPV5 plasma membrane stabilization after sialidase treatment is a result of reduced caveolae-mediated endocytosis. The importance of ß-galactosidase for TRPV5 membrane stabilization and thereby Ca^{2+} transport is outlined in **chapter 4**. β-galactosidase is present, as an active protein, in the pro-urine from where it apically can stimulates the expression of TRPV5 at the plasma membrane. A TRPV5 homology model, based on a previously published TRPV1 structure is presented in **chapter 5**. Using the homology model, a gating mechanism for TRPV5 has been characterized. TRPV5 is gated via a tryptophan (W)-gate, in combination with a glycine (G)-hinge. Mutations at the W-gate and the G-hinge have been designed and characterized, showing the importance of this system for TRPV5 regulation. Finally, the studies presented in this thesis are summarized and discussed in **chapter 6**.

I

References

1. Hart, G. W., and Copeland, R. J. (2010) Glycomics hits the big time. *Cell* **143**, 672-676
2. Bertozzi, C. R., and Sasisekharan, R. (2009) Glycomics
3. Gabius, H. J., Andre, S., Jimenez-Barbero, J., Romero, A., and Solis, D. (2011) From lectin structure to functional glycomics: principles of the sugar code. *Trends Biochem Sci* **36**, 298-313
4. Spiro, R. G. (2002) Protein glycosylation: nature, distribution, enzymatic formation, and disease implications of glycopeptide bonds. *Glycobiology* **12**, 43R-56R
5. Apweiler, R., Hermjakob, H., and Sharon, N. (1999) On the frequency of protein glycosylation, as deduced from analysis of the SWISS-PROT database. *Biochim. Biophys. Acta-Gen. Subj.* **1473**, 4-8
6. Jung, E., Veuthey, A. L., Gasteiger, E., and Bairoch, A. (2001) Annotation of glycoproteins in the SWISS-PROT database. *Proteomics* **1**, 262-268
7. Varki, A., Cummings, R. D., Esko, J. D., Freeze, H. H., Stanley, P., Bertozzi, C. R., Hart, G. W., and Etzler, M. E. (2009) Essentials of Glycobiology, 2nd edition. *Cold Spring Harbor (NY)*
8. Zielinska, D. F., Gnad, F., Wisniewski, J. R., and Mann, M. (2010) Precision mapping of an in vivo N-glycoproteome reveals rigid topological and sequence constraints. *Cell* **141**, 897-907
9. Ruddock, L. W., and Molinari, M. (2006) N-glycan processing in ER quality control. *J Cell Sci* **119**, 4373-4380
10. Helenius, A., and Aebi, M. (2004) Roles of N-linked glycans in the endoplasmic reticulum. *Annu Rev Biochem* **73**, 1019-1049
11. Petrescu, A. J., Milac, A. L., Petrescu, S. M., Dwek, R. A., and Wormald, M. R. (2004) Statistical analysis of the protein environment of N-glycosylation sites: implications for occupancy, structure, and folding. *Glycobiology* **14**, 103-114
12. Gabius, H. J., and Kayser, K. (2014) Introduction to glycopathology: the concept, the tools and the perspectives. *Diagn Pathol* **9**, 4
13. Lau, K. S., and Dennis, J. W. (2008) N-Glycans in cancer progression. *Glycobiology* **18**, 750-760
14. Rambaruth, N. D., and Dwek, M. V. (2011) Cell surface glycan-lectin interactions in tumor metastasis. *Acta Histochem* **113**, 591-600
15. Tanha, N., Troelsen, L., From Hermansen, M. L., Kjaer, L., Faurschou, M., Garred, P., and Jacobsen, S. (2014) MBL2 gene variants coding for mannose-binding lectin deficiency are associated with increased risk of nephritis in Danish patients with systemic lupus erythematosus. *Lupus* **23**, 1105-1111
16. Moreto, A., Farinas-Alvarez, C., Puente, M., Ocejo-Vinyals, J. G., Sanchez-Velasco, P., Horcajada, J. P., Batlle, A., Montes, C., Santos, F., Conde, E., and Farinas, M. C. (2014) Mannose-binding lectin gene variants and infections in patients receiving autologous stem cell transplantation. *Bmc Immunol* **15**
17. Dennis, J. W., Lau, K. S., Demetriou, M., and Nabi, I. R. (2009) Adaptive Regulation at the Cell Surface by N-Glycosylation. *Traffic* **10**, 1569-1578
18. Cooper, D. N. (2002) Galectinomics: finding themes in complexity. *Biochim Biophys Acta* **1572**, 209-231
19. Leffler, H., Carlsson, S., Hedlund, M., Qian, Y., and Poirier, F. (2004) Introduction to galectins. *Glycoconj J* **19**, 433-440
20. Viguier, M., Advedissian, T., Delacour, D., Poirier, F., and Deshayes, F. (2014) Galectins in epithelial functions. *Tissue Barriers* **2**, e29103
21. Rondanino, C., Poland, P. A., Kinlough, C. L., Li, H., Rbaibi, Y., Myerburg, M. M., Al-bataineh, M. M., Kashlan, O. B., Pastor-Soler, N. M., Hallows, K. R., Weisz, O. A., Apodaca, G., and Hughey, R. P. (2011) Galectin-7 modulates the length of the primary cilia and wound repair in polarized kidney epithelial cells. *Am J Physiol-Renal* **301**, 622-633
22. Hughes, R. C. (2002) Galectins in kidney development. *Glycoconjugate J* **19**, 621-629
23. Boons, G. J. (2010) Bioorthogonal chemical reporter methodology for visualization, isolation and analysis of glycoconjugates. *Carbohydr Chem* **36**, 152-167
24. (Retrieved 28 May 2014) International Union of Pure and Applied Chemistry (IUPAC).
25. Reusch, W. (1999) *Virtual Text of Organic Chemistry*
26. Lemieux, G. A., and Bertozzi, C. R. (1998) Chemoselective ligation reactions with proteins, oligosaccharides and cells. *Trends Biotechnol.* **16**, 506-513
27. Mahal, L. K., Yarema, K. J., and Bertozzi, C. R. (1997) Engineering chemical

reactivity on cell surfaces through oligosaccharide biosynthesis. *Science* **276**, 1125-1128
28. Zeng, Y., Ramya, T. N., Dirksen, A., Dawson, P. E., and Paulson, J. C. (2009) High-efficiency labeling of sialylated glycoproteins on living cells. *Nat Methods* **6**, 207-209
29. Nauman, D. A., and Bertozzi, C. R. (2001) Kinetic parameters for small-molecule drug delivery by covalent cell surface targeting. *Biochim. Biophys.***1568**, 147-154
30. Agarwal, P., van der Weijden, J., Sletten, E. M., Rabuka, D., and Bertozzi, C. R. (2013) A Pictet-Spengler ligation for protein chemical modification. *P Natl Acad Sci USA* **110**, 46-51
31. Saxon, E., and Bertozzi, C. R. (2000) Cell surface engineering by a modified Staudinger reaction. *Science* **287**, 2007-2010
32. Ning, X., Guo, J., Wolfert, M. A., and Boons, G. J. (2008) Visualizing metabolically labeled glycoconjugates of living cells by copper-free and fast huisgen cycloadditions. *Angew Chem Int Ed Engl* **47**, 2253-2255
33. Griffin, R. J. (1994) The medicinal chemistry of the azido group. *Prog Med Chem* **31**, 121-232
34. Debets, M. F., van der Doelen, C. W., Rutjes, F. P., and van Delft, F. L. (2010) Azide: a unique dipole for metal-free bioorthogonal ligations. *ChemBioChem* **11**, 1168-1184
35. Agard, N. J., and Bertozzi, C. R. (2009) Chemical approaches to perturb, profile, and perceive glycans. *Acc Chem Res* **42**, 788-797
36. Almaraz, R. T., Aich, U., Khanna, H. S., Tan, E., Bhattacharya, R., Shah, S., and Yarema, K. J. (2012) Metabolic oligosaccharide engineering with N-Acyl functionalized ManNAc analogs: Cytotoxicity, metabolic flux, and glycan-display considerations. *Biotechnol Bioeng* **109**, 992-1006
37. Prescher, J. A., Dube, D. H., and Bertozzi, C. R. (2004) Chemical remodelling of cell surfaces in living animals. *Nature* **430**, 873-877
38. Rostovtsev, V. V., Green, L. G., Fokin, V. V., and Sharpless, K. B. (2002) A stepwise huisgen cycloaddition process: copper(I)-catalyzed regioselective "ligation" of azides and terminal alkynes. *Angew Chem* **41**, 2596-2599
39. Torne, C. W., Christensen, C., and Meldal, M. (2002) Peptidotriazoles on solid phase: [1,2,3]-triazoles by regiospecific copper(I)-catalyzed 1,3-dipolar cycloadditions of terminal alkynes to azides. *J Org Chem* **67**, 3057-3064
40. Agard, N. J., Prescher, J. A., and Bertozzi, C. R. (2004) A strain-promoted [3 + 2] azide-alkyne cycloaddition for covalent modification of biomolecules in living systems. *J Am Chem Soc* **126**, 15046-15047
41. Hong, V., Steinmetz, N. F., Manchester, M., and Finn, M. G. (2010) Labeling Live Cells by Copper-Catalyzed Alkyne-Azide Click Chemistry. *Bioconj Chem* **21**, 1912-1916
42. del Amo, D. S., Wang, W., Jiang, H., Besanceney, C., Yan, A. C., Levy, M., Liu, Y., Marlow, F. L., and Wu, P. (2010) Biocompatible Copper(I) Catalysts for in Vivo Imaging of Glycans. *J Am Chem Soc* **132**, 16893-16899
43. Besanceney-Webler, C., Jiang, H., Zheng, T. Q., Feng, L., del Amo, D. S., Wang, W., Klivansky, L. M., Marlow, F. L., Liu, Y., and Wu, P. (2011) Increasing the Efficacy of Bioorthogonal Click Reactions for Bioconjugation: A Comparative Study. *Angew Chem* **50**, 8051-8056
44. Codelli, J. A., Baskin, J. M., Agard, N. J., and Bertozzi, C. R. (2008) Second-generation difluorinated cyclooctynes for copper-free click chemistry. *J Am Chem Soc* **130**, 11486-11493
45. Jewett, J. C., Sletten, E. M., and Bertozzi, C. R. (2010) Rapid Cu-free click chemistry with readily synthesized biarylazacyclooctynones. *J Am Chem Soc* **132**, 3688-3690
46. Debets, M. F., van Berkel, S. S., Schoffelen, S., Rutjes, F., van Hest, J. C. M., and van Delft, F. L. (2010) Aza-dibenzocyclooctynes for fast and efficient enzyme PEGylation via copper-free (3+2) cycloaddition. *Chemical Communications* **46**, 97-99
47. Dommerholt, J., Schmidt, S., Temming, R., Hendriks, L. J., Rutjes, F. P., van Hest, J. C., Lefeber, D. J., Friedl, P., and van Delft, F. L. (2010) Readily accessible bicyclononynes for bioorthogonal labeling and three-dimensional imaging of living cells. *Angew Chem* **49**, 9422-9425
48. Debets, M. F., van Berkel, S. S., Dommerholt, J., Dirks, A. T., Rutjes, F. P., and van Delft, F. L. (2011) Bioconjugation with strained alkenes and alkynes. *Acc Chem Res* **44**, 805-815
49. Baskin, J. M., Prescher, J. A., Laughlin, S. T., Agard, N. J., Chang, P. V., Miller, I.

A., Lo, A., Codelli, J. A., and Bertozzi, C. R. (2007) Copper-free click chemistry for dynamic in vivo imaging. *Proc Natl Acad Sci U S A* **104**, 16793-16797
50. Baskin, J. M., Dehnert, K. W., Laughlin, S. T., Amacher, S. L., and Bertozzi, C. R. (2010) Visualizing enveloping layer glycans during zebrafish early embryogenesis. *Proc Natl Acad Sci U S A* **107**, 10360-10365
51. Laughlin, S. T., Baskin, J. M., Amacher, S. L., and Bertozzi, C. R. (2008) In vivo imaging of membrane-associated glycans in developing zebrafish. *Science* **320**, 664-667
52. Chang, P. V., Prescher, J. A., Sletten, E. M., Baskin, J. M., Miller, I. A., Agard, N. J., Lo, A., and Bertozzi, C. R. (2010) Copper-free click chemistry in living animals. *Proc Natl Acad Sci U S A* **107**, 1821-1826
53. Borrmann, A., Milles, S., Plass, T., Dommerholt, J., Verkade, J. M. M., Wiessler, M., Schultz, C., van Hest, J. C. M., van Delft, F. L., and Lemke, E. A. (2012) Genetic Encoding of a Bicyclo[6.1.0]nonyne-Charged Amino Acid Enables Fast Cellular Protein Imaging by Metal-Free Ligation. *ChemBioChem* **13**, 2094-2099
54. Nikic, I., Plass, T., Schraidt, O., Szymanski, J., Briggs, J. A. G., Schultz, C., and Lemke, E. A. (2014) Minimal Tags for Rapid Dual-Color Live-Cell Labeling and Super-Resolution Microscopy. *Angew Chem* **53**, 2245-2249
55. Dimke, H., Hoenderop, J. G., and Bindels, R. J. (2011) Molecular basis of epithelial Ca^{2+} and Mg^{2+} transport: insights from the TRP channel family. *J Physiol* **589**, 1535-1542
56. de Groot, T., Bindels, R. J. M., and Hoenderop, J. G. J. (2008) TRPV5: an ingeniously controlled calcium channel. *Kidney Int* **74**, 1241-1246
57. Peng, J. B., Brown, E. M., and Hediger, M. A. (2001) Structural conservation of the genes encoding CaT1, CaT2, and related cation channels. *Genomics* **76**, 99-109
58. Berridge, M. J. (2012) Calcium signalling remodelling and disease. *Biochem Soc T* **40**, 297-309
59. van der Eerden, B. C. J., Hoenderop, J. G. J., de Vries, T. J., Schoenmaker, T., Buurman, C. J., Uitterlinden, A. G., Pols, H. A. P., Bindels, R. J. M., and van Leeuwen, J. P. T. M. (2005) The epithelial Ca^{2+} channel TRPV5 is essential for proper osteoclastic bone resorption. *P Natl Acad Sci USA* **102**, 17507-17512
60. Hoenderop, J. G., van der Kemp, A. W., Hartog, A., van de Graaf, S. F., van Os, C. H., Willems, P. H., and Bindels, R. J. (1999) Molecular identification of the apical Ca^{2+} channel in 1,25-dihydroxyvitamin D3-responsive epithelia. *J Biol Chem* **274**, 8375-8378
61. Hoenderop, J. G., van Leeuwen, J. P., van der Eerden, B. C., Kersten, F. F., van der Kemp, A. W., Merillat, A. M., Waarsing, J. H., Rossier, B. C., Vallon, V., Hummler, E., and Bindels, R. J. (2003) Renal Ca2+ wasting, hyperabsorption, and reduced bone thickness in mice lacking TRPV5. *J Clin Invest* **112**, 1906-1914
62. Felsenfeld, A., Rodriguez, M., and Levine, B. (2013) New insights in regulation of calcium homeostasis. *Curr Opin Nephrol Hypertens* **22**, 371-376
63. Hoorn, E. J., and Zietse, R. (2013) Disorders of calcium and magnesium balance: a physiology-based approach. *Pediatr Nephrol* **28**, 1195-1206
64. Dimke, H., Hoenderop, J. G., and Bindels, R. J. (2010) Hereditary tubular transport disorders: implications for renal handling of Ca^{2+} and Mg^{2+}. *Clin Sci (Lond)* **118**, 1-18
65. Friedman, P. A., and Gesek, F. A. (1995) Cellular calcium transport in renal epithelia: measurement, mechanisms, and regulation. *Physiol Rev* **75**, 429-471
66. Greger, R., Lang, F., and Oberleithner, H. (1978) Distal site of calcium reabsorption in the rat nephron. *Pflugers Arch* **374**, 153-157
67. Glaudemans, B., Knoers, N. V. A. M., Hoenderop, J. G. J., and Bindels, R. J. M. (2010) New molecular players facilitating Mg^{2+} reabsorption in the distal convoluted tubule. *Kidney Int* **77**, 17-22
68. Hoenderop, J. G. J., van Leeuwen, J. P. T. M., van der Eerden, B. C. J., Kersten, F. F. J., van der Kemp, A. W. C. M., Merillat, A. M., Waarsing, J. H., Rossier, B. C., Vallon, V., Hummler, E., and Bindels, R. J. M. (2003) Renal Ca^{2+} wasting, hyperabsorption, and reduced bone thickness in mice lacking TRPV5. *Journal of Clinical Investigation* **112**, 1906-1914
69. Loh, N. Y., Bentley, L., Dimke, H., Verkaart, S., Tammaro, P., Gorvin, C. M., Stechman, M. J., Ahmad, B. N., Hannan, F. M., Piret, S. E., Evans, H., Bellantuono, I., Hough, T. A., Fraser, W. D., Hoenderop, J. G. J., Ashcroft, F. M., Brown, S. D. M., Bindels, R. J. M., Cox, R. D., and Thakker, R. V. (2013) Autosomal Dominant Hypercalciuria in a Mouse Model Due to a Mutation of the Epithelial Calcium Channel, TRPV5. *Plos One* **8**
70. Sooy, K., Kohut, J., and Christakos, S. (2000) The role of calbindin and

1,25dihydroxyvitamin D3 in the kidney. *Curr Opin Nephrol Hypertens* **9**, 341-347
71. Schwaller, B. (2009) The continuing disappearance of "pure" Ca^{2+} buffers. *Cell Mol Life Sci* **66**, 275-300
72. Ko, S. H., Choi, K. C., Oh, G. T., and Jeung, E. B. (2009) Effect of dietary calcium and 1,25-(OH)2D3 on the expression of calcium transport genes in calbindin-D9k and -D28k double knockout mice. *Biochem Biophys Res Commun* **379**, 227-232
73. Hwang, I., Hong, E. J., Yang, H., Kang, H. S., Ahn, C., An, B. S., and Jeung, E. B. (2014) Regulation of tight junction gene expression in the kidney of calbindin-D9k and/or-D28k knockout mice after consumption of a calcium- or a calcium/vitamin D-deficient diet. *Bmc Biochem* **15**
74. Bonny, O., Stoudmann, C., Zavadova, V., Hilgemann, D. W., and Moe, O. W. (2013) Mice with Kidney-Specific Deletion of the Sodium/Calcium Exchanger 1 Have Increased Intestinal Calcium Absorption. *Journal of the American Society of Nephrology* **24**
75. Okunande, G. W., Miller, M. L., Pyne, G. J., Sutliff, R. L., O'Connor, K. T., Neumann, J. C., Andringa, A., Miller, D. A., Prasad, V., Doetschman, T., Paul, R. J., and Shull, G. E. (2004) Targeted ablation of plasma membrane Ca^{2+}-ATPase (PMCA) 1 and 4 indicates a major housekeeping function for PMCA1 and a critical role in hyperactivated sperm motility and male fertility for PMCA4. *Journal of Biological Chemistry* **279**, 33742-33750
76. Weber, K., Erben, R. G., Rump, A., and Adamski, J. (2001) Gene structure and regulation of the murine epithelial calcium channels ECaC1 and 2. *Biochem Bioph Res Co* **289**, 1287-1294
77. Nilius, B., Vennekens, R., Prenen, J., Hoenderop, J. G. J., Droogmans, G., and Bindels, R. J. M. (2001) The single pore residue Asp(542) determines Ca2+ permeation and Mg2+ block of the epithelial Ca^{2+} channel. *J Bioll Chem* **276**, 1020-1025
78. Chang, Q., Gyftogianni, E., van de Graaf, S. F. J., Hoefs, S., Weidema, F. A., Bindels, R. J. M., and Hoenderop, J. G. J. (2004) Molecular determinants in TRPV5 channel assembly. *J Biol Chem* **279**, 54304-54311
79. van de Graaf, S. F. J., Bindels, R. J. M., and Hoenderop, J. G. J. (2007) Physiology of epithelial Ca2+ and Mg2+ transport. *Rev Physiol Bioch P* **158**, 77-160
80. Liao, M. F., Cao, E. H., Julius, D., and Cheng, Y. F. (2013) Structure of the TRPV1 ion channel determined by electron cryo-microscopy. *Nature* **504**, 107-112
81. de Groot, T., Verkaart, S., Xi, Q., Bindels, R. J. M., and Hoenderop, J. G. J. 2010) The Identification of Histidine 712 as a Critical Residue for Constitutive TRPV5 Internalization. *Journal of Biological Chemistry* **285**, 28481-28487
82. Erler, I., Hirnet, D., Wissenbach, U., Flockerzi, V., and Niemeyer, B. A. (2004) Ca2+-selective transient receptor potential V channel architecture and function require a specific ankyrin repeat. *Journal of Biological Chemistry* **279**, 34456-34463
83. Phelps, C. B., Huang, R. J., Lishko, P. V., Wang, R. R., and Gaudet, R. (2008) Structural analyses of the ankyrin repeat domain of TRPV6 and related TRPV ion channels. *Biochemistry-Us* **47**, 2476-2484
84. Van de Graaf, S. F. J., Hoenderop, J. G. J., Gkika, D., Lamers, D., Prenen, J., Rescher, U., Gerke, V., Staub, O., Nilius, B., and Bindels, R. J. M. (2003) Functional expression of the epithelial Ca^{2+} channels (TRPV5 and TRPV6) requires association of the S100A10-annexin 2 complex. *Embo Journal* **22**, 1478-1487
85. van de Graaf, S. F. J., Chang, Q., Mensenkamp, A. R., Hoenderop, J. G. J., and Bindels, R. J. M. (2006) Direct interaction with Rab11a targets the epithelial Ca2+ channels TRPV5 and TRPV6 to the plasma membrane. *Mol Cell Biol* **26**, 303-312
86. Gkika, D., Mahieu, F., Nilius, B., Hoenderop, J. G. J., and Bindels, R. J. M. (2004) 80K-H as a new Ca^{2+} sensor regulating the activity of the epithelial Ca2+ channel transient receptor potential cation channel V5 (TRPV5). *J Biol Chem* **279**, 26351-26357
87. Embark, H. M., Setiawan, W., Poppendieck, S., van de Graaf, S. F. J., Boehmer, C., Palmada, M., Wieder, T., Gerstberger, R., Cohen, P., Yun, C. C., Bindels, R. J. M., and Lang, F. (2004) Regulation of the epithelial Ca^{2+} channel TRPV5 by the NHE regulating factor NHERF2 and the serum and glucocorticoid inducible kinase Isoforms SGK1 and SGK3 expressed in Xenopus oocytes. *Cell Physiol Biochem* **14**, 203-212
88. de Groot, T., Lee, K., Langeslag, M., Xi, Q., Jalink, K., Bindels, R. J. M., and Hoenderop, J. G. J. (2009) Parathyroid Hormone Activates TRPV5 via PKA-Dependent Phosphorylation. *J Am Soc Nephrol* **20**, 1693-1704
89. Gkika, D., Topala, C. N., Chang, Q., Picard, N., Thebault, S., Houillier, P., Hoenderop, J. G., and Bindels, R. J. (2006) Tissue kallikrein stimulates Ca^{2+} reabsorption via PKC-dependent plasma membrane accumulation of TRPV5. *EMBO J* **25**, 4707-4716

90. Tudpor, K., Lainez, S., Kwakernaak, A. J., Kovalevskaya, N. V., Verkaart, S., van Genesen, S., van der Kemp, A., Navis, G., Bindels, R. J., and Hoenderop, J. G. (2012) Urinary plasmin inhibits TRPV5 in nephrotic-range proteinuria. *J Am Soc Nephrol* **23**, 1824-1834
91. Chang, Q., Hoefs, S., van der Kemp, A. W., Topala, C. N., Bindels, R. J., and Hoenderop, J. G. (2005) The beta-glucuronidase klotho hydrolyzes and activates the TRPV5 channel. *Science* **310**, 490-493
92. Bergwitz, C., and Juppner, H. (2010) Regulation of Phosphate Homeostasis by PTH, Vitamin D, and FGF23. *Annu Rev Med* **61**, 91-104
93. Hoenderop, J. G. J., van der Kemp, A. W. C. M., Urben, C. M., Strugnell, S. A., and Bindels, R. J. M. (2004) Effects of vitamin D compounds on renal and intestinal Ca^{2+} transport proteins in 25-hydroxyvitamin D-3-1 alpha-hydroxylase knockout mice. *Kidney Int* **66**, 1082-1089
94. Jones, G., Strugnell, S. A., and DeLuca, H. F. (1998) Current understanding of the molecular actions of vitamin D. *Physiological Reviews* **78**, 1193-1231
95. Nilius, B., Prenen, J., Vennekens, R., Hoenderop, J. G., Bindels, R. J., and Droogmans, G. (2001) Modulation of the epithelial calcium channel, ECaC, by intracellular Ca^{2+}. *Cell Calcium* **29**, 417-428
96. Nilius, B., Weidema, F., Prenen, J., Hoenderop, J. G., Vennekens, R., Hoefs, S., Droogmans, G., and Bindels, R. J. (2003) The carboxyl terminus of the epithelial Ca(2+) channel ECaC1 is involved in Ca^{2+}-dependent inactivation. *Pflugers Arch* **445**, 584-588
97. de Groot, T., Kovalevskaya, N. V., Verkaart, S., Schilderink, N., Felici, M., van der Hagen, E. A. E., Bindels, R. J. M., Vuister, G. W., and Hoenderop, J. G. (2011) Molecular Mechanisms of Calmodulin Action on TRPV5 and Modulation by Parathyroid Hormone. *Mol Cell Biol* **31**, 2845-2853
98. Boros, S., Xi, Q., Dimke, H., van der Kemp, A. W., Tudpor, K., Verkaart, S., Lee, K. P., Bindels, R. J., and Hoenderop, J. G. (2012) Tissue transglutaminase inhibits the TRPV5-dependent calcium transport in an N-glycosylation-dependent manner. *Cell Mol Life Sci* **69**, 981-992
99. Cha, S. K., Kim, J. H., and Huang, C. L. (2013) Flow-induced activation of TRPV5 and TRPV6 channels stimulates Ca(2+)-activated K(+) channel causing membrane hyperpolarization. *Biochim Biophys Acta* **1833**, 3046-3053
100. Yeh, B. I., Kim, Y. K., Jabbar, W., and Huang, C. L. (2005) Conformational changes of pore helix coupled to gating of TRPV5 by protons. *Embo Journal* **24**, 3224-3234
101. Palmada, M., Poppendieck, S., Embark, H. M., van de Graaf, S. F., Boehmer, C., Bindels, R. J., and Lang, F. (2005) Requirement of PDZ domains for the stimulation of the epithelial Ca2+ channel TRPV5 by the NHE regulating factor NHERF2 and the serum and glucocorticoid inducible kinase SGK1. *Cell Physiol Biochem* **15**, 175-182
102. Cha, S. K., and Huang, C. L. (2010) WNK4 kinase stimulates caveola-mediated endocytosis of TRPV5 amplifying the dynamic range of regulation of the channel by protein kinase C. *J Biol Chem* **285**, 6604-6611
103. Jing, H., Na, T., Zhang, W., Wu, G., Liu, C., and Peng, J. B. (2011) Concerted actions of NHERF2 and WNK4 in regulating TRPV5. *Biochem Biophys Res Commun* **404**, 979-984
104. Lambers, T. T., Oancea, E., de Groot, T., Topala, C. N., Hoenderop, J. G., and Bindels, R. J. (2007) Extracellular pH dynamically controls cell surface delivery of functional TRPV5 channels. *Mol Cell Biol* **27**, 1486-1494
105. Wolf, M. T., Wu, X. R., and Huang, C. L. (2013) Uromodulin upregulates TRPV5 by impairing caveolin-mediated endocytosis. *Kidney Int* **84**, 130-137
106. Cha, S. K., Ortega, B., Kurosu, H., Rosenblatt, K. P., Kuro-O, M., and Huang, C. L. (2008) Removal of sialic acid involving Klotho causes cell-surface retention of TRPV5 channel via binding to galectin-1. *P Natl Acad Sci USA* **105**, 9805-9810
107. Chin, D., and Means, A. R. (2000) Calmodulin: a prototypical calcium sensor. *Trends Cell Biol* **10**, 322-328
108. Voets, T., Janssens, A., Prenen, J., Droogmans, G., and Nilius, B. (2003) Mg^{2+}-dependent gating and strong inward rectification of the cation channel TRPV6. *Journal of General Physiology* **121**, 245-260
109. Lee, J., Cha, S. K., Sun, T. J., and Huang, C. L. (2005) PIP2 activates TRPV5 and releases its inhibition by intracellular Mg^{2+}. *J Gen Physiol* **126**, 439-451
110. Brown, E. M., Gamba, G., Riccardi, D., Lombardi, M., Butters, R., Kifor, O., Sun, A., Hediger, M. A., Lytton, J., and Hebert, S. C. (1993) Cloning and Characterization of an Extracellular Ca2+-Sensing Receptor from Bovine Parathyroid. *Nature* **366**, 575-580
111. Chen, R. A., and Goodman, W. G. (2004) Role of the calcium-sensing receptor in parathyroid gland physiology. *Am J Physiol-Renal* **286**, F1005-F1011

112. Houillier, P. (2013) Calcium-sensing in the kidney. *Curr Opin Nephrol Hypertens* **22**, 566-571
113. van Abel, M., Hoenderop, J. G. J., van der Kemp, A. W. C. M., Friedlaender, M. M., van Leeuwen, J. P. T. M., and Bindels, R. J. M. (2005) Coordinated control of renal Ca2+ transport proteins by parathyroid hormone. *Kidney Int* **68**, 1708-1721
114. Martin, A., David, V., and Quarles, L. D. (2012) Regulation and Function of the Fgf23/Klotho Endocrine Pathways. *Physiological Reviews* **92**, 131-155
115. Andrukhova, O., Smorodchenko, A., Egerbacher, M., Streicher, C., Zeitz, U., Goetz, R., Shalhoub, V., Mohammadi, M., Pohl, E. E., Lanske, B., and Erben, R. G. (2014) FGF23 promotes renal calcium reabsorption through the TRPV5 channel. *EMBO J*
116. Cha, S. K., Wu, T., and Huang, C. L. (2008) Protein kinase C inhibits caveolae-mediated endocytosis of TRPV5. *Am J Physiol-Renal* **294**, F1212-F1221
117. Nijenhuis, T., Renkema, K. Y., Hoenderop, J. G., and Bindels, R. J. (2006) Acid-base status determines the renal expression of Ca2+ and Mg2+ transport proteins. *J Am Soc Nephrol* **17**, 617-626
118. Yeh, B. I., Yoon, J., and Huang, C. L. (2006) On the role of pore helix in regulation of TRPV5 by extracellular protons. *J Membr Biol* **212**, 191-198
119. Yeh, B. I., Sun, T. J., Lee, J. Z., Chen, H. H., and Huang, C. L. (2003) Mechanism and molecular determinant for regulation of rabbit transient receptor potential type 5 (TRPV5) channel by extracellular pH. *J Biol Chem* **278**, 51044-51052
120. Cha, S. K., Jabbar, W., Xie, J., and Huang, C. L. (2007) Regulation of TRPV5 single-channel activity by intracellular pH. *J Membr Biol* **220**, 79-85
121. Bonny, O., and Edwards, A. (2013) Calcium reabsorption in the distal tubule: regulation by sodium, pH, and flow. *Am J Physiol Renal Physiol* **304**, F585-600
122. Ito, S., Fujimori, T., Hayashizaki, Y., and Nabeshima, Y. (2002) Identification of a novel mouse membrane-bound family 1 glycosidase-like protein, which carries an atypical active site structure. *Biochim Biophys Acta* **1576**, 341-345
123. Chen, C. D., Podvin, S., Gillespie, E., Leeman, S. E., and Abraham, C. R. (2007) Insulin stimulates the cleavage and release of the extracellular domain of Klotho by ADAM10 and ADAM 17. *P Natl Acad Sci USA* **104**, 19796-19801
124. Chang, Q., Hoefs, S., van der Kemp, A. W., Topala, C. N., Bindels, R. J., and Hoenderop, J. G. (2005) The beta-glucuronidase klotho hydrolyzes and activates the TRPV5 channel. *Science* **310**, 490-493
125. Tohyama, O., Imura, A., Iwano, A., Freund, J. N., Henrissat, B., Fujimori, T., and Nabeshima, Y. (2004) Klotho is a novel beta-glucuronidase capable of hydrolyzing steroid beta-glucuronides. *J Biol Chem* **279**, 9777-9784
126. Huang, C. L. (2010) Regulation of ion channels by secreted Klotho: mechanisms and implications. *Kidney Int* **77**, 855-860
127. Griffin, M., Casadio, R., and Bergamini, C. M. (2002) Transglutaminases: Nature's biological glues. *Biochem J* **368**, 377-396
128. Weinbaum, S., Duan, Y., Satlin, L. M., Wang, T., and Weinstein, A. M. (2010) Mechanotransduction in the renal tubule. *Am J Physiol-Renal* **299**, F1220-F1236

II

CHAPTER 2

Copper-free click reactions with polar bicyclononyne derivatives for modulation of cellular imaging

Elizabeth H.P. Leunissen[1,3], Mandy H.L. Meuleners[1,3], Jorge M.M. Verkade[2], Jan Dommerholt[3], Joost G.J. Hoenderop[1], Floris L. van Delft [2,3]

[1]Department of Physiology, Radboud university medical center, Radboud Institute for Molecular Life Sciences, Nijmegen, The Netherlands
[2]SynAffix B.V., Molenstraat 110, 5342 CC Oss, The Netherlands
[3]Synthetic Organic Chemistry, Institute for Molecules and Materials, Radboud University Nijmegen, The Netherlands

ChemBioChem 15(10):1446-1451, 2014

Abstract

The ability of cells to incorporate azidosugars metabolically is a useful tool for extracellular glycan labelling. The exposed azide moiety can covalently react with alkynes, such as bicyclo[6.1.0]nonyne (BCN), by strain-promoted alkyne-azide cycloaddition (SPAAC). However, the use of SPAAC can be hampered by low specificity of the cycloalkyne. In this article we describe the synthesis of more polar BCN derivatives and their properties for selective cellular glycan labelling. The new polar derivatives [amino-BCN, glutarylamino-BCN and bis(hydroxymethyl)-BCN] display reaction rates similar to those of BCN and are less cell-permeable. The labelling specificity in HEK293 cells is greater than that of BCN, as determined by confocal microscopy and flow cytometry. Interestingly, amino-BCN appears to be highly specific for the Golgi apparatus. In addition, the polar BCN derivatives label the N-glycan of the membrane calcium channel TRPV5 in HEK293 cells with significantly enhanced signal-to-noise ratios.

Introduction

Glycosylation is the most abundant form of post-translational protein modification in nature, with a wide range of functional implications. Whereas intracellular glycosylation contributes to signalling, dimer formation, membrane trafficking and polarised sorting of glycoproteins (1,2), extracellular glycans of plasma membrane proteins are involved in additional signalling processes, apoptosis and cell-cell contacts. The composition of extracellular glycans is strictly regulated by the activity of extracellular glycosidases,(3,4) which have important implications for the properties of membrane glycoproteins. Membrane stabilisation of the epithelial calcium channel, known as transient receptor potential vanilloid type 5 (TRPV5), for example, is closely associated with the composition of its N-glycan (5). Klotho, a hormone expressed in the pro-urine, can regulate TRPV5 channel activity through modification of the extracellular TRPV5 N-glycan (6,7).

Increasing interest in the biological role of cell-surface glycans has enhanced the development of new tools for selective labelling of extracellular glycoproteins. In particular, bioorthogonal reactions have numerous applications for in vitro glycan labelling.(8-10). This was first demonstrated in 2000 in a Staudinger reaction between an azide and a phosphine, two abiotic functional groups that are mutually reactive, but inert toward native biomolecular functionality (11). Despite its promises, the utility of the Staudinger ligation is compromised by the oxygen-sensitivity of the requisite phosphine reagents and the slow reaction rates (12). In the past decade, the 1,3-dipolar cycloaddition of an azide with a terminal acetylene in the presence of copper(I) (13,14), typically referred to as a “click” reaction, has been shown to react *in vitro* with increased reaction rates. However, extensive optimisation of reaction conditions might be necessary, to reduce concomitant oxidative damage to biomolecular structures and copper(I) toxicity, and this limits its application in living systems (15). In 2004, metal-free cycloaddition between cyclooctynes and azides, the so-called strain-promoted alkyne-azide cycloaddition (SPAAC), was first applied as a tool for bioconjugation (16). Because initial reaction rates were relatively low, a vast number of cyclooctyne derivatives with increased reaction rates were developed in subsequent years; these include dimethoxyazacyclooctyne (DIMAC) (18), difluorocyclooctyne (DIFO) (19,20) and bisarylazacyclooctynone (BARAC) (21).

Currently, the most frequently used, cyclooctynes that are commercially available are dibenzocyclooctynol (DIBO) (22,23), dibenzoazacyclooctyne (DIBAC / DBCO) (23,24) and bicyclo[6.1.0]nonyne (BCN)(25) (Fig 1). These three cyclooctynes display moderate to high reactivity in 1,3-dipolar cycloadditions, not only with azides, but also with nitrones (26,27), nitrile oxides (28,29) and diazo compounds (29). Most recently, it was found that BCN –unlike the dibenzofused cyclooctynes DIBO and DBCO– undergoes (4+2) cycloaddition with diphenyltetrazine at reaction rates at least 1000 times faster than with the azide (30). For example, genetic encoding of BCN into green fluorescent protein (GFP), followed by reaction with tetrazine proved to be highly efficient (31,32).

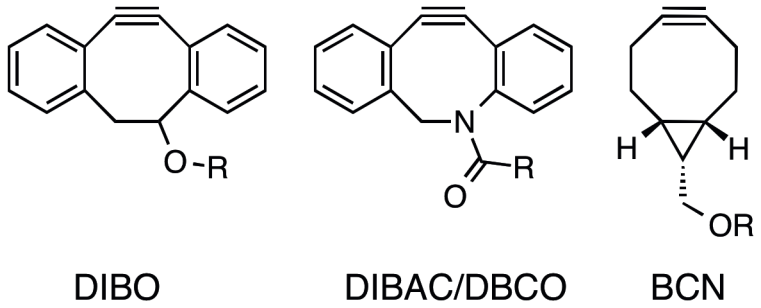

Figure 1. Structures of the most commonly used cyclooctynes.

Lipophilicity is a prime consideration in the selection of a particular cyclooctyne for bioconjugation or *in vitro* labelling. Under physiological conditions, hydrophobic interactions or thiol-yne additions (17,33) can give rise to unspecific signals and compromise studies of live cell endocytosis and protein mobility. To avoid this, Bertozzi *et al.* developed a highly polar cyclooctyne (DIMAC) from a carbohydrate precursor, but the lengthy synthesis and attenuated reactivity have hampered its broad application (18). The benzoannulated cyclooctynes (DIBO, DBCO, BARAC and others) show improved reactivity, but at the expense of increased size and lipophilicity. To overcome this, a more hydrophilic, sulfonylated variant of DIBO was synthesised and shown to exhibit reduced unspecific staining in human skin fibroblast (34). Leeper *et al.* synthesised a more hydrophilic DIBO variant through the introduction of four methoxy substituents (TMDIBO); it displayed increased reaction specificity in Lewis lung carcinoma cells (35).

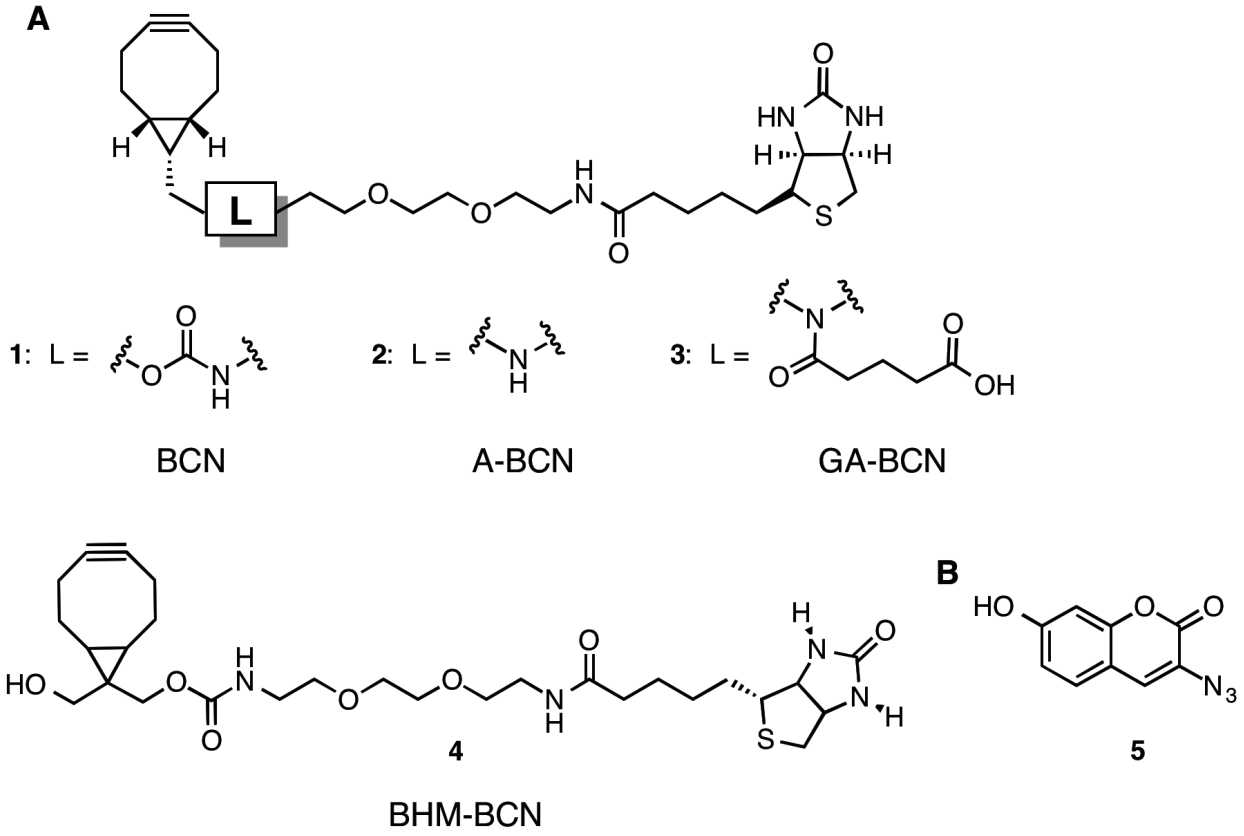

Figure 2. Structures of the synthesized derivatives.

A) Structure of BCN-biotin (**1**) and the newly developed hydrophilic BCN probes **2**-**4**, conjugated to biotin. **B)** fluorogenic azidocoumarin (**5**).

We reasoned that BCN, the only non-benzoannulated cyclooctynes with practical reactivity and straightforward synthetic accessibility, would form a logical starting point for the development of a more polar, potentially water-soluble cyclooctyne.

Here we report a new set of BCN-derived structures (Fig 2A) with enhanced hydrophilicity, retained reactivity and high labelling specificity. Three BCN variants were developed: amino-BCN (A-BCN, **2**), glutarylamino-BCN (GA-BCN, **3**) and bis(hydroxymethyl)-BCN (BHM-BCN, **4**). In each of these variants a biotin moiety was attached as a functional group to enable cellular and biochemical imaging. The polarities of the BCN probes strongly influence membrane permeability and reaction specificity in HEK293 cells, thereby leading to significantly improved signal-to-noise ratios (SNRs). In particular, the A-BCN derivative **2** was found to display selectivity in Golgi staining, thereby offering considerable promise for the study of glycan-controlled protein trafficking.

Experimental procedures

Reaction kinetics

1 equiv of **5** (0.5 mM) was added to 2 equiv of (1*R*,8*S*,9*s*)-bicyclo [6.1.0]non-4-yn-9-ylmethanol, **1**, **2**, **3** or **4** (1 mM) in MeCN:H_2O 1:2. After 1, 2, 4, 8, 15, 30 and 45 min 10 µl was taken and diluted 400 times in MeCN:H_2O 1:2. Fluorescence was measured (ex: 395 nm, em: 460 nm) on a LS55 Perkin Elmer fluorescence spectrometer.

Fluorescence confocal microscopy.

HEK293 cells were plated on 12 mm glass coverslips coated with 50 µg/ml fibronectin (Roche Diagnostics, Mannheim, Germany). Next, they were treated for 48 h with 60 µM Ac_4ManNAz, or left untreated. The cells were washed once with with ice-cold PBS (pH 8.0, adjusted with NaOH) containing 1 mM $MgCl_2$ and 0.5 mM $CaCl_2$ (PBSB) and treated with 60 µM **1**, **2**, **3** or **4** in PBSB for 1 h at RT. After incubation, the cells were washed three times with PBSB and fixed with 1% (w/v) paraformaldehyde (Sigma-Aldrich, St. Louis, MO, USA) in PBS for 5 min. Afterwards, the cells were washed twice with PBS and permeabilised for 10 min using 0.3% (v/v) Triton X-100, 0.1% (w/v) Bovine Serum Albumin (BSA) (Sigma life Science, St. Louis, MO, USA) in PBS. Finally, the cells were incubated with 50 mM NH_4Cl (Merck, Boom B.V. Meppel, Darmstadt, Germany) in PBS for 15 min and washed with PBS. After incubation for 30 min at RT with goat serum dilution buffer (GSDB; 16% goat serum, 0.3% (v/v) triton X-100 and 0.3 M NaCl in PBS), the cells were incubated overnight with a Golgi 58K antibody (Sigma, Saint Louis, Missouri, USA)(1:800) at 4 °C in GSDB. The cells were then washed with PBSB and incubated with a combination of streptavidin-Alexa Fluor 488 (Invitrogen, Eugene, OR, USA) (1:200) and Alexa Fluor 647 conjugated to goat anti-mouse IgG (Invitrogen, Eugene, OR, USA) (1:2000) in PBSB for 1 h. The cells were washed twice with PBS and stained with 4',6-diamidino-2-phenylindole (DAPI, Roche Diagnostics, Mannheim, Germany) in PBSB for 10 min. After three wash steps with PBSB, the coverslips were attached to a glass microscope slide with polyvinyl alcohol (Mowiol; Hoechst, Frankfurt, Germany). Cells were imaged using an Olympus FV1000 Confocal laser scanning microscope with the 488 nm argon laser, the 405 nm and the 635 nm diode lasers. Images were acquired using Olympus FluoView software.

FACS analysis.

HEK293 cells were incubated for 48 h with or without 60 µM Ac_4ManNAz. Next, cells were detached using 0.02% EDTA (Merck, Darmstadt, Germany) in PBS. After centrifugation

(1250 rpm, 4 min), the cells were washed twice with PBS and plated on a 96-well cell culture plate. The cells were resuspended and incubated with 60 µM of **1**, **2**, **3** or **4** in PBS for 1 h at 4, 20 or 37 °C. After centrifugation and three wash steps with PBS, the cells were incubated for 30 min at 4°C in streptavidin-Alexa Fluor 488 (Invitrogen, Eugene, OR, USA) (1:200) in PBS. Finally, the cells were washed twice with PBS and once with PBS enriched with 0.5% (w/v) BSA and suspended in a total volume of 400 µl PBS. Just prior to analysis, 2.5 µg/ml propidium iodide (MACS, Miltenyi Biotec Inc. Auburn, CA, USA) was added to the cells. The cells were analyzed by flow cytometry using FACSCalibur (Becton Dickinson BD Biosciences, California, USA) with BD CellQuest™ Pro software. Images were acquired using FCS Express 4 Plus research edition (De Novo software).

DNA constructs

The pCINeo/IRES-GFP plasmid encoding TRPV5 was generated as described previously (36). All constructs were verified by DNA sequence analysis. HEK293 cells were transiently transfected with the relevant DNA constructs using Lipofectamine TM2000 (Invitrogen, Carlsbad, CA, USA), following the manufacturer's instructions.

Immunoblotting

TRPV5 protein expression was determined with 8 % (w/v) SDS-PAGE and Western-blotting, using anti-HA (6E2) (Cell Signalling Technology, Danvers, MA, USA)(1:5000), and peroxidase-labeled goat anti-mouse IgG (1:10.000, Sigma-Aldrich, St. Louis, MO, USA) antibodies.

Plasma membrane biotinylation

HEK293 cells were transiently transfected with TRPV5 in pCINeo/IRES-GFP or the empty pCINeo/IRES-GFP vector (mock) and cultured for 2 days in the presence or absence of 60 µM Ac_4ManNAz. Next, cells were washed twice with ice-cold PBSB and biotinylated via treatment with 60 µM of **1, 2** or **3** in PBSB for 1 h at RT. The cells were then washed three times with ice-cold PBSB and disrupted in 1 ml lysis buffer [1 % (v/v) NP-40, 150 mM NaCl, 5 mM EDTA, 50 mM Tris (pH 7.5 adjusted with HCl), 1 mM PMSF, 10 µg/ml leupeptin, 10 µg/ml pepstatin, 5 µg/ml proteinase A]. TRPV5 protein expression containing the azido-glycan and in total cell lysate was investigated as described previously (5).

Reversed-Phase HPLC

RP-HPLC, on a C18 150 mm long column (prodigy ODS-3 C18, Phenomenex, Torrance, CA, USA), used 50 mM phosphate buffer adjusted to pH 7.4 as mobile phase A and MeCN as mobile phase B, at 1 ml/min. A run of 50 min with 95% mobile phase A up to 80% of phase B over 30 min, was used to detect the retention time of the compounds. The compounds were detected using the 214 nm detector. The RP-HPLC was performed on a Shimadzu LC-20A Prominence system (Shimadzu, 's-Hertogenbosch, The Netherlands).

Synthesis

(1*R*,8*S*,9*s*)-bicyclo [6.1.0]non-4-yne-9-carbaldehyde (6)

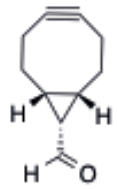

To (1*R*,8*S*,9*s*)-bicyclo [6.1.0]non-4-yn-9-ylmethanol (0.499 g; 3.32 mmol; 1.0 equiv.) dissolved in DCM (330 ml) was added Dess-Martin periodinane (2.10 g; 4.95 mmol; 1.5 equiv.). The reaction mixture was stirred for 2 h at RT. The complete reaction mixture was filtered over celite and immediately used for further synthesis.

***N*-(2-(2-(2-aminoethoxy)ethoxy)ethyl)-5-((3*aS*,4*S*,6*aR*)-2- oxohexahydro-1H-thiono[3,4-*d*]imidazol-4-yl)pentanamide *(Biotin-amine)* (7)**

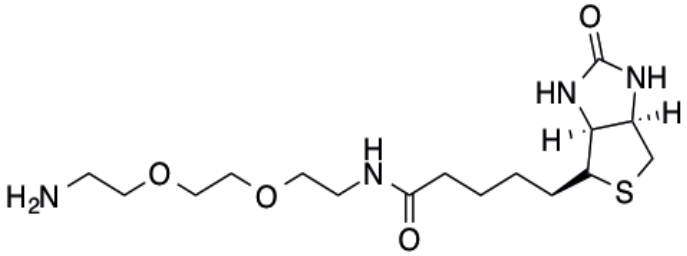

To 2,2'-(ethane-1,2-diylbis(oxy)) diethanamine (4.55 ml; 30.7 mmol; 3.0 equiv.) dissolved in DMF (700 ml) was added dropwise a solution of biotin-OSu (3.5 g, 10.3 mmol; 1.0 equiv.) in DMF (700 ml). The reaction mixture was stirred overnight at RT. The solvent was removed *in vacuo* and the crude product was purified by silica column chromatography with 7N ammonia in MeOH: MeOH: DCM / 2:13:85 as the eluent to give the title compound as a white solid. Yield 2.66 g (69%), R_f 0.40 (7N ammonia in MeOH: DCM / 1:4).

^{1}H NMR (DMSO-d_6, 300 MHz): 7.84 (m, 1H), 6.42 (s, 1H), 6.35 (s, 1H), 4.33–4.29 (m, 1H), 4.15–4.11 (m, 1H), 3.51 (s, 4H), 3.38 (q, *J* = 6.0 Hz, 4H), 3.18 (q, *J* = 6.0 Hz, 3H), 3.11–3.07 (m, 1H), 2.79, 2.83 (2 × d, *J* = 6.0 Hz, 1H), 2.67 (t, *J* = 5.7 Hz, 2H), 2.06 (t, *J* = 7.2 Hz, 2H), 1.68–1.37 (m, 4H), 1.37–1.24 (m, 2H). ^{13}C NMR (DMSO-d_6, 75 MHz): 172.1, 162.7, 72.5, 69.5 (2C), 69.1, 61.0, 59.2, 55.4, 41.1, 40.3, 40.1, 35.1, 28.2, 28.0, 25.2. IR (cm^{-1}): 3278, 2924, 2855, 1692, 1645, 1260, 1113, 698, 594. [ESI-MS]: calculated for $C_{16}H_{30}N_4O_4S$, 374.20, found: (M+H$^+$) 375.21 and (M+Na$^+$) 397.19.

***N*-(2-(2-(2-(((1*R*,8*S*,9*s*)-bicyclo[6.1.0]non-4-yn-9-ylmethyl)amino)ethoxy) ethoxy)ethyl)-5-((3*aR*,4*R*,6*aS*)-2-oxohexahydro-1H-thieno[3,4-*d*]imidazol-4-yl) pentanamide (A-BCN) (2)**

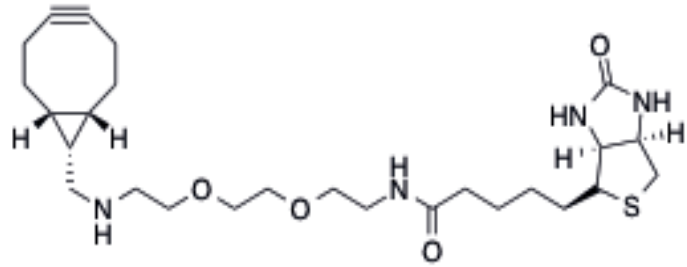

Biotin-amine (**7**) (1.25 g; 3.32 mmol; 1.0 equiv.) and sodium cyanoborohydride (0.775 g; 3.66 mmol; 1.1 equiv.) were dissolved in DCM (15 ml). **6** (0.493 g; 3.33 mmol; 1.0 equiv.) dissolved in DCM (330 ml) was added dropwise. 0.1 M aqueous sodium hydroxide solution (300 ml) was added to the reaction mixture. The aqueous layer was extracted with DCM (3 × 100 ml). The combined organic washings were dried (Na_2SO_4), and the solvent was removed *in vacuo*. The residue was purified by silica column chromatography with 7N ammonia in MeOH: DCM / 1:99 → 2:98 → 5:95 as the eluent to give the title compound as a yellow solid. Yield 695 mg (41%), R_f 0.60 (7N ammonia in MeOH: DCM / 1:4) (37).

^{1}H NMR ($CDCl_3$, 300 MHz): 6.85 (m, 1H), 6.57 (s, 1H), 5.61 (s, 1H), 4.46 (m, 1H), 4.28 (m,

1H), 3.58 (s, 4H), 3.57–3.52 (m, 4H), 3.43–3.38 (m, 3H), 3.10 (sex, *J* = 4.5 Hz, 1H), 2.84, 2.90 (2 × d, *J* = 6.0 Hz, 1H), 2.78, (t, *J* = 5.1 Hz, 2H), 2.64, (d, *J* = 7.2 Hz, 2H), 2.27–2.13 (m, 7H), 2.05–1.35 (m, 10H), 1.21–1.02 (m, 1 H), 0.86–0.79 (m, 2H). ^{13}C NMR ($CDCl_3$, 75 MHz): 173.5, 164.2, 99.1 (2C), 70.7, 70.3 (2C), 70.2, 62.0, 60.4, 55.8, 49.4, 45.7, 40.7, 39.3, 36.2, 29.3 (2C), 28.3, 25.8, 21.7 (2C), 21.5, 19.6 (2C), 19.4. IR (cm^{-1}): 3283, 2920, 2846, 1701, 1640, 1550, 1243, 1117, 728. [ESI-MS]: calculated for $C_{26}H_{42}N_4O_4S$, 506.29, found: ($M+H^+$) 507.30; ($M+Na^+$) 529.28.

II

6-((1*R*,8*S*,9*s*)-bicyclo[6.1.0]non-4-yn-9-ylmethyl)-5,16-dioxo-20-((3*aR*,4*R*,6*aS*)-2-oxohexahydro-1H-thieno[3,4-*d*]imidazol-4-yl)-9,12-dioxa-6,15-diazaicosan-1-oic acid (GA-BCN) (3)

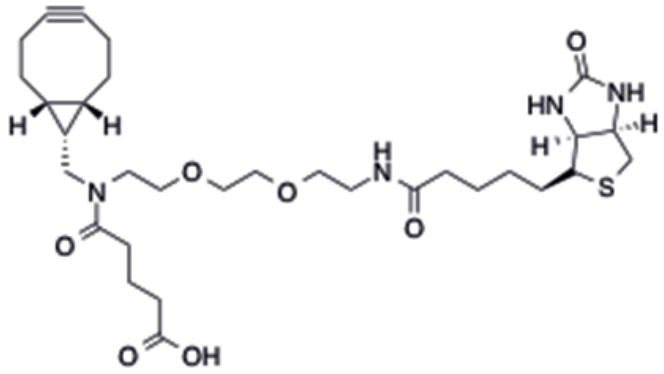

To a solution of **2** (121 mg; 0.240 mmol; 1.0 equiv.) in DCM (30 ml) were added 4-(dimethylamino) pyridine (20.4 mg; 0.167 mmol; 0.7 equiv.) and glutaric anhydride (51.8 mg; 0.462 mmol; 1.9 equiv.). The resulting mixture was stirred for 16 h at RT. The organic layer was washed with 30 ml 0.1 M aqueous hydrochloric acid. The aqueous layer was extracted with DCM (30 mL) and the combined organic layers were dried over Na_2SO_4. The solvent was removed *in vacuo* and the crude product was purified by silica column chromatography with MeOH: DCM / 1:15 with 1% acetic acid as the eluent to give **3** as an opaque colorless oil. Yield 116 mg (78%), R_f 0.13 (7N ammonia in MeOH: DCM / 1:4).
^{1}H NMR ($CDCl_3$, 300 MHz): 8.07 (s, 1H), 7.14 (m, 1H), 6.84 (m, 1H), 5.70 (s, 1H), 4.54 (m, 1H), 4.38 (m, 1H), 3.61 (s, 4H), 3.68–3.36 (m, 8H), 3.20 (q, *J* = 7.2 Hz, 1H), 2.92, 2.98 (2 × d, *J* = 6.0 Hz, 1H), 2.77 (t, *J* = 6.9 Hz, 5H), 2.54, (t, *J* = 7.2 Hz, 2H), 2.48–2.16 (m, 6H), 2.04 (m, 4H), 1.81–1.63 (m, 4H), 1.54–1.43 (m, 4H), 1.27–1.15 (m, 1H), 0.99–0.86 (m, 2H). ^{13}C NMR ($CDCl_3$, 75 MHz): 175.1, 174.1, 173.4 (2C), 99.0, 98.9, 71.1, 70.9, 70.3, 68.7, 62.1, 60.6, 55.6, 46.6, 45.3, 44.5, 40.6, 39.5, 35.9, 32.4, 29.3 (2C), 28.2, 25.7, 21.5 (2C), 20.8, 19.7 (2C), 19.5, 17.6. IR (cm^{-1}): 3291, 2920, 1697, 1636, 1450, 1264, 1126, 733. [ESI-MS]: calculated for $C_{31}H_{48}N_4O_7S$, 620.32, found: ($M+H^+$) 621.32; ($M+Na^+$) 643.31.

(*Z*)-diethyl bicyclo[6.1.0]non-4-ene-9,9-dicarboxylate (8)

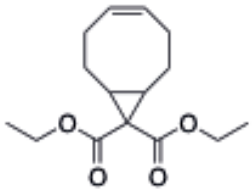

To a solution of 1,5-cyclooctadiene (3.29 mL; 26.8 mmol; 5.0 equiv.) and rhodium(II) acetate (23.3 mg; 0.053 mmol; 0.2 mol%) in DCM (5 ml) was added dropwise a solution of diethyl 2-diazomalonate (1.00 g; 5.39 mmol; 1.0 equiv.) in DCM (5 ml) under nitrogen conditions. The mixture was stirred for 24 h at RT. The solvent was removed *in vacuo* and the crude product was purified by silica column chromatography (pentane as the first eluent to remove 1,5-cyclooctadiene → ethyl acetate: pentane / 1:10 as the second eluent) to give the compound as colorless oil. Yield 893 mg (62%), R_f 0.31 (ethyl acetate: heptane / 1:10) (25).
^{1}H NMR ($CDCl_3$, 300 MHz): 5.60–5.53 (m, 2H), 4.16 (q, *J* = 6.9 Hz, 2H), 4.10 (q, *J* = 6.9 Hz, 2H), 2.35–2.29 (m, 2H), 2.11–2.05 (m, 4H), 1.80–1.68 (m, 4H), 1.26 (t, *J* = 7.2 Hz, 3H),

1.21 (t, *J* = 7.2 Hz, 3H). ^{13}C NMR ($CDCl_3$, 75 MHz): 171.3, 167.7, 129.6 (2C), 61.6, 61.1, 39.3, 31.3 (2C), 27.0 (2C), 24.7 (2C), 14.3 (2C). IR (cm^{-1}): 2980, 1718, 1316, 1260, 1217, 1169, 1104, 1027, 715. [ESI-MS]: calculated for $C_{15}H_{22}O_4$ 266.15, found: ($M+Na^+$) 289.14.

Bicyclo[6.1.0]non-4-ene-9,9-diyldimethanol (9)

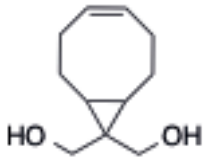

To a suspension of lithium aluminium hydride (294 mg; 7.75 mmol; 2.1 equiv.) in diethyl ether (25 ml) was added dropwise, a solution of **8** (966 mg; 3.63 mmol; 1.0 equiv.) in diethyl ether (10 ml). The suspension was stirred for 15 min at RT. The reaction mixture was cooled to 0°C and water (10 ml) was added carefully until the grey solid turned white. The solid was filtered and washed thoroughly with diethyl ether (50 ml). The aqueous and organic layers were separated and the aqueous layer was extracted with diethyl ether (3 × 50 ml). The combined organic layers were dried over Na_2SO_4. The solvent was removed *in vacuo* and the crude product was purified by silica column chromatography with ethyl acetate: pentane / 2:1 as the eluent to give (*Z*)-bicyclo[6.1.0]non-4-ene-9,9-diyldimethanol as a white solid. Yield 546 mg (83%), R_f 0.25 (ethyl acetate: heptane / 2:1) (25).

Bicyclo[6.1.0]non-4-yne-9,9-diyldimethanol (10)

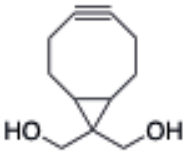

To a solution of **9** (546 mg; 3.00 mmol; 1.0 equiv.) in DCM (30 ml) was added dropwise at 0°C, a solution of bromine (0.290 ml; 5.63 mmol; 1.8 equiv.) in DCM (10 ml). The reaction mixture was quenched with a 10% sodium thiosulfate solution (15 ml), extracted with DCM (2 × 20 ml) and combined organic layers were dried over Na_2SO_4. The solvent was removed *in vacuo* and the crude product (4,5-dibromobicyclo[6.1.0]nonane-9,9-diyl) dimethanol) was purified by silica column chromatography with ethyl acetate: pentane / 10:1 as the eluent to give the title compound as a white solid. Yield 705 mg (69%), R_f 0.35 (ethyl acetate: heptane / 10:1) (25). Next, to a solution of (4,5-dibromobicyclo[6.1.0] nonane-9,9-diyl)dimethanol) (201 mg; 0.588 mmol; 1.0 equiv.) in THF (25 ml) was added dropwise at 0°C a solution of 1 M potassium *tert*-butoxide (2.57 ml; 2.57 mmol; 4.4 equiv.) in THF and the reaction mixture was refluxed for 2 h. This experiment was carried out under nitrogen conditions, with dry solvents and oven dry glassware. After cooling down to RT, the reaction mixture was quenched with saturated aqueous ammonium chloride solution (20 ml) and extracted with DCM (3 × 20 ml). The combined organic layers were dried over Na_2SO_4. The solvent was removed *in vacuo* to give the title compound as an opaque colorless solid. Yield 101 mg (66%), R_f 0.26 (ethyl acetate: heptane / 10:1) (25). ^{1}H NMR ($CDCl_3$, 300 MHz): 3.88 (s, 2H), 3.62 (s, 2H), 2.34–2.16 (m, 6H), 1.68–1.56 (m, 2H), 0.88–0.79 (m, 2H). ^{13}C NMR ($CDCl_3$, 75 MHz): 98.9 (2C), 73.7, 63.5, 30.7, 29.7 (2C), 26.3 (2C), 21.5 (2C). [ESI-MS]: calculated for $C_{11}H_{16}O_2$, 180.24, found: ($M+Na^+$) 203.10517.

Spiro[bicyclo[6.1.0]non[4]yne-9,5'-[1,3]dioxan]-2'-one (11)

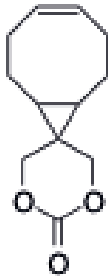

This experiment was accomplished under nitrogen conditions, with dry solvents and oven dry glassware. To a solution of **10** (115 mg; 0.588 mmol; 1.0 equiv.) and pyridine (0.127 ml; 1.60 mmol; 2.7 equiv.) in THF (20 ml) at -78°C, was added a solution of triphosgene (74.8 mg; 0.253 mmol; 0.4 equiv.) in DCM (20 ml). The reaction mixture was warmed to RT and continued to stir for 1 h. The solvent was removed *in vacuo* and the crude product was purified by silica column chromatography (ethyl acetate: pentane / 1:4 → 1:1 as the eluent) to give the title compound as a white

solid. Yield 41.2 mg (34 %), R_f 0.24 (ethyl acetate: heptane / 1:1) (38). ^{1}H NMR ($CDCl_3$, 300 MHz): 4.36 (s, 2H), 4.17 (s, 2H), 2.36–2.21 (m, 6H), 1.62–1.47 (m, 2H), 1.14–1.05 (m, 2H). ^{13}C NMR ($CDCl_3$, 75 MHz): 149.3, 98.4 (2C), 68.9 (2C), 28.9 (2C), 25.9 (2C), 21.9, 21.0 (2C). IR (cm^{-1}): 2920, 2846, 1744, 1407, 1264, 1169, 1130. [ESI-MS]: calculated for $C_{12}H_{14}O_3$, 206.09, found: ($M+Na^+$) 229.08493.

(9-(hydroxymethyl)bicyclo[6.1.0]non-4-yn-9-yl)methyl (2-(2-(2-aminoethoxy) ethoxy)ethyl)carbamate (12)

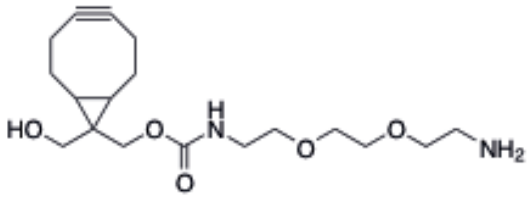

To a solution of **11** (20 mg; 0.097 mmol; 1.0 equiv.) in MeCN (2 ml) was added 2,2'-(ethane-1,2-diylbis(oxy))diethanamine (0.044 ml; 0.294 mmol; 3.0 equiv.), this mixture was stirred for 24 h at RT. The reaction mixture was warmed to 50 °C and stirred continuously for 12 h. Water (10 ml) and DCM (10 ml) were added to the reaction mixture and the aqueous layer was extracted with DCM (2 × 10 ml). The combined organic layers were dried over Na_2SO_4. The solvent was removed *in vacuo* and the crude product was purified by silica column chromatography (7N ammonia in MeOH: DCM / 2:98 → 5:95 as the eluent). This synthesis yielded **12** as a white solid. Yield 14.9 mg (43%). The product was obtained as a mixture of diastereomers.

^{1}H NMR ($CDCl_3$, 300 MHz): 5.54–5.49 (m, 1H, both diastereomers), 4.26 (s, 1H), 4.00 (s, 1H), 3.63–3.54 (m, 7H), 3.49 (t, *J* = 5.0 Hz, 2H), 3.39–3.35 (m, 3H), 2.85 (t, *J* = 5.2 Hz, 1H, diastereomer 1), 2.84 (t, *J* = 5.2 Hz, 1H, diastereomer 2), 2.26–2.14 (m, 8H), 1.63–1.57 (m, 2H), 0.85–0.81 (m, 2H). ^{13}C NMR ($CDCl_3$, 75 MHz): 157.4, 98.8 (2C), 73.4, 70.4 (2C), 70.1, 69.4, 59.2, 41.9, 41.1, 29.5, 29.3 (2C), 26.3 (2C), 21.5 (2C).

(9-(hydroxymethyl)bicyclo[6.1.0]non-4-yn-9-yl)methyl (2-(2-(2-(5-((3*aR*, 4*R*,6*aS*)-2-oxohexahydro-1H-thieno[3,4-*d*]imidazol-4-yl)pentanamido)ethoxy)ethoxy)ethyl) carbamate (BHM-BCN) (4)

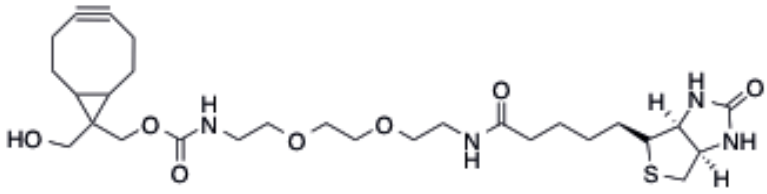

To a solution of **12** (14.9 mg; 0.042 mmol; 1.0 equiv.) and triethylamine (0.0176 ml; 0.126 mmol; 3.0 equiv.) in DMF (2 ml) was added dropwise biotin-OSu (15.8 mg; 0.046 mmol; 1.1 equiv.) in DMF (2 ml). The reaction mixture was stirred for 1 h at RT. DCM (5 ml) was added to the reaction mixture and the organic layer was washed successively with saturated aqueous ammonium chloride (5 ml) and saturated aqueous sodium bicarbonate (5 ml). The aqueous layers were extracted with DCM. The combined organic layers were dried over Na_2SO_4 and the solvent was removed *in vacuo* to give the title compound as a white solid. Yield 14.0 mg (57%), R_f 0.48 (7 N ammonia in MeOH: DCM / 1:4).

^{1}H NMR ($CDCl_3$, 300 MHz): 6.69 (m, 1H), 6.48 (m, 1H), 5.68 (m, 1H), 5.58 (m, 1H), 4.47 (t, *J* = 6.0 Hz, 1H), 4.30–4.26 (m, 1H), 4.01 (s, 1H), 3.66 (s, 1H), 3.59 (s, 4H), 3.54 (t, *J* = 5.1 Hz, 4H), 3.44–3.34 (m, 4H), 3.11 (q, *J* = 4.5 Hz, 1H), 2.93 (s, 1H), 2.85 (s,1H), 2.85, 2.90 (2 × d, *J* = 6.0 Hz, 1H), 2.73 (s, 1H), 2.68 (s, 1H), 2.27–2.15 (m, 7H), 1.75–1.57 (m, 6H), 1.45–1.36 (m, 2H), 1.22 (s, 1H), 0.85–0.82 (m, 2H). ^{13}C NMR ($CDCl_3$, 75 MHz): 173.7, 164.2, 157.6, 98.8 (2C), 72.5, 70.2 (2C), 69.9, 63.7, 62.0, 60.4, 59.9, 55.8, 41.1, 40.7, 39.4, 36.6, 36.1, 29.3, 28.4 (2C), 28.3, 26.3 (2C), 25.8, 21.5 (2C). IR (cm^{-1}): 3304,

2924, 1697, 1537, 1459, 1260, 1117, 1027. ESI-MS: calculated for $C_{28}H_{44}N_4O_7S$ 580.29: ($M+H^+$) 581.30, found; ($M+Na^+$) 603.28.

Results and Discussion

Synthesis

Synthesis of compounds **2** and **3** commenced with oxidation of commercially available BCN alcohol to the corresponding aldehyde **6**. Aldehyde **6** was found to be highly unstable, and hence unsuitable for storage or purification, and was therefore further processed crude after oxidation. Reductive amination with $NaCNBH_3$ in the presence of biotin-amine **7**, led to the desired amino-linked conjugate **2**. Subsequent acylation of **2** with glutaric anhydride yielded the second desired BCN derivative **3** (Scheme 1).

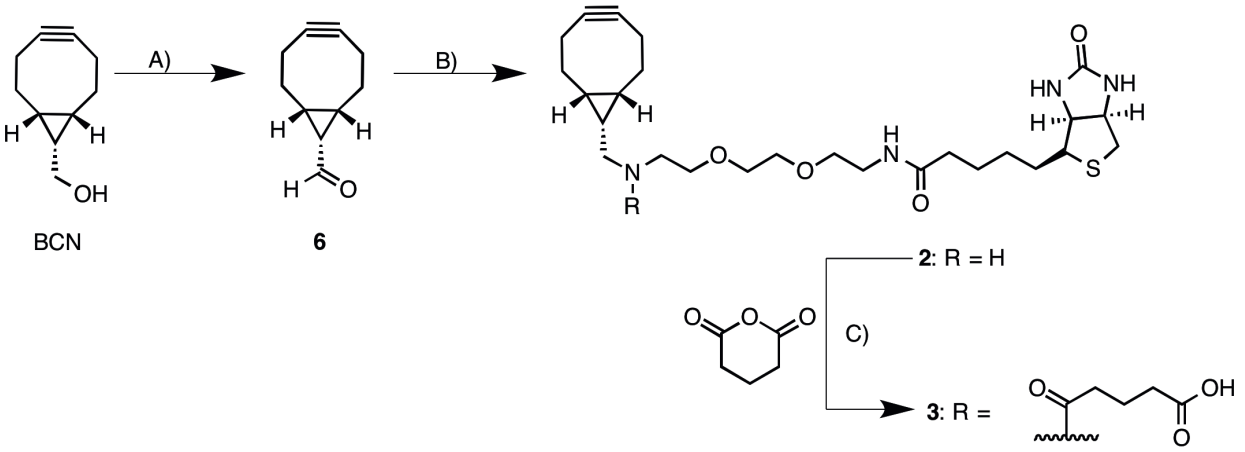

Scheme 1. Synthesis of A-BCN (2) and GA-BCN (3).
A) Dess–Martin periodinane, CH_2Cl_2, RT, 2 h. **B)** Biotin-amine **7**, $NaCNBH_3$, CH_2Cl_2, RT, 2 h (41%). **C)** 4-dimethylaminopyridine (DMAP), CH_2Cl_2, RT, 16 h (78 %).

The synthesis of compound **4**, featuring a BHM-BCN scaffold, could not be achieved from the same BCN starting material but required a different approach from simple starting materials. To this end, a synthetic route resembling that to the earlier reported BCN alcohol was devised (25). Cycloocta-1,5-diene (in excess) was treated with diethyl diazomalonate (39), in the presence of rhodium acetate. The resulting cyclopropanated derivative **8** was subjected to a three-step procedure involving lithium aluminumhydride reduction, bromination and then double elimination and afforded the bishydroxymethyl bicyclo[6.1.0]non-4-yne (**10**) in reasonable yield. Conversion of **10** into the projected biotin derivative **4** required a slight modification of the earlier procedure. As expected, treatment of **10** with triphosgene, did not afford a mono-activated NHS-carbonate derivative, but led to cyclic carbonate **11** instead. Interestingly, we discovered that the cyclic carbonate **11** possessed sufficient electrophilicity for spontaneous acylation of an alkylamine, potentially due to the strained character of the spiro system. Thus, treating **11** with (excess) diamine led to monoselective ring opening, and after purification and acylation the desired carbamate-linked BCN-biotin conjugate **4** was obtained in good yield as a mixture of diastereomers (Scheme 2).

Kinetics

The reactivity of the new bicyclo[6.1.0]nonyne analogues **2**-**4** was determined for a prototypical SPAAC reaction with the fluorogenic substrate 3-azido-7-hydroxycoumarin (**5**, Fig2B), by monitoring and quantifying the resulting fluorescent signal over time. A

kinetic olot is made and the reaction rate is determined. In a mixture of acetonitrile and water (1:2), the different BCN-biotin analogues displayed nearly similar reaction rates with **5** (Table 1), which was expected, given the fact that the reactive bicyclononyne moiety is constant across the set of probes. We were surprised, however, that the rate constant of approximately 2 $M^{-1}s^{-1}$ is almost 10-fold higher than the rate established earlier (0.29 $M^{-1}s^{-1}$) for cycloaddition of BCN with benzyl azide (25). Apparently, the aromatic coumarin substituent on the azide has a profound influence on its reactivity, an effect that cannot be readily explained at this stage, all the more so because Hosoya *et al.* recently reported that the reaction of phenyl azide with a dibenzofused cyclooctyne is 6.8 times slower than for a benzyl azide (an aliphatic azide) (40). At this point, however, no further attention was given to this observation, since, apart from the permeability studies, subsequent experiments were performed exclusively with aliphatic azides.

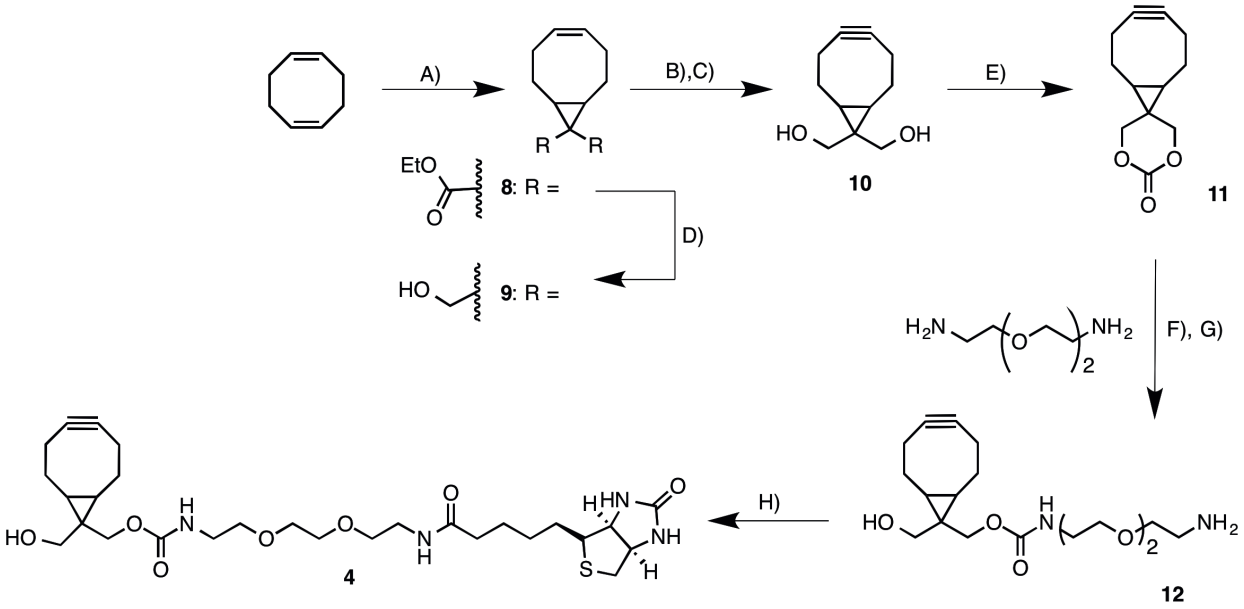

Scheme 2. Synthesis of BHM-BCN (4).
A) $Rh_2(OAc)_4$, diethyl 2-diazomalonate, CH_2Cl_2, RT, 24 h (62%). **B)** Br_2, CH_2Cl_2, 0 ºC, 30 min. **C)** KOtBu, THF, 0 ºC, 30 min, RT, 2 h (46 %). **D)** $LiAlH_4$, Et_2O, RT, 15 min (83%). **E)** pyridine, THF,-78 ºC, 30 min, triphosgene, CH_2Cl_2, RT, 1 h (34%). **F)** CH_3CN, RT, 24 h. **G)** 50 ºC, 12 h (43%). **H)** biotin-OSu, Et_3N, DMF, RT, 1 h (57 %).

Table 1. Rate constants ± SEM of the reaction between **5** and the indicated cyclooctyne at RT in MeCN:H_2O = 1:2

Cyclooctyne	**BCN**	**1**	**2**	**3**	**4**
Rate [$M^{-1}s^{-1}$]	2.64±0.01	1.52±0.01	2.64±0.23	1.56±0.14	1.86±0.21

Polarity

To assess the relative hydrophilicities of compounds **1**-**4**, each individual analogue was subjected to reversed-phase HPLC (RP-HPLC) analysis, with a 50 mM phosphate buffer (pH 7.4) and MeCN as eluents and a 30 min solvent gradient from 95:5 to 20:80 of phosphate buffer versus MeCN. The higher polarities of the newly synthesised **2**-**4** were nicely reflected in the significantly reduced retention times, which varied between 11.59, 11.63 and 13.27, respectively (Fig 3); in comparison, the known BCN (**1**) appeared after 16.27 min with this gradient. These particularly high hydrophilicities of compounds **2** and **3** can be explained on the basis of pKa values published previously,

which predict that compounds **2** and **3** should be positively and negatively charged, respectively, at neutral pH 7.4 (41).

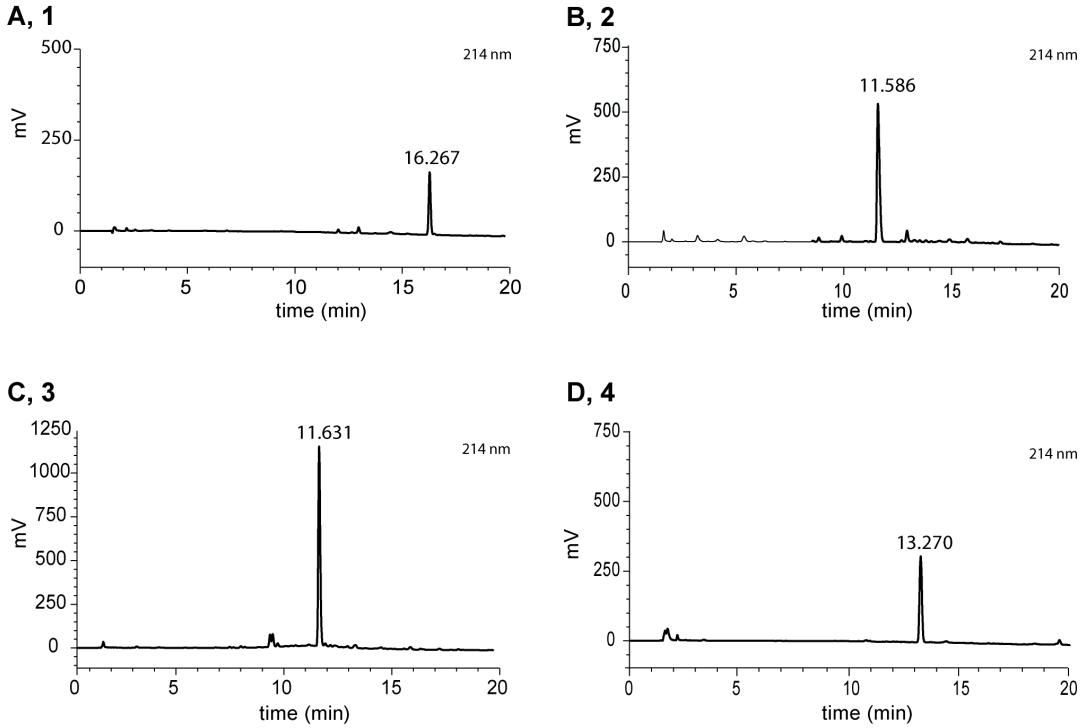

Figure 3. **RP-HPLC profiles from the BCN derivatives.**
RP-HPLC on a C18 column was performed using 50 mM phosphate buffer adjusted to pH 7.4 as mobile phase A, and MeCN as mobile phase B. The gradient profile started with 95% mobile phase A up to 80% mobile phase B in 30 min. **A)** As expected the retention time of **1** was highest (16.27 min). **B)** Compound **2** is likely to be charged at pH 7.4 and therefore had a retention time of 11.59 min. **C)** GA-BCN (**3**) is probably negatively charged at pH 7.4 and therefore more polar (11.63 min). **D) 4** is slightly more hydrophilic than **1** with a retention time of 13.27 min.

Membrane permeability

Cyclooctynes may penetrate the cell membrane and give rise to enhanced background signal, because removal by washing steps is not possible as long as the cells are intact. We reasoned that the more polar BCN analogues (**2**-**4**) should display a reduced tendency for transport across the plasma cell membrane relative to BCN (**1**). Therefore, the uptake of BCN into HEK293 cells was evaluated by confocal microscopy, to ascertain the effects of active transport mechanisms and differences in membrane lipid composition of living cells. HEK293 cells were cultured for 24 h on glass cover slips before treatment with 60 µM of one of the biotinylated BCN probes (**1-4**) for 1 h at room temperature. Cells were then fixed and permeabilised with paraformaldehyde (PFA), and incubated with streptavidin-Alexa Fluor 488 (green) for the direct detection of the BCN distribution through the cells. At the same time, DAPI staining was used to visualise the cell nucleus (blue), whereas the Golgi 58k antibody allowed the detection of the Golgi apparatus (red).

As anticipated, cells treated with the least polar BCN (**1**) showed high fluorescence distributed throughout the cell (Fig 4A), whereas the more hydrophilic BCN analogues **2**-**4**

showed a reduced fluorescence intensity (Fig 4B-D), thus indicating that internalization is reduced compared to the mother compound BCN. Treatment with GA-BCN (**3**) resulted in the lowest fluorescent intensity, comparable to the intensity found without BCN treatment (Fig 4B). Furthermore, no specific co-localisation with the nucleus or the Golgi apparatus was found for the BCN analogues, and no cross-over between the different channels was detected; this supports the conclusion that the developed probes give reduced background staining.

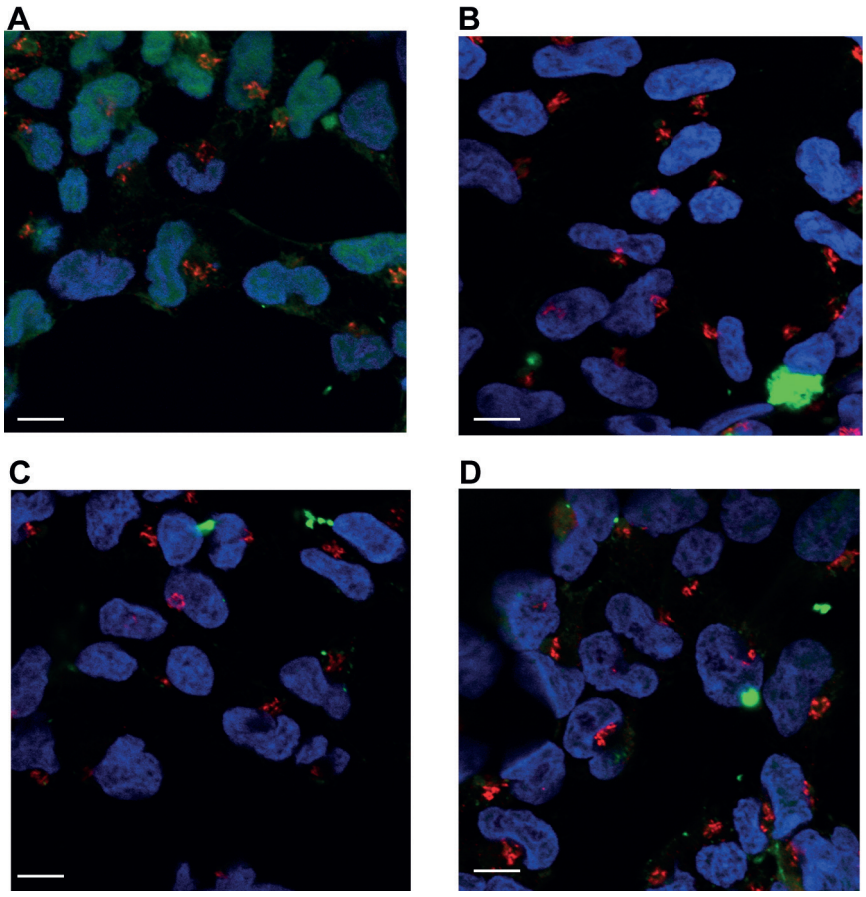

Figure 4. Representative confocal images of HEK293 cells treated with cyclooctyne-biotin followed by secondary labelling with streptavidin-Alexa Fluor 488 (green).
Blue represents nucleus staining with DAPI and red represents the Golgi apparatus. **A)** Treatment with BCN (**1**) results in a strong intracellular signal. **B) 2**. **C) 3** or **D)** 4 results in weak intracellular signal. Bar: 10μm.

Metabolic incorporation

We analysed the specific binding and labelling capacities of the different BCN analogues for cellular staining of metabolically labelled azidoglycans. HEK293 cells were grown on glass cover slips and treated with 60 μM peracetylated N-azidoacetyl-D-mannosamine (Ac4ManNAz) for 3 days. Subsequently, cells were incubated with one of the BCN-biotin probes (**1**-**4**) (60 μM) for 1 h, washed, permeabilised and stained with streptavidin-Alexa Fluor 488. As expected, we found that labelling with **1** resulted in marginal membrane detection in combination with a strong intracellular signal (Fig 5A). In previous studies, the cells were not permeabilised, so only BCN bound to the cell membrane is visualized,(25) a method that is often used in combination with glycan labelling. Labelling with A-BCN (**2**), unlike with **1**, resulted in clear and selective membrane visualisation. In addition, the Golgi apparatus was labelled consistently (Fig 5B), a phenomenon reported before for DIBO and DIFO (20,42). This effect might be a result of the extreme high concentration

of ManNaz in the trans-Golgi where the glycan is composed. GA-BCN (**3**) also showed selective membrane labelling but with a relatively low fluorescent intensity, thus indicating that the membrane staining was highly specific, but less efficient (Fig 5C). Treatment with BHM-BCN (**4**) gave rather weak fluorescent signals for both extracellular and intracellular staining (Fig 5D). No cross-over between the different channels was detected.

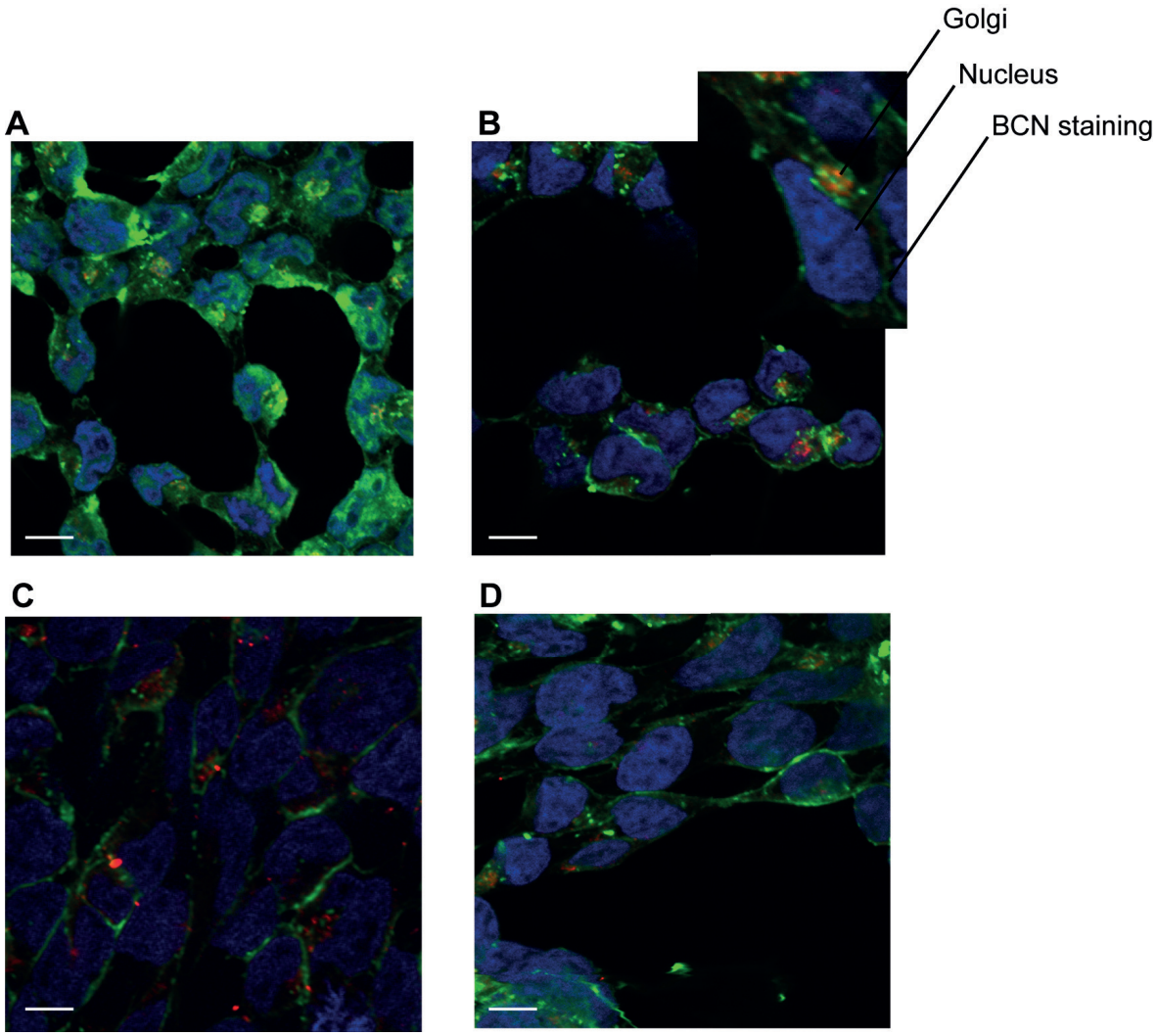

Figure 5. Representative confocal images of HEK293 cells after Ac_4ManNAz treatment followed by reaction with cyclooctyne-biotin and secondary labelling with streptavidin-Alexa Fluor 488 (green). Blue represents nucleus staining with DAPI, whereas the Golgi apparatus is labelled red. **A)** BCN (**1**) labelling is not restricted to plasma membrane labelling. **B)** Treatment with A-BCN (**2**) results in low background labelling. Membrane and Golgi network are detected. **C)** Biotinylation with probe **3** shows relatively low background labelling. Clear membrane staining is visible, but the Golgi apparatus is not clearly stained. **D)** A higher background signal is detected after labelling with probe **4**, however the membrane is stained. Bar: 10μm.

To quantify the plasma membrane labelling efficiencies of the different BCN analogues, the fluorescent intensities were measured by flow cytometry. To this end, HEK293 cells were either treated with 60 μM Ac_4ManNAz for 3 days or left untreated as a control. The reaction efficiencies of all four BCN probes were tested at three different temperatures (4 °C, RT, 37°C), and the cyclooctynes were visualised by binding of streptavidin-Alexa Fluor 488 and analysed by Fluorescence Activated Cell Sorting (FACS). Because streptavidin is not internalized at 4 °C and whole, non-permeabilised cells are measured, only extracellular BCN can be labelled and detected. Rather strong unspecific signals on

the cell membranes were found for BCN (**1**) and BHM-BCN (**4**) in HEK293 cells (Fig 6). To our satisfaction, the most hydrophilic compounds **2** and **3** were found to give better signal-to-noise ratio (SNR) then **1** at all temperatures (Table 2, Fig 6). Labelling with either A-BCN (**2**) or GA-BCN (**3**) gave significantly higher SNR's. For **2** the SNR was increased with a factor of two with respect to **1**, and this is consistent with the confocal microscopy data. Specific membrane labelling was most efficient at 37°C, independent of the cyclooctyne (Fig 6C).

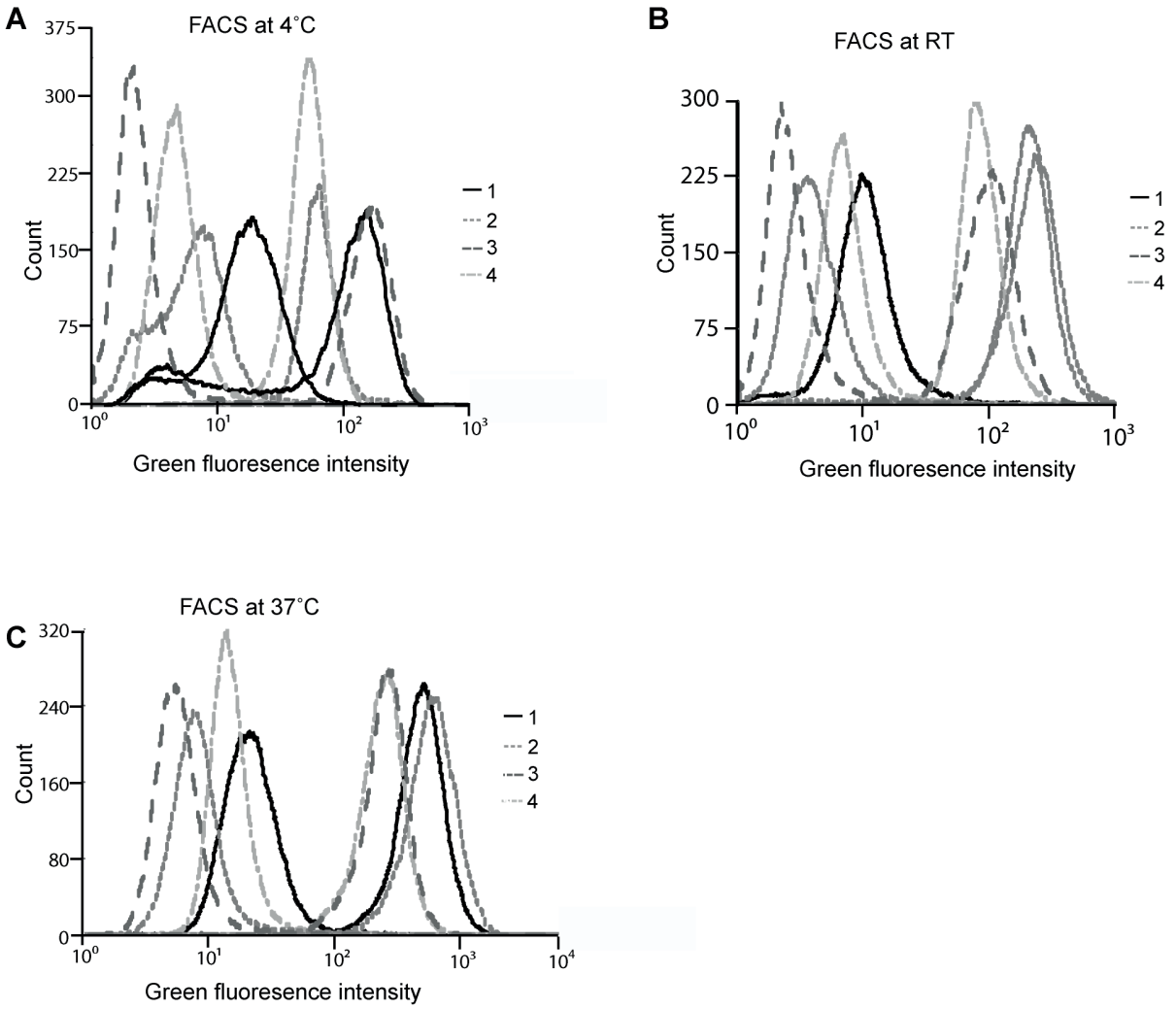

Figure 6. Metabolic labelling efficiencies assessed by flow cytometry.
Representative graphs of the fluorescent intensities from the BCN analogues. The peaks on the left represent the unspecific signal (without Ac_4ManNAz treatment). The peaks on the right side represent the signal after Ac_4ManNAz treatment. **A)** Representative graph of the fluorescent intensities from the BCN analogues at 4°C, **B)** at RT, **C)** at 37°C.

Table 2. SNR ± SEM of the indicated cyclooctyne at the different temperatures

Cyclooctyne	**1**	**2**	**3**	**4**
SNR at 4°C	6.4 ± 1.4	18.9 ± 5.0	12.8 ± 3.0	5.8 ±1.8
SNR at RT	18.6 ± 2.0	32.2 ± 6.7	25.6 ± 5.9	9.9 ± 1.0
SNR at 36°C	46.2 ± 11.4	76.4 ± 8.4	53.7 ± 11.4	17.6 ± 3.2

Finally, we tested whether the newly developed cyclooctynes could label specific membrane glycoproteins, with use of the complex N-glycosylated TRPV5 membrane channel as our model protein. This epithelial calcium transporter functions as the rate-limiting step in renal calcium reabsorption. Because modification of the TRPV5 N-glycan is known to influence the membrane retention of the channel significantly (5,6,43), a direct glycoprotein read-out would be valuable for obtaining further insight into the role of glycosylation for TRPV5 function. Because BHM-BCN (**4**) had a low SNR after FACS analysis, this probe was not evaluated. HEK293 cells overexpressing TRPV5, or the empty vector ("mock"), were either treated with 60 μM Ac_4ManNAz or left untreated. This was followed by labelling with one of the BCN-biotin analogues at room temperature for 1 h. Analysis by SDS-PAGE, followed by western blot, indicated that treatment with BCN (**1**) resulted in a strong TRPV5-biotinylated signal. However, an unspecific biotinylation signal was detected as well (SNR of 3.96 ± 0.93, n=9; 3 independent experiments, bottom panel, Fig 7A), probably due to unspecific thiol-yne additions. Treatment with A-BCN (**2**) significantly increased the specific biotinylation, with reduced background labelling and a SNR of 7.91 ± 1.55 ($p<0.05$ with respect to BCN, n=9; 3 independent experiments, bottom panel, Fig 7B). The more hydrophilic GA-BCN (**3**) also showed a reduction in background labelling, with a SNR of 7.03 ± 1.59 (p= 0.13, ns with respect to BCN, n=11; 4 independent experiments, bottom panel, Fig 7C). The total loading of TRPV5 was determined as a control (top panels, Fig 7).

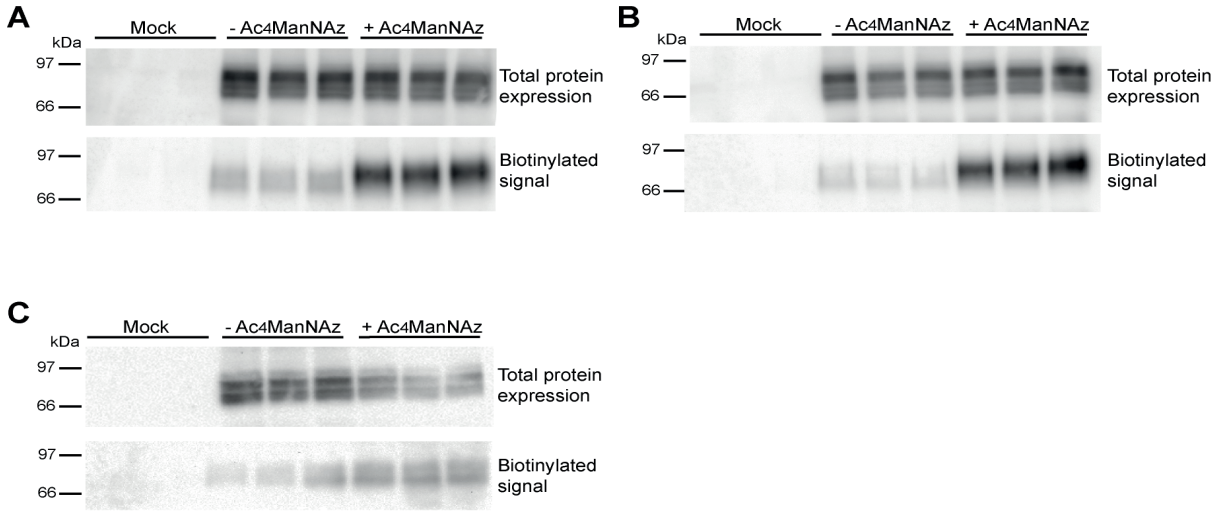

Figure 7. Western blots showing the TRPV5 channel through glycan labelling.
Top panel in each case represents the total TRPV5 expression, bottom panel represents the biotinylated fraction of TRPV5 with and without Ac_4ManNAz treatment. Representative blots of three independent experiments. **A)** Treatment with BCN (**1**) results in a relatively high unspecific background labelling compared to the total signal. **B)** Biotinylation with A-BCN (**2**) showed a weak background signal compared to the Ac_4ManNAz signal. **C)** Labelling with probe **3** resulted in a slightly weaker background signal than in the case of BCN.

Conclusions

The ability to introduce azide-functionalized glycans into biomolecules, followed by SPAAC gives rise to many opportunities in the glycobiology field (20,44,45). The high reaction rates of the non-benzoannulated, relative non-lipophilic bicyclo[6.1.0]nonyne make this cyclooctyne derivative particularly suitable for labelling in living systems (25). We have designed, synthesized and evaluated a second-generation of BCN analogues with

reduced intracellular labelling capacity. In passing we noted the exceptional reactivity of BCN and its analogues for **5**, an effect that we are currently investigating in our laboratory.

All BCN derivatives were evaluated for their relative lipophilicities; the newly synthesised derivatives were found to be more hydrophilic than the mother compound **1**. Metabolic labelling studies in HEK293 cells showed that the polar BCN probes had a reduced tendency to pass through the plasma membrane. After treatment of HEK293 cells with Ac_4ManNAz, followed by probe **2** or **3**, plasma membrane staining became apparent. Interestingly, probe **2** also showed selective staining of the Golgi apparatus after Ac_4ManNAz treatment. Golgi labelling by means of copper-free click chemistry can be used to study dynamic glycan trafficking (20,42). The SNRs of the reactions of the most hydrophilic compounds, **2** and **3**, at the cell surfaces were increased compared to those with the unmodified BCN. The key advantages in using more hydrophilic BCN analogues are their reduced tendency to undergo membrane transport in HEK293 cells and their increased labelling specificities. Treatment with probe **2** resulted in the most specific labelling of the TRPV5 N-glycan. The SNR is significantly better than that achieved with the commonly used BCN. We therefore expect that the polar BCN probes **2**-**4**, with retained reaction rate and reduced unspecific labelling, will find useful application in the visualisation of glycans of cell membrane proteins in living cells and live-cell imaging.

Acknowledgements
We would like to thank S. Schmidt for his help with the FACS experiments and the Microscopic Imaging Centre (MIC) in Nijmegen for making available the Olympus FV1000 Confocal laser scanning microscope. This work was supported by a grant of the Radboud Institute for Molecular Life Sciences (RIMLS) to J.G.J. Hoenderop and F.L. van Delft.

References

1. Takahashi, M., Yokoe, S., Asahi, M., Lee, S. H., Li, W., Osumi, D., Miyoshi, E., and Taniguchi, N. (2008) N-glycan of ErbB family plays a crucial role in dimer formation and tumor promotion. *Biochimica Et Biophysica Acta-General Subjects* **1780**, 520-524
2. Moen, A., Hafte, T. T., Tveit, H., Egge-Jacobsen, W., and Prydz, K. (2011) N-Glycan synthesis in the apical and basolateral secretory pathway of epithelial MDCK cells and the influence of a glycosaminoglycan domain. *Glycobiology* **21**, 1416-1425
3. Zhuo, Y., and Bellis, S. L. (2011) Emerging Role of alpha 2,6-Sialic Acid as a Negative Regulator of Galectin Binding and Function. *J of Biol Chem* **286**, 5935-5941
4. Kawamura, S., Sato, I., Wada, T., Yamaguchi, K., Li, Y., Li, D., Zhao, X., Ueno, S., Aoki, H., Tochigi, T., Kuwahara, M., Kitamura, T., Takahashi, K., Moriya, S., and Miyagi, T. (2012) Plasma membrane-associated sialidase (NEU3) regulates progression of prostate cancer to androgen-independent growth through modulation of androgen receptor signaling. *Cell Death and Differentiation* **19**, 170-179
5. Chang, Q., Hoefs, S., van der Kemp, A. W., Topala, C. N., Bindels, R. J., and Hoenderop, J. G. (2005) The beta-glucuronidase klotho hydrolyzes and activates the TRPV5 channel. *Science* **310**, 490-493
6. Leunissen, E. H., Nair, A. V., Bull, C., Lefeber, D. J., van Delft, F. L., Bindels, R. J., and Hoenderop, J. G. (2013) The epithelial calcium channel TRPV5 is regulated differentially by klotho and sialidase. *J Biol Chem* **288**, 29238-29246
7. Cha, S. K., Ortega, B., Kurosu, H., Rosenblatt, K. P., Kuro-O, M., and Huang, C. L. (2008) Removal of sialic acid involving Klotho causes cell-surface retention of TRPV5 channel via binding to galectin-1. *P Natl Acad Sci USA* **105**, 9805-9810
8. van Berkel, S. S., van Eldijk, M. B., and van Hest, J. C. M. (2011) Staudinger Ligation as a Method for Bioconjugation. *Angew Chem* **50**, 8806-8827
9. Sletten, E. M., and Bertozzi, C. R. (2009) Bioorthogonal Chemistry: Fishing for Selectivity in a Sea of Functionality. *Angew Chem Int Edit* **48**, 6974-6998
10. Debets, M. F., van der Doelen, C. W. J., Rutjes, F. P. J. T., and van Delft, F. L. (2010) Azide: A Unique Dipole for Metal-Free Bioorthogonal Ligations. *ChemBioChem* **11**, 1168-1184
11. Saxon, E., and Bertozzi, C. R. (2000) Cell surface engineering by a modified reaction. *Science* **287**, 2007-2010
12. Lin, F. L., Hoyt, H. M., van Halbeek, H., Bergman, R. G., and Bertozzi, C. R. (2005) Mechanistic investigation of the Staudinger ligation. *J Am Chem Soc* **127**, 2686-2695
13. Rostovtsev, V. V., Green, L. G., Fokin, V. V., and Sharpless, K. B. (2002) A stepwise Huisgen cycloaddition process: Copper(I)-catalyzed regioselective “ligation” of azides and terminal alkynes. *Angew Chem* **41**, 2596-2599
14. Tornoe, C. W., Christensen, C., and Meldal, M. (2002) Peptidotriazoles on solid phase: [1,2,3]-triazoles by regiospecific copper(I)-catalyzed 1,3-dipolar cycloadditions of terminal alkynes to azides. *J Org Chem* **67**, 3057-3064
15. Soares, E. V., Hebbelinck, K., and Soares, H. M. (2003) Toxic effects caused by heavy metals in the yeast Saccharomyces cerevisiae: a comparative study. *Can J Microbiol* **49**, 336-343
16. Agard, N. J., Prescher, J. A., and Bertozzi, C. R. (2004) A strain-promoted [3+2] azide-alkyne cycloaddition for covalent modification of biomolecules in living systems. *J Am Chem Soc* **126**, 15046-15047
17. Debets, M. F., Van Berkel, S. S., Dommerholt, J., Dirks, A. J., Rutjes, F. P. J. T., and Van Delft, F. L. (2011) Bioconjugation with Strained Alkenes and Alkynes. *Accounts Chem Res* **44**, 805-815
18. Sletten, E. M., and Bertozzi, C. R. (2008) A hydrophilic azacyclooctyne for Cu-free click chemistry. *Org Lett* **10**, 3097-3099
19. Codelli, J. A., Baskin, J. M., Agard, N. J., and Berozzi, C. R. (2008) Second-generation difluorinated cyclooctynes for copper-free click chemistry. *J Am Chem Soc* **130**, 11486-11493
20. Baskin, J. M., Prescher, J. A., Laughlin, S. T., Agard, N. J., Chang, P. V., Miller, I. A., Lo, A., Codelli, J. A., and Bertozzi, C. R. (2007) Copper-free click chemistry for dynamic in vivo imaging. *P Natl Acad Sci USA* **104**, 16793-16797
21. Jewett, J. C., Sletten, E. M., and Bertozzi, C. R. (2010) Rapid Cu-Free Click Chemistry with Readily Synthesized Biarylazacyclooctynones. *J Am Chem Soc* **132**, 3688-3690

22. Ning, X. H., Guo, J., Wolfert, M. A., and Boons, G. J. (2008) Visualizing metabolically labeled glycoconjugates of living cells by copper-free and fast huisgen cycloadditions. *Angew Chem Int* **47**, 2253-2255
23. Poloukhtine, A. A., Mbua, N. E., Wolfert, M. A., Boons, G. J., and Popik, V. V. (2009) Selective Labeling of Living Cells by a Photo-Triggered Click Reaction. *J Am Chem Soc* **131**, 15769-15776
24. Debets, M. F., van Berkel, S. S., Schoffelen, S., Rutjes, F. P. J. T., van Hest, J. C. M., and van Delft, F. L. (2010) Aza-dibenzocyclooctynes for fast and efficient enzyme PEGylation via copper-free (3+2) cycloaddition. *Chem Commun* **46**, 97-99
25. Dommerholt, J., Schmidt, S., Temming, R., Hendriks, L. J. A., Rutjes, F. P. J. T., van Hest, J. C. M., Lefeber, D. J., Friedl, P., and van Delft, F. L. (2010) Readily Accessible Bicyclononynes for Bioorthogonal Labeling and Three-Dimensional Imaging of Living Cells. *Angew Chem Int* **49**, 9422-9425
26. Ning, X. H., Temming, R. P., Dommerholt, J., Guo, J., Ania, D. B., Debets, M. F., Wolfert, M. A., Boons, G. J., and van Delft, F. L. (2010) Protein Modification by Strain-Promoted Alkyne-Nitrone Cycloaddition. *Angew Chem Int* **49**, 3065-3068
27. Mckay, C. S., Moran, J., and Pezacki, J. P. (2010) Nitrones as dipoles for rapid strain-promoted 1,3-dipolar cycloadditions with cyclooctynes. *Chem Commun* **46**, 931-933
28. Jawalekar, A. M., Reubsaet, E., Rutjes, F. P. J. T., and van Delft, F. L. (2011) Synthesis of isoxazoles by hypervalent iodine-induced cycloaddition of nitrile oxides to alkynes. *Chem Commun* **47**, 3198-3200
29. Sanders, B. C., Friscourt, F., Ledin, P. A., Mbua, N. E., Arumugam, S., Guo, J., Boltje, T. J., Popik, V. V., and Boons, G. J. (2011) Metal-Free Sequential [3+2]-Dipolar Cycloadditions using Cyclooctynes and 1,3-Dipoles of Different Reactivity. *J Am Chem Soc* **133**, 949-957
30. Chen, W. X., Wang, D. Z., Dai, C. F., Hamelberg, D., and Wang, B. H. (2012) Clicking 1,2,4,5-tetrazine and cyclooctynes with tunable reaction rates. *Chem Commun* **48**, 1736-1738
31. Borrmann, A., Milles, S., Plass, T., Dommerholt, J., Verkade, J. M. M., Wiessler, M., Schultz, C., van Hest, J. C. M., van Delft, F. L., and Lemke, E. A. (2012) Genetic Encoding of a Bicyclo[6.1.0]nonyne-Charged Amino Acid Enables Fast Cellular Protein Imaging by Metal-Free Ligation. *ChemBioChem* **13**, 2094-2099
32. Lang, K., Davis, L., Wallace, S., Mahesh, M., Cox, D. J., Blackman, M. L., Fox, J. M., and Chin, J. W. (2012) Genetic Encoding of bicyclononynes and trans-cyclooctenes for site-specific protein labeling in vitro and in live mammalian cells via rapid fluorogenic Diels-Alder reactions. *J Am Chem Soc* **134**, 10317-10320
33. van Geel, R., Pruijn, G. J. M., van Delft, F. L., and Boelens, W. C. (2012) Preventing Thiol-Yne Addition Improves the Specificity of Strain-Promoted Azide-Alkyne Cycloaddition. *Bioconjugate Chem* **23**, 392-398
34. Friscourt, F., Ledin, P. A., Mbua, N. E., Flanagan-Steet, H. R., Wolfert, M. A., Steet, R., and Boons, G. J. (2012) Polar dibenzocyclooctynes for selective labeling of extracellular glycoconjugates of living cells. *J Am Chem Soc* **134**, 5381-5389
35. Stockmann, H., Neves, A. A., Stairs, S., Ireland-Zecchini, H., Brindle, K. M., and Leeper, F. J. (2011) Development and evaluation of new cyclooctynes for cell surface glycan imaging in cancer cells. *Chem Sci* **2**, 932-936
36. Van de Graaf, S. F. J., Hoenderop, J. G. J., Gkika, D., Lamers, D., Prenen, J., Rescher, U., Gerke, V., Staub, O., Nilius, B., and Bindels, R. J. M. (2003) Functional expression of the epithelial Ca^{2+} channels (TRPV5 and TRPV6) requires association of the S100A10-annexin 2 complex. *Embo J* **22**, 1478-1487
37. Cotton, R., Johnstone, A. N. C., and North, M. (1995) Asymmetric-Synthesis of 3-Carboxyproline and Derivatives Suitable for Peptide-Synthesis. *Tetrahedron* **51**, 8525-8544
38. Curphey, T. J. (1981) Preparation of Para-Toluenesulfonyl Azide - a Cautionary Note. *Org Prep Proced Int* **13**, 112-115
39. Tullis, S. J., and Helquist, P. (1997) Rhodium-catalyzed heterocycloaddition of a diazomalonate and a nitrile 4-carbomethoxy-5-methoxy-2-phenyl-1,3-oxazole. *Organic Syntheses* **74**, 229
40. Yoshida, S., Shiraishi, A., Kanno, K., Matsushita, T., Johmoto, K., Uekusa, H., and Hosoya, T. (2011) Enhanced clickability of doubly sterically-hindered aryl azides. *Sci Rep-Uk* **1**
41. Bordwell, F. G. (1988) Equilibrium Acidities in Dimethyl-Sulfoxide Solution. *Acc Chem Res* **21**, 456-463
42. Mbua, N. E., Flanagan-Steet, H., Johnson, S., Wolfert, M. A., Boons, G. J., and

Steet, R. (2013) Abnormal accumulation and recycling of glycoproteins visualized in Niemann-Pick type C cells using the chemical reporter strategy. *P Natl Acad Sci USA* **110**, 10207-10212
43. van de Graaf, S. F., Bindels, R. J., and Hoenderop, J. G. (2007) Physiology of epithelial Ca^{2+} and Mg^{2+} transport. *Rev Physiol Biochem Pharmacol* **158**, 77-160
44. Laughlin, S. T., Baskin, J. M., Amacher, S. L., and Bertozzi, C. R. (2008) In vivo imaging of membrane-associated glycans in developing zebrafish. *Science* **320**, 664-667
45. Chang, P. V., Prescher, J. A., Sletten, E. M., Baskin, J. M., Miller, I. A., Agard, N. J., Lo, A., and Bertozzi, C. R. (2010) Copper-free click chemistry in living animals. *P Natl Acad Sci USA* **107**, 1821-1826

CHAPTER 3

The epithelial calcium channel TRPV5 is regulated differentially by klotho and sialidase

Elizabeth H.P. Leunissen [1], Anil V. Nair [1], Christian Büll [1], Dirk J. Lefeber [2], Floris L. van Delft [3], René J.M. Bindels [1], Joost G.J. Hoenderop [1]

[1]Department of Physiology and [2] Laboratory of Medicine, Radboud university medical center, Radboud Institute for Molecular Life Sciences, Nijmegen, The Netherlands
[3] Synthetic Organic Chemistry, Institute for Molecules and Materials, Radboud University Nijmegen, The Netherlands

J. Biol. Chem. 288(41): 29238-29246, 2013

Abstract

The transient receptor potential vanilloid type 5 (TRPV5) Ca^{2+} channel facilitates transcellular Ca^{2+} transport in the distal convoluted tubule (DCT) of the kidney. The channel is glycosylated with a complex type N-glycan and it has been postulated that hydrolysis of the terminal sialic acid(s) stimulate TRPV5 activity. The present study delineates the role of the N-glycan in TRPV5 activity using biochemical assays in Human embryonic kidney 293 cells expressing TRPV5, isoelectric focusing and total internal reflection fluorescent microscopy. The anti-aging hormone klotho and other glycosidases stimulate TRPV5-dependent Ca^{2+} uptake. Klotho was found to increase the plasma membrane stability of TRPV5, via the TRPV5 N-glycan. Sialidase mimicked this stimulatory action. However, this effect was independent of the N-glycosylation state of TRPV5, since the N-glycosylation mutant ($TRPV5^{N358Q}$) was activated to the same extent. We showed that the increased TRPV5 activity after sialidase treatment is caused by inhibition of lipid-raft-mediated internalization. In addition, sialidase modified the N-glycan of transferrin, a model glycoprotein, differently from klotho. Previous studies showed that after klotho treatment, galectin-1 binds the TRPV5 N-glycan and thereby increases TRPV5 activity. However, galectin-3, but not galectin-1, was expressed in the DCT. Besides, an increase in TRPV5-mediated Ca^{2+} uptake was detected after galectin-3 treatment. In conclusion, two distinct TRPV5 stimulatory mechanisms were demonstrated; a klotho-mediated effect that is dependent on the N-glycan of TRPV5 and a sialidase-mediated stimulation that is lipid raft-dependent and independent of the N-glycan of TRPV5.

Introduction

Calcium (Ca^{2+}) plays a crucial role in multiple physiological processes such as muscle contraction, neuronal excitability, enzymatic activity, bone formation, cell membrane formation and exocytosis. It is of physiological importance to tightly regulate intra- and extracellular Ca^{2+} levels. To this end, the Ca^{2+} balance is maintained by the bone, kidney, duodenum and parathyroid glands (1). Secretion of parathyroid hormone (PTH) by the parathyroid glands results in increased Ca^{2+} re(ab)sorption from both bone and kidney. The rate-limiting step in renal active Ca^{2+} reabsorption is the uptake by the transient receptor potential vanilloid type 5 (TRPV5) channel, which is apically expressed in the distal convoluted tubule (DCT) of the kidney (2-5). The channel is responsible for 3-7% of the total Ca^{2+} reabsorption (6). TRPV5 is a tetrameric membrane protein containing 6 transmembrane segments, with a cytosolic amino- and carboxyl-terminus and an extracellular N-glycan at Asn 358. The N-glycan is an important post-translational regulatory site, that can affect the plasma membrane retention of the channel (7).

Previous studies have shown that intracellular N-glycans contribute to signalling processes, dimer formation, membrane trafficking and polarized sorting of glycoproteins to the apical surface of epithelial cells (8,9). Extracellular N-glycans of plasma membrane glycoproteins are involved in signalling processes, apoptosis and cell-cell contacts. The composition of these glycans and the properties of the glycoproteins can be influenced by the activity of extracellular glycosidases (10-12). For example, previous studies demonstrated that sialidase, a glycosidase, affects caveolar-mediated endocytosis by interacting with glycolipids in the plasma membrane (13). Trafficking of TRPV5 is crucial for controlling its abundance at the plasma membrane and therefore, the Ca^{2+} reabsorption.

A protein that modifies the extracellular N-glycan of TRPV5 is the type-1 glycoprotein, klotho (7,14,15). Klotho is a glycosidase that participates in the degradation of glycans and thereby affects different glycoproteins (7,15-17). Other glycosidases, such as -glucuronidase and sialidase, mimic the plasma membrane stabilization effect of klotho on TRPV5 by modifying its N-glycan. It was hypothesized that klotho had β-glucuronidase activity, because this enzyme had homology with β-glucuronidase and is able to hydrolyze glucuronic acids (16). Treatment of Human embryonic kidney 293 cells (HEK293) expressing TRPV5 with β-glucuronidase also increased the Ca^{2+} uptake through TRPV5 (7). However, Tohyama *et al.* found that the β-glucuronidase activity of klotho is approximately 26 times lower than that of β-glucuronidase (16). In addition, two highly conserved glutamate residues, essential for the enzymatic activity of β-glucuronidase, are not conserved in klotho. Furthermore, glucuronic acids are uncommon moieties in N-glycans of membrane proteins such as TRPV5. Cha *et al.* proposed that klotho operates instead as an exo-sialidase, specifically breaking the α-2,6 linked bonds of the negatively charged sialic acids (14). They postulated that in Chinese hamster ovary (CHO) cells, cleavage of sialic acids by klotho exposes the underlying disaccharide galactose-β-(1-4)-*N*-acetylglucosamine, followed by binding of galectins, a group of carbohydrate-binding proteins with a high affinity for the exposed galactose-*N*-acetylglucosamine disaccharides.

One of the galectin family members is galectin-1, a polyvalent protein expressed in various tissues and with a wide range of biological activities. It is suggested that galectin-1 forms a stable complex with TRPV5, resulting in a stimulatory effect on Ca^{2+} reabsorption by TRPV5 retention at the cell surface (14). Galectin-1 is present in both extra- and intracellular compartments, where it binds to carbohydrate and non-carbohydrate molecules, respectively (18). Galectin-1 is found in human tubular epithelial cells and in extensive amounts in the porcine kidney (19).

The aim of the present study was to investigate the underlying molecular mechanism of the klotho-mediated TRPV5 regulation and the involvement of galectins. To this end, we delineated the action of different glycosidases, *viz*. klotho and sialidase. Total Internal Reflection Fluorescent Microscopy (TIRF-M) combined with a photo-switchable fluorescent protein enabled us to study the dynamics of TRPV5 proteins on the plasma membrane in HEK293 cells. Finally, isoelectric focusing (IEF), allowed the detection of klotho-mediated sialic acid hydrolysis on a model glycoprotein, transferrin.

Experimental procedures

DNA constructs

The pCINeo/IRES-GFP plasmid encoding TRPV5 was generated as described previously (20). TRPV5^{N358Q} was obtained by *in vitro* mutagenesis of TRPV5-pCINeo/IRES-GFP cDNA according to the manufacturer's instructions (Stratagene, La Jolla, CA, USA). The pcDendra-2 (Evrogen, Moscow, Russia) was amplified by PCR and ligated into the pCINeo/IRES-HA TRPV5 construct using the *NheI* and *EcoNI* (New England Biolabs, Ipswich, MA, USA) restriction sites. All constructs were verified by DNA sequence analysis.

Immunoblotting and protein concentration determination

TRPV5 protein expression was determined by 8 % (w/v) SDS-PAGE and Western-blotting using anti-TRPV5 (1:4.000, (21)) with peroxidase-labeled goat anti-mouse IgG (1:10.000, Sigma-Aldrich, St. Louis, MO, USA) antibodies. Protein concentration was measured using the BCA protein assay kit (Thermo Scientific, Rockford, IL, USA), according to the manufacturer's manual.

Electrophysiology

Whole-cell currents were measured with an EPC-10 (HEKA electronic) amplifier using Patchmaster V2.20 software. The borosilicate glass electrode resistance was between 2.5 and 4 MΩ. The ramp protocol for measuring the current-voltage (*I*/*V*) relationship of Na^+ consisted of linear voltage ramps from -100 to +100 mV within 450 ms repeated every 5 s. The step protocol for measuring the Ca^{2+} current consisted of a 10 s long voltage-step applied from +70 to -100 mV. Current traces were sampled at 0.5 ms for the ramp and 2 ms for step protocol. Reported current densities were calculated from the current at -80 mV during the ramp protocol. The standard extracellular solution contained 150 mM NaCl, 6 mM CsCl, 10 mM HEPES (pH 7.4 adjusted with NaOH), 50 µM EDTA and 10 mM glucose. For Ca^{2+} current measurements NaCl was replaced with equimolar NMDG-Cl and 10 mM $CaCl_2$ was added. Osmotic differences were adjusted by adding a respective amount of mannitol. The internal (pipette) solution contained 20 mM CsCl, 100 mM Cs-aspartate, 1 mM $MgCl_2$, 10 mM BAPTA, 4 mM Na_2ATP and 10 mM HEPES (pH 7.2 adjusted with CsOH). Data was analyzed using Igor-pro software (WaveMetrics, Oswego, OR, USA).

$^{45}Ca^{2+}$ uptake assay

HEK293 cells were transiently transfected with TRPV5 in pCINeo/IRES-GFP, TRPV5^{N358Q} in pCINeo/IRES-GFP or the empty pCINeo/IRES-GFP vector (mock). One day after transfection, cells were reseeded on poly-L-lysine-coated (0.1 mg/ml) culture dishes and incubated with recombinant klotho (2 µg/ml, R&D systems, Minneapolis, MN, USA), sialidase from *Vibrio Cholerae* (27 mU/ml, Sigma-Aldrich), β-glucuronidase from bovine liver (310 U/ml, Sigma-Aldrich), endoF (1 kU/ml, New England), a combination of glycosidases, or human galectin-3 (0.67 µg/ml, Prospec, Ness Ziona, Israel) for 16 h at 37 °C. Radioactive $^{45}Ca^{2+}$-

uptake in TRPV5-transfected HEK293 cells was determined as described previously (22).

Plasma membrane biotinylation and TRPV5 cell surface turnover
HEK293 cells were transiently transfected with TRPV5 in pCINeo/IRES-GFP, TRPV5^{N358Q} in pCINeo/IRES-GFP or the empty pCINeo/IRES-GFP vector (mock). One day after transfection, cells were reseeded on poly-L-lysine-coated (0.1 mg/ml) culture dishes and incubated with recombinant klotho (2 µg/ml, R&D systems), sialidase from *Vibrio Cholerae* (27 mU/ml, Sigma-Aldrich), β-glucuronidase from bovine liver (310 U/ml, Sigma-Aldrich), or endoF (1 kU/ml, New England Biolabs) for 16 h at 37 °C. Subsequently, cells were biotinylated as described previously (7). For time point 0 h cells were collected from the plates and disrupted in 1 ml lysis buffer [1 % (v/v) NP-40, 150 mM NaCl, 5 mM EDTA, 50 mM Tris (pH 7.5 adjusted with HCl), 1 mM PMSF, 10 µg/ml leupeptin, 10 µg/ml pepstatin, 5 µg/ml proteinase A] immediately after biotinylation. For the other investigated time points, cells were cultured in the absence of glycosidases for an additional 1 or 3 h at 37 °C, subsequently washed with ice-cold PBS and homogenized in 1 ml lysis buffer. TRPV5 protein expression at the cell surface and in total cell lysate was investigated as described previously (7).

III

Total Internal Reflection Microscopy (TIRF-M)
HEK293 cells were transiently transfected with pcDNA3-Dendra2-HA-TRPV5 and pcDNA3-Dendra2-HA-TRPV5^{N358Q} 24 h before the experiment. TIRF-M cells were harvested in 15 ml tubes and resuspended in conditioned medium containing recombinant klotho (2 µg/ml, R&D systems) or sialidase from *Vibrio Cholerae* (27 mU/ml, Sigma-Aldrich). The tubes were rotated for 1.5 h at 37 °C to increase the effective reactive surface of the cells. Cells were reseeded on small petri dishes (WilCo, Amsterdam, The Netherlands) coated with 50 µg/ml fibronectin and cultured for 2-7 h before subjected to TIRF-M. Dishes were washed and placed in a custom-made chamber with Krebs buffer (135 mM NaCl, 5 mM KCl, 1.5 mM $MgCl_2$, 1.5 mM $CaCl_2$, 20 mM HEPES (pH 7.4 with NaOH), 10 mM D-glucose,) and imaged at room temperature. The Olympus Fluoview FV1000-IX81 confocal microscope, with fully integrated TIRF module, and equipped with a PLAPON60xO/TIRFM-SP – PlanApochromatic objective 60x oil, NA 1.45 and WD = 0,10 mm lens was used to measure fluorescence. Photoconversion of Dendra2 was carried out using a 405 nm laser for 2 s. TRPV5 membrane trafficking was followed for about 36 min and every 3 min images were acquired of unswitched (488 nm laser, 20 frames/5 s) and switched (559 nm laser, 20 frames/5 s) dendra-TRPV5 proteins. All imaging acquisition was performed with Cell^M (Tokyo, Japan).

Biotinylation of TRPV5
HEK293 cells transiently transfected with TRPV5 in pCINeo/IRES-GFP, TRPV5^{N358Q} in pCINeo/IRES-GFP, or the empty pCINeo/IRES-GFP vector (mock) were reseeded on poly-L-lysine-coated (0.1 mg/ml) culture dishes one day after transfection and incubated with sialidase from *Vibrio Cholerae* (27 mU/ml, Sigma-Aldrich) or recombinant klotho (2 µg/ml, R&D systems) for 16 h at 37 °C. Subsequently, cells were biotinylated, lysed, and the biotinylated proteins were precipitated from the cell lysate with neutravidin beads (Pierce, Etten-leur, The Netherlands) as described previously (7). For the biotinylation after filipin treatment, the same protocol was used, but the cells were treated with filipin (5 µg/ml, Sigma-Aldrich) for 45 min prior to lysis.

Transferrin Isoelectric focusing (tIEF)
The IEF assay was carried out as previously described (23), with the following differences. Briefly, plasma samples were incubated for 30 min, with a solution of 6.7 mM ferric citrate and 0.17 M sodium hydrogen carbonate, in a ratio of 1:1 (plasma to solution), to saturate the transferrin with iron. The iron-saturated plasma was treated with 2 U/ml sialidase (Roche Applied Science, Mannheim, Germany), 150 µg/ml recombinant klotho (R&D systems) or left untreated for each of the investigated time points (1, 2, 4, 7 h or overnight). Subsequently, the samples were applied to a hydrated immobiline gel (pH 5-7) on a PhastSystem (GE-Healthcare Life Sciences, Piscataway, USA). Transferrin isoforms were detected after immunofixation with rabbit anti-human transferrin antibody (Dako, Glostrup, Denmark) and Coomassie brilliant blue staining.

COPAS Sorting and PCR
Transgenic mice expressing eGFP under the control of the TRPV5 promoter have been described previously (24). Fluorescently labeled DCT/CNT tubules were isolated from transgenic animals, using a Complex Object Parametric Analyzer and Sorter (COPAS) sorter (Union Biometrica, Somerville, MA) as previously described (25,26). The animal ethics board of the Radboud University Nijmegen approved all of the experimental procedures. Tubular, HEK293 and CHO cell RNA was extracted using TRIzol Total RNA Isolation Reagent (Life Technologies BRL, The Netherlands) and processed into cDNA. The cDNA was mixed with Power SYBR green PCR Mastermix (Applied Biosystems, Foster City, CA) and exon-overlapping primers against TRPV5 and galectin-1 and -3.

Statistical analysis
In all experiments, the data are expressed as mean ± S.E.M. Statistical significance ($p < 0.05$) was determined by analysis of variance and a Bonferroni post-hoc test.

Results
Stimulation of TRPV5 plasma membrane retention by glycosidases
To study the molecular mechanism of the klotho-dependent TRPV5 stimulation, we investigated the effect of various glycosidases on the activity of the channel. HEK293 cells transiently over-expressing TRPV5 were treated with recombinant mouse klotho (2 µg/ml), sialidase (27 mU/ml), β-glucuronidase (310 U/ml) or endoglycosidase-F (endoF) (1 kU/ml) for 16 h and subjected to patch clamp analysis. HEK293 cells transfected with TRPV5 all showed typical representative inwardly-rectifying I/V curves. Fig 1A represents cells transiently transfected with TRPV5, untreated or treated with klotho or endoF. The tested glycosidases significantly increased the TRPV5-mediated Na^+ current density (Fig 1B), while the current density of mock-transfected cells was not affected (data not shown). The stimulation of TRPV5 channel activity was confirmed by measuring $^{45}Ca^{2+}$ uptake in cells after glycosidase treatment (Fig 1C). EndoF showed the highest stimulation of TRPV5 (205±6%), but also β-glucuronidase, sialidase and klotho increased significantly the TRPV5-dependent Ca^{2+} uptake (166±4%, 147±8%, 155±4%, respectively, $P<0.05$).

Subsequently, we investigated the plasma membrane retention via time-chase analysis. HEK293 cells expressing TRPV5 were treated for 16 h with different glycosidases and subjected to cell-surface biotinylation. To follow the fate of the biotinylated proteins, the cells were incubated for 0, 1 or 3 h without glycosidases. In untreated cells, the amount of biotinylated TRPV5 decreased significantly after 1 and 3 h compared to the initial time point (0 h) (Fig 1D*, upper panels*). For klotho, sialidase and endoF treated

cells, only a small decrease of biotinylated TRPV5 channels was detected after 1 and 3 h (Fig 1D*, upper panels*). The total expression of TRPV5 was not significantly altered by the glycosidase treatment (Fig 1D*, lower panels*).

To further e lucidate the mechanism responsible for the increase in TRPV5 activity after glycosidase treatment, the N-glycosylation-deficient mutant TRPV5^{N358Q}, was subjected to time-chase analysis. Compared to wild-type TRPV5 the plasma membrane abundance of the mutant TRPV5^{N358Q} channel was markedly stable, even after 3 h of incubation (Fig 1E).

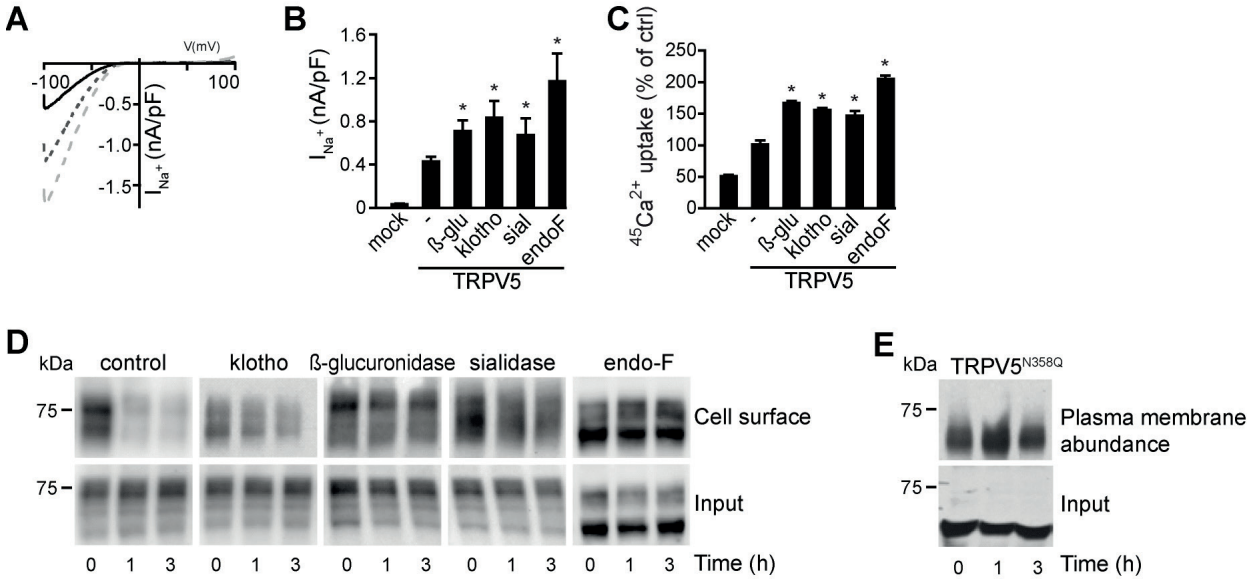

Figure 1. Different glycosidases increase the TRPV5-mediated Ca^{2+}uptake via plasma membrane stabilization of the channel.
A) The I/V relationships of untreated, klotho- or endoF-treated HEK293 cells expressing TRPV5 are presented. Solid line represents untreated cells, dashed line represents klotho-treated cells (light grey) and the dotted line represents endoF-treated cells (dark grey). **B)** The TRPV5-mediated Na^+ current in HEK293 cells was measured. Treatment with β-glucuronidase, klotho, sialidase or endoF all resulted in a significantly increased current (n=17-42). **C)** $^{45}Ca^{2+}$ uptake assays of HEK293 cells transfected with TRPV5 or the empty vector (mock). These cells were untreated or treated with glycosidase (β-glucuronidase, klotho, sialidase or endoF). **D)** Time-chase assay of cells transfected with TRPV5. The membrane proteins were biotinylated at 0 h. After 3 h incubation without glycosidase, the membrane fraction of TRPV5 was decreased. **E)** Time-chase assay of cells transfected with TRPV5^{N358Q}. All data are presented as mean ± SEM; n=3; *P< 0.05, statistically significant.

Glycosidase treatment retains TRPV5 at the plasma membrane

Traditional time-chase experiments are not able to distinguish between delayed recycling of proteins from the plasma membrane or reduced degradation. To overcome this limitation, we established a novel approach by combining live-cell TIRF-M with a photo-convertible (green to red) fluorescent protein, Dendra-2, that was fused to the N-terminus of the TRPV5 channel (27). Via this technique an evanescent field at the glass-cell membrane interface permitted specific detection and excitation of the channels close to the plasma membrane (~ 70-100 nm). Proteins in close vicinity to the plasma membrane were photo-switched in TIRF mode using evanescent UV light (λ=405 nm). TIRF-M images are shown of the control and treated conditions for Dendra-2-TRPV5 and Dendra-2-TRPV5^{N358Q}, captured at the initial time point after photo-switching and after 30 min (Fig 2A,B). The ratio of fluorescent intensity at an initial time point was calculated by (Fi-Fo)/Fo, where Fo= fluorescent intensity at an initial time point and Fi= fluorescent intensity at a new time point. To follow the presence of the protein at the plasma membrane in time, the ratio

between the switched red fraction (F_{559}) and unswitched green fraction (F_{488}) was calculated ((F_{559} /F_{488})/(F_{559} /F_{488})$_{max}$). After treatment with sialidase (70±3%) or klotho (75±4%) the ratio at 30 min was significantly increased compared to control (47±8%) indicating that TRPV5 is more stable at the plasma membrane (Fig 2C). To investigate whether there is a glycosidase-dependent effect on the N-glycosylation-deficient mutant, Dendra-2-TRPV5^{N358Q} was subjected to klotho and sialidase treatment. After glycosidase treatment, no significant decrease in the fluorescent ratio of Dendra-2-TRPV5^{N358Q} was found (Fig 2D).

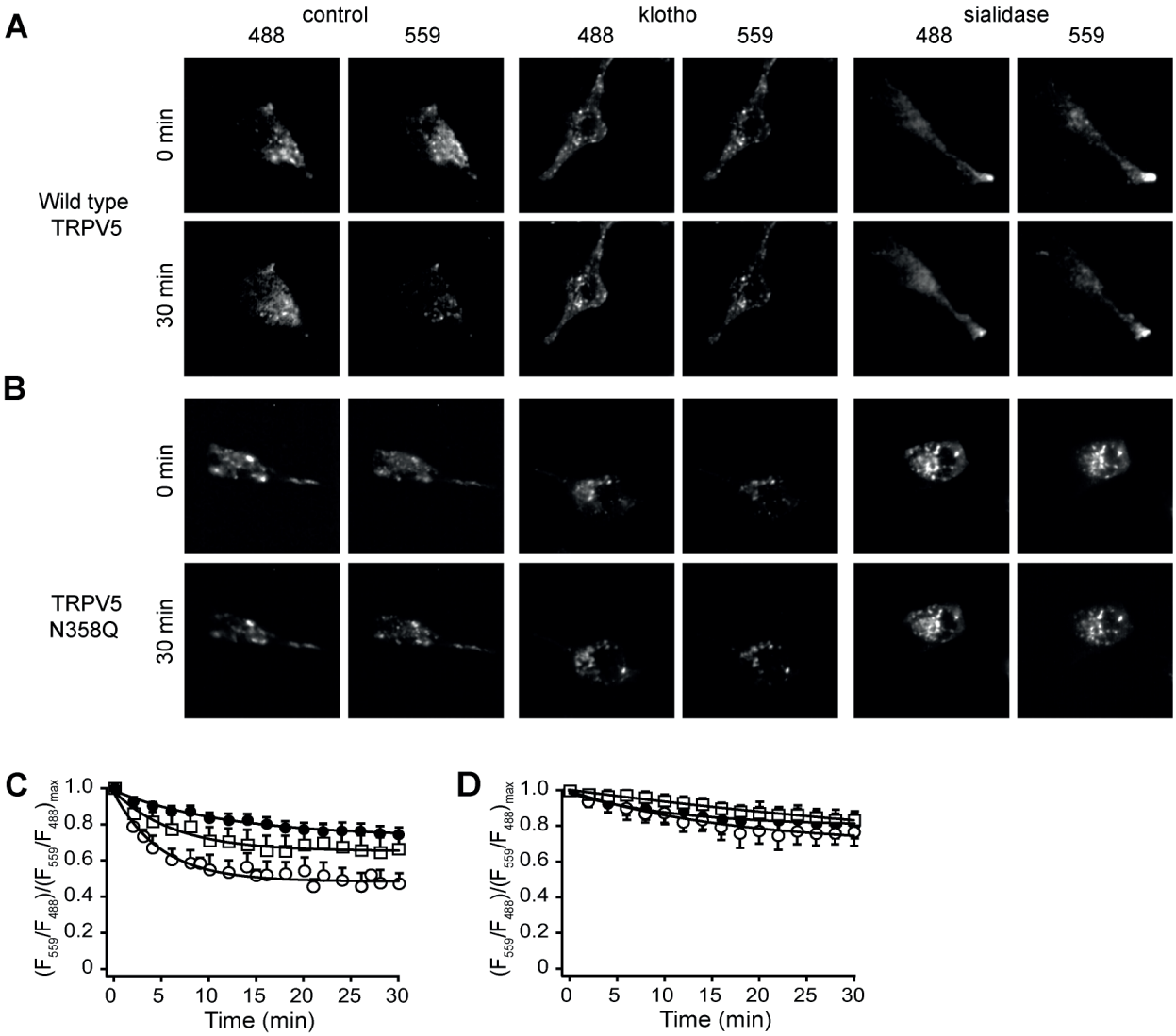

Figure 2. Klotho and sialidase stabilize TRPV5 on the plasma membrane.
A, B) TIRF-M images of HEK293 cells expressing Dendra-2-TRPV5 or Dendra-2-TRPV5^{N358Q} in both red and green channels, after 0 and 30 min. **C)** Ratio of switched red/unswitched green fraction of HEK293 cells expressing Dendra-2-TRPV5. These cells were subjected to live-cell TIRF-M. At 0 min Dendra-2 was subjected to UV light (λ=405 nm), resulting in a switch from green to red. **D)** Ratio of switched red/unswitched green fraction of HEK293 cells expressing Dendra-2-TRPV5^{N358Q} These cells showed no increase in plasma membrane retention after glycosidase treatment. ○ Control; □ klotho treated; ● sialidase treated. All data are expressed as mean ± SEM; n=3.

Klotho and sialidase regulate TRPV5 plasma membrane retention differently

TIRF-M showed that the cells expressing TRPV5^{N358Q} appeared brighter after sialidase treatment, but not after klotho treatment. The difference between sialidase-treated and klotho-treated HEK293 cells expressing TRPV5^{N358Q} was further investigated. Treatment with klotho of the cells expressing TRPV5^{N358Q} did not alter the plasma

membrane availability of this mutant as detected by cell surface biotinylation (104±6%, P>0.2) (Fig 3A,B). For the cells transfected with wild-type TRPV5, the TRPV5 plasma membrane fraction significantly increased after klotho treatment (140±9%, P<0.05). In contrast, sialidase treatment enhanced the plasma membrane fraction of both TRPV5 and TRPV5^{N358Q} (151±8% and 153±7%, respectively, P<0.05) (Fig 3C,D). The distinct actions of klotho and sialidase were further studied by $^{45}Ca^{2+}$ uptake assays. In line with our biochemical observations, klotho augmented the $^{45}Ca^{2+}$ influx in HEK293 cells transfected with TRPV5 (120±2%), but not in cells expressing TRPV5^{N358Q} (103±5%) (Fig 3E). In contrast, sialidase increased TRPV5-mediated $^{45}Ca^{2+}$ uptake in TRPV5-expressing cells (150±11%) as well as in cells expressing TRPV5^{N358Q} (149±10%) (Fig 3E). Co-treatment with sialidase and klotho resulted in an additive increase in TRPV5-mediated Ca^{2+} influx (170±8%). In contrast, no additional $^{45}Ca^{2+}$ influx was observed after treatment of cells over-expressing TRPV5^{N358Q} (149±10% versus 144±9%). The TRPV5 blocker ruthenium red was applied to determine the magnitude of the TRPV5-mediated $^{45}Ca^{2+}$ influx (28).

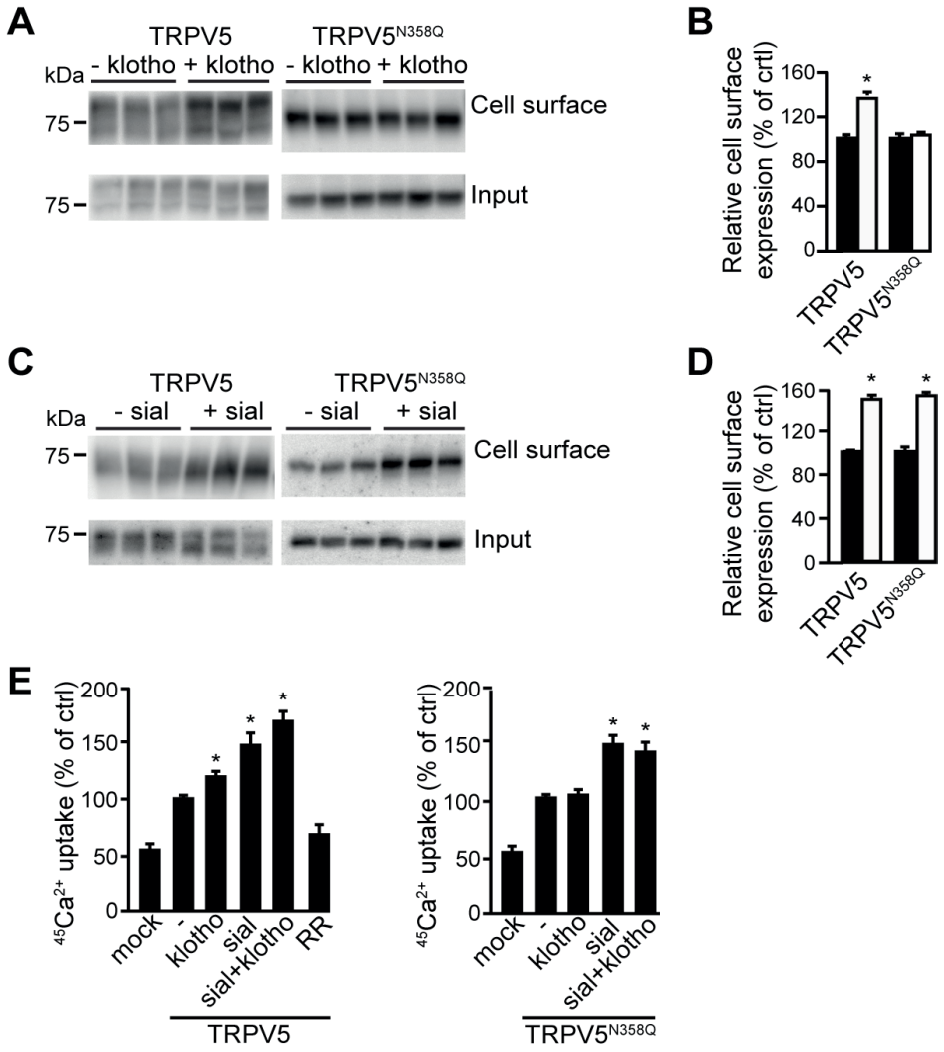

Figure 3. TRPV5 stabilization via klotho is N-glycan dependent.
A) Biotinylation of HEK293 cells expressing TRPV5 or TRPV5^{N358Q} after klotho treatment, a representative blot is depicted; **B)** Relative TRPV5 cell surface expression with or without klotho treatment (white and black bar, respectively); **C)** Biotinylation of HEK293 cells expressing TRPV5 or TRPV5^{N358Q} after sialidase treatment, a representative blot is depicted; **D)** Relative TRPV5 cell surface expression with or without sialidase treatment (n=3) (white and black bar, respectively); **E)** $^{45}Ca^{2+}$ uptake assay of cells transfected with TRPV5 or TRPV5^{N358Q} after treatment with klotho, sialidase, a combination of these glycosidases, ruthenium red or left untreated. All data are presented as mean ± SEM; n=3; *P< 0.05, statistically significant.

Disruption of lipid rafts increases TRPV5 plasma membrane abundance

Sialidase is known to affect protein trafficking by interacting with glycolipids in lipid rafts (13). To determine whether TRPV5 is present in lipid rafts, lipid rafts in HEK293 cells expressing either TRPV5 or TRPV5^{N358Q} were disrupted using the cholesterol-chelating drug filipin. After filipin treatment, cell surface biotinylation showed a significant increase in TRPV5 and TRPV5^{N358Q} abundance at the plasma membrane (120±8% versus 121±4%, respectively, P<0.05) (Fig 4A,B,C). Likewise, $^{45}Ca^{2+}$ uptake assays revealed a proportional increase in the functional activity of TRPV5 and TRPV5^{N358Q} after filipin treatment (119±3% versus 122±4%, respectively, P<0.05) (Fig 4D). A combination of filipin and klotho significantly stimulated TRPV5-mediated $^{45}Ca^{2+}$ uptake (100±6% versus 143±10%, P<0.05). No additional $^{45}Ca^{2+}$ uptake was observed after combining sialidase with filipin (100±6% versus 113±6%) (Fig 4E).

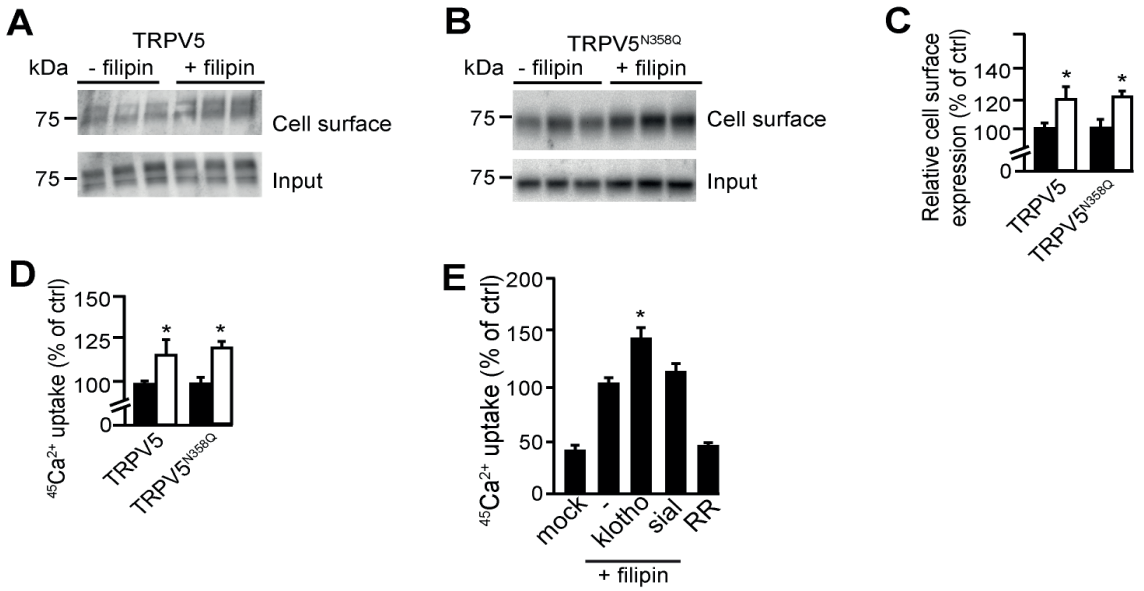

Figure 4. TPRV5 plasma membrane retention is regulated via lipid rafts.
A) Biotinylation of HEK293 cells expressing TRPV5 after filipin treatment, a representative blot is depicted. **B)** Biotinylation of cells expressing TRPV5^{N358Q} after filipin treatment, a representative blot is depicted. **C)** Relative cell surface expression, with or without filipin treatment (white and black bar, respectively), of TRPV5 (n=6) or TRPV5^{N358Q} (n=3) over-expressing cells. **D)** $^{45}Ca^{2+}$ uptake assay in the presence of filipin (n=3). Filipin significantly increases $^{45}Ca^{2+}$ uptake independent on the N-glycan of TRPV5 (white bar). **E)** $^{45}Ca^{2+}$ uptake assay in the presence of filipin and klotho or sialidase (n=3). Klotho significantly increased TRPV5-dependent $^{45}Ca^{2+}$-uptake in the presence of flilipin, while sialidase treatment gave no additional effect. All data are presented as mean ± SEM; *P< 0.05, statistically significant.

Sialidase and klotho modify the N-glycan of transferrin in a different manner

The difference between klotho and sialidase was further confirmed by isoelectric focusing (IEF), using human blood transferrin as a model glycoprotein. Via this technique, proteins are separated based on their isoelectric focus point. Since sialic acids are negatively charged, a change in the isoelectric focusing pattern can be detected after sialidase treatment. Plasma transferrin was used as model glycoprotein, since its isoelectric focusing point after removal of the sialic acids has been characterized. The main isoform of human plasma transferrin contains two complex biantennary N-glycans, each terminated by two α-2,6-linked sialic acids (23). The protein was treated with klotho (150 µg/ml) or sialidase (2 U/ml) for different time intervals. Sialidase treatment resulted in a clear shift in the IEF pattern of transferrin, indicating the loss of sialic acids (Fig 5A). Before treatment, a main isoform with four sialic

acids was detected and after 2 h of sialidase treatment all sialic acids were cleaved. Treatment with klotho did not significantly alter the IEF pattern of transferrin (Fig 5B).

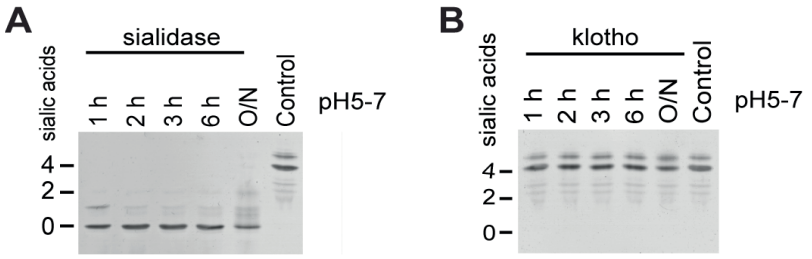

Figure 5. The isoelectric focusing pattern of transferrin is not modified by klotho.
A) Isoelectric focusing of transferrin (tIEF) after sialidase treatment. Hydrolysis of sialic acids by sialidase treatment results in a shift of the IEF pattern. **B)** Isoelectric focusing of transferrin after klotho treatment. Klotho has no influence on the amount of sialic acids.

III

Galectin-3 partially mediates klotho-dependent TRPV5 activity

The premise that klotho might not be a specific sialidase, would add new mechanistic data to the hypothesis proposed by Cha *et al*., who suggested that galectin-1 stabilizes TRPV5 on the plasma membrane after N-glycan modification by klotho-mediated sialidase activity. In CHO cells they showed that the stimulatory klotho effect on TRPV5 was absent after the knock down of galectin-1 (14). However, immunohistochemistry of mouse kidney sections failed to show co-localization between TRPV5 and galectin-1 (Fig 6A). In addition, galectin-1 was expressed in CHO cells, but not in HEK293 cells, that were used for this study (Fig 6B). Since the potential ligands for galectin-1 and galectin-3 are similar (29), the expression of galectin-3 in mice sections, HEK293 cells and in Complex Object Parametric Analyzer and Sorter (COPAS)-sorted distal convoluted and connecting tubules (DCT/CNT) was checked. Galectin-3 showed a clear co-localization with TRPV5 in mice kidney sections. Some tubuli were positive for galectin-3, but not for TRPV5, indicating that galectin-3 activity is not restricted to TRPV5-expressing tubuli (Fig 6C). Galectin-3 also expressed in HEK293 cells, as was shown by RT-PCR (Fig 6D). The expression of galectins in the DCT/CNT was further studied after collecting the nephron segments from mouse kidney, by the COPAS large particle flow cytometry (25). In isolated DCT/CNT segments, only galectin-3 mRNA was detected by RT-PCR (Fig 6E). In addition, in mouse urine, only galectin-3 was found, which implies that it has access to the glycan of TRPV5 (Fig 6F).

The involvement of galectin-3 in TRPV5 regulation was further investigated. HEK293 cells, transiently over-expressing TRPV5 were treated with 0.67 µg/mL recombinant human galectin-3. $^{45}Ca^{2+}$ uptake assays revealed an increase in TRPV5 channel activity after galectin-3 treatment (100±2% versus 131±6%, $P<0.05$) (Fig 7A), while the activity of the $TRPV5^{N358Q}$ mutant was not affected by galectin-3 treatment (100±2% versus 104±4%) (Fig 7A). Combining galectin-3 and klotho-treatment, or galectin-3 and sialidase-treatment, did not result in additional stimulation of channel activity (Fig 7B).

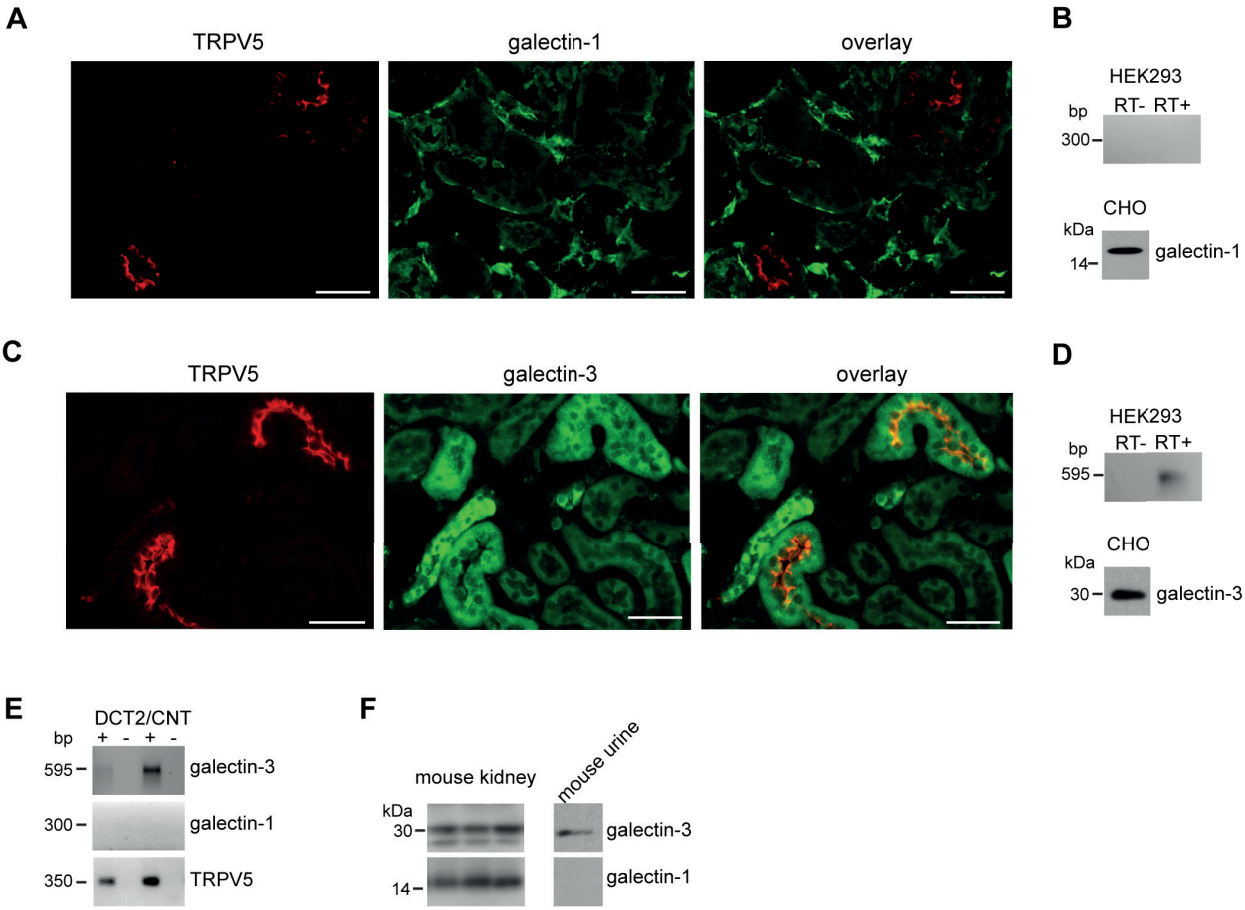

Figure 6. Galectin-3 is a candidate mediator of the klotho effect on TRPV5.
A) Immunohistochemistry on DCT/CNT for TRPV5 and galectin-1 shows no co-localization. **B)** Immunoblot of CHO cell lysate demonstrated that galectin-1 was present. After RT-PCR on the cDNA of HEK293 cells, no galectin-1 was detected. **C)** Immunohistochemistry on DCT/CNT for TRPV5 and galectin-3 demonstrate a co-localization. **D)** Immunoblot of CHO cell lysate demonstrated that galectin-3 was expressed. After RT-PCR on the cDNA of HEK293 cells, galectin-3 was detected. **E)** The cDNA of the DCT/CNT cells was analyzed by RT-PCR and only galectin-3 was detected. **F)** Total kidney lysate of mouse contains both galectin-1 and galectin-3, while mouse urine only contains galectin-3.

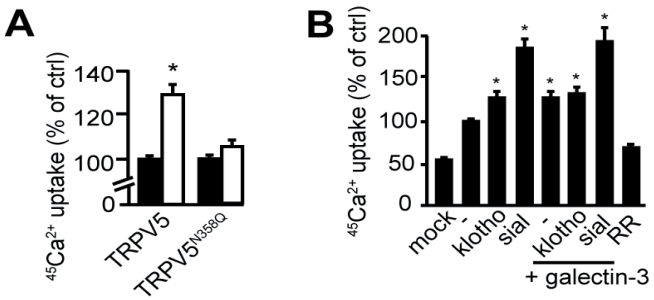

Figure 7. TRPV5 channel activity is regulated by extracellular galectin-3.
A) $^{45}Ca^{2+}$-uptake assay in cells over-expressing TRPV5 (n=5) or TRPV5^{N358Q} (n=3) in the presence and absence of human galectin-3. Galectin-3 significantly increased wild type TRPV5 (white bar) but not TRPV5^{N358Q} channel activity (white bar). All data are presented as mean ± SEM; *P<0.05, statistically significant. **B)** $^{45}Ca^{2+}$ uptake assay of cells over-expressing TRPV5 treated with klotho, sialidase, galectin-3 or a combination of these enzymes. No additional stimulation was detected after treatment with klotho and galectin-3. All data are presented as mean ± SEM; n=5; *P< 0.05, statistically significant.

Discussion

Our study demonstrates that glycosidases augment the plasma membrane retention of TRPV5, where klotho and sialidase increase the TRPV5 plasma membrane fraction via distinct mechanisms. The effect of sialidase, in contrast to klotho, is independent of the glycosylation status of TRPV5. Moreover, galectin-3 is a potential mediator for klotho-dependent TRPV5 stabilization. Our conclusions are based on the following observations: *i*) biochemical assays show that klotho, sialidase, β-glucuronidase and endoF increase the TRPV5 channel activity and membrane retention; *ii*) the plasma membrane stability of $TRPV5^{N358Q}$ is altered by sialidase, but not by klotho; *iii*) IEF demonstrate no modification of the N-glycan sialic acids after klotho treatment in transferrin; *iv*) only galectin-3, but not galectin-1, co-localizes with TRPV5 in DCT/CNT of the kidney; *v*) galectin-3 increases the TRPV5-mediated Ca^{2+} influx N-glycan dependent.

It was demonstrated that glycosidase treatment increases the TRPV5 channel activity. This effect was detected by treatment with different types of glycosidase (endoF, sialidase and β-glucuronidase). TRPV5 channel activity was measured via time-chase experiments in combination with functional analyses (7,14). A general mechanism or pathway for all the applied glycosidases remains unknown, since their enzymatic effects are distinct: endoF cleaves the entire N-glycan (30), sialidase hydrolyses end-standing sialic acids, while β-glucuronidase cleaves glucuronic acids (31). One hypothesis is that any modification of the N-glycan improves the plasma membrane stabilization of TRPV5. Alternatively, since all glycans on the plasma membrane were hydrolyzed, the detected stabilizing effect could be independent of the N-glycan of TRPV5. This would mean that the plasma membrane stabilization is due to an indirect effect on TRPV5. However, the stimulatory effect of klotho is dependent on the N-glycan of TRPV5.

Plasma membrane retention can occur via two distinct routes; a delayed retrieval from the plasma membrane and subsequent degradation of the channel, or via an accelerated/increased insertion at the plasma membrane. It is difficult to distinguish between both routes based on time-chase experiments. To pinpoint the fate of glycosidase-treated TRPV5, we developed a novel assay, combining the live-cell imaging technique, TIRF-M, with photoactivatable fluorophores. Important advantages of TIRF-M over confocal microscopy are the higher Z resolution, high signal to noise ratio, increased contrast in fluorescence and reduced bleaching. The ease in combining kinetic studies with local information in living samples results in fast data acquisition (32). We showed that TRPV5 has a reduced mobile fraction after sialidase- or klotho-treatment, indicating that these glycosidases enable TRPV5 to reside longer on the plasma membrane. Our control, $TRPV5^{N358Q}$ lacks N-glycosylation and is devoid of any glycosylation-dependent regulation. This mutant demonstrated no decrease in the mobile fraction after glycosidase treatment. Overall this mutant had a smaller mobile fraction compared to TRPV5.

While conducting the TIRF-M based live-cell imaging it was observed that after sialidase treatment, the cells expressing $TRPV5^{N358Q}$ appeared brighter. This effect was not detected after klotho treatment. This prompted us to investigate the effect of sialidase on $TRPV5^{N358Q}$. An increased plasma membrane abundance of $TRPV5^{N358Q}$ was detected via biotinylation, after sialidase treatment. It was noticed that biotinylated TRPV5 often runs as a smear band on SDS-PAGE. The reason for this effect remains unclear, however, it suggests that membrane TRPV5 is more heterogeneous compared to intracellular TRPV5.

The effect of sialidase treatment on the $TRPV5^{N358Q}$ mutant was confirmed using $^{45}Ca^{2+}$ uptake experiments. TRPV5-mediated $^{45}Ca^{2+}$ uptake was increased after treatment with both sialidase and klotho in an additive manner, indicating that klotho and sialidase act

via different pathways. Interestingly, Cha *et al.* postulated that sialidase did not increase the plasma membrane abundance of TRPV5^{N358Q} (14). However, in their study CHO cells were used as a model system, while in the present study HEK293 cells were employed

We proved that filipin, an inhibitor of microdomain clustering, increases the cell surface expression of TRPV5/TRPV5^{N358Q} and $^{45}Ca^{2+}$ uptake through TRPV5 and TRPV5^{N358Q}. This finding indicated that TRPV5 and TRPV5^{N358Q} channels are present and internalized in clustered microdomains. Recently, it has been suggested that sialidase prevents microdomain clustering and lipid raft formation by hydrolyzing sialic acids from glycosphingolipids (13). Microdomain clustering is known to stimulate caveolae-mediated endocytosis and since sialidase treatment inhibits this microdomain clustering, the endocytosis is reduced (13). Because TRPV5 is present in these microdomains, the channel is most likely stabilized on the plasma membrane by sialidase via reduced lipid raft formation and thereby a decreased caveolae-mediated endocytosis. In agreement with this hypothesis, sialidase treatment did not result in additional stimulation of $^{45}Ca^{2+}$ uptake after disrupting the lipid rafts by filipin. This finding, together with the sialidase-mediated stimulation of Ca^{2+} uptake via TRPV5^{N358Q}, and increased wild type TRPV5 activation after klotho treatment in the presence of filipin, suggested that klotho and sialidase act via two different pathways to modulate channel activity. Sialidase, in contrast to klotho, stimulates TRPV5 via a mechanism that is independent of the N-glycan of TRPV5.

To further confirm this hypothesis IEF was used, with the well-characterized transferrin as a model protein. Sialidase altered the IEF pattern of transferrin, a substrate exposing terminal sialic acids, including α2,6 linked sialic acids (33,34). Klotho-treatment did not result in any modification, suggesting a lack of sialidase activity of klotho. Alternatively, it is possible that sialidase activity of klotho is tightly structure-related, cleaving only one sialic acid that is presented in a specific sugar signature, which may be absent in transferrin. The difference between sialidase and klotho prompted us to investigate the following step in the proposed mechanism. Cha *et al.* suggested that galectin-1 is a key player in the regulation of TRPV5. Interestingly, immunohistochemistry on renal mouse cortex sections showed no co-localization of galectin-1 with TRPV5. Galectin-1 is not expressed in HEK293 cells and therefore the *in vitro* measured effect of klotho is likely to be galectin-1 independent. Since the potential ligands for galectin-1 and galectin-3 are highly similar, we investigated the role of galectin-3 in this process. Galectin-3 is a carbohydrate-binding protein that is highly abundant in type A intercalated cells of the cortical collecting duct and the distal tubules (35,36). An important difference between galectin-1 and galectin-3 is that the dimer galectin-1 requires a terminal galactose for binding, while the oligomer galectin-3 binds to repeating [-3Gal-β-(1-4)-GlcNAc-β-1-]$_n$ or poly-N-acetyllactosamine sequences that not necessarily contain a terminal β-galactoside residue (37). Galectin-3 co-localized with TRPV5, although the presence of galectin-3 is not restricted to TRPV5-expressing tubuli. In addition, COPAS sorted DCT/CNT cells were enriched with galectin-3 mRNA, while galectin-1 mRNA was not detected, indicating that galectin-3 may be involved in TRPV5 regulation. In contrast to the TRPV5^{N358Q} mutant, wild type TRPV5 channel activity was increased upon treatment with galectin-3. This suggests that galectin-3-mediated channel activity is dependent on the N-glycan of TRPV5. Interestingly, co-treatment with galectin-3 and klotho did not additively stimulate TRPV5 activity implying that klotho and galectin-3 stimulate TRPV5 activity in a similar manner. An interesting observation, as detected with TIRF-M, biotinylation, $^{45}Ca^{2+}$ uptake experiments and electrophysiology was the stable expression of TRPV5^{N358Q} mutant on the plasma membrane without any treatment. It

was proposed that galectin stabilizes TRPV5 on the plasma membrane. However, due to the absence of an N-glycan on the TRPV5^{N358Q} mutant, it is striking that this mutant retains on the plasma membrane. Since the TRPV5^{N358Q} mutant was transiently over-expressed, one could hypothesize that some glycosylation-deficient channels are forced to the plasma membrane. Since the entire N-glycan is absent, the protein cannot be appropriately regulated by the cell and will remain stable on the plasma membrane.

Interestingly, Kohno *et al.* demonstrated a significant difference between the internalization rates of the wild type endothelial differentiation gene-1 product (Edg-1, a G-coupled receptor) and the nonglycosylated N30D-Edg-1 mutant (38). The wild type G-coupled receptor was internalized at higher rates compared to the nonglycosylated N30D-Edg-1 receptor. However, more research for TRPV5 is needed to understand this internalization process. Another explanation could be that the channel is destabilized due to steric hindrance in the presence of the N-glycan, resulting in a reduced amount of TRPV5 on the cell surface. Consequently, any reduction of the N-glycan of TRPV5 will result in an increase of plasma membrane stability and, therefore, channel activity.

Acknowledgements

We would like to thank Dr. S. Boros (Dept. of Physiology, Nijmegen) for his help with the performed experiments, and F. van Zeeland and E. Lenssen for their assistance and support with the COPAS experiments. This work was supported by grants of the Radboud Institute for Molecular Life Sciences (RIMLS) to J.G.J. Hoenderop and F.L. van Delft, the Dutch kidney foundation (C06.2170, CP10.11), the Netherlands Organization for Scientific Research (NWO-CW 700.55.302) and EURenOmics funding from the European Union Seventh Framework Programme (FP7/2007-2013, agreement n° 305608).

III

References

1. Huang, C. L., and Moe, O. W. (2011) Klotho: a novel regulator of calcium and phosphorus homeostasis. *Pflug Arch Eur J Phy* **462**, 185-193
2. Venkatachalam, K., and Montell, C. (2007) TRP channels. *Annu Rev Biochem* **76**, 387-417
3. van de Graaf, S. F., Bindels, R. J., and Hoenderop, J. G. (2007) Physiology of epithelial Ca2+ and Mg2+ transport. *Rev Physiol Biochem Pharmacol* **158**, 77-160
4. Suzuki, Y., Landowski, C. P., and Hediger, M. A. (2008) Mechanisms and regulation of epithelial Ca2+ absorption in health and disease. *Annual review of physiology* **70**, 257-271
5. Hoenderop, J. G., and Bindels, R. J. (2008) Calciotropic and magnesiotropic TRP channels. *Physiology (Bethesda, Md* **23**, 32-40
6. Hoenderop, J. G. J., Willems, P. H. G. M., and Bindels, R. J. M. (2000) Toward a comprehensive molecular model of active calcium reabsorption. *Am J Physiol-Renal* **278**, F352-F360
7. Chang, Q., Hoefs, S., van der Kemp, A. W., Topala, C. N., Bindels, R. J., and Hoenderop, J. G. (2005) The beta-glucuronidase klotho hydrolyzes and activates the TRPV5 channel. *Science* **310**, 490-493
8. Takahashi, M., Yokoe, S., Asahi, M., Lee, S. H., Li, W., Osumi, D., Miyoshi, E., and Taniguchi, N. (2008) N-glycan of ErbB family plays a crucial role in dimer formation and tumor promotion. *Bba-Gen Subjects* **1780**, 520-524
9. Moen, A., Hafte, T. T., Tveit, H., Egge-Jacobsen, W., and Prydz, K. (2011) N-Glycan synthesis in the apical and basolateral secretory pathway of epithelial MDCK cells and the influence of a glycosaminoglycan domain. *Glycobiology* **21**, 1416-1425
10. Zhuo, Y., and Bellis, S. L. (2011) Emerging Role of alpha 2,6-Sialic Acid as a Negative Regulator of Galectin Binding and Function. *J Biol Chem* **286**, 5935-5941
11. Kawamura, S., Sato, I., Wada, T., Yamaguchi, K., Li, Y., Li, D., Zhao, X., Ueno, S., Aoki, H., Tochigi, T., Kuwahara, M., Kitamura, T., Takahashi, K., Moriya, S., and Miyagi, T. (2012) Plasma membrane-associated sialidase (NEU3) regulates progression of prostate cancer to androgen-independent growth through modulation of androgen receptor signaling. *Cell Death and Differentiation* **19**, 170-179
12. Miyagi, T., and Yamaguchi, K. (2012) Mammalian sialidases: physiological and pathological roles in cellular functions. *Glycobiology*, 1460-2423
13. Singh, R. D., Marks, D. L., Holicky, E. L., Wheatley, C. L., Kaptzan, T., Sato, S. B., Kobayashi, T., Ling, K., and Pagano, R. E. (2010) Gangliosides and beta1-integrin are required for caveolae and membrane domains. *Traffic* **11**, 348-360
14. Cha, S. K., Ortega, B., Kurosu, H., Rosenblatt, K. P., Kuro, O. M., and Huang, C. L. (2008) Removal of sialic acid involving Klotho causes cell-surface retention of TRPV5 channel via binding to galectin-1. *Proc Natl Acad Sci U S A* **105**, 9805-9810
15. Lu, P., Boros, S., Chang, Q., Bindels, R. J., and Hoenderop, J. G. (2008) The beta-glucuronidase klotho exclusively activates the epithelial Ca^{2+} channels TRPV5 and TRPV6. *Nephrol Dial Transpl* **23**, 3397-3402
16. Tohyama, O., Imura, A., Iwano, A., Freund, J. N., Henrissat, B., Fujimori, T., and Nabeshima, Y. (2004) Klotho is a novel beta-glucuronidase capable of hydrolyzing steroid beta-glucuronides. *J Biol Chem* **279**, 9777-9784
17. Cohen, D. M. (2006) Regulation of TRP channels by N-linked glycosylation. *Semin Cell Dev Biol* **17**, 630-637
18. Cho, M. J., and Cummings, R. D. (1995) Galectin-1, a Beta-Galactoside-Binding Lectin in Chinese-Hamster Ovary Cells .1. Physical and Chemical Characterization. *J Biol Chem* **270**, 5198-5206
19. Burger, A., Filsinger, S., Cooper, D. N. W., and Hansch, G. M. (1996) Expression of the 14 kDa galactose-binding protein, galectin-1, on human tubular epithelial cells. *Kidney International* **50**, 754-759
20. van de Graaf, S. F., Hoenderop, J. G., Gkika, D., Lamers, D., Prenen, J., Rescher, U., Gerke, V., Staub, O., Nilius, B., and Bindels, R. J. (2003) Functional expression of the epithelial Ca(2+) channels (TRPV5 and TRPV6) requires association of the S100A10-annexin 2 complex. *The EMBO journal* **22**, 1478-1487
21. Hoenderop, J. G., van der Kemp, A. W., Hartog, A., van de Graaf, S. F., van Os, C. H., Willems, P. H., and Bindels, R. J. (1999) Molecular identification of the apical Ca^{2+} channel in 1, 25-dihydroxyvitamin D3-responsive epithelia. *J Biol Chem* **274**, 8375-8378

22. de Groot, T., Lee, K., Langeslag, M., Xi, Q., Jalink, K., Bindels, R. J., and Hoenderop, J. G. (2009) Parathyroid hormone activates TRPV5 via PKA-dependent phosphorylation. *J Am Soc Nephrol* **20**, 1693-1704
23. van Eijk, H. G., and van Noort, W. L. (1992) The analysis of human serum transferrins with the PhastSystem: quantitation of microheterogeneity. *Electrophoresis* **13**, 354-358
24. Meyer, A. H., Katona, I., Blatow, M., Rozov, A., and Monyer, H. (2002) In vivo labeling of parvalbumin-positive interneurons and analysis of electrical coupling in identified neurons. *J Neurosci* **22**, 7055-7064
25. Dimke, H., San-Cristobal, P., de Graaf, M., Lenders, J. W., Deinum, J., Hoenderop, J. G., and Bindels, R. J. (2011) gamma-Adducin stimulates the thiazide-sensitive NaCl cotransporter. *J Am Soc Nephrol* **22**, 508-517
26. Miller, R. L., Zhang, P., Chen, T., Rohrwasser, A., and Nelson, R. D. (2006) Automated method for the isolation of collecting ducts. *American Journal of Physiology - Renal Physiology* **291**, F236-245
27. Gurskaya, N. G., Verkhusha, V. V., Shcheglov, A. S., Staroverov, D. B., Chepurnykh, T. V., Fradkov, A. F., Lukyanov, S., and Lukyanov, K. A. (2006) Engineering of a monomeric green-to-red photoactivatable fluorescent protein induced by blue light. *Nat Biotechnol* **24**, 461-465
28. Hoenderop, J. G., Vennekens, R., Muller, D., Prenen, J., Droogmans, G., Bindels, R. J., and Nilius, B. (2001) Function and expression of the epithelial Ca^{2+} channel family: comparison of mammalian ECaC1 and 2. *J Physiol* **537**, 747-761
29. Varki, A. (2009) *Essentials of glycobiology*, 2nd ed., Cold Spring Harbor Laboratory Press, Cold Spring Harbor, N.Y.
30. Suzuki, T., Park, H., and Lennarz, W. J. (2002) Cytoplasmic peptide:N-glycanase (PNGase) in eukaryotic cells: occurrence, primary structure, and potential functions. *Faseb J* **16**, 635-641
31. Chen, X., and Varki, A. (2010) Advances in the biology and chemistry of sialic acids. *ACS Chem Biol* **5**, 163-176
32. Toomre, D., and Bewersdorf, J. (2010) A New Wave of Cellular Imaging. *Annu Rev Cell Dev Bi* **26**, 285-314
33. Coddeville, B., Regoeczi, E., Strecker, G., Plancke, Y., and Spik, G. (2000) Structural analysis of trisialylated biantennary glycans isolated from mouse serum transferrin. Characterization of the sequence Neu5Gc(alpha 2-3)Gal(beta 1-3)[Neu5Gc(alpha 2-6)]GlcNAc(beta 1-2)Man. *Biochimica et biophysica acta* **1475**, 321-328
34. Spik, G., Debruyne, V., Montreuil, J., van Halbeek, H., and Vliegenthart, J. F. (1985) Primary structure of two sialylated triantennary glycans from human serotransferrin. *FEBS letters* **183**, 65-69
35. Winyard, P. J. D., Bao, Q., Hughes, R. C., and Woolf, A. S. (1997) Epithelial galectin-3 during human nephrogenesis and childhood cystic diseases. *J Am Soc Nephrol* **8**, 1647-1657
36. Kikuchi, Y., Kobayashi, S., Hemmi, N., Ikee, R., Hyodo, N., Saigusa, T., Namikoshi, T., Yamada, M., Suzuki, S., and Miura, S. (2004) Galectin-3-positive cell infiltration in human diabetic nephropathy. *Nephrol Dial Transpl* **19**, 602-607
37. Patnaik, S. K., Potvin, B., Carlsson, S., Sturm, D., Leffler, H., and Stanley, P. (2006) Complex N-glycans are the major ligands for galectin-1, -3, and -8 on Chinese hamster ovary cells. *Glycobiology* **16**, 305-317
38. Kohno, T., Wada, A., and Igarashi, Y. (2002) N-glycans of sphingosine 1-phosphate receptor Edg-1 regulate ligand-induced receptor internalization. *Faseb J* **16**, 983-992

IV

CHAPTER 4

Urinary β-galactosidase stimulates Ca^{2+} transport by stabilizing TRPV5 at the plasma membrane

Elizabeth H.P. Leunissen, Maxime G. Blanchard, Marla Lavrijsen, René J.M. Bindels, Joost G.J. Hoenderop

Department of Physiology, Radboud university medical center, Radboud Institute for Molecular Life Sciences, The Netherlands

Submitted, 2015

Abstract

Transcellular Ca^{2+} transport in the late distal convoluted tubule and connecting tubule (DCT2/CNT) of the kidney is a finely controlled process mediated by the transient receptor potential vanilloid type 5 (TRPV5) channel. A complex-type N-glycan is bound at the extracellular residue Asn358 of TRPV5 through post-translational glycosylation. This N-glycan has been postulated to regulate TRPV5 channel activity. Using *in vitro* Ca^{2+} transport assays, immunoblot analysis, immunohistochemistry, patch clamp electrophysiology and total internal reflection fluorescence microscopy, it is demonstrated that the glycosidase β-galactosidase (β-gal), an enzyme that hydrolyzes galactose, stimulates TRPV5 channel activity. This stimulation depends on the presence of the TRPV5 N-glycan, since the activity of the non-glycosylated $TRPV5^{N358Q}$ mutant was not altered in the presence of β-gal, and resulted from plasma membrane stabilization. In addition, β-gal was found to stimulate transcellular Ca^{2+} transport in isolated mouse primary DCT2/CNT cells. β-gal expression was detected at the apical membrane of the proximal tubules and in mice urine. In summary, β-gal is expressed in the pro-urine from where it is thought to stimulate TRPV5 activity.

Introduction

The extracellular calcium (Ca^{2+}) concentration is tightly regulated due to the critical involvement of Ca^{2+} in numerous signalling cascades, muscle contraction and bone mineralization (1). The transient receptor potential vanilloid type 5 (TRPV5) channel mediates the apical entry of Ca^{2+} in the kidney epithelial cell, which constitutes a finely regulated rate-limiting step in renal Ca^{2+} reabsorption (2,3). TRPV5 is expressed in the epithelial cells of the late distal convoluted tubule (DCT2) and connecting tubule (CNT) segments of the nephron, where it mediates ~5-10% of the total Ca^{2+} reabsorption in the kidney (4,5). The channel is regulated by a variety of factors including 1,25-dihydroxyvitamin D_3, parathyroid hormone, dietary Ca^{2+}, acid/base status and glycosylation (6-8).

Each subunit of the tetrameric TRPV5 channel contains an intracellular C- and N-terminus, and six transmembrane segments. TRPV5 possesses a single N-glycan on the Asn358 (N358) amino acid located in the extracellular loop situated between the first and second transmembrane domain. This glycan plays an important role in regulating the plasma membrane expression of TRPV5 channels (9-11).

Glycosylation is one of the most common post-translational modification in eukaryotic cells, as it is estimated that ~50% of the proteome is glycosylated (12). Extracellular N-glycans of plasma membrane glycoproteins are involved in signalling processes, such as apoptosis and cell-cell contacts (13). Mammalian extracellular glycosidases modify the structure of cell surface glycans by hydrolyzing specific sugars (14). For example, sialidase (also known as neuraminidase) hydrolyzes terminal sialic acids from N-glycans and gangliolipids (15), while β-galactosidase (β-gal) hydrolyzes galactose units (13). Modification of the glycan of proteins can alter substrate binding, enzymatic activity or protein stability at the plasma membrane (13,16).

Previous studies have shown that glycosidases influence TRPV5 channel activity via the N-glycan. For instance, the putative pro-urinary glycosidase klotho stabilizes TRPV5 at the plasma membrane, an effect that is absent in the non-glycosylated N358Q mutant (9-11).

A different glycosidase, β-gal, is present in its active form in the urine of human subjects (17). Deficiencies of β-gal cause human metabolic disorders such as GM1 gangliosidosis (OMIM nr.230500) and Morquio B disease (OMIM nr.253010), both characterized by heterogeneous clinical phenotypes (18,19). A common phenotype among these patients is bone malformations. Interestingly, TRPV5 knockout (-/-) mice also exhibit significant disturbances in bone structure (20).

Here, we hypothesized that β-gal regulates the activity of TRPV5 via the TRPV5 N-glycan. To investigate this hypothesis, a combination of techniques including immunoblotting, radioactive $^{45}Ca^{2+}$ uptake assays, electrophysiology and Total Internal Reflection Fluorescent Microscopy (TIRF-M) were applied. The physiological relevance of such mechanism was investigated using $^{45}Ca^{2+}$ transport assays in primary mice DCT2/CNT cells. In addition, the expression of β-gal in kidney and its presence in mouse urine were investigated.

Experimental procedures

DNA constructs

The pCINeo/IRES-GFP plasmid encoding TRPV5 was generated as described previously (21). The $TRPV5^{N358Q}$ mutant was obtained by *in vitro* site-directed mutagenesis of wild type (wt)-TRPV5-pCINeo/IRES-GFP (Stratagene, La Jolla, CA, USA). The pcDNA3-Dendra2-HA-TRPV5 and pcDNA3-Dendra2-HA-$TRPV5^{N358Q}$ vectors were generated as previously described (9). Mouse β-galactosidase (Biosource Bioscience

LifeSciences, Cambridge, UK) was subcloned into the pCINeo/IRES-GFP vector using the *XhoI* and *AscI* restriction sites. All constructs were verified using DNA sequencing.

Cell culture and transfections
HEK293 cells were grown in Dulbecco's modified eagle's medium (DMEM, Bio Whittakker-Europe, Verviers, Belgium) containing 10% (v/v) fetal calf serum (PAA, Liz Australia), 2mM L-glutamine and 10 μg/ml non-essential amino acids at 37 ºC in a humidity-controlled incubator with 5% (v/v) CO_2. HEK293 cells were transiently transfected using lipofectamine 2000 (Invitrogen, Carlsbad, CA, USA), or Polyethyleneimine (PEI) (Brunswig/PolySciences). Transfections were performed according to manufacturer's protocol.

Immunoblotting and determination of protein concentration
TRPV5 protein expression was determined by 8 % (w/v) SDS-PAGE and immunoblotted using anti-HA-tag (1:5,000, Cell Signalling Technology, Beverly, MA, USA) with peroxidase-labelled sheep anti-mouse IgG (1:10,000, Chemie Brunschwig, Basel, Switzerland) antibodies. Protein concentration was measured with a BCA protein assay kit (Thermo Scientific, Rockford, IL, USA), according to manufacturer's instructions. Two days after transfection, cells were lysed in 0.5 mL lysis buffer containing: Triton X-100 (1% v/v), 150 mM NaCl, 5 mM EDTA, 50 mM Tris/HCl pH 7.5, 1 mM phenylmethanesulfonylfluoride (PMSF), 10 μg/mL leupeptin, 10 μg/mL pepstatin A, 5 μg/mL protinin and subjected to immunoblotting. β-gal protein expression was determined by 10 % (w/v) SDS-PAGE and immunoblotting using goat anti-β-galactosidase antibody (1:250, Santa Cruz Biotechnology, Texas, USA; C-20, polyclonal) with peroxidase-labelled mouse anti-sheep IgG (1:10,000, Jackson ImmunoResearch Laboratories, Suffolk, UK) antibodies. 16μL wt mice urine was treated with 4 μL Leammli for 30 minutes at 37°C. Next, the β-gal protein expression in these samples was determined via immunoblotting.

$^{45}Ca^{2+}$ uptake assay
HEK293 cells were transfected with TRPV5, TRPV5^{N358Q} or the empty pCINeo/IRES-GFP vector (mock). One day after transfection, cells were reseeded on poly-L-lysine-coated (0.1 mg/mL) culture dishes and incubated with β-gal from *E. coli* (1 U/mL, Worthington Biochemical Corporation, Lakewood, NJ, USA), β(1-4)-gal from *Bacteroides fragilis* (20 mU/mL, New England Biolabs, Ipswich, MA, USA), β(1,3)-gal from *Xanthomonas manihotis* (20 mU/mL, New England Biolabs), or D-(+)galactose (2 μg/mL or 3 μg/mL, Sigma, St. Louis, MO, USA) for 16 h at 37 °C. Radioactive $^{45}Ca^{2+}$ uptake in TRPV5-transfected HEK293 cells was determined as previously described (22).

Electrophysiology
Experiments were performed using an EPC-9 amplifier and the Patchmaster software (HEKA electronics, Lambrecht, Germany). The sampling interval was set to 200 ms for whole-cell recordings and 20 ms for single-channel recordings. Whole-cell recordings were acquired with a low-pass filter set at 3.6 kHz, while single-channel recordings had a low-pass filter set at 5 kHz. The electrical noise was reduced further using the Humbug 50/60 Hz noise eliminator (Quest Scientific, Vancouver, Canada). Whole-cell patch clamp pipettes were pulled from thin-walled borosilicate glass (Harvard Apparatus, March-Hugstetten, Germany) and had resistances between 1 and 3 MΩ when filled with the pipette solution. Series resistance compensation was set to 75-95% in all whole-cell experiments. Single-channel patch clamp pipettes were made of thick-walled borosilicate

glass (Harvard Apparatus and World Precision Instruments) and had resistances between 8 and 11 MΩ when filled with the pipette solution. Single-channel recordings were analyzed using the Qub software package (23). Three different extracellular solutions were used to obtain whole-cell recordings of TRPV5 activity. A nominally divalent-free (nDVF) solution comprised of (in mM): 150 NaCl, 6 CsCl, 10 glucose, 10 HEPES and CsOH to adjust the pH adjusted to 7.4. A divalent-free (DVF) solution based on nDVF solution with 50 μM EGTA. A Krebs solution containing (in mM): 150 NaCl, 6 CsCl, 1 $CaCl_2$, 1 $MgCl_2$, 10 glucose, 10 HEPES and pH adjusted to 7.4 using CsOH. The pipette solution was comprised of (in mM): 20 CsCl, 100 CsAspartate, 1 $MgCl_2$, 10 BAPTA, 4 Na_2ATP, 10 HEPES and pH adjusted to 7.2 using CsOH. The extracellular solution for cell-attached recordings contained (in mM): 150 NaCl, 6 CsCl, 10 Glucose, 10 HEPES and pH adjusted to 7.4 using CsOH. The pipette solution comprised (in mM): 150 NaCl, 10 EGTA, 10 HEPES and pH adjusted to 7.3 using CsOH (24). Cells were initially bathed in nDVF extracellular solution. The whole-cell EGTA-sensitive current was obtained by measuring the current sensitive to the perfusion of 50 μM EGTA. At the end of the recording protocol, the Ca^{2+}-sensitive current was obtained by perfusion of Krebs solution containing 1 mM of $CaCl_2$.

Total Internal Reflection Fluorescent Microscopy (TIRF-M)

HEK293 cells were transfected with Dendra2-HA-TRPV5 or Dendra2-HA-TRPV5^{N358Q} two days prior to the experiment. Following treatment with β(1-4)-gal (16 h, 20 mU/mL), cells were harvested and resuspended in medium containing β(1-4)-gal (20 mU/mL). The tubes were rotated for 2 h at 37 °C. Cells were reseeded on petri dishes (WilCo, Amsterdam, The Netherlands) coated with 50 μg/mL fibronectin and cultured for 4-7 h in the presence or absence of β(1-4)-gal (20 mU/mL). Monolayers were washed with Krebs buffer containing (in mM): 135 NaCl, 5 KCl, 1.5 $MgCl_2$, 1.5 $CaCl_2$, 20 HEPES, 10 D-glucose, pH adjusted to 7.4 with NaOH, and imaged at room temperature. Fluorescence was measured by an Olympus Fluoview confocal microscope (FV1000-IX81) with fully integrated TIRF module, -PLAPON60xO/TIRFM-SP - PlanApochromatic objective (60x oil, NA=1.45 and WD=0,10 mm) lens. A 2 s 405 nm laser pulse photo-converted Dendra2. Unswitched (488 nm) and switched (559 nm) Dendra2-TRPV5 proteins were imaged in a 4 Hz series of 5 s every minute for a total duration of 20 min. To calculate the time-dependent expression of the protein at the plasma membrane, the ratio between the switched red signal (F_{559}) and unswitched green signal (F_{488}) was calculated using the following equation: $((F_{559}/F_{488})/(F_{559}/F_{488})_{max})$. All imaging acquisition was performed with the Cell^M software (Tokyo, Japan).

COPAS Sorting

Transgenic mice expressing eGFP under the control of the TRPV5 promoter were generated as described previously (25,26). Fluorescent DCT2/CNT tubules were isolated from transgenic animals, using the Complex Object Parametric Analyzer and Sorter (COPAS) (Union Biometrica, Somerville, MA), as previously described (25). In short: mice aged 4-6 weeks were anesthetized (ketamine 0.1 mg/g body weight and xylazine 0.01 mg/g) and perfused with ice-cold KREBS buffer. The kidney cortex was dissected, minced and subjected to digestion. Finally, the mice are sacrificed by cervical dislocation. The animal ethics board of the Radboud University Nijmegen approved all the experimental procedures involving mice (permit number: RU-DEC 2013-095).

$^{45}Ca^{2+}$ transport in primary DCT2/CNT cells

COPAS sorted DCT2/CNT tubules were cultured for 7-8 days as previously described

(25). The epithelial resistance was measured one day prior to the $^{45}Ca^{2+}$ transport assay. Cell monolayers were incubated for 16 h with β(1-4)-gal (32 mU/mL) or left untreated. 30 min prior to the $^{45}Ca^{2+}$ transport assay, indomethacin (5 μM final concentration, Sigma) was added to the culture medium, on both apical and basolateral sides. The assay was performed at 37 °C with pre-heated buffers. Cells were washed with physiological salt solution (PSS) containing (in mM): 140 NaCl, 2 KCl, 1 K_2HPO_4, 1 $MgCl_2$, 1 $CaCl_2$, 5 D-glucose, 5 L-alanine, 0.005 indomethacin, 10 HEPES/Tris pH 7.4. Subsequently, apical buffer was replaced with PSS (100 μl) containing 3 μCi/mL $^{45}Ca^{2+}$. PSS containing forskolin (10 μM, Sigma) or β(1-4)-gal (32 mU/mL) in combination with 3 μCi/mL $^{45}Ca^{2+}$ were added apically as needed. Basolateral buffer (600 μl) was replaced with PSS. A 10 μl sample was taken from the apical and basolateral compartments at time point 0. Next, basolateral samples were taken at subsequent time points: 15, 30, 60 and 120 min and analyzed for radioactivity using a liquid scintillation counter as previously described (22).

Immunohistochemistry

Kidneys of wt C57BL/6N mice were harvested and fixed in 1% (w/v) poly-L-lysine paraformaldehyde. Kidneys were immerged in 15% (w/v) sucrose (MP Biomedicals, California, USA), after which they were snap frozen in liquid nitrogen. Co-staining for β-gal with TRPV5, breast cancer resistant protein (BCRP) or uromodulin were performed on 5-μm kidney sections, which were incubated for 16 h at 4 °C with chicken anti-β-gal (1:100, Abcam, Cambridge, UK), guinea pig anti-TRPV5 (27) (1:50), rat anti-BCRP (1:250, Kamiya Biomedical Company, Seattle, WA, USA) or sheep anti-uromodulin (1:750, Biotrend, Cologne, Germany; polyclonal) primary antibodies. Finally, kidney sections were incubated for 45 min at room temperature with a FITC-conjugated secondary anti-chicken antibody (1:200, Jackson ImmunoResearch, West Grove, PA, USA) combined with an Alexa Fluor 594-conjugated antibody (goat anti-guinea pig, goat anti-rat or donkey anti-sheep (1:300, life technologies, CA, USA) for TRPV5, BCRP or uromodulin respectively). Images were acquired with an AxioCam camera and processed using the AxioVision software (Zeiss, Sliedrecht, the Netherlands).

Statistical analysis

All data are shown as mean ± S.E.M. Statistical significance ($p < 0.05$) was determined by analysis of variance and a Dunn post-hoc test. For electrophysiological data, unpaired student t-test was used to assess statistical significance.

Results

β-Galactosidase stimulates TRPV5 activity in the presence of the TRPV5 N-glycan.

To investigate the effect of β-gal on either TRPV5, HEK293 cells were transfected with TRPV5, $TRPV5^{N358Q}$ or empty vector. After 48 h, the activity of TRPV5 was assessed using a $^{45}Ca^{2+}$ uptake assay. Ruthenium red, a TRPV5 inhibitor (10 μM, (28)), significantly inhibited $^{45}Ca^{2+}$ uptake. β-gal (16 h, 1 U/mL) significantly stimulated $^{45}Ca^{2+}$ uptake in cells expressing TRPV5, but had no effect on cells expressing $TRPV5^{N358Q}$ (Figure 1A). PCR analysis performed on cDNA from HEK293 cells using specific β-gal primers showed that HEK293 cells endogenously express β-gal (Figure 1B). Exogenous galactose can inhibit endogenous β-gal activity and may therefore reduce TPRV5 activity. The addition of D(+)-galactose (2-3 μg/mL, 16 h) significantly inhibited $^{45}Ca^{2+}$ uptake of TRPV5, but not that of $TRPV5^{N358Q}$ (Figure 1C). β-gal hydrolyses both end-standing β(1-3) and β(1-4) linkages (13). To clarify the mechanism of β-gal-stimulated TRPV5 activity, the effect of enzymes specific for β(1-3)

(β(1-3)-gal, 20 mU/mL) or β(1-4) linkages (β(1-4)-gal, 20 mU/mL) were investigated. While the β(1-3)-gal enzyme did not stimulate $^{45}Ca^{2+}$ uptake, β(1-4)-gal significantly enhanced TRPV5-mediated Ca^{2+} uptake in a similar manner as β-gal (Figure 1D). Importantly, β(1-4)-gal treatment did not alter the expression levels of TRPV5 protein (Figure 1D). $TRPV5^{N358Q}$ was insensitive to both β(1-3)-gal and β(1-4)-gal treatment (Figure 1E).

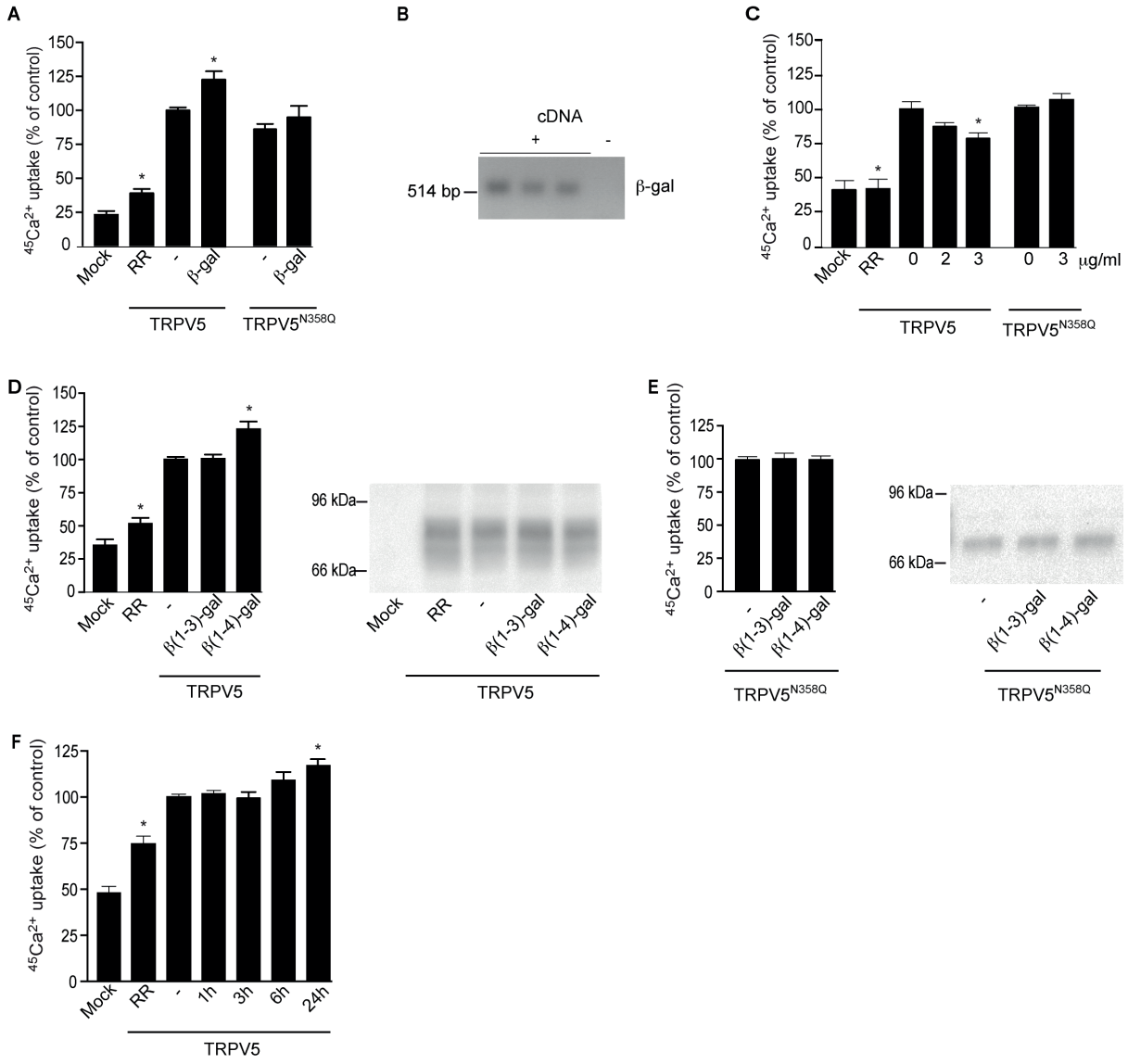

Figure 1. β-gal specifically stimulates TRPV5 activity.
A) β-gal (1 U/mL, 16 h) stimulates TRPV5-mediated $^{45}Ca^{2+}$ uptake in an N-glycan-dependent manner. Ruthenium Red (RR, 10 µM) inhibits $^{45}Ca^{2+}$ uptake (n=17-19, from five independent experiments). **B)** Endogenous β-gal is detected in the presence of HEK293 cDNA (+), but not in its absence (-). **C)** Exogenous D(+)-galactose (2-3 µg/mL) treatment prevents β-gal-mediated stimulation of TRPV5 (n=19-20, from four independent experiments). **D)** β(1-4)-gal, but not β(1-3)-gal, stimulates TRPV5 activity (n=19-20, from five independent experiments). **E)** Neither β(1-4)-gal nor β(1-3)-gal (20 mU/mL) alter the activity of $TRPV5^{N358Q}$ (n=19-20, from five independent experiments). Data shown are mean ± SEM and statistical significance is denoted by * (p<0.05). **F)** Time-course of ß(1-4)-gal-mediated TRPV5 stimulation (n=11-12, from four independent experiments).

β(1-4)-gal stimulates the activity of TRPV5

To validate the specificity of the β(1-4)-gal-mediated TRPV5 stimulation, the function of TRPV5 and $TRPV5^{N358Q}$ was studied by whole-cell patch clamp measurements. Using Na^+

as the main charge carrier, Ca^{2+}-sensitive inwardly rectifying currents were observed in cells expressing TRPV5 or TRPV5^{N358Q} (Figure 2A). The shape of the EGTA-sensitive current-voltage curve was similar for TRPV5 and TRPV5^{N358Q} (Figure 2B-C). Pre-treatment with β(1-4)-gal significantly increased the current density of TRPV5-expressing cells at -100 mV, but did not affect the currents of the TRPV5^{N358Q} mutant (Figure 2B-C). Further analysis observable macroscopic parameters at -100 mV. Subsequently, cells expressing TRPV5 or TRPV5^{N358Q} were subjected to cell-attached patch clamp, as previously described (29). Using this approach, single-channel activity was detected for both TRPV5 and TRPV5^{N358Q} (Figure 3A). Detailed analysis revealed that the single-channel conductance (Figure 3B) and open probability (Figure 3C) were not different between TRPV5 and TRPV5^{N358Q}.

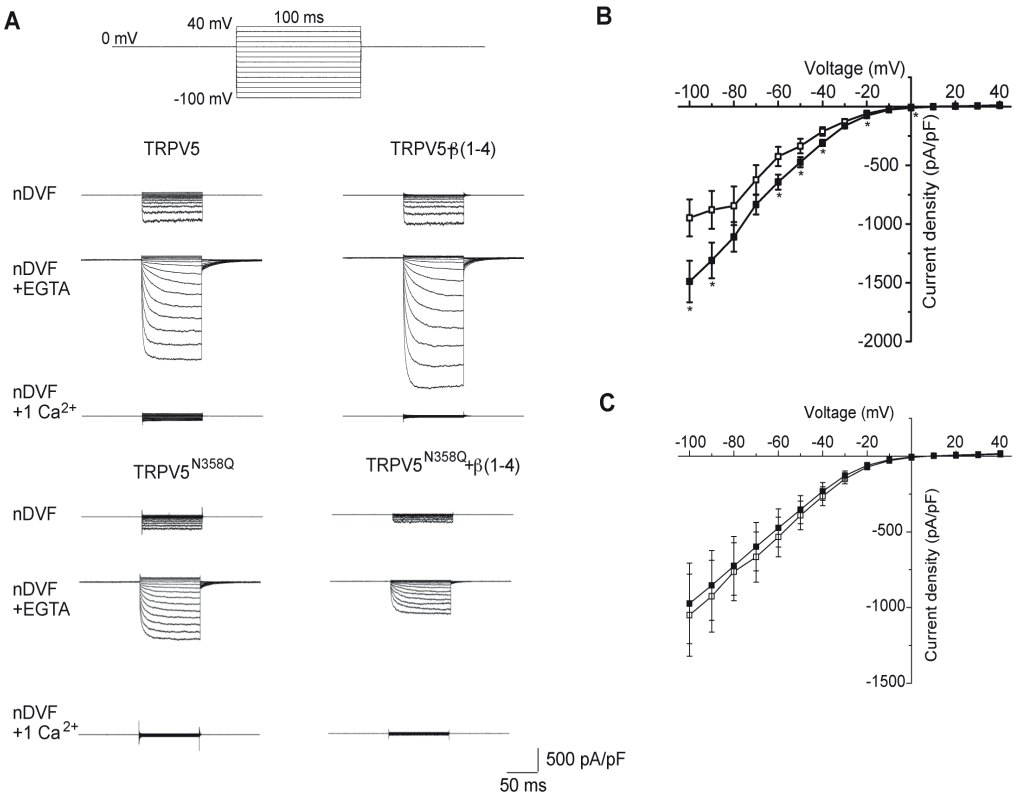

Figure 2. Patch clamp measurement of TRPV5 and TRPV5^{N358Q} with or without β(1-4)-gal treatment. **A)** Inwardly-rectifying currents were observed in response to a voltage step protocol (top inset). Currents were sequentially measured in a solution lacking divalent cations (nDVF), nDVF solution containing 50 μM EGTA and finally in Krebs buffer. Maximal current values were obtained by averaging a 25 ms time window at the end of each voltage pulse. **B)** The current-voltage curve of TRPV5 in the presence of 50 μM EGTA is significantly increased with β(1-4)-gal pre-treatment (n=19-23). **C)** The current density of TRPV5^{N358Q} is insensitive to β(1-4)-gal at all tested voltages (n=8-13). □TRPV5/ TRPV5^{N358Q}; ■TRPV5/TRPV5^{N358Q} + β(1-4)-gal. Data shown are mean ± SEM and statistical significance is denoted by * (p<0.05).

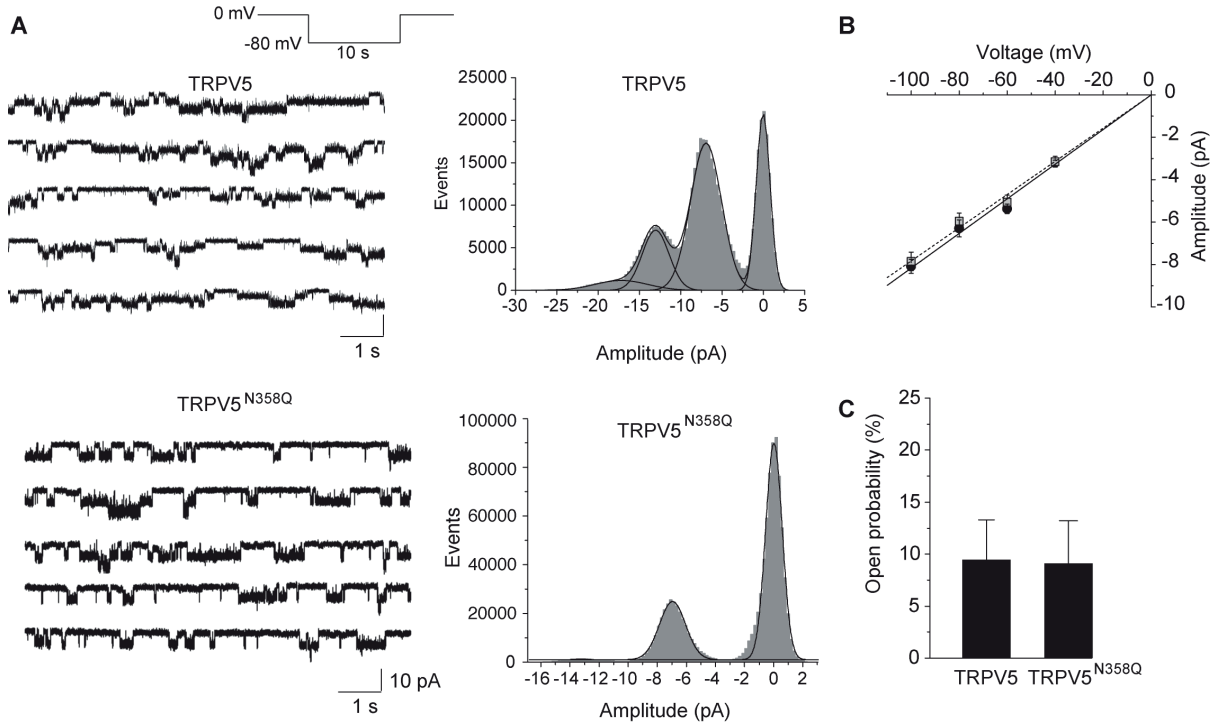

Figure 3. TRPV5 and TRPV5^{N358Q} demonstrate similar intrinsic properties at the single-channel level. **A)** Single channel activity was detected in cell-attached mode in cells expressing TRPV5 or TRPV5^{N358Q}. Channel activity was observed in response to a series of 10 x 10 s hyperpolarization from 0 to -80 mV in nDVF solution. Typical traces with corresponding amplitude histograms were shown for TRPV5 (top, 3 channel) and TRPV5^{N358Q} (bottom, 2 channels). **B)** Average current-voltage curves were obtained by fitting amplitude histograms obtained at -100, -80, -60 and -40 mV for TRPV5 (n=6, open symbol) and TRPV5^{N358Q} (n=5, filled symbol). The conductance, taken as the slope of the IV curve, was 81.7 ± 2.1 and 78.3 ± 1.8 pS for TRPV5 and TRPV5^{N358Q}, respectively. **C)** The open probability at -80 mV was calculated by weighting the average areas of the different open states in individual histograms (n=5-6). ● TRPV5; ■ TRPV5^{N358Q}. Data shown are mean ± SEM.

IV

β(1-4)-gal promotes retention of TRPV5 at the plasma membrane

Live-cell TIRF-M was performed on cells expressing a Dendra-2-TRPV5 fusion protein (9,30,31), as described previously (9), permitting the time-dependent visualization of channels situated in close vicinity to the plasma membrane (~70-100 nm). The Dendra2 proteins were photo-converted using a brief UV-light pulse (405 nm, 2 s). A typical field of view for Dendra2-TRPV5 and Dendra2-TRPV5^{N358Q} is shown (Figure 4A). To assess the time-dependence of plasma membrane TRPV5 and TRPV5^{N358Q} expression, the ratio between the switched red fraction (F_{559}) and unswitched green fraction (F_{488}) was monitored over approximately 20 min. Subsequently, a region in the TIRF field was selected and the ratio between the switched red fraction (F_{559}) and unswitched green fraction (F_{488}) was calculated ((F_{559}/F_{488})/(F_{559}/F_{488})$_{max}$). Before subjected to TIRF-M, cells were either treated with β(1-4)-gal for 16 h or left untreated, similarly to the cells in $^{45}Ca^{2+}$ assays. This analysis revealed a significant increase of TRPV5 in plasma membrane retention time following β(1-4)-gal treatment (Figure 4B). Dendra2-TRPV5^{N358Q} was subjected to an identical protocol. Under these conditions, the basal plasma membrane retention time increased, while β(1-4)-gal had no additional effect (Figure 4C).

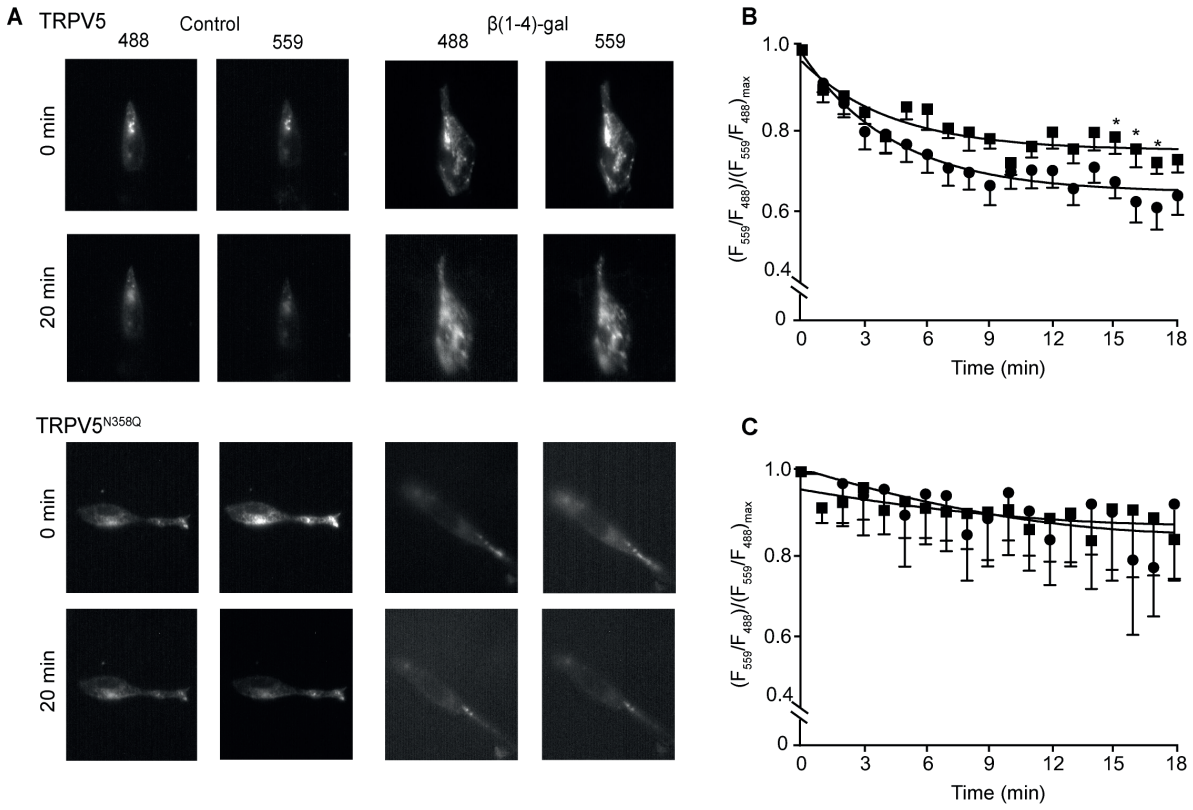

Figure 4. β-gal stabilizes TRPV5 at the plasma membrane.
Cells were subjected to live-cell TIRF-M. At 0 min, Dendra-2 was switched from green to red using an UV light pulse (λ=405 nm, 2 s) and fluorescence was followed over time. **A)** Typical TIRF-M field of view in HEK293 cells of the control and β(1-4)-gal treated conditions for Dendra2-TRPV5 and Dendra2-TRPV5^{N358Q}, captured at the initial time point after photo-switching and after 18 min. **B)** Ratio of switched red/unswitched green fraction in HEK293 cells expressing Dendra2-TRPV5 over time (n=18). **C)** Ratio of switched red/unswitched green fraction in HEK293 cells expressing Dendra2-TRPV5^{N358Q} (n=11). ● Control; ■ β(1-4)-gal treated. Data shown are mean ± SEM and statistical significance is denoted by * (p<0.05).

β-gal is expressed in the proximal tubule and enhances $^{45}Ca^{2+}$ transport in mouse DCT2/CNT

Immunoblot analysis indicated that β-gal was present in mice urine (Figure 5A). In addition, tubular β-gal protein expression was present in kidney sections, with an apparently stronger signal on the apical side. Co-localization was not observed between TRPV5 (DCT2/CNT marker) or uromodulin (thick ascending limb (TAL) marker) and β-gal. BCRP, a proximal tubule marker (32), did co-localized with β-gal (Figure 5B).

Kidneys obtained from mice expressing enhanced GFP (eGFP) under the TRPV5 gene promoter were utilised (25,33) to assess the effect of β-gal on Ca^{2+} transport in a physiological setting. GFP-positive segments (DCT2/CNT) were sorted by COPAS (see Experimental procedures) and seeded on permeable transwell filters. After 7 days in culture, these DCT2/CNT primary cells developed a monolayer with a transepithelial resistance of 547 ± 37 Ωcm^2 (n=33). The monolayers were treated apically with β(1-4)-gal for 16 h (32 mU/mL) while forskolin, a known TRPV5 activator, was used as a positive control (34,35). Forskolin stimulates the cAMP/PKA pathway resulting in TRPV5 phosphorylation and thereby increasing channel activity (36).

Transepithelial Ca^{2+} transport was followed over time by supplying apical $^{45}Ca^{2+}$ and sampling basolateral medium at different time points (t= 0, 15, 60 and 120 min) (Figure 5C). Treatment with either β(1-4)-gal or the positive control forskolin (10 μM) significantly increased Ca^{2+} transport across primary mouse DCT2/CNT monolayers (Figure 5D).

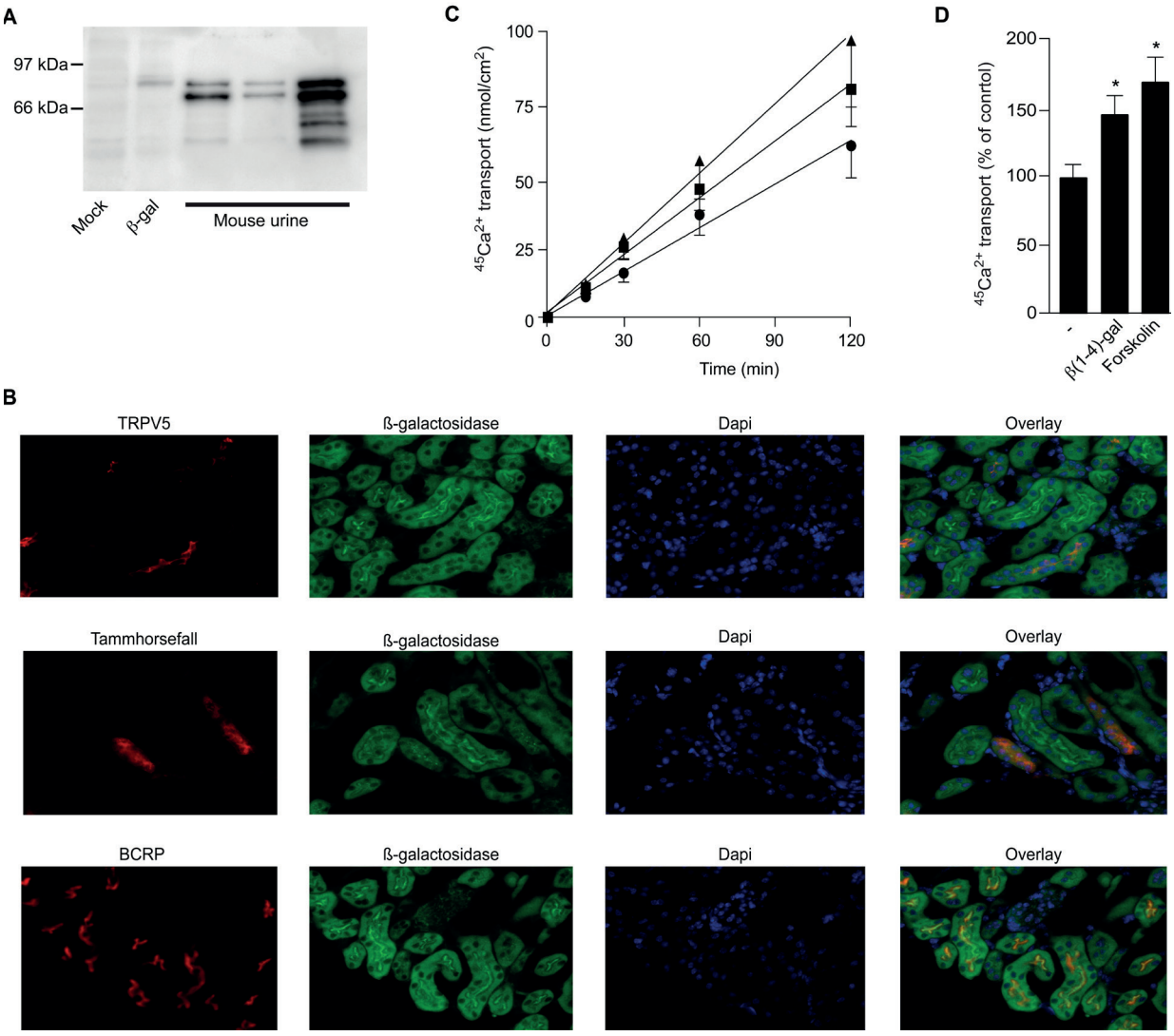

Figure 5. Expression of β-gal in mouse kidney and the $^{45}Ca^{2+}$ transport in mouse DCT2/CNT.
A) β-gal is expressed in mice urine (three different mouse urine samples). HEK293 cells transfected with mouse β-gal were used as positive control (β-gal). **B)** The localization of β-gal in mice kidney sections. β-gal is apically expressed in the proximal tubules along the nephron. Co-localization was found between β-gal and BCRP, a proximal tubule marker. **C)** $^{45}Ca^{2+}$ transport in COPAS sorted primary mouse DCT2/CNT cells in time. ● Control; ■ β(1-4)-gal (32 mU/mL); ▲ forskolin (10 μM). **D)** The slope of $^{45}Ca^{2+}$ transport was significantly increased upon forskolin and β(1-4)-gal treatment (n=13, from five independent experiments). Data shown are mean ± SEM and statistical significance is denoted by * (p<0.05).

Discussion

This study revealed a new regulatory mechanism of transepithelial Ca^{2+} transport by which the extracellular glycosidase β(1-4)-gal stimulates TRPV5 channel activity via the TRPV5 N-glycan. This conclusion is based on the following observations: *i*) β(1-4)-gal enhanced TRPV5 activity; *ii*) this stimulatory effect was absent in the non-glycosylated $TRPV5^{N358Q}$ mutant; *iii*) β(1-4)-gal stabilized TRPV5 on the cell plasma membrane; *iv*) β-gal was present in mouse urine; *v*) apical β-gal stimulated Ca^{2+} transport in primary DCT2/CNT cells.

This study demonstrated that $TRPV5^{N358Q}$ and β(1-4)-gal-treated TRPV5 channels had increased plasma membrane stability without a significant change in their intrinsic biophysical properties. Even though β(1-4)-gal could affect numerous glycoproteins, the effect on the Ca^{2+} uptake is specific for TRPV5 as the $TRPV5^{N358Q}$ expressing cells are not responsive to β(1-4)-gal treatment. Other members of the TRPV family have also been shown to present glycosylation-dependent regulation (37,38). For instance,

ablation of the unique N-glycan in TRPV4 enhanced plasma membrane residency of the channel without affecting its function (37). In contrast, preventing glycosylation of TRPV1 at the residue N604 altered its ionic permeability and capsaicin sensitivity. An N-glycan-mediated alteration of plasma membrane stability of TRPV1 cannot be excluded, due to the presence of multiple glycosylation sites in TRPV1 (38). Our findings suggest that the N358 residue does not take part in the gating or structural constituents of the pore of TRPV5. In accordance, mutational ablation of the TRPV5 N-glycan could reduce clathrin-mediated internalization, as previously suggested for sphingosine 1-phosphate receptor Edg-1 and the dendritic cell-specific intracellular adhesion molecule-3-grabbing nonintegrin (DC-SIGN) (9,39,40). Further experiments studying the details of TRPV5 trafficking will be necessary to validate this hypothesis.

Extracellular galectins are glycan-binding proteins with high affinity for *N*-acetyllactosamine (LacNAc), a saccharide repeat of Gal-(β-1,4)-GlcNAc units (41). Galectin-1, -3, -8 and -9 are expressed in mammalian kidneys (42). A galectin-mediated regulation of TRPV5 could be a new regulatory mechanism of Ca^{2+} transport. Previous reports have suggested that binding of galectin-1 and galectin-3 stabilizes TRPV5 at the plasma membrane (9,10). Furthermore, TRPV5 co-localized with galectin-3, but not with galectin-1. Finally, TRPV5-mediated Ca^{2+} uptake in HEK293 cells was stimulated by extracellular galectin-3 and galectin-1 (9,10). In contrast, galectin-3 can also stimulate the internalization of proteins after binding (9,43-45). Galectin-mediated interactions may restrict the mobility of plasma membrane proteins to clathrin-enriched regions (40). Ablation of the glycan would results in larger membrane exploration and reduced interaction with clathrin, thereby compromising clathrin-dependent internalization. It is, therefore, tempting to hypothesize that galectins bind to the TRPV5 N-glycan and thereby reduce the plasma membrane mobility of the channel, and thus favouring clathrin-mediated endocytosis. Treatment with β-gal can alter the binding of galectins, thereby inhibiting clathrin-mediated endocytosis.

Ca^{2+} transport is increased in isolated mice DCT cells expressing endogenous TRPV5 by apical β(1-4)-gal treatment. However, it remains uncertain if the β-gal derived in the proximal tubules can have the same effect. Future research should show the direct effect of proximal β-gal on TRPV5 activity. Interestingly, a correlation between TRPV5 and β-gal is found in diabetic mellitus diseased patients. This disease is associated with renal Ca^{2+} wasting, although the molecular mechanisms underlying these findings are not known. A compensatory upregulation of TRPV5 mRNA and protein levels have been observed in diabetic rats (46). Interestingly, diabetes mellitus type 1 patients show elevated β-gal levels in blood as well as in urine, suggesting that β-gal upregulation may represent an additional mechanism of compensation to prevent renal Ca^{2+} wasting (47,48).

Finally, patients with a deficiency in β-gal expression commonly present skeletal anomalies (18,19). GM1 gangliosidosis is associated with flattening of vertebral bodies, while Morquio B disease is associated with skeletal dysplasia. This phenotype is comparable to the $TRPV5^{-/-}$ mice, which show significant alterations in bone structure (20). Future *in vivo* studies may substantiate the link between the observed phenotype in β-gal-diseased patients and TRPV5 dysregulation.

Acknowledgements
We would like to thank Femke Latta for her support with the COPAS experiments and the Microscopic Imaging Centre (MIC) in Nijmegen for their technical support.

References

1. Felsenfeld, A., Rodriguez, M., and Levine, B. (2013) New insights in regulation of calcium homeostasis. *Curr Opin Nephrol Hypertens* **22**, 371-376
2. van de Graaf, S. F. J., Hoenderop, J. G. J., and Bindels, R. J. M. (2006) Regulation of TRPV5 and TRPV6 by associated proteins. *Am J Physiol-Renal* **290**, F1295-F1302
3. Renkema, K. Y., Nijenhuis, T., van der Eerden, B. C. J., van der Kemp, A. W. C. M., Weinans, H., van Leeuwen, J. P. T. M., Bindels, R. J. M., and Hoenderop, J. G. J. (2005) Hypervitaminosis D mediates compensatory Ca2+ hyperabsorption in TRPV5 knockout mice. *J Am Soc Nephrol* **16**, 3188-3195
4. Hoenderop, J. G. J., Hartog, A., Stuiver, M., Doucet, A., Willems, P. H. G. M., and Bindels, R. J. M. (2000) Localization of the epithelial Ca2+ channel in rabbit kidney and intestine. *J Am Soc Nephrol* **11**, 1171-1178
5. Dimke, H., Hoenderop, J. G. J., and Bindels, R. J. M. (2011) Molecular basis of epithelial Ca2+ and Mg2+ transport: insights from the TRP channel family. *J Physiol-London* **589**, 1535-1542
6. Boros, S., Bindels, R. J. M., and Hoenderop, J. G. J. (2009) Active Ca^{2+} reabsorption in the connecting tubule. *Pflug Arch Eur J Phy* **458**, 99-109
7. Wolf, M. T., Wu, X. R., and Huang, C. L. (2013) Uromodulin upregulates TRPV5 by impairing caveolin-mediated endocytosis. *Kidney Int* **84**, 130-137
8. Nilius, B., Prenen, J., Hoenderop, J. G. J., Vennekens, R., Hoefs, S., Weidema, A. F., Droogmans, G., and Bindels, R. J. M. (2002) Fast and slow inactivation kinetics of the Ca2+ channels ECaC1 and ECaC2 (TRPV5 and TRPV6) - Role of the intracellular loop located between transmembrane segments 2 and 3. *J Biol Chem* **277**, 30852-30858
9. Leunissen, E. H., Nair, A. V., Bull, C., Lefeber, D. J., van Delft, F. L., Bindels, R. J., and Hoenderop, J. G. (2013) The epithelial calcium channel TRPV5 is regulated differentially by klotho and sialidase. *J Biol Chem* **288**, 29238-29246
10. Cha, S. K., Ortega, B., Kurosu, H., Rosenblatt, K. P., Kuro-O, M., and Huang, C. L. (2008) Removal of sialic acid involving Klotho causes cell-surface retention of TRPV5 channel via binding to galectin-1. *P Natl Acad Sci USA* **105**, 9805-9810
11. Chang, Q., Hoefs, S., van der Kemp, A. W., Topala, C. N., Bindels, R. J., and Hoenderop, J. G. (2005) The beta-glucuronidase klotho hydrolyzes and activates the TRPV5 channel. *Science* **310**, 490-493
12. Apweiler, R., Hermjakob, H., and Sharon, N. (1999) On the frequency of protein glycosylation, as deduced from analysis of the SWISS-PROT database. *Bba-Gen Subjects* **1473**, 4-8
13. Varki, A., Cummings, R. D., Esko, J. D., Freeze, H. H., Stanley, P., Bertozzi, C. R., Hart, G. W., and Etzler, M. E. (2009) Essentials of Glycobiology, 2nd edition. *Cold Spring Harbor (NY)*
14. Cummings, R. D., and Pierce, J. M. (2014) The Challenge and Promise of Glycomics. *Chem Biol* **21**, 1-15
15. Parker, R. B., and Kohler, J. J. (2010) Regulation of Intracellular Signaling by Extracellular Glycan Remodeling. *Acs Chem Biol* **5**, 35-46
16. Nagae, M., and Yamaguchi, Y. (2012) Function and 3D Structure of the N-Glycans on Glycoproteins. *Int J Mol Sci* **13**, 8398-8429
17. Xu, G., Zhu, L., Hong, J., Cao, Y., and Xia, T. (1999) Rapid colorimetric assay of urinary beta-galactosidase and N-acetyl-beta-D-glucosaminidase with Cobas Mire Auto-analyzer. *J Clin Lab Anal* **13**, 95-98
18. Yoshida, K., Oshima, A., Sakuraba, H., Nakano, T., Yanagisawa, N., Inui, K., Okada, S., Uyama, E., Namba, R., Kondo, K., and et al. (1992) GM1 gangliosidosis in adults: clinical and molecular analysis of 16 Japanese patients. *Ann Neurol* **31**, 328-332
19. Oshima, A., Yoshida, K., Shimmoto, M., Fukuhara, Y., Sakuraba, H., and Suzuki, Y. (1991) Human beta-galactosidase gene mutations in morquio B disease. *Am J Hum Genet* **49**, 1091-1093
20. Hoenderop, J. G. J., van Leeuwen, J. P. T. M., van der Eerden, B. C. J., Kersten, F. F. J., van der Kemp, A. W. C. M., Merillat, A. M., Waarsing, J. H., Rossier, B. C., Vallon, V., Hummler, E., and Bindels, R. J. M. (2003) Renal Ca^{2+} wasting, hyperabsorption, and reduced bone thickness in mice lacking TRPV5. *J Clin Invest* **112**, 1906-1914
21. van de Graaf, S. F., Hoenderop, J. G., Gkika, D., Lamers, D., Prenen, J., Rescher, U., Gerke, V., Staub, O., Nilius, B., and Bindels, R. J. (2003) Functional expression of the epithelial Ca^{2+} channels (TRPV5 and TRPV6) requires association of the S100A10-annexin 2 complex. *The EMBO journal* **22**, 1478-1487

22. de Groot, T., Lee, K., Langeslag, M., Xi, Q., Jalink, K., Bindels, R. J., and Hoenderop, J. G. (2009) Parathyroid hormone activates TRPV5 via PKA-dependent phosphorylation. *J Am Soc Nephrol* **20**, 1693-1704
23. Milescu, L. S., Nicolai, C., and Bannen, J. (2000-2013) Qub Software.
24. Vennekens, R., Hoenderop, J. G., Prenen, J., Stuiver, M., Willems, P. H., Droogmans, G., Nilius, B., and Bindels, R. J. (2000) Permeation and gating properties of the novel epithelial Ca(2+) channel. *J Biol Chem* **275**, 3963-3969
25. van der Hagen, E. A., Lavrijsen, M., van Zeeland, F., Praetorius, J., Bonny, O., Bindels, R. J., and Hoenderop, J. G. (2014) Coordinated regulation of TRPV5-mediated Ca(2+) transport in primary distal convolution cultures. *Pflugers Arch* **466**, 2077-2087
26. Hofmeister, M. V., Fenton, R. A., and Praetorius, J. (2009) Fluorescence isolation of mouse late distal convoluted tubules and connecting tubules: effects of vasopressin and vitamin D3 on Ca^{2+} signaling. *Am J Physiol Renal Physiol* **296**, F194-203
27. Hoenderop, J. G., van der Kemp, A. W., Hartog, A., van de Graaf, S. F., van Os, C. H., Willems, P. H., and Bindels, R. J. (1999) Molecular identification of the apical Ca^{2+} channel in 1, 25-dihydroxyvitamin D3-responsive epithelia. *J Biol Chem* **274**, 8375-8378
28. Nilius, B., Prenen, J., Vennekens, R., Hoenderop, J. G. J., Bindels, R. J. M., and Droogmans, G. (2001) Pharmacological modulation of monovalent cation currents through the epithelial Ca^{2+} channel ECaC1. *Brit J Pharmacol* **134**, 453-462
29. Nilius, B., Vennekens, R., Prenen, J., Hoenderop, J. G. J., Bindels, R. J. M., and Droogmans, G. (2000) Whole-cell and single channel monovalent cation currents through the novel rabbit epithelial C^{a2+} channel ECaC. *J Physiol-London* **527**, 239-248
30. Gurskaya, N. G., Verkhusha, V. V., Shcheglov, A. S., Staroverov, D. B., Chepurnykh, T. V., Fradkov, A. F., Lukyanov, S., and Lukyanov, K. A. (2006) Engineering of a monomeric green-to-red photoactivatable fluorescent protein induced by blue light. *Nat Biotechnol* **24**, 461-465
31. Gurskaya, N. G., Verkhusha, V. V., Shcheglov, A. S., Staroverov, D. B., Chepurnykh, T. V., Fradkov, A. F., Lukyanov, S., and Lukyanov, K. A. (2006) Engineering of a monomeric green-to-red photoactivatable fluorescent protein induced by blue light. *Nature Biotechnology* **24**, 461-465
32. Huls, M., Brown, C. D. A., Windass, A. S., Sayer, R., van den Heuvel, J. J. M. W., Heemskerk, S., Russel, F. G. M., and Masereeuw, R. (2008) The breast cancer resistance protein transporter ABCG2 is expressed in the human kidney proximal tubule apical membrane. *Kidney International* **73**, 220-225
33. Markadieu, N., San-Cristobal, P., Nair, A. V., Verkaart, S., Lenssen, E., Tudpor, K., van Zeeland, F., Loffing, J., Bindels, R. J., and Hoenderop, J. G. (2012) A primary culture of distal convoluted tubules expressing functional thiazide-sensitive NaCl transport. *Am J Physiol Renal Physiol* **303**, F886-892
34. van Baal, J., Raber, G., de Slegte, J., Pieters, R., Bindels, R. J. M., and Willems, P. H. G. M. (1996) Vasopressin-stimulated Ca^{2+} reabsorption in rabbit cortical collecting system: effects on cAMP and cytosolic Ca^{2+}. *Pfluegers Arch* **433**, 109-115
35. Hoenderop, J. G. J., Hartog, A., Willems, P. H. G. M., and Bindels, R. J. M. (1998) Adenosine-stimulated Ca^{2+} reabsorption is mediated by apical A(1) receptors in rabbit cortical collecting system. *Am J Physiol-Renal* **274**, F736-F743
36. Diepens, R. J., den Dekker, E., Bens, M., Weidema, A. F., Vandewalle, A., Bindels, R. J., and Hoenderop, J. G. (2004) Characterization of a murine renal distal convoluted tubule cell line for the study of transcellular calcium transport. *Am J Physiol Renal Physiol* **286**, F483-489
37. Xu, H., Fu, Y., Tian, W., and Cohen, D. M. (2006) Glycosylation of the osmoresponsive transient receptor potential channel TRPV4 on Asn-651 influences membrane trafficking. *Am J Physiol Renal Physiol* **290**, F1103-1109
38. Veldhuis, N. A., Lew, M. J., Abogadie, F. C., Poole, D. P., Jennings, E. A., Ivanusic, J. J., Eilers, H., Bunnett, N. W., and McIntyre, P. (2012) N-glycosylation determines ionic permeability and desensitization of the TRPV1 capsaicin receptor. *J Biol Chem* **287**, 21765-21772
39. Kohno, T., Wada, A., and Igarashi, Y. (2002) N-glycans of sphingosine 1-phosphate eceptor Edg-1 regulate ligand-induced receptor internalization. *FASEB J* **16**, 983-992
40. Torreno-Pina, J. A., Castro, B. M., Manzo, C., Buschow, S. I., Cambi, A., and Garcia-Parajo, M. F. (2014) Enhanced receptor-clathrin interactions induced by

N-glycan-mediated membrane micropatterning. *P Natl Acad Sci USA* **111**, 11037-11042
41. Cooper, D. N. W. (2002) Galectinomics: finding themes in complexity. *Bba-Gen Subjects* **1572**, 209-231
42. Hughes, R. C. (2004) Galectins in kidney development. *Glycoconjugate J* **19**, 621-629
43. Dumic, J., Dabelic, S., and Flogel, M. (2006) Galectin-3: An open-ended story. *Bba-Gen Subjects* **1760**, 616-635
44. Furtak, V., Hatcher, F., and Ochieng, J. (2001) Galectin-3 mediates the endocytosis of beta-1 integrins by breast carcinoma cells. *Biochem Bioph Res Co* **289**, 845-850
45. Dennis, J. W., Lau, K. S., Demetriou, M., and Nabi, I. R. (2009) Adaptive Regulation at the Cell Surface by N-Glycosylation. *Traffic* **10**, 1569-1578
46. Lee, C. T., Lien, Y. H. H., Lai, L. W., Chen, J. B., Lin, C. R., and Chen, H. C. (2006) Increased renal calcium and magnesium transporter abundance in streptozotocin-induced diabetes mellitus. *Kidney International* **69**, 1786-1791
47. Kohler, E., Sheth, K. J., and Good, T. A. (1979) Urinary Acidic Glycohydrolases as an Index of Kidney Damage in Juvenile Diabetes-Mellitus. *Acta Diabetol Lat* **16**, 247-255
48. Serrano, M. A., Reglero, A., Cabezas, J. A., Diez, L. C. G., Corrales, J. J., Decastro, S., and Miralles, J. M. (1983) Serum Glycosidases in Diabetes-Mellitus in Relation to the Retinopathy and to the Length of the Disease. *Clinica Chimica Acta* **132**, 23-27

V

CHAPTER 5

The Ca^{2+} permeation pathway of the TRPV5 channel is composed of a tryptophan-gate and a glycine-hinge

Elizabeth H.P. Leunissen[1], Maxime G. Blanchard[1], Jenny van der Wijst[1], Hanka Venselaar[2], Sjoerd Verkaart[1], René J.M. Bindels, Joost G.J. Hoenderop[1]

[1]Department of Physiology, [2]Centre for Molecular and Biomolecular Informatics, Radboud university medical center, Radboud Institute for Molecular Life Sciences, Nijmegen, The Netherlands

Abstract

The transient receptor potential vanilloid type 5 (TRPV5) Ca^{2+} channel facilitates transcellular Ca^{2+} reabsorption in the kidney. It is of importance that this epithelial Ca^{2+} channel is tightly regulated, as it is responsible for the fine-tuning of Ca^{2+} excretion. Based on the recently elucidated TRPV1 structure, a TRPV5 homology model has been designed by an automatic script using the YASARA and WHAT IF Twinset. Structural analysis of this homology model proposes a gating mechanism based on an aromatic gate in combination with a helix hinge. The present study delineates two residues that are essential in the gating mechanism of the TRPV5 channel. First, a tryptophan (W583) that is located at the end of the inner pore helix, transmembrane six, with its side chain facing the permeation pathway. Mutation of this residue heavily increased the TRPV5-mediated Ca^{2+} influx. The expression of mutated TRPV5 channels led to high basal Ca^{2+} levels and consequently to an increased cell death. Substitution to an aromatic residue had intermediate effects with a nearly 10-fold increase in Ca^{2+} uptake levels, while replacement with a non-aromatic residue yielded a stronger phenotype of an averaged 30-fold increase in Ca^{2+} uptake levels. Moreover, the open probability of the non-aromatic mutant channels was increased. A flexible glycine residue (G579), located one α-helical turn above the tryptophan residue, was shown to be important for channel opening. Replacement of this residue with alanine ablated TRPV5-mediated Ca^{2+} transport and decreased the open probability ~5-fold. It is concluded that the TRPV5 gating machinery is composed of the highly conserved tryptophan-gate in combination with a glycine-hinge.

Introduction

The transient receptor potential vanilloid type 5 (TRPV5) channels form the apical gate for transepithelial Ca^{2+} reabsorption in the kidney (1). TRPV5, formerly known as ECaC1/CaT2, is expressed in the late distal convoluted tubule and connecting tubule of the nephron in the kidney, the early intestine and the placenta (1-4). Functional channels are composed of four subunits, each containing six transmembrane (TM) segments and intracellular amino (N)- and carboxyl (C)-termini (5,6). The Ca^{2+}-selective pore is formed at the interface of the four subunits, by TM segment five, six and the pore loop between these two segments. TRPV5 is a constitutively active Ca^{2+}-selective cation channel, with a substantial permeability at physiological membrane potentials and a Ca^{2+}-dependent feedback regulation (7).

The TRP family consists of ion channels with a similar structure but a great variety in their mechanisms of activation. TRPV5 is most homologous to TRPV6, a Ca^{2+}-selective channel expressed in the intestine. Compared to TRPV1-4, TRPV5 and TRPV6 display a specific selectivity filter sequence, allowing a more pronounced selectivity for Ca^{2+} over monovalent cations (8). The TRPV5 Ca^{2+}-selectivity filter is composed of a ring of four aspartic acid residues (D542), which are localized in the pore loop (9). This single residue is crucial for the channel characteristics such as a high Ca^{2+} permeability, block by Mg^{2+}, and Ca^{2+}-dependent current decay (7). Mutation of this residue into an alanine abolishes Ca^{2+} permeability without altering the permeability for monovalent cations (7).

A high intracellular Ca^{2+} level functions as a negative feedback mechanism and will inhibit TRPV5 channel activity (10). This inhibition is controlled by the concentration of Ca^{2+} in a micro domain near the inner mouth of the channel. Calmodulin (CaM), a ubiquitous Ca^{2+}-binding protein, has been postulated to mediate part of the Ca^{2+}-dependent inactivation by binding to the C-terminus of TRPV5 (11-13). A high intracellular Ca^{2+} concentration enhances the CaM binding. CaM binding decreases TRPV5-mediated Ca^{2+}-uptake by reducing the open probability. Removal of the C-terminal fragment of TRPV5 (S696X) abolishes the sensitivity for CaM (12). Moreover, PTH-mediated T709 phosphorylation diminishes the CaM binding and thereby increases TRPV5-mediated Ca^{2+} transport (12).

The current knowledge about the gating mechanism of TRPV5 and other Ca^{2+} selective channels is limited. In contrast, several mechanisms have been proposed for the gating of voltage-gated K^+ channels (14): *i)* rotation of the inner pore helix around the pore axis, *ii)* kinking of the inner pore helix, and *iii)* helix kinking in combination with an aromatic gate. Most eukaryotic K^+ channels are regulated by kinking of the inner pore helix at a proline-valine-proline (PVP) sequence (15), a motif that is absent in TRPV5. Prokaryotic K^+ channel gating is often mediated by helix kinking in combination with an aromatic gate (15). Channel regulation via an aromatic gate is often accompanied by a flexible hinge point at the bottom of the α-helix, composed of a glycine (14).

Recently, the first high resolution 3D structure of a TRP channel (TRPV1) has been solved at 3.4 Å. Electron cryo-microscopy elucidated the structure of TRPV1 in a closed conformation (16). Rat TRPV1 may serve as a suitable template for homology modeling of the rabbit TRPV5 structure (17). The present study shows a homology model of TRPV5 that is used to delineate the gating mechanism of TRPV5. The tryptophan residue at position 583 (W583) is investigated in view of its localization at the intracellular end of the pore and the unusual orientation of its side chain pointing towards the solvent. Mutation of this residue is severely affecting the channel function of TRPV5. In addition, a glycine residue (G579) has been detected one α-helical turn above W583. Mutation of this residue in the rigid and slightly bigger alanine abolishes Ca^{2+} transport through the channel. These results provide the first evidence that the gating mechanism of

TRPV5 involves the combination of an aromatic tryptophan gate and glycine hinge point.

Experimental procedures

Generating the TRPV5 homology model

The YASARA (18) & WHAT IF (19) Twinset was used to build a homology model of TRPV5, based on the TRPV1 structure as a modelling template (29% sequence identity, PDB file 3j5p) (16). An automatic script with standard parameters was used. The model contained residue 1-644 of rabbit TRPV5.

DNA constructs and transfections

The pCINeo/IRES-GFP plasmid encompassing either HA-tagged rabbit TRPV5 or untagged rat CaM were generated as described previously (11,20). The $TRPV5^{G579A}$ and all $TRPV5^{W583}$ mutants were obtained by site-directed mutagenesis of TRPV5-pCINeo/IRES-GFP. The $TRPV5^{D542A}$ mutation was introduced by site-directed mutagenesis of TRPV5-pCINeo/IRES-GFP. Subsequently, this construct was digested with BspEI and AgeI and a PCR product of $TRPV5^{698X}$ was introduced. All constructs were verified by DNA sequencing.

Cell culture and transfections

HEK293 cells were grown in Dulbecco's modified eagle's medium (DMEM, Bio Whittakker-Europe, Verviers, Belgium) containing 10% (v/v) fetal calf serum (PAA, Liz Australia), 2 mM L-glutamine and 10 μg/ml non-essential amino acids at 37 ºC in a humidity-controlled incubator with 5% (v/v) CO_2. The cells were transiently transfected with the respective DNA construct using lipofectamine 2000 (Invitrogen, Carlsbad, CA, USA) according to manufacturer's instructions.

V

Immunoblotting and determination of protein concentration

HEK293 cells expressing TRPV5 and indicated mutants were disrupted in lysis buffer containing Triton X-100 1% (v/v), 150 mM NaCl, 5 mM EDTA, 50 mM Tris/HCl pH 7.5, 1 mM phenylmethanesulfonylfluoride (PMSF), 10 μg/ml leupeptin, 10 μg/ml pepstatin A, 5 μg/ml aprotinin. Protein concentration was measured using the BCA protein assay kit (Thermo Scientific, Rockford, IL, USA), according to manufacturer's instructions. Cell lysates were subjected to 8 % (w/v) SDS-PAGE and immunoblotted using anti-HA-tag (1:5,000, Cell Signalling Technology, Beverly, MA, USA) with peroxidase-labelled goat anti-mouse IgG (1:10,000, Chemie Brunschwig, Basel, Switzerland) antibodies.

$^{45}Ca^{2+}$ uptake assay

HEK293 cells were transfected with TRPV5, indicated mutants, or the empty pCINeo/IRES-GFP vector (mock). One day after transfection, cells were reseeded on poly-L-lysine-coated (0.1 mg/ml) culture dishes. Radioactive $^{45}Ca^{2+}$ uptake in TRPV5-transfected HEK293 cells was determined as previously described (21). If required, cells were incubated with 10 μM ruthenium red (RR) 30 min prior to the $^{45}Ca^{2+}$ uptake measurements.

Trypan blue assay

HEK293 cells were transfected as indicated. Two days after transfection the cells were collected and precipitated by centrifugation (2 min, 200 g). The supernatant was discarded and cells were resuspended in phosphate buffered saline (PBS), pH 7.4, adding 4 % (w/v) trypan blue (Sigma) to a final concentration of 0.08%. Cells were counted using a hemocytometer.

Intracellular Ca^{2+} measurements using fura-2-AM
HEK293 cells were seeded on fibronectin-coated coverslips (diameter, 25 mm) and transfected as indicated. After one day, cells were loaded for 20 min with 3 μM fura-2-acetoxymethyl ester (fura-2-AM; Molecular Probes) and 0.01% (v/v) Pluronic F-129 (Molecular Probes) in Krebs solution (5.5 mM KCl, 147 mM NaCl, 1.2 mM $MgCl_2$, 1.5 mM $CaCl_2$, 10 mM glucose, and 10 mM HEPES/NaOH, pH 7.4) at 37°C. Subsequently, the cells were washed once with Krebs solution and allowed to equilibrate at 37°C for another 10 min. Details of microscopy procedures and quantitative image analysis have been described previously (22). In short, fura-2-loaded cells were placed on an inverted microscope using an incubation chamber containing Krebs solution and intracellular Ca^{2+} levels were determined with fura-2 excited at 340 and 380 nm. All measurements were performed at room temperature.

Electrophysiology
Experiments were performed using an EPC-9 amplifier and the Patchmaster software (HEKA electronics, Lambrecht, Germany). The sampling interval was set to 200 ms for whole-cell recordings and 100 ms for single-channel recordings. Whole-cell recordings were acquired with a low-pass filter set at 3.6 kHz, while single-channel recordings had a low-pass filter set at 5 kHz. The electrical noise was further reduced using the Humbug 50/60 Hz noise eliminator (Quest Scientific, Vancouver, Canada). Whole-cell patch clamp pipettes were pulled from thin-walled borosilicate glass (Harvard Apparatus, March-Hugstetten, Germany) and had resistances between 1 and 3 MΩ when filled with the pipette solution. Series resistance compensation was set to 75-95% in all whole-cell experiments. Single-channel patch clamp pipettes were made of thick-walled borosilicate glass (Harvard Apparatus and World Precision Instruments) and had resistances between 8 and 11 M when filled with the pipette solution. Two different extracellular solutions were used to obtain whole-cell recordings. A nominally divalent-free (nDVF) solution comprising (in mM): 150 NaCl, 6 CsCl, 10 glucose, 10 HEPES and pH adjusted to 7.4 using NaOH. A divalent-free (DVF) solution based on nDVF solution with 50 μM of added EGTA. The pipette solution comprised (in mM): 20 CsCl, 100 CsAspartate, 1 $MgCl_2$, 10 BAPTA, 4 Na_2ATP, 10 HEPES and pH adjusted to 7.2 using CsOH. Cells were initially bathed in nDVF extracellular solution. The whole-cell EGTA-sensitive current was obtained by measuring the current sensitive to the perfusion of 50 μM EGTA. A voltage step protocol, consisting of voltage steps from -100 to +40 mV was applied from a holding potential of +20 mV. Current densities were calculated by normalizing the current amplitude at −80 mV to the cell membrane capacitance. The extracellular solution for cell-attached recordings contained (in mM): 150 NaCl, 6 CsCl, 10 glucose, 10 HEPES and pH adjusted to 7.4 using NaOH. The pipette solution comprised (in mM): 140 NaCl, 10 EGTA, 10 HEPES and pH adjusted to 7.2 using NaOH (23). Single channel activity was monitored upon a 10s step to -80 mV from a holding potential 0 mV. All experiments were performed at room temperature. The analysis and display of whole-cell recordings were performed using Igor Pro software (WaveMetrics, Lake Oswego, USA). Single-channel recordings were analyzed using the Qub software package (24).

Cell surface biotinylation assay
HEK293 cells were transiently transfected with TRPV5, the indicated mutants, or the empty pCINeo/IRES-GFP vector. One day after transfection, cells were reseeded on poly-L-lysine-coated (0.1 mg/ml) culture dishes. Subsequently, cells were biotinylated

as described previously (25) and disrupted in 1 ml lysis buffer; 1 % (v/v) Triton-X100, 150 mM NaCl, 5 mM EDTA, 50 mM Tris (pH 7.5 adjusted with HCl), 1 mM PMSF, 10 μg/ml leupeptin, 10 μg/ml pepstatin A, 5 μg/ml aprotinin. TRPV5 protein expression at the cell surface and in total cell lysate was determined as described previously (25).

CaM binding assay

HEK293 cells were transiently transfected with $TRPV5^{D542A,\ S698X}$, $TRPV5^{D542A,\ S698X,\ W583L}$, $TRPV5^{D542A,\ S698X,\ W583F}$ in pCINeo/IRES-GFP or the empty pCINeo/IRES-GFP vector. Two days after transfection, cells were washed twice with ice-cold PBS pH 7.4 and disrupted in 0.5 ml lysis buffer; 0.5 % (v/v) Triton-X100, 150 mM NaCl, 50 mM Tris (pH 7.5 adjusted with HCl), 1 mM PMSF, 10 μg/ml leupeptin, 10 μg/ml pepstatin A, 5 μg/ml aprotinin, enriched with $CaCl_2$ (1 mM) or EGTA (2.5 mM, Sigma). Following, the cells were centrifuged for 10 min at 14,000 g at 4°C. For input samples, 30 μl supernatant was treated with Leammli buffer, enriched with 100 mM dithiothreitol (DTT), for 30 min at 37°C. Remaining supernatant was added to 200 μL CaM agarose beads (Sigma, St. Louis, MO, USA) and rotated overnight at 4°C. The beads were washed 6 times with wash buffer; 0.1 % (v/v) Triton-X100, 150 mM NaCl, 50 mM Tris (pH 7.5 adjusted with HCl), 1 mM PMSF, 10 μg/ml leupeptin, 10 μg/ml pepstatin A, 5 μg/ml aprotinin, enriched with either $CaCl_2$ (1 mM) or EGTA (2.5 mM). Finally, proteins were eluted by incubation with Leammli buffer, enriched with 100 mM DTT, for 30 min at 37°C and the TRPV5 protein was assessed by immunoblotting as described.

Statistical analysis

All data are shown as mean ± standard error of the mean (SEM). Statistical significance ($p < 0.05$) was determined by analysis of variance and a Dunn post-hoc test. For electrophysiological data, unpaired student t-test was used to assess statistical significance.

V

Results

TRPV5 homology model

A TRPV5 homology model was generated using the recently determined structure of rat TRPV1 (16) (Fig 1A). The Sander-Schneider plot indicates that 29% amino acid identity between rabbit TRPV5 and rat TRPV1 is sufficient for homology modelling (17). To validate the TRPV5 homology model, some regulatory motifs of TRPV5, including the aspartic acid D542, asparagine N358 and the ankyrin repeats, were inspected (7,25,26). First, the localization and orientation of the D542 Ca^{2+}-selectivity filter in the homology model was assessed (7,9,27) and appeared correctly localized and oriented, forming a negatively charged ring at the entry of the channel (Fig 1B). Ankyrin repeats were detected on the intracellular side as small α-helices, with the expected twist between the 4^{th} and 5^{th} ankyrin repeat (26). Based on these known amino acid residues and the overall validity of the homology model, the TRPV5 structure was further examined for amino acids that might critically affect the channel gating.

A visual inspection outlined the W583 residue situated at the intracellular end of TM six, with its side chain pointing towards the ion permeation pathway (Fig 1C). Given the hydrophobic nature of the tryptophan side chain, this conformation appears energetically unfavourable. The W583 residue is localized in a region that is highly conserved among different species (Table 1). It is conserved in TRPV6, but not in other members of the TRPV family (Table 2). The side chain of a tryptophan can convert to different rotameric positions. One of these rotamers constituted a

conformation prohibiting Ca^{2+} permeation (Fig 1D, E). Dehydrated Ca^{2+} ions have a diameter of 0.99 Å. Passage of Ca^{2+} ions is prohibited when the W583 side chains are facing each other. The estimated distance between the centers of the side chains is ~3.1 Å, and therefore, the passage size will be ~0.8 Å. This is too small for dehydrated Ca^{2+} to pass the channel pore (28) (Fig 1E). However, the absolute values of these measurements should be handled with care as this data is based on a homology model.

Channel	Alignment of different TRP channels
hTRPV1	VILTYILLLNMLIALMGETVNKIAQESKNIWKLQRAITILD
hTRPV2	VLLTYILLLNMLIALMSETVNSVATDSWSIWKLQKAISVLE
hTRPV3	IILTFVLLLNMLIALMGETVGQVSKESKHIWKLQWATTILD
hTRPV4	VILTFVLLLNMLIALMGETVENVSKESERIWRLQRARTILE
hTRPV5	AIIATLLMLNLFIAMMGDTHWRVAQERDELWRAQVVATTVM
hTRPV6	AIIATLLMLNLLIAMMGDTHWRVAHERDELWRAQIVATTVM
	::: :*:**::**:*.:* :: : :*: * . : :

Table 1: Sequence alignment between TRPV5 of different species. The region containing the W583 residue is conserved between the different species (* = exact match).

Organism	Alignment TRPV5
Mouse	AIIATLLMLNLFIAMMGDTHWRVAQERDELWRAQVVATTVM
Rat	AIIATLLMLNLFIAMMGDTHWRVAQERDELWRAQVVATTVM
Rabbit	AIIATLLMLNLFIAMMGDTHWRVAQERDELWRAQVVATTVM
Human	AIIATLLMLNLFIAMMGDTHWRVAQERDELWRAQVVATTVM
Chimpanzee	AIIATLLMLNLFIAMMGDTHWRVAQERDELWRAQVVATTVM
	**************************************

Table 2: Sequence alignment of TRPV channels. W583 is only conserved in the highly homologous TRPV6 channel (* = exact match; : = strongly similar properties; . = weakly similar properties).

Gain of function in TRPV5 upon W583 mutation

To investigate the involvement of W583 in TRPV5 channel gating, site-directed mutagenesis was applied to substitute W583 into different amino acids (aromatic: $TRPV5^{W583Y}$ and $TRPV5^{W583F}$; non aromatic: $TRPV5^{W583Q}$, $TRPV5^{W583L}$ and $TRPV5^{W583A}$). The activity of the mutated channels was assessed using $^{45}Ca^{2+}$ uptake assays. The TRPV5 blocker ruthenium red was applied to determine the magnitude of the TRPV5-mediated $^{45}Ca^{2+}$ influx (29). The $^{45}Ca^{2+}$ uptake was similar between mutant and wild type TRPV5 (Fig 2A). However, the TRPV5 protein expression was significantly reduced in cells expressing mutants compared to wild type TRPV5 (Fig 2A). After correcting for expressional differences, a significant increase in $^{45}Ca^{2+}$ uptake was detected for all mutants (Fig 2B). In general, non-aromatic W583 mutants ($TRPV5^{W583Q}$, $TRPV5^{W583L}$ and $TRPV5^{W583A}$) yielded poor expression and a ~25 to 43-fold enhancement in Ca^{2+} uptake, while both aromatic $TRPV5^{W583Y}$ and $TRPV5^{W583F}$ mutants showed intermediate Ca^{2+} influx (~7 to 10-fold increase). Of note, partial but significant inhibition by ruthenium red treatment was observed in all TRPV5 mutants (Fig 2C).

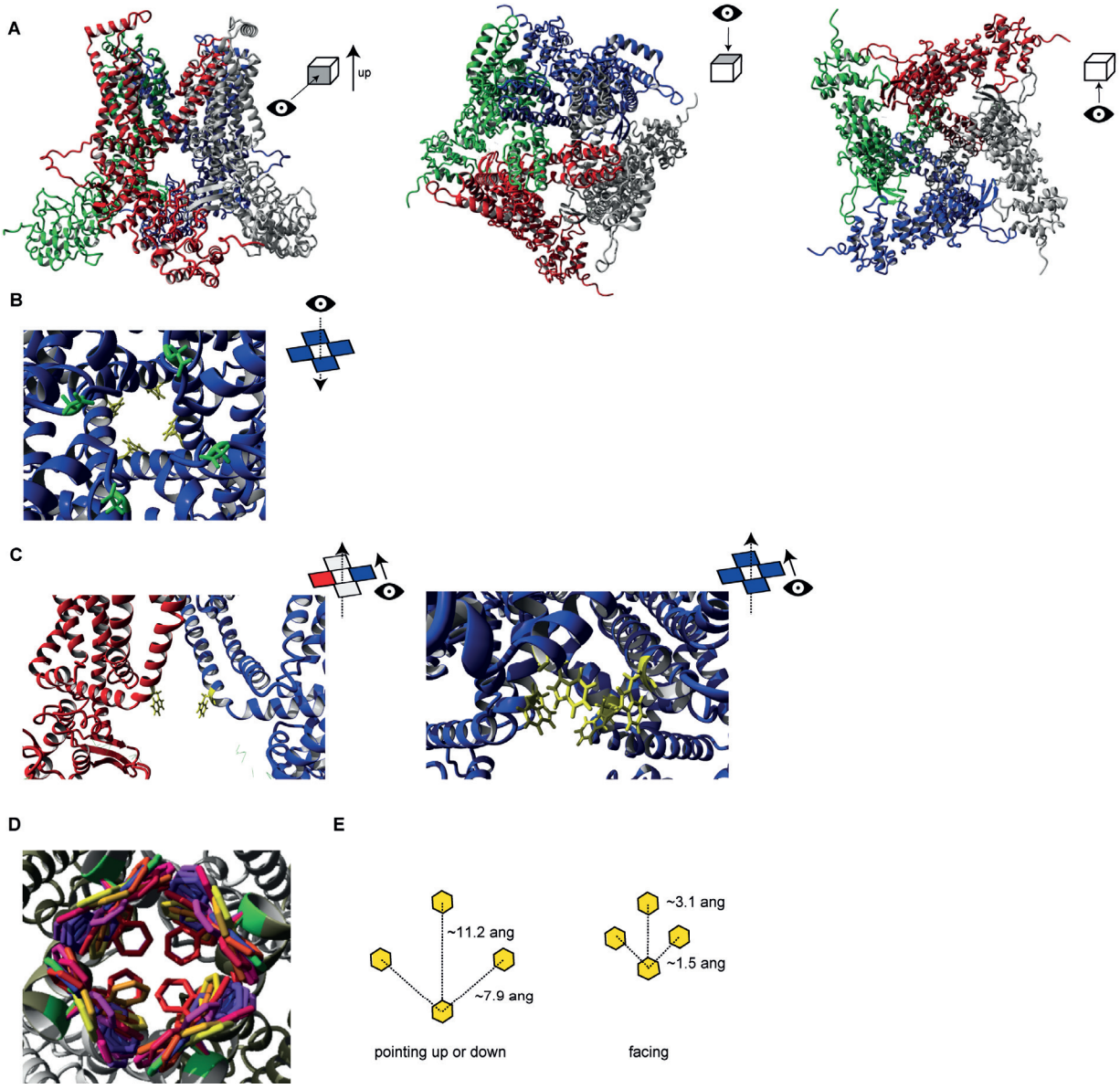

Figure 1. Homology model of TRPV5.
A) Side, top and bottom view of the tetrameric TRPV5 channel. Each subunit is displayed in a different color. **B)** Localization of the selectivity filter, composed of four D542 residues that are depicted in green. These residues are located at the top of the channel, at the bottom are presented the W583 residues in yellow. **C)** Side view of the W583 residue (yellow), presented at the interface of the lipid membrane layer and the cytosol. The hydrophobic side chains stick into the solvent. **D)** All possible rotameric positions for the W583 side chains. Three main rotameric positions are detected; with the side chains sticking up, pointing down or pointing towards each other. **E)** Distance between the W583 side chains based on the TRPV5 homology model in the main rotameric positions.

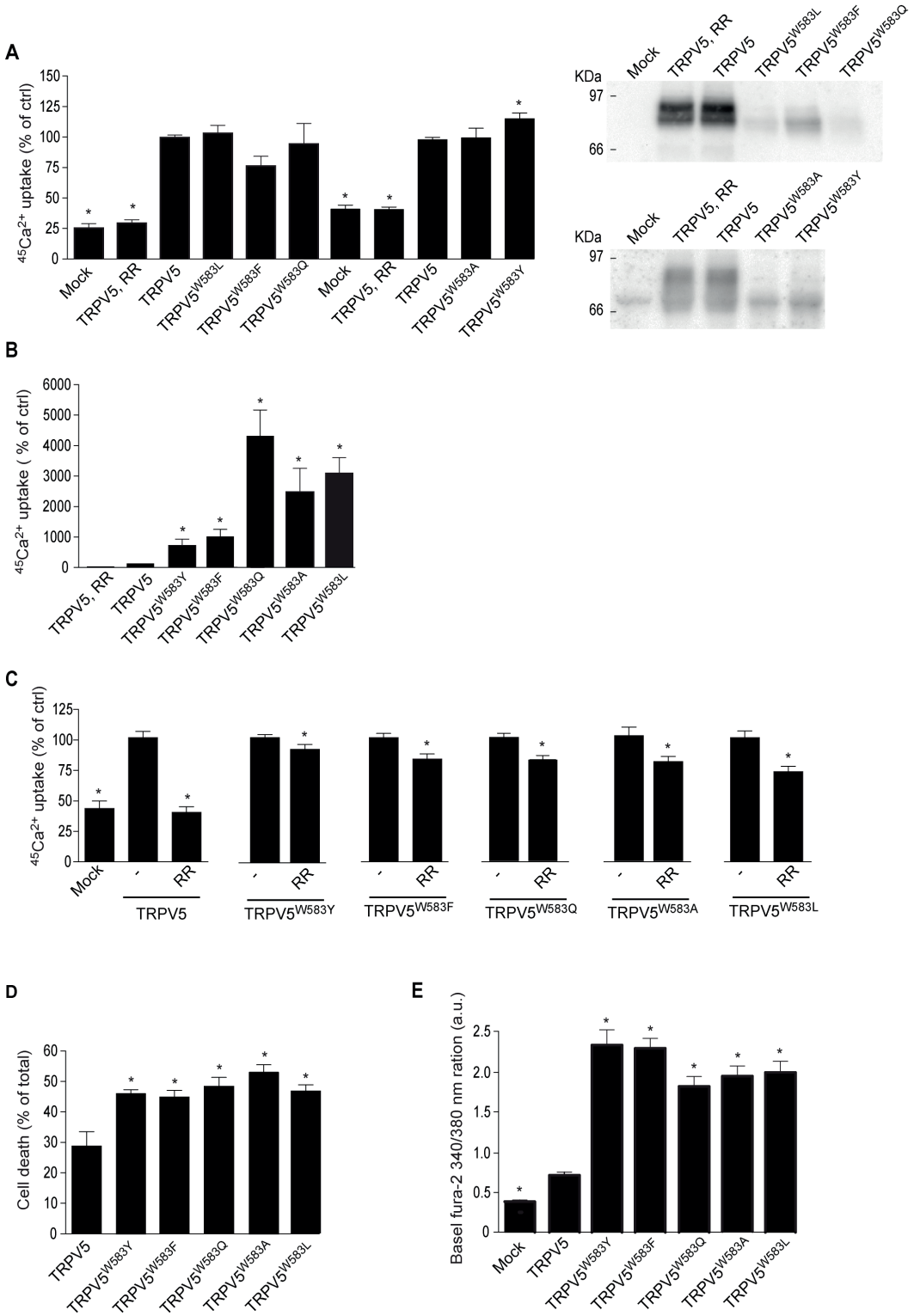

Figure 2. W583 mutation increases the Ca^{2+} uptake, resulting in cell death.
A) $^{45}Ca^{2+}$ uptake assay and the protein expression of HEK293 cells transfected with TRPV5, TRPV5^{W583L}, TRPV5^{W583F}, TRPV5^{W583Q}, TRPV5^{W583A} or TRPV5^{W583Y} (n=9, from three independent experiments). Ruthenium red (RR) was used as a negative control. **B)** $^{45}Ca^{2+}$ uptake assay of HEK293 cells transfected with TRPV5, TRPV5^{W583Y}, TRPV5^{W583F}, TRPV5^{W583Q}, TRPV5^{W583A} or TRPV5^{W583L} corrected for protein expression. **C)** $^{45}Ca^{2+}$ uptake of the W583 mutants can be blocked by treatment with the TRPV5 inhibitor RR (10 μM) (n=9-12, from three independent experiments). **D)** Cell viability assay of HEK293 cells expressing TRPV5 or any of the W583 mutants. Modulation of the W583 residue results in cell mortality (n=6, from three independent experiments). **E)** The basal intracellular Ca^{2+} levels, as measured by fura-2-AM, are significantly increased for all W583 mutants compared to TRPV5 expressing cells (n>30, from two independent experiments). Data shown are mean ± SEM, statistical significance is reflected by * (p<0.05).

In line with the reduced protein expression, we observed a decrease in cell survival upon transfection with the TRPV5 mutants, which was confirmed by a trypan blue assay demonstrating enhanced cell mortality for all TRPV5 mutants, compared to wild type TRPV5 (Fig 2D). To support the link between enhanced TRPV5 Ca^{2+} uptake and reduced cell survival, the basal intracellular Ca^{2+} levels were assessed using fura-2-AM, a cell-permeant ratiometric fluorescent Ca^{2+} indicator. Compared to a basal Ca^{2+} level of 0.7 arbitrary units (a.u.) in wild type TRPV5, the basal levels of the W583 mutants were approximately 3-fold enhanced (1.8 - 2.3 a.u.) (Fig 2E). These high intracellular Ca^{2+} levels might cause the observed cell death.

TRPV5 W583 mutants are functional at the plasma membrane

Next, a non-aromatic and aromatic mutant TRPV5 channel ($TRPV5^{W583L}$ and $TRPV5^{W583F}$) were subjected to whole-cell patch clamp recording to examine the channel characteristics. Figure 3A shows representative traces of TRPV5, $TRPV5^{W583L}$ and $TRPV5^{W583F}$ that are recorded using a voltage step protocol (from -100 to 40 mV). Importantly, the mutant channels exhibited the characteristic Na^+ inward-rectifying current in nominally divalent-free (nDVF) bath solution, which were enhanced upon extracellular addition of EGTA (DVF) (Fig 3A). Of note, the absolute currents of both TRPV5 mutants were 3-4 fold smaller than wild type TRPV5. To confirm channel expression at the plasma cell membrane, a cell surface biotinylation was performed on HEK293 cells expressing TRPV5, $TRPV5^{W583L}$ and $TRPV5^{W583F}$. Even though the overall protein expression was reduced, the relative plasma membrane abundance of both $TRPV5^{W583L}$ and $TRPV5^{W583F}$ was not altered (Fig 3B).

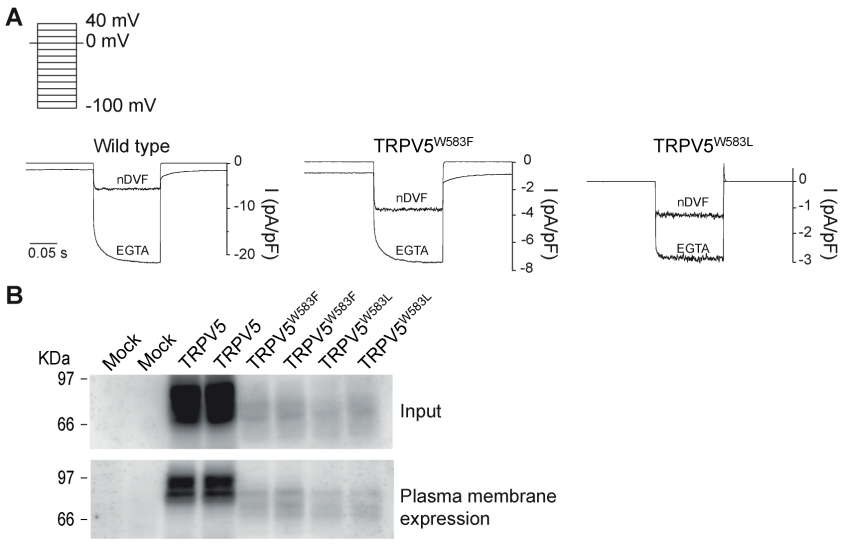

Figure 3. TRPV5 W mutants are functional at whole-cell level and expressed at the plasma membrane. **A)** Representative traces of the whole-cell Na^+ currents of TRPV5, $TRPV5^{W583L}$ and $TRPV5^{W583F}$ are measured from a step protocol (-100 to +40 mV) in nominally DVF (nDVF) and divalent-free (EGTA) solutions. **B)** Cell surface biotinylation of TRPV5, $TRPV5^{W583L}$ and $TRPV5^{W583F}$. Top panel displays the total protein expression, while the bottom panel displays the fraction of TRPV5 present on the plasma membrane. Representative immunoblot of three independent experiments is depicted.

Mutation of W583 increases the open probability of TRPV5

In order to assess putative changes in the intrinsic properties of the mutant TRPV5 channels, cells expressing wild type TRPV5, $TRPV5^{W583F}$, $TRPV5^{W583L}$, $TRPV5^{W583Y}$, $TRPV5^{W583A}$ and $TRPV5^{W583Q}$ were subjected to cell-attached patch clamp. Briefly, TRPV5 activity was measured by applying a series of 10 s voltage steps to -80 mV from a holding

voltage of 0 mV, using Na^+ as the charge carrier. By applying this protocol, frequent patches containing one to three channels were obtained and analyzed for amplitude of openings and open probability. Representative channel openings and amplitude histograms are depicted in Figure 4. While TRPV5^{W583F} showed no difference in openings compared to wild type TRPV5, the TRPV5^{W583L}, TRPV5^{W583Y}, TRPV5^{W583A} and TRPV5^{W583Q} mutants presented altered single-channel activity with shorter closing and opening times (Fig 4A-F). Analysis of these recordings revealed a ~2-fold increase in the open probability of TRPV5^{W583Q}, TRPV5^{W583L}, TRPV5^{W583Y}, and TRPV5^{W583A} compared to TRPV5 (Fig 4G). On the other hand, the open probability of TRPV5^{W583F} was decreased compared to the wild type channel (Fig 4C, G). The amplitude of opening at -80 mV was not significantly different between wild type and the mutants (Fig 4H).

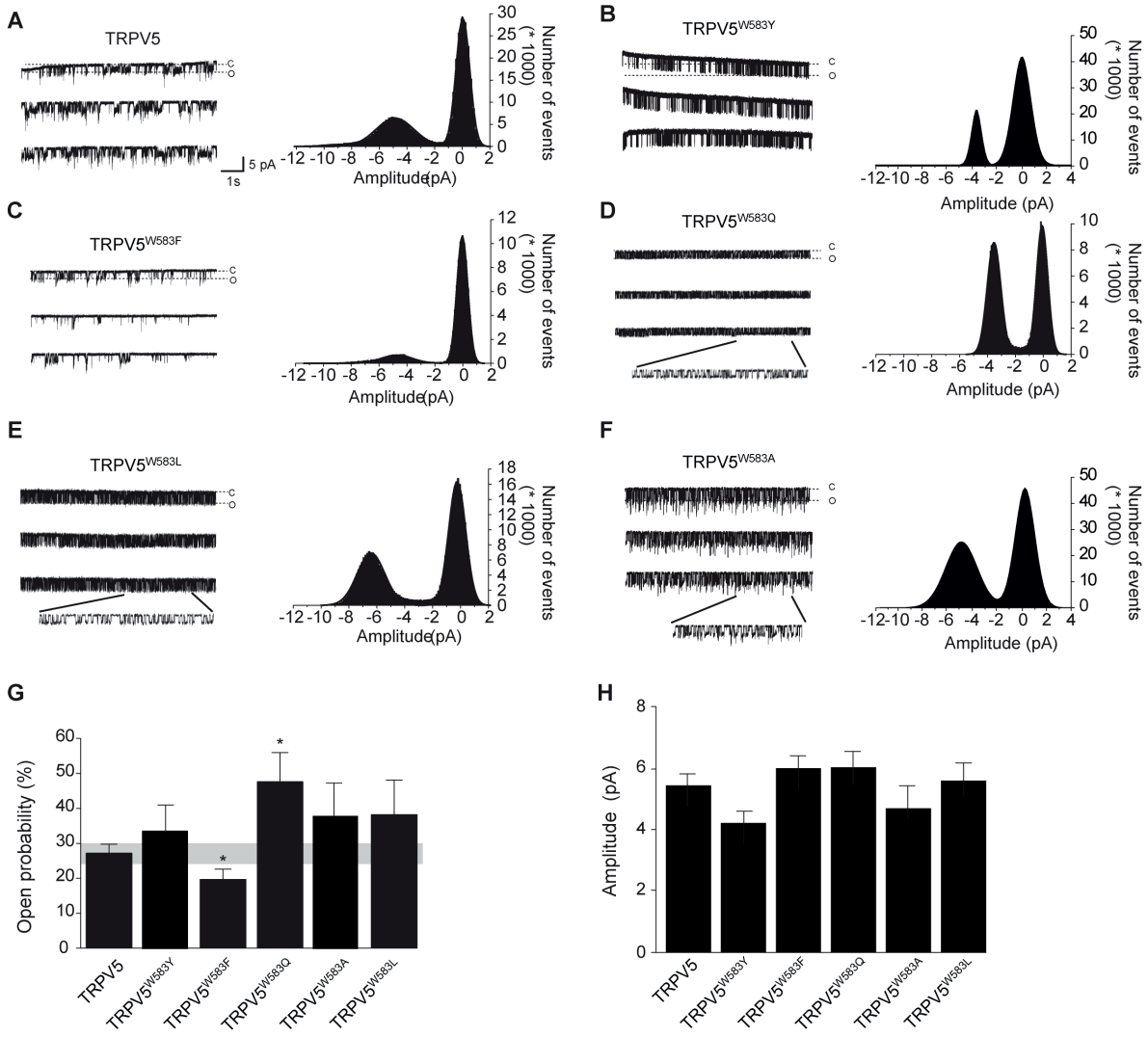

Figure 4. Single channel activity is increased in the TRPV5 W583 mutants.
Cell-attached single channel recordings were measured during a 10 s step to -80 mV (holding potential 0 mV) in **A)** wild type TRPV5, **B)** TRPV5^{W583Y}, **C)** TRPV5^{W583F}, **D)** TRPV5^{W583Q}, **E)** TRPV5^{W583A}, **F)** TRPV5^{W583L}. Representative amplitude histograms are shown with a Gaussian fit function corresponding to the closed and open states. **G)** The average open probability and **H)** amplitude are plotted for wild type and mutant TRPV5 (n>7 per condition). Data shown are mean ± SEM, statistical significance is reflected by * (p<0.05).

W583 does not participate in CaM binding

To address the role of the TRPV5 W583 residue in CaM binding and its involvement on TRPV5 activity, a CaM binding assay was performed for wild type TRPV5, TRPV5^{W583F} and

TRPV5^{W583L}. It has previously been demonstrated that CaM binds to or near the intracellular C-terminal region of TRPV5, involving the W702 residue (12). Mutation of this residue or deletion of the TRPV5 C-terminal region (TRPV5^{S689X}) significantly enhanced Ca^{2+} influx and cell death. Since CaM can bind at different positions in TRPV5, we hypothesized that W583 could also be involved in CaM binding. Hence, the TRPV5^{S689X} mutant was used to prevent CaM from binding to the C-terminal region. In order to enhance the cell survival of TRPV5^{S689X}, an additional D542A pore mutation (7) was incorporated as mutation of this residue is known to block the Ca^{2+} influx (7). The resulting TRPV5$^{D542A, S698X}$ double mutant was used to assess whether W583 may form or participate in an additional binding site(s) of CaM (12). Calmodulin immobilized on agarose beads was used to precipitate TRPV5$^{D542A, S698X}$ in the absence (EGTA) or presence of Ca^{2+}. Clear binding of TRPV5$^{D542A, S698X}$ was observed in the presence of Ca^{2+}, and a weak background CaM binding under Ca^{2+}-free conditions (Fig 5A). The precipitation of the TRPV5$^{D542A, W583F, S698X}$ and TRPV5$^{D542A, W583L, S698X}$ mutants by CaM was similar compared to wild type TRPV5, implying that W583 is not involved in CaM binding (Fig 5B). Patch clamp analysis revealed that co-transfection with CaM significantly increases the open probability for TRPV5, but decreased the elevated open probability of TRPV5^{W583Q} (Fig 5C).

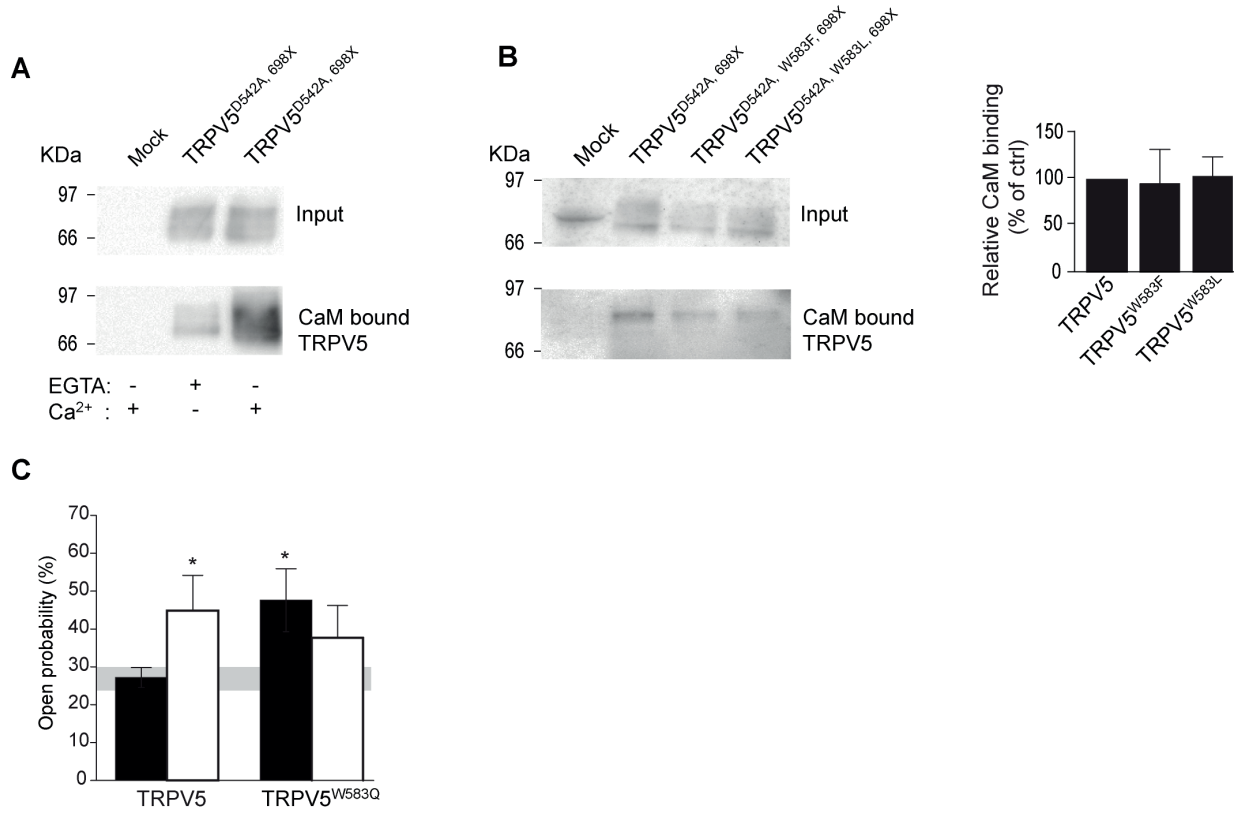

Figure 5. W583 is not involved in CaM binding.
A) TRPV5$^{D542, S698X}$ binds CaM in the presence of Ca^{2+}. The top panel displays the total channel expression and the bottom panel illustrates the CaM bound TRPV5 fraction. **B)** Both TRPV5$^{D542, S698X, W583F}$ and TRPV5$^{D542, S698X, W583L}$ bind CaM in the presence of Ca^{2+}. Quantification is performed over three independent experiments. **C)** The average open probability of TRPV5 and TRPV5^{W583Q} without or with CaM co-expression. Black bars represent control; white bars represent co-expression with CaM. Data shown are mean ± SEM, statistical significance is reflected by * (p<0.05).

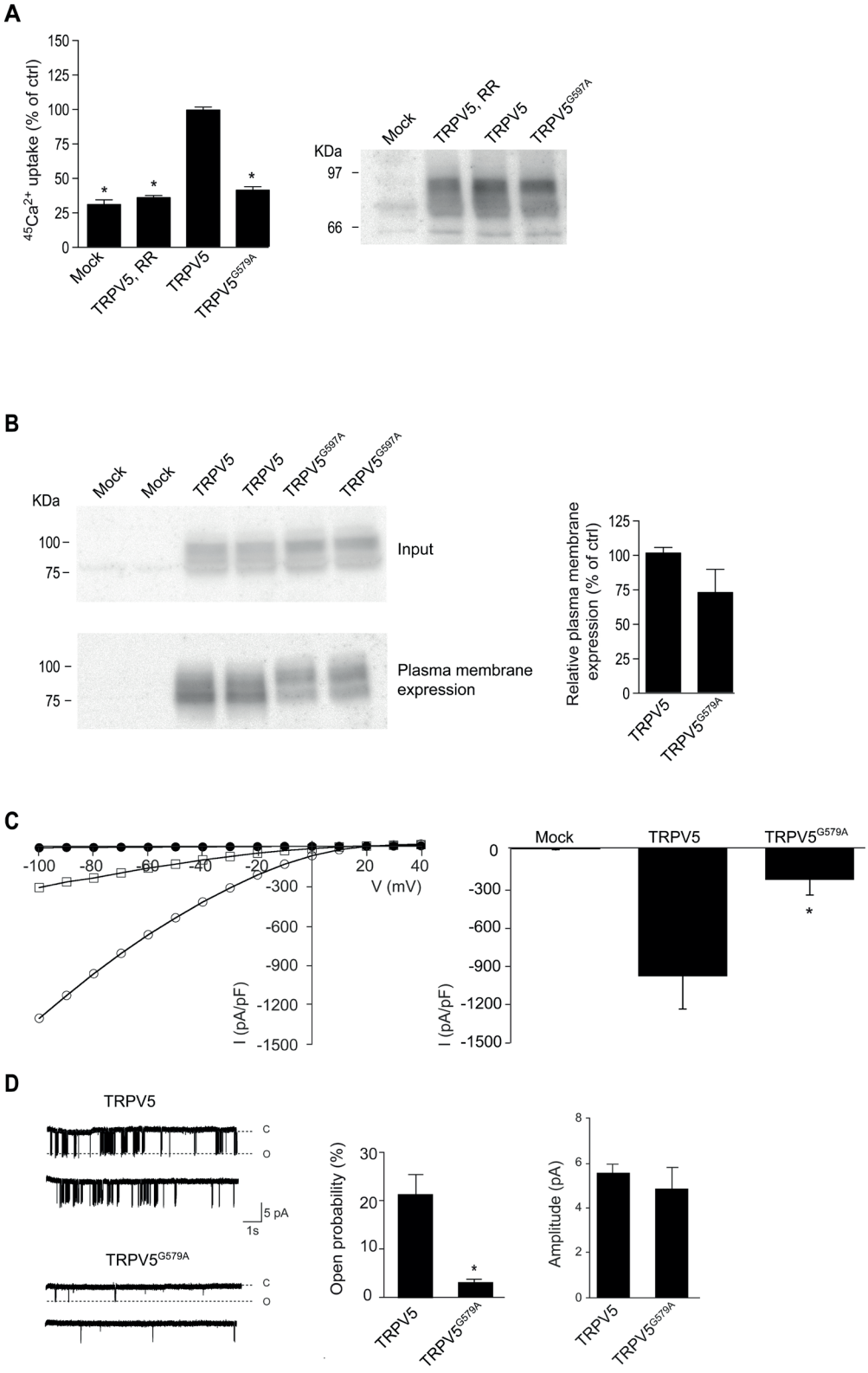

Figure 6. TRPV5^{G579A} mutation blocks TRPV5-mediated Ca^{2+} uptake and channel activity.
A) $^{45}Ca^{2+}$ uptake assay of the TRPV5^{G579A} mutant. The protein expression level is not altered (n=9, from three independent experiments). **B)** TRPV5^{G579A} protein expression at the plasma membrane. The top panel displays the total channel expression, and the bottom panel illustrates the plasma membrane fraction. Representative immunoblot of three independent experiments is depicted. **C)** The I-V relation of mock, wild type TRPV5 and TRPV5^{G579A} is extracted through a voltage step protocol in DVF solution (left). Averaged Na^+ current densities at -80 mV are presented in the right panel. **D)** The open probability at -80 mV is assessed using cell-attached patch clamp in cells expressing the TRPV5^{G579A} mutant. Typical single-channel behaviour is shown for TRPV5^{G579A}. The average open probability is determined (n>7 per condition). Data shown are mean ± SEM, statistical significance is reflected by * (p<0.05).

G579 forms the inner pore helix hinge

In addition to the identification of W583, we detected a flexible hinge point one α-helical turn above the aromatic gate. This G579 residue could form a structural hinge point, allowing the W583 residues to change position. In order to test this hypothesis, G579 was mutated into the more rigid alanine. Radioactive Ca^{2+} uptake experiments demonstrated that $TRPV5^{G579A}$ function is significantly reduced (41 ± 3% vs 100 ± 2%) and comparable to ruthenium red-inhibited uptake levels (36 ± 2%). Total protein expression was not altered (Fig 6A). Cell surface biotinylation assays showed that $TRPV5^{G579A}$ is present at the plasma membrane, although at slightly reduced levels (100 ± 4% vs. 72 ± 16%) (Fig 6B). Whole-cell patch clamp recording demonstrated a significantly diminished current density for $TRPV5^{G579A}$, with no difference in the current/voltage relationship (Fig 6C). Cell-attached single channel analysis of the $TRPV5^{G579A}$ mutant revealed a decreased open probability of 3 ± 0.6% compared of 21 ± 4% for wild type (Fig 6D). Of note, the amplitude of opening is not changed (Fig 6D).

Discussion

This study presents a new model for TRPV5 channel gating in which the channel is mediated by an aromatic gate (W583) in combination with a gating hinge (G579) (Fig 7). This conclusion is based on the following observations: *i*) $^{45}Ca^{2+}$ uptake is increased for all W583 mutants; *ii*) basal intracellular Ca^{2+} levels are higher in all W583 mutants; *iii*) the open probability of the W583 mutants, except for $TRPV5^{W583F}$, is increased, and *iv*) $^{45}Ca^{2+}$ influx and the open probability of the $TRPV5^{G579A}$ mutant is decreased.

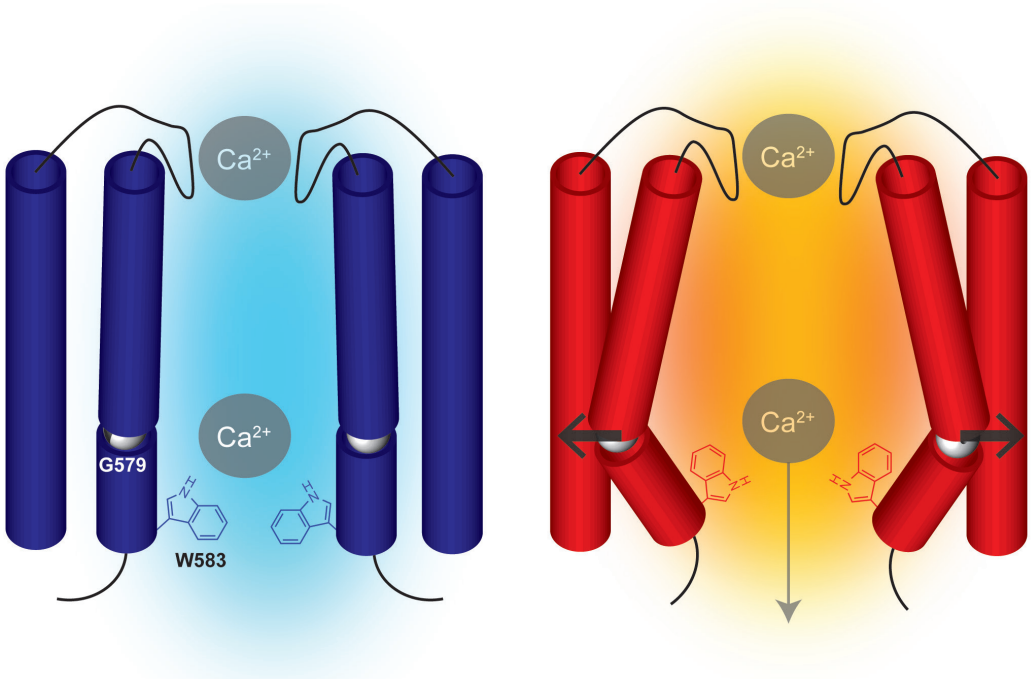

Figure 7. Proposed gating mechanism of TRPV5.
The gate of TRPV5 is composed of a glycine hinge and a tryptophan gating residue at the end of TM domain six (blue). A currently unknown stimulus induces the bending of the inner pore helix, changing the relative position of the tryptophan residues resulting in channel opening (red).

A TRPV5 homology model was developed based on the recently solved TRPV1 structure. The rotameric conformations of W583 were analyzed and three major side chain positions were detected: pointing down, pointing up or facing each other. Unless Ca^{2+} is protein bound, the ion is surrounded by a hydration shell of nine to ten water

molecules (30). The passage of Ca^{2+} with a hydration shell requires 2.95 Å, while dehydrated Ca^{2+} ions only have a diameter of 0.99 Å (28). Passage of Ca^{2+} with a hydration shell is likely to be impeded, independent of the rotameric position of W583. When the W583 side chains are facing each other, passage of dehydrated Ca^{2+} ions will be hampered since the estimated distance between the centers of the side chains is ~3.1 Å, implying that the size for passage is ~0.8 Å (Fig 1E). Both other rotameric positions are not likely to hinder the dehydrated Ca^{2+} flow, as the gate radius is ~11.2 Å.

Often, aromatic residues anchor proteins into the cell membrane through interactions with the lipid head groups (31). These residues are then localized at the interfacial regions of a TM α-helix and the solvent, acting to anchor the helix into the cell membrane (31). Tryptophan residues generally localize to the extracellular face in α-helical membrane proteins (32), in contradiction to what is observed here for TRPV5. In addition, the current homology model suggests that W583 is pointing in opposite direction from the lipids. These observations, together with the present findings suggest that W583 may not participate in the interaction of the α-helix with lipids, but has a role in channel gating. As a result of their size and oblateness, a small rotation in the aromatic residue can lead to a large change in width of the gate (14).

It was demonstrated that substitution of W583 with a non-aromatic residue ($TRPV5^{W583Q}$, $TRPV5^{W583L}$, $TRPV5^{W583A}$) results in massive $^{45}Ca^{2+}$ influx and cell death, while change to an aromatic residue ($TRPV5^{W583F}$, $TRPV5^{W583Y}$) seems to have a more intermediate phenotype. The open probability of $TRPV5^{W583F}$ is even decreased compared to wild type TRPV5. Possibly, $TRPV5^{W583F}$ is leaky towards Ca^{2+}, but can still close the channel to some extent as a result of its hydrophobic aromatic characteristics. The reduced cell viability of the W583 mutants is likely a result of high intracellular Ca^{2+} concentration, as evidenced using ratiometric fura-2-AM imaging. The overall deleterious effect and scarcity of suitable cells did not allow for accurate quantification and comparison of current densities between the TRPV5 W583 mutants and wild type TRPV5. A similar effect on the cell viability was observed for the overactive $TRPV5^{M490P}$ and $TRPV5^{S698X}$ mutants (22,33). The observed ruthenium red-mediated inhibition of the W583 mutants was smaller compared to TRPV5. Ruthenium red blocks TRPV5 function in a voltage-dependent manner, by binding to the extracellular side of the channel (29). A possible explanation for the partial ruthenium red inhibition is that cells expressing W583 mutants might not have an intact transmembrane voltage, given their poor viability.

CaM is previously described as the mediator of Ca^{2+}-dependent TRPV5 inhibition (12). The high intracellular Ca^{2+} levels in cells expressing the W583 mutants might imply that W583 is involved in the TRPV5 interaction with CaM. However, our TRPV5 homology model implies that CaM (PDB: 3CLN) cannot reach W583, as a result of steric hindrance. Furthermore, there was no difference in CaM binding observed for the tested $TRPV5^{D542A,\ S698X,\ W583L}$ and $TRPV5^{D542A,\ S698X,\ W583F}$. Based on these indirect data it is not likely that CaM is involved int his regulation pathway, however it cannot be excluded. Interestingly, co-expression of TRPV5 with CaM increased the single-channel open probability, an effect that appears counter-intuitive based on the previously described inhibitory role of CaM (12). A likely explanation is that over-expressed CaM is sufficient to buffer intracellular Ca^{2+} and thereby increases the TRPV5 channel open probability. This effect would be absent in $TRPV5^{W583Q}$ due to the high basal intracellular Ca^{2+} concentration. Further experiments will be needed to address this question.

A gating function for aromatic residues has been observed previously for other ion channels. The proton-selective influenza virus M_2 channel is regulated by a so-called

tryptophan gate (34). This tryptophan gate is stabilized by aspartate residues through a network of hydrogen bonds, which support the closed state conformation of the channel (35). Upon lowering the outside pH, four histidine residues in this network are protonated, leading to a change in conformation of the tryptophan gate. Moreover, the prokaryotic K^+ channel KcsA is regulated by a phenylalanine gate and mutations at this position have a size-dependent effect on gating kinetics (36). Small side-chain substitution results in impaired inactivation kinetics, while substitution with larger side chain residues has minor effects on channel characteristics. The prokaryotic K^+ inwardly rectifying KirBac 1.1 channel functions in a similar manner through four phenylalanine residues at the cytoplasmic end of the pore (37). These residues are displaced by bending a so-called gating hinge (a glycine) in the inner pore helices, thereby allowing channel opening (14,38). A similar gating mechanism has been proposed for the closely related KirBac 3.1 channel, using a tyrosine residue (39). The TRPV5 homology model reveals a highly conserved glycine (G579), located one α-helical turn above the aromatic gate that may cause such a helix kink. Mutation of G579 into an alanine completely blocked the $^{45}Ca^{2+}$ uptake by reducing the open probability, leading to the hypothesis that G579 is essential for proper channel gating. Substitution of this residue confers the channel pore into a rigid closed state.

Future work aims at studying the stimulus for this conformational change. The TRPV5 TM six α-helix is known to change its conformation upon extracellular acidification (40). In addition, the pore helix is rotated along its axis as a result of intra- or extracellular acidification (41). A pH sensitive histidine (582) is located directly above the tryptophan gate. Protonation of the histidine residue might cause the hinge to change the relative positions of the tryptophan residues, thereby opening or closing the channel. In addition, external factors such as phosphatidylinositol 4,5-bisphosphate (PIP_2) can potentially regulate the TRPV5 gating mechanism. PIP_2 stabilizes TRPV5 in its open conformation (42). The TRP domain, located directly below the tryptophan gate, is involved in the PIP_2-mediated stimulation (43). Interestingly, TRPV5, TRPV6 and the K^+ channels displaying a similar type of gating are all stimulated by PIP_2 (14,44). In contrast, TRPV1 shows no conservation of the tryptophan gate and is inhibited by PIP_2 (43). Future studies should determine the stimulus underlying the conformational changes that result in TRPV5 channel gating.

References

1. Hoenderop, J. G., van der Kemp, A. W., Hartog, A., van de Graaf, S. F., van Os, C. H., Willems, P. H., and Bindels, R. J. (1999) Molecular identification of the apical Ca^{2+} channel in 1, 25-dihydroxyvitamin D3-responsive epithelia. *J biol chem* **274**, 8375-8378
2. Hoenderop, J. G. J., van der Kemp, A. W. C. M., Hartog, A., van Os, C. H., Willems, P. H. G. M., and Bindels, R. J. M. (1999) The Epithelial Calcium Channel, ECaC, Is Activated by Hyperpolarization and Regulated by Cytosolic Calcium. *Biochemical and biophysical research communications* **261**, 488-492
3. Nilius, B., Vennekens, R., Prenen, J., Hoenderop, J. G., Bindels, R. J., and Droogmans, G. (2000) Whole-cell and single channel monovalent cation currents through the novel rabbit epithelial Ca^{2+} channel ECaC. *J Physiol* **527 Pt 2**, 239-248
4. Vennekens, R., Hoenderop, J. G., Prenen, J., Stuiver, M., Willems, P. H., Droogmans, G., Nilius, B., and Bindels, R. J. (2000) Permeation and gating properties of the novel epithelial Ca^{2+} channel. *J biol chem* **275**, 3963-3969
5. Dimke, H., Hoenderop, J. G. J., and Bindels, R. J. M. (2011) Molecular basis of epithelial Ca^{2+} and Mg^{2+} transport: insights from the TRP channel family. *Journal of Physiology-London* **589**, 1535-1542
6. Hoenderop, J. G., and Bindels, R. J. (2008) Calciotropic and magnesiotropic TRP channels. *Physiology (Bethesda)* **23**, 32-40
7. Nilius, B., Vennekens, R., Prenen, J., Hoenderop, J. G., Droogmans, G., and Bindels, R. J. (2001) The single pore residue Asp542 determines Ca^{2+} permeation and Mg^{2+} block of the epithelial Ca2+ channel. *J Biol Chem* **276**, 1020-1025
8. Owsianik, G., Talavera, K., Voets, T., and Nilius, B. (2006) Permeation and selectivity of TRP channels. *Annu Rev Physiol* **68**, 685-717
9. Dodier, Y., Dionne, F., Raybaud, A., Sauve, R., and Parent, L. (2007) Topology of the selectivity filter of a TRPV channel: rapid accessibility of contiguous residues from the external medium. *Am J Physiol Cell Physiol* **293**, C1962-1970
10. Nilius, B., Prenen, J., Vennekens, R., Hoenderop, J. G., Bindels, R. J., and Droogmans, G. (2001) Modulation of the epithelial calcium channel, ECaC, by intracellular Ca^{2+}. *Cell Calcium* **29**, 417-428
11. Lambers, T. T., Weidema, A. F., Nilius, B., Hoenderop, J. G. J., and Bindels, R. J. M. (2004) Regulation of the Mouse Epithelial Ca^{2+} Channel TRPV6 by the Ca^{2+}-sensor Calmodulin. *The Journal of biological chemistry* **279**, 28855-28861
12. de Groot, T., Kovalevskaya, N. V., Verkaart, S., Schilderink, N., Felici, M., van der Hagen, E. A., Bindels, R. J., Vuister, G. W., and Hoenderop, J. G. (2011) Molecular mechanisms of calmodulin action on TRPV5 and modulation by parathyroid hormone. *Mol Cell Biol* **31**, 2845-2853
13. Niemeyer, B. A., Bergs, C., Wissenbach, U., Flockerzi, V., and Trost, C. (2001) Competitive regulation of CaT-like-mediated Ca2+ entry by protein kinase C and calmodulin. *Proc Natl Acad Sci U S A* **98**, 3600-3605
14. Zhou, H. X., and McCammon, J. A. (2010) The gates of ion channels and enzymes. *Trends Biochem Sci* **35**, 179-185
15. Elinder, F., Nilsson, J., and Arhem, P. (2007) On the opening of voltage-gated ion channels. *Physiol Behav* **92**, 1-7
16. Liao, M. F., Cao, E. H., Julius, D., and Cheng, Y. F. (2013) Structure of the TRPV1

ion channel determined by electron cryo-microscopy. *Nature* **504**, 107-112
17. Sander, C., and Schneider, R. (1991) Database of homology-derived protein structures and the structural meaning of sequence alignment. *Proteins* **9**, 56-68
18. Krieger, E., Koraimann, G., and Vriend, G. (2002) Increasing the precision of comparative models with YASARA NOVA - a self-parameterizing force field. *Proteins* **47**, 393-402
19. Vriend, G. (1990) What If - a Molecular Modeling and Drug Design Program. *J Mol Graphics* **8**, 52-58
20. van de Graaf, S. F., Hoenderop, J. G., Gkika, D., Lamers, D., Prenen, J., Rescher, U., Gerke, V., Staub, O., Nilius, B., and Bindels, R. J. (2003) Functional expression of the epithelial Ca^{2+} channels (TRPV5 and TRPV6) requires association of the S100A10-annexin 2 complex. *EMBO J* **22**, 1478-1487
21. de Groot, T., Lee, K., Langeslag, M., Xi, Q., Jalink, K., Bindels, R. J., and Hoenderop, J. G. (2009) Parathyroid hormone activates TRPV5 via PKA-dependent phosphorylation. *J Am Soc Nephrol* **20**, 1693-1704
22. de Groot, T., Verkaart, S., Xi, Q., Bindels, R. J. M., and Hoenderop, J. G. J. (2010) The Identification of Histidine 712 as a Critical Residue for Constitutive TRPV5 Internalization. *J biol chem* **285**, 28481-28487
23. de Groot, T., Lee, K., Langeslag, M., Xi, Q., Jalink, K., Bindels, R. J. M., and Hoenderop, J. G. J. (2009) Parathyroid Hormone Activates TRPV5 via PKA-Dependent Phosphorylation. *J Am Soc Nephrol* **20**, 1693-1704
24. Milescu, L. S., Nicolai, C., and Bannen, J. (2000-2013) Qub Software.
25. Chang, Q., Hoefs, S., van der Kemp, A. W., Topala, C. N., Bindels, R. J., and Hoenderop, J. G. (2005) The beta-glucuronidase klotho hydrolyzes and activates the TRPV5 channel. *Science* **310**, 490-493
26. Phelps, C. B., Huang, R. J., Lishko, P. V., Wang, R. R., and Gaudet, R. (2008) Structural analyses of the ankyrin repeat domain of TRPV6 and related TRPV ion channels. *Biochemistry* **47**, 2476-2484
27. Dodier, Y., Dionne, F., Raybaud, A., Sauvé, R., and Parent, L. (2007) Topology of the selectivity filter of a TRPV channel: rapid accessibility of contiguous residues from the external medium. *Am j physiol cell physiol* **293**, 1962-1970
28. Maguire, M. E., and Cowan, J. A. (2002) Magnesium chemistry and biochemistry. *Biometals* **15**, 203-210
29. Nilius, B., Prenen, J., Vennekens, R., Hoenderop, J. G. J., Bindels, R. J. M., and Droogmans, G. (2001) Pharmacological modulation of monovalent cation currents through the epithelial Ca^{2+} channel ECaC1. *Brit J Pharmacol* **134**, 453-462
30. Palinkas, G., and Heinzinger, K. (1986) Hydration shell structure of calcium-ion. *Chemical Physics Letters* **126**, 251-254
31. Pilpel, Y., Ben-Tal, N., and Lancet, D. (1999) kPROT: a knowledge-based scale for the propensity of residue orientation in transmembrane segments. Application to membrane protein structure prediction. *J Mol Biol* **294**, 921-935
32. Ulmschneider, M. B., and Sansom, M. S. P. (2001) Amino acid distributions in integral membrane protein structures. *Biochimica Et Biophysica Acta-Biomembranes* **1512**, 1-14
33. Lee, K. P., Nair, A. V., Grimm, C., van Zeeland, F., Heller, S., Bindels, R. J. M., and Hoenderop, J. G. J. (2010) A helix-breaking mutation in the epithelial Ca^{2+} channel TRPV5 leads to reduced Ca^{2+}-dependent inactivation. *Cell calcium* **48**, 275-287
34. Tang, Y. J., Zaitseva, F., Lamb, R. A., and Pinto, L. H. (2002) The gate of the

influenza virus M-2 proton channel is formed by a single tryptophan residue. *J Biol Chem* **277**, 39880-39886
35. Ma, C. L., Fiorin, G., Carnevale, V., Wang, J., Lamb, R. A., Klein, M. L., Wu, Y. B., Pinto, L. H., and DeGrado, W. F. (2013) Asp44 Stabilizes the Trp41 Gate of the M2 Proton Channel of Influenza A Virus. *Structure* **21**, 2033-2041
36. Cuello, L. G., Jogini, V., Cortes, D. M., Pan, A. C., Gagnon, D. G., Dalmas, O., Cordero-Morales, J. F., Chakrapani, S., Roux, B., and Perozo, E. (2010) Structural basis for the coupling between activation and inactivation gates in K+ channels. *Nature* **466**, 272-U154
37. Kuo, A. L., Gulbis, J. M., Antcliff, J. F., Rahman, T., Lowe, E. D., Zimmer, J., Cuthbertson, J., Ashcroft, F. M., Ezaki, T., and Doyle, D. A. (2003) Crystal structure of the potassium channel KirBac1.1 in the closed state. *Science* **300**, 1922-1926
38. Vemparala, S., Domene, C., and Klein, M. L. (2008) Interaction of anesthetics with open and closed conformations of a potassium channel studied via molecular dynamics and normal mode analysis. *Biophys J* **94**, 4260-4269
39. Kuo, A., Domene, C., Johnson, L. N., Doyle, D. A., and Venien-Bryan, C. (2005) Two different conformational states of the KirBac3.1 potassium channel revealed by electron crystallography. *Structure* **13**, 1463-1472
40. Yeh, B. I., Sun, T. J., Lee, J. Z., Chen, H. H., and Huang, C. L. (2003) Mechanism and molecular determinant for regulation of rabbit transient receptor potential type 5 (TRPV5) channel by extracellular pH. *J Biol Chem* **278**, 51044-51052
41. Yeh, B.-I., Kim, Y. K., Jabbar, W., and Huang, C.-L. (2005) Conformational changes of pore helix coupled to gating of TRPV5 by protons. *The EMBO journal* **24**, 3224-3234
42. Lee, J., Cha, S. K., Sun, T. J., and Huang, C. L. (2005) PIP2 activates TRPV5 and releases its inhibition by intracellular Mg2+. *J Gen Physiol* **126**, 439-451
43. Rohacs, T., Lopes, C. M. B., Michailidis, I., and Logothetis, D. E. (2005) PI(4,5)P-2 regulates the activation and desensitization of TRPM8 channels through the TRP domain. *Nat Neurosci* **8**, 626-634
44. Suh, B. C., and Hille, B. (2005) Regulation of ion channels by phosphatidylinositol 4,5-bisphosphate. *Curr Opin Neurobiol* **15**, 370-378

VI

CHAPTER 6

General Discussion and Summary

Introduction

Glycosylation of a protein is the most complex and diverse form of posttranslational modification. Moreover, it is highly abundant as more than 50% of the total proteome is modified with a glycan (1). The composition of a glycan can influence protein activity, membrane trafficking and many other processes (2). However, due to the high degree of variability in glycan structure, it is difficult to investigate regulatory pathways in detail. In addition, only few labeling methods enable direct detection of glycans *in vitro* and *in vivo* (3).

The Transient Receptor Potential Vanilloid type 5 (TRPV5) Ca^{2+} channel is an example of a protein whose activity is regulated via a glycan located at an extracellular asparagine (N) side chain (therefore called N-glycan). The TRPV5 channel facilitates the gatekeeper function to regulate renal Ca^{2+} handling and determines the fine-tuning of Ca^{2+} excretion via the urine (4). This active transcellular Ca^{2+} reabsorption takes place in the late distal convoluted tubule (DCT2) and connecting tubule (CNT). Here, Ca^{2+} enters the epithelial cells via the constitutively active and Ca^{2+}-selective TRPV5 channel. The intrinsic activity, expression and plasma membrane abundance of the channel regulates the total amount of TRPV5-mediated Ca^{2+} influx, as illustrated in **chapter 1**. Control of TRPV5 function via the N-glycan is poorly understood as a result of the high complexity of glycan regulation and inadequate glycan labeling tools. This thesis elucidated the role of the N-glycan of TRPV5 in the physiological process of renal Ca^{2+} handling.

Glycan labeling via click chemistry

There is a need for glycan detection methods that do not interfere with the cell dynamics, are easy to use and have high labeling specificity. To this end, it is essential that the particular chemical reaction, which visualizes a glycan, takes place at a high rate and with low substrate concentration. Bioorthogonal reactions meet these criteria; with the most prominent glycan labeling method used nowadays being the copper-catalyzed azide–alkyne (3+2) cycloaddition, also known as the click reaction. The click reaction quickly and reliably joins two small molecules together, thereby enabling specific saccharide labeling. The attractiveness of this reaction can be attributed to its high biocompatibility and simplicity. Besides the popular copper(I)-catalyzed azide–alkyne cycloaddition (CuAAC), a copper-free version of the click reaction, known as strain-promoted azide–alkyne cycloaddition (SPAAC), has gained significant recognition (5). However, SPAAC is hampered by low specificity *in vitro* and *in vivo* (6,7). Reaction rate and selectivity are the two key factors determining the suitability of particular chemical reaction for bioconjugation (8).

As described in **chapter 1**, the chemical reporter strategy used for glycan labeling involves two steps, first the introduction of an abiotic molecular tag, followed by bioorthogonal conjugation with a molecule of choice with designed complementary reactivity. To date, the azide group ($–N_3$) is the most utilized bioorthogonal tag, as it is small and inert towards most components. In **chapter 2,** an azide-functionalized saccharide, *N*-azido-acetylmannosamine (ManNAz), was metabolically incorporated into proteins expressed in Human embryonic Kidney 293 (HEK293) cells at the position of the sialic acids. To ensure a good reactivity of SPAAC, optimal conditions for ManNAz incorporation were determined. The incorporation of ManNAz can differ between several cell lines, and the use of Chinese hamster ovarian (CHO) cells instead of HEK293 cells might improve labeling efficiency as a result of difference in metabolic incorporation and glycosylation patterns (9). In addition, ManNAz is also highly incorporated in gangliolipids, glycosylated lipids in the plasma membrane, which compose 75% of the total signal (10). Therefore, blocking the synthesis of gangliolipids can increase the labeling specificity for protein

N-glycans. ManNAz compete with the natural saccharide (N-acetylmannosamine) and has a lower affinity to metabolic enzymes compared to endogenous sugars, therefore only a fraction of proteins have the non-natural glycan incorporated. It remains to be elucidated if the non-natural sugar distribution reflects the *in vivo* glycan distribution.

Cyclooctynes, their strengths and weaknesses

The second step in the chemical reporter strategy involves the bioorthogonal conjugation. In **chapter 2**, the SPAAC reaction is used to label sialic acids in HEK293 cells with specific developed conjugating molecules, cyclooctynes. The past few years, the effectiveness of cyclooctynes used for SPAAC is greatly enhanced by structural modifications. The rate of most cyclooctynes used in SPAAC is high enough for *in vitro* and *in vivo* use (0.012 – 0.96 $M^{-1}s^{-1}$) (8). Biarylazacyclooctynone (BARAC) is the cyclooctyne with the highest reactivity, however broad application is hampered by its lengthy synthesis and low stability (11,12). As a result of their good reactivity, stability and accessibility, dibenzoazacyclooctyne (DIBAC) (13) and bicyclo[6.1.0]nonyne (BCN) (14) are the most commonly used cyclooctynes.

SPAAC is limited by its selectivity, as thiol-yne additions and unspecific hydrophobic interactions are common side reactions *in vitro* and *in vivo* (6,7). Thiol-yne additions, the reaction between a cyclooctyne and a free thiol, takes place at a relatively low rate compared to the SPAAC reaction (15). Though, once the cyclooctyne is residing intracellular or internalized by the animal, it cannot be removed that quickly, allowing thiol-yne additions. *In vitro*, free thiols can be blocked with iodoacetamide (IAM) prior to addition of a cyclooctyne, thereby preventing unspecific thiol-yne additions (6,16). However, administration of IAM is not suitable for living systems and, therefore, its use is restrained. *In vivo*, unspecific thiol-yne additions also limit specific detection, as cyclooctynes injected in mice react in an azide-independent manner with the free thiol group in serum albumin (17). Recently, a cyclooctyne displaying only low unspecific thiol-yne additions was developed (18). However, this might be attributed to the cell line used for these experiments and future studies should indicate the use of this cyclooctyne (19).

The hydrophobicity of cyclooctynes does not only result in poorly water-soluble compounds, but also in potential unspecific hydrophobic interactions with proteins or with the cell lipid bilayer. The calculated partition-coefficient (^{c}logP) indicates the distribution of a compound between two solutions, typically n-octanol and water, and is a measure of lipophilicity. Most cyclooctynes have a calculated ^{c}log P value between 0.8 and 4.8 (8) (Table 1). One can hypothesize that more polar cyclooctynes display a higher labeling specificity *in vitro* and *in vivo*. Leeper *et al.* developed a more polar variant of DIBO (20), called tetramethoxydibenzocyclooctyne (TMDIBO), with a reaction rate of ~ 9.8×10^{-2} $M^{-1}s^{-1}$ in the (3+2) cycloaddition with benzyl azide. The signal-to-noise ratio was greatly improved for this probe compared to DIFO3, a 3rd generation variant of difluorocyclooctyne (DIFO). Based on the ^{c}log P value, this improvement was unforeseen as the hydrophobicity for TMDIBO is higher than for DIFO3 (^{c}log P 3.7 vs. 3.3) (18). No direct correlation was detected between the labeling specificity and hydrophilicity of the cyclooctynes (Table 1 and Table 2), and therefore it can be assumed that unspecific signaling is caused by a combination of hydrophobic interactions and thiol-yne additions. Hence, the 'ideal' cyclooctyne will display low unspecific thiol-yne additions and hydrophobic interactions, which can be achieved by preventing intracellular accumulation of the cyclooctynes. The cyclooctyne can be easily removed when it is restricted to the outside of the cell, limiting its reaction time and thereby preventing the slow thiol-yne additions. This method is only valuable if extracellular labeling is requested. One way this can be accomplished,

is by implementing a charge which will also restrict unspecific hydrophobic interactions.

Chapter 2 describes the development of three polar derivatives of BCN, which were analyzed for their specificity. BCN and its derivatives have a similar reaction rate of ~ 2 $M^{-1}s^{-1}$ in the (3+2) cycloaddition with azidocoumarin. The reaction rates were almost 10 times higher than earlier determined for BCN, via (3+2) cycloaddition with benzyl azide (14×10^{-2} $M^{-1}s^{-1}$) (14) (**chapter 2**) (Table 2). A phenomenon that can be explained by the finding that BCN reacts much faster with aromatic azides than with aliphatic azides, as a result of the inverse electron demand mechanism that is operative when reacting with an aliphatic cyclooctyne such as BCN (21). The newly developed probes were functionalized with a biotin tag and have calculated ^{c}log P values between 0.3-2.1 in their anionic state. To compare the ^{c}log P values with other cyclooctynes, the value of the *N*-methyl carbamate derivative of alcohols or acetyl derivative of the amine was calculated (Table 1).

Cyclooctyne	Structure	Reaction rate ($M^{-1}s^{-1}$)	^{c}log P[a]	Specificity	Ref.
BARAC	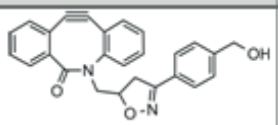	96×10^{-2} (CD_3CN)	3.9	--	(8,12,23, 24)
BCN	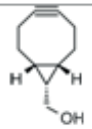	14×10^{-2} ($CD_3CN:D_2O$, 3:1); 1.52[a]	1.2	+	(6,14,25, 26)
DIBAC	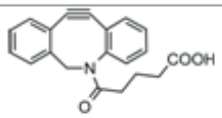	31×10^{-2} (CD_3OD)	3.7	+	(6,8,13)
DIBO	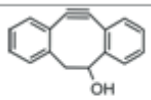	5.7×10^{-2} (MeOH)	4.4	++	(6,8,26-28)
DIFO	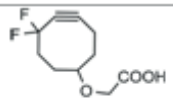	7.6×10^{-2} ($CDCl_3$)	1.4	--	(8,16,29)
DIFO2	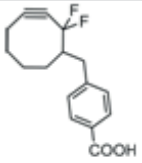	4.2×10^{-2} ($CDCl_3$)	4.1	N.D.	(8,30)
DIFO3	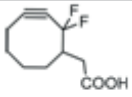	6.8×10^{-2} ($CDCl_3$)	3.3	+	(18)
DIMAC	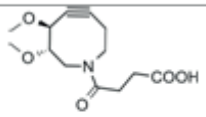	0.3×10^{-2} (CD_3CN)	0.8	N.D.	(8,31)
TMDIBO	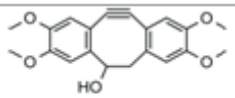	9.8×10^{-2} ($CDCl_3$)	3.7	++	(18)

Table 1: Overview of commonly used cyclooctynes.
BARAC = biarylazacyclooctynone, BCN = bicyclo[6.1.0]nonyne, DIBAC = dibenzoazacyclooctyne, DIBO = dibenzocyclooctyne, DIFO = difluorocyclooctyne, DIMAC = dimethoxyazacyclooctyne, TMDIBO = tetramethoxydibenzocyclooctyne. Reaction rate is determined by reaction with benzyl azide, unless stated otherwise. N.D. is not determined. [a] Calculated for the *N*-methylamide derivatives of carboxylic acids, the *N*-methyl carbamate derivatives of alcohols and the acetyl derivative of primary and secondary amines.

As expected, the hydrophobicity is lower than for most other cyclooctynes. Charged cyclooctynes displayed a higher labeling specificity *in vitro* as illustrated in **chapter 2**. However, solely increasing the hydrophilicity, as shown for BHM-BCN, did not improve the labeling specificity.

Importantly, specific Golgi-staining with SPAAC via A-BCN was presented in **chapter 2**. Since glycans are matured with sialic acids in the *trans*-Golgi, this signal seems rather specific. So far, only few cyclooctynes were found to exhibit specific intracellular labeling (22). It would be interesting to make a panel of *cis*-, *medial*-, *endo*- and *trans*-Golgi stainings in combination with a sialic acid labeling using A-BCN to fully determine the specificity of this staining. As the role of glycosylation in diseases such as infection, inflammation and cancer metastasis is now widely recognized, A-BCN can potentially aid in developing a method to identify abnormal localization and accumulation of glycoproteins in these diseases (22).

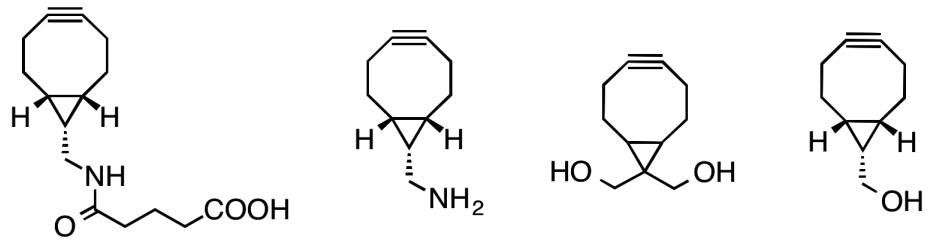

	A-BCN	GA-BCN	BHM-BCN	BCN
Reaction rate ($M^{-1}s^{-1}$)[a]	2.64	1.86	1.56	1.52
[c]log P[b]	0.7[c]	1.5[c]	0.8	1.2
Specificity	++	++	-	+

Table 2: overview of developed BCN derivatives.
[a] Measured in (MeCN:H_2O, 1:2) by reaction with azidocoumarin. [b] Calculated for the *N*-methylamide derivatives of carboxylic acids, the *N*-methyl carbamate derivatives of alcohols and the acetyl derivative of primary and secondary amines. [c] Calculated for the neutral compound.

Overall, the BCN derivatives synthesized in **chapter 2** can assist in future studies aiming at optimizing *in vivo* use of SPAAC. So far, only few studies were performed to compare the two most popular (3+2) cycloaddition reactions, SPAAC and CuAAC (23,25). SPAAC displays shorter reaction times and needs only low equivalents of reagents, both beneficial for the cell viability. Moreover, there is no need for accessory reagents such as a ligand and thus no extensive optimization is required. The labeling efficiency of SPAAC, using BARAC, was compared with several ligand-enriched CuAAC reactions, via application of the chemical reporter strategy with ManNAz in living cells and zebrafish. This study implies that the use of CuAAC in combination with a ligand results in more specific glycan labeling in cell lysates compared to SPAAC (23). As BARAC is rather hydrophobic and instable, it would be interesting to perform a similar study with a different cyclooctyne such as BCN or DIBAC.

Dual labeling of the protein and the glycan

At present, the cycloaddition reactions used for glycan labeling are saccharide- but not protein-specific. Cellular protein-specific glycan labeling can aid in the study of

glycosylation patterns and their involvement in protein regulation and trafficking pathways. Dual labeling with a Förster resonance energy transfer (FRET) donor-acceptor pair can be used to accomplish *in vitro* dual labeling of protein and glycan. The glycan of a chosen protein can be visualized, as close proximity between a FRET donor-acceptor pair (~ 10 nm) results in a specific excitation wavelength. Cell surface glycans of determined proteins can be labeled by combining CuAAC on the N-glycan with an amino(N)-terminal protein label. By labeling the protein and the N-glycan positions with a FRET donor-acceptor pair, the glycan of the specific protein can be visualized (32,33). Unfortunately, only cell membrane proteins with an extracellular N-terminus can be visualized using this method, as the extracellular N-glycan has to be in close proximity. Alternatively, genetic encoding can be used to tag the protein, which in principle allows the incorporation of a non-natural amino acid at any chosen position in the protein. In short, the mRNA sequence is altered such that an unnatural amino acid (UAA) gets incorporated at the location of an introduced amber stop codon. To this end, the cell is provided with additional machinery: 1) a tRNA molecule that will recognise the amber stop codon and the UAA and 2) an aminoacyl-tRNA synthetase for *in vivo* assembly of tRNA-UAA. Following, the UAA will be incorporated at the position of the amber stop codon. This technique has previously been used to incorporate an azido group into a G protein-coupled receptor (34), but can also function for the incorporation of cyclooctynes (35-37).

For dual labeling of the protein and the N-glycan, two successive, mutually orthogonal reactions have to be performed. For example, the Diels–Alder reaction with inverse electron-demand (IEDDA), a reaction between a terminal alkene and a tetrazine, can be used in concert with SPAAC (38) (Fig 1). Thus, an alkene can be incorporated into the protein via genetic encoding (39), followed by implementation of an azide into the glycan as described in **chapter 2**. Next, the alkene can react with a tetrazine via the IEDDA, and the azide can react with a cyclooctyne as indicated previously (38). In addition, a similar system can be developed using strain-promoted inverse-electron-demand Diels-Alder cycloaddition (SPIEDAC) between a *trans*-cyclooctyne and a tetrazine in combination with SPAAC (37). In this way, a *trans*-cyclooctyne will be built into the protein via genetic encoding, after which it is allowed to react with a tetrazine. The azide can be metabolically incorporated in the glycan and react with a strained cyclooctyne as described in **chapter 2**.

Labeling TRPV5 in a dual manner via both its N-glycan and the protein can provide information on how TRPV5 is regulated and localized by its N-glycan. Moreover, direct evidence that klotho does or does not cleave sialic acids from the TRPV5 N-glycan can be provided via such a method. In addition, the effect of sialic acids on internalization or plasma membrane stabilization of TRPV5 can be investigated. The study can be easily expended to other saccharides such as glucosamine, galactosamine and fucose analogs (3,40). To develop such a method, the incorporation of an azido-saccharide into the N-glycan of TRPV5, as developed in **chapter 2**, is necessary. In addition, an alkene moiety should be implemented into the channel protein via genetic encoding (39). Finally, both moieties can react via the SPAAC and IEDDA with their bioorthognal partners that are tagged with a FRET donor or acceptor. However, there are some concerns one should consider when developing this method. First, the alkene has to reside extracellularly, as the distance between the FRET donor-acceptor pair should be small. Since, both the N- and C- terminal regions of TRPV5 reside intracellular, the amber stop codon should be positioned in the small region between two membrane-spanning domains, which may cause difficulties in protein folding. Second, as the incorporation of the UAA at the amber stop codon is in competition with the endogenous

system, TRPV5 expression will be suppressed. The expression of membrane proteins is rather low, applying genetic encoding may cause detection problems.

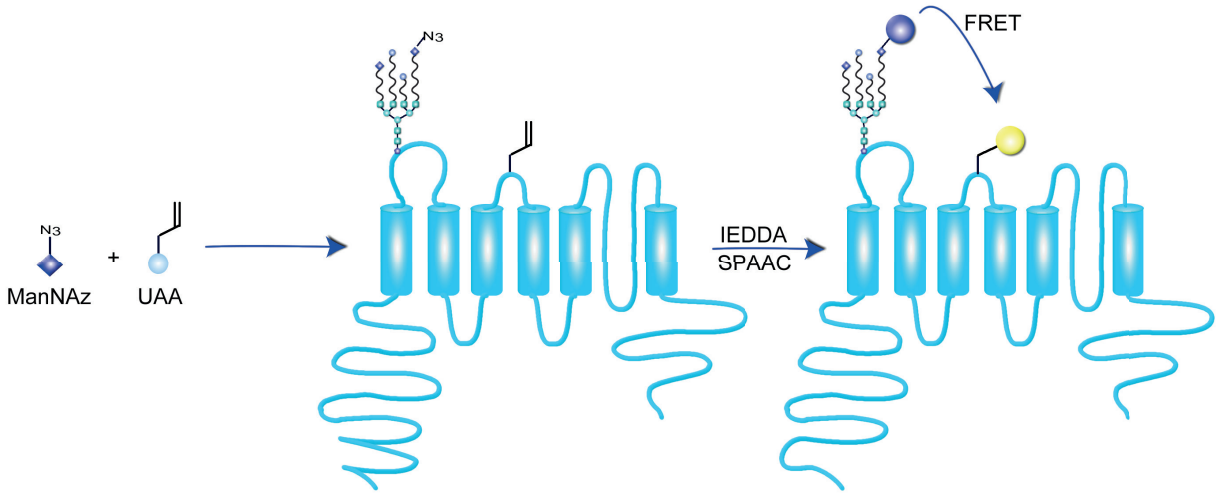

Figure 1. Dual labeling allows specific TRPV5 glycan detection.
The glycan can be labeled with an azide and detected via the SPAAC reaction as described previously. In addition, the TRPV5 protein should be labeled specifically. This can be done by genetic encoding. A specific amino acid with an alkene can be incorporated in TRPV5 specifically. Subsequently, the Diels–Alder reaction with inverse electron-demand can performed and a label can be added this linker. Subsequently, FRET can take place between these two dyes, only if they are in close proximity.

Another interesting experiment would be to implement an artificial glycan at the N358 position of TRPV5. This would allow us to study the effect of different (tetra) saccharides on TRPV5 localization and activity. Genetic encoding with the amber stop codon positioned at the N358 position and a cyclooctyne labeled UAA may allow the implementation of a reactive moiety. (36,37). Following, azide-functionalized saccharides can react via SPAAC with the UAA, allowing the incorporation of a specific chosen saccharide on TRPV5. Functionality of the channel can be tested via patch-clamp and radioactive Ca^{2+} assays, while total internal reflection fluorescence microscopy (TIRF-M) can be used to detect the protein trafficking.

Klotho glycosidase activity remains elusive

Klotho is a type-1 transmembrane protein that is predominantly expressed in the kidney, parathyroid glands and epithelial cells of the choroid plexus in the brain (41). The protein consists of one transmembrane and two similar extracellular domains, KL1 and KL2 (~ 440 amino acids) (41). The extracellular domains can be cleaved at two different positions by A Disintegrin and Metalloprotease (ADAM) 10 or ADAM17 (42), resulting in three fragments; KL1, KL2 and KL1-KL2. Soluble klotho (KL1, KL2 or KL1-KL2) is detected in the blood, urine and cerebrospinal fluid (43).

In 2005, soluble klotho has been found to stimulate TRPV5-mediated Ca^{2+} influx via a mechanism dependent on the TRPV5 N-glycan (44). To understand the molecular mechanism of klotho-mediated TRPV5 regulation, it is important to determine the enzymatic activity of klotho. Based on homology studies, it was suggested that klotho has glycosidase activity, as the KL1 and KL2 domains have an amino acid sequence identity of 20–40% with family 1 glycosidases (41,45). Interestingly, two glutamate (E) residues, critical for enzymatic activity, are not conserved between klotho and the

family 1 glycosidases (Table 3). Since the discovery of klotho as a potential glycosidase, much effort has been made to determine its specific activity. Klotho was shown to possess β-glucuronidase activity towards β-glucuronic acids from 4-methylumbelliferyl β-D-glucuronide, though this activity was 26 times lower than the control bovine β-glucuronidase activity (46). Furthermore, glucuronic acids are uncommon moieties in N-glycans, therefore it is unlikely that TRPV5 is regulated by β-glucuronidase activity (47).

In 2008, Cha *et al.* hypothesized that klotho exerts sialidase activity (48). Removal of the end-standing sialic acids from the TRPV5 N-glycan by klotho will then expose an *N*-acetyllactosamine (LacNAc) repeat, a region composed of repeating disaccharide Gal-(β1-4)-GlcNAc units. Galectin-1 is a glycan binding protein that was found to bind this repeat and thereby stabilize the channel on the plasma membrane (48) (Fig 2A). They showed that blocking of sialyltransferase ST6-gal1, which catalyses the transfer of sialic acids via α2-6-linkage to galactose residues of Gal-(β1-4)-GlcNAc, abolished the klotho-mediated stimulation (48), indicating that klotho needs α2-6-linked sialic acids for its function. In addition, the klotho-mediated effect was absent in the presence of the sialidase inhibitor, *N*-acetyl-2,3-dehydro-2-deoxyneuraminic acid (DANA) (48). However, this compound inhibits specifically the sialic acid hydrolysis of glycosphingolipids (49), implying that the effect might be independent of the TRPV5 N-glycan.

In **chapter 3**, the effect of sialidase treatment on the non-glycosylated $TRPV5^{N358Q}$ mutant was further investigated. Cha *et al.* described that the non-glycosylated $TRPV5^{N358Q}$ mutant is insensitive to sialidase treatment (48). In contrast to literature (48), sialidase stimulated TRPV5 channel activity independent of the TRPV5 N-glycan. Our data suggests that sialidase-mediated TRPV5 stimulation is not specific via the TRPV5 N-glycan, as opposed to klotho-mediated TRPV5 stimulation.

Previously, sialidase was reported to prevent microdomain clustering and lipid raft formation by hydrolyzing sialic acids from glycosphingolipids, glycosylated lipids highly expressed in lipid rafts (50). Lipid rafts are involved in caveolae-dependent endocytosis and, hence, disruption of these lipid membrane compositions via sialidase may reduce endocytosis. **Chapter 3** confirmed that the sialidase-mediated TRPV5 stimulation is caused by reduced caveolae-dependent endocytosis (Fig 2B), resulting from disturbed lipid raft formation (50). Interruption of the lipid rafts via filipin, a compound known to dislocate these microdomains, eliminated the effect of sialidase on TRPV5. In contrast, filipin did not influence the klotho-mediated stimulation on TRPV5, implying that klotho acts independent of caveolae-mediated endocytosis. Additionally, sialidase hydrolysed the sialic acids of the model glycoprotein transferrin that contains end-standing α2-6-linked sialic acids, while klotho did not alter the glycan structure as described in **chapter 3**.

Glycosidase	1st glutamic acid	2nd glutamic acid
GpcBGL	RVRQWITINEPNVLCAMGYD	TYNNPVIYITENGFPQDDPPS
rLPH	RVKFWMTFNEPWCHVVLGYS	EYGNIPIYITENGQGLEN-PT
mKL1	QVKYWITIDNPYVVAWHGYA	EYNHPPIFIVENGWFVSGTTK
mKL2	WVNLWITMNEP--------	KYGDLPMYVTANG-IDDDPHA

Table 3: Alignment of mouse KL1 and KL2 domains with family 1 glycosidases. ClustalW alignment of mouse KL1, mouse KL2, guinea pig cystosolic β-glucosidase (GpcBGL) and rat lactase-phlorizin hydrolase (rLPH). The conserved glutamate residues are indicated in gray. mKL1 has an N at the first conserved E position, while the mKL2 domain has an alanine (A) at the second conserved E site. Adapted from Ito *et al*. (45).

However, one could hypothesize that klotho does not show sialidase activity on transferrin because it needs a particular 'glycan signature' for cleavage, which is absent in transferrin. Based on the data illustrated in **chapter 3**, it cannot be excluded that klotho has sialidase activity, although no evidence is found demonstrating this enzymatic activity.

Klotho controls TRPV5 membrane expression

The enhanced TRPV5 function after klotho treatment results from higher plasma membrane abundance as shown in previous studies (44,48). Biotinylation assays demonstrated that the amount of TRPV5 channels reaching the plasma membrane is increased upon klotho treatment. However, this method was not able to differentiate between increased trafficking to the cell surface or a decreased protein turnover at the membrane. Therefore, TIRF-M was combined with a photoswitchable TRPV5-Dendra-2 protein in **chapter 3**. Using this technique, it was demonstrated that klotho increases the plasma membrane stability of TRPV5. The plasma membrane without any treatment. Interestingly, N-glycans are known to allow the localization of proteins towards clathrin-enriched regions. Non-glycosylated proteins are no longer localized to clathrin-enriched areas, resulting in diminished endocytosis (51). TRPV5 can be endocytosed via the clathrin- and caveolae-mediated pathways (52,53), and ablation of the N-glycan reduces clathrin-mediated endocytosis resulting in the observed membrane stabilization (51) (**chapter 3**).

Other ion channels, such as Transient Receptor Potential Vanilloid type 6 (TRPV6), the renal outer medullary K^+ channel (ROMK), and the Na^+-K^+-ATPase pump are also regulated by klotho (54-56). TRPV6 is a Ca^{2+} channel closely related to TRPV5 (75% amino acid identity). It contains a similar N-glycosylation site situated at the extracellular loop between transmembrane (TM) domain 1 and 2, and channel function can be activated upon klotho treatment (55). However, klotho is not expressed in the intestine where TRPV6 is located. The physiological relevance of klotho-mediated TRPV6 regulation remains elusive, but soluble klotho may be transported towards the intestine (57). More distant channels such as TRPV4 (29% amino acid identity) and TRPM6 (19% amino acid identity) are not stimulated by klotho (55). Similar to TRPV5, klotho treatment increases ROMK plasma membrane expression (54) in an N-glycan-dependent manner (Fig 3). However, the stabilization pathway through which klotho regulates ROMK and TRPV5 is different. Klotho-mediated ROMK stimulation results from reduced clathrin-mediated endocytosis (54), while the TRPV5 plasma membrane stabilization was proposed to be caveolae-dependent (48). It seems striking that klotho influences different endocytosis pathways for these channels, while the final outcome is similar. **Chapter 3** illustrated that disruption of lipid rafts, and thereby caveolae-mediated endocytosis, does not influence TRPV5 stimulation by klotho. This data suggests that the membrane stabilization of TRPV5 by klotho is actually clathrin-dependent. Interestingly, the N-glycan is also often involved in the localization of proteins towards clathrin-enriched regions, connecting klotho to glycan-mediated regulation pathways (51). Finally, klotho stimulated the recruitment of the Na^+-K^+-ATPase pump to the plasma membrane, via binding to the Na^+-K^+-ATPase α1 subunit (56) (Fig 3). A subset of Na^+-K^+-ATPase proteins appeared to traffic from the ER to the cell surface in conjunction with klotho (56). Recently, klotho was shown to stimulate the Na^+,K^+-ATPase pump activity in *Xenopus laevis* oocytes (58).

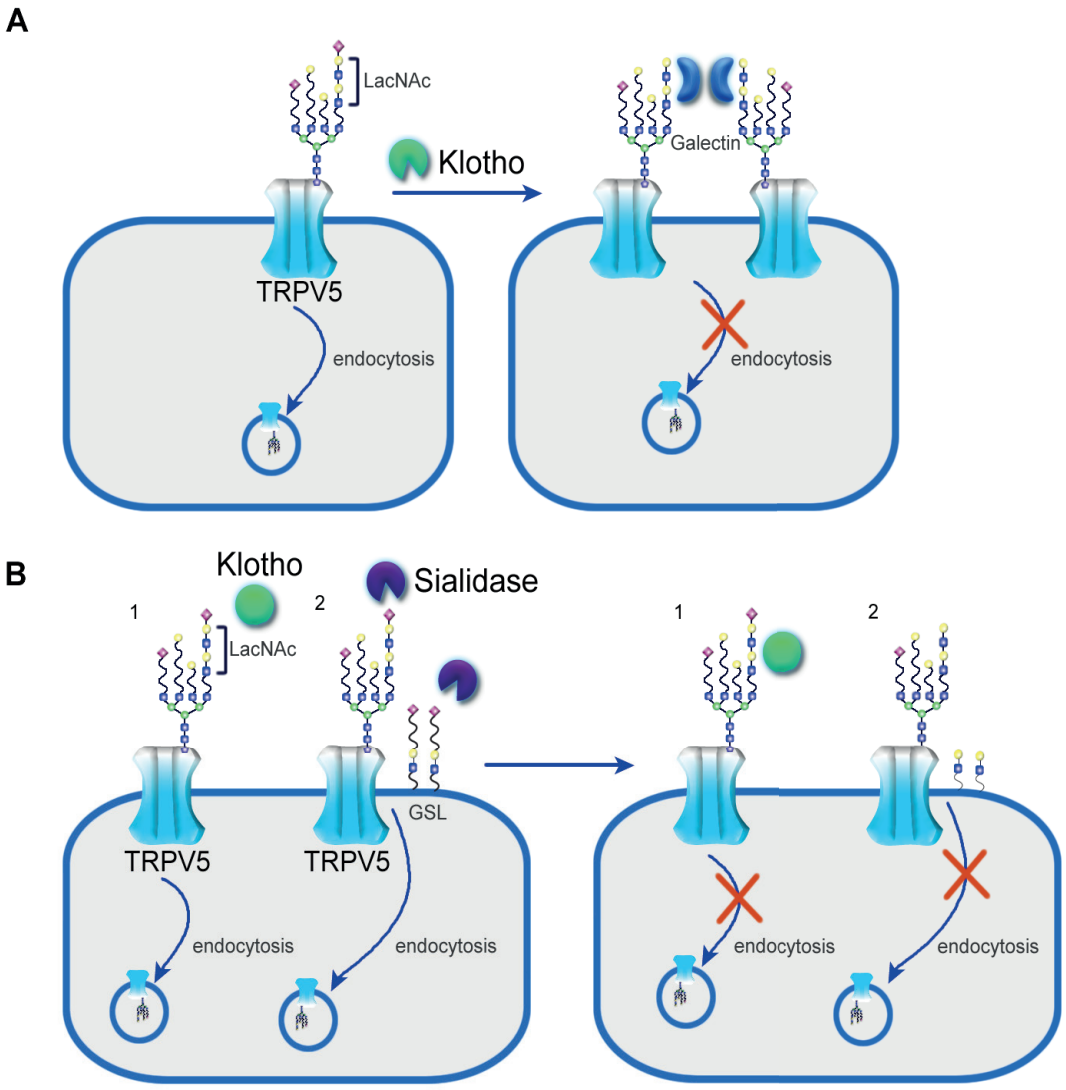

Figure 2. Molecular mechanisms involved in klotho-mediated TRPV5 regulation.
A) Klotho hydrolyses sialic acids from the TRPV5 N-glycan, exposing a terminal LacNAc region. To this region, galectin-1 can bind, stabilizing TRPV5 at the plasma membrane (48). **B)** 1. The activity of Kloto remains to be elucidated. 2. Sialidase hydrolyses the sialic acids of both the TRPV5 N-glycan and glycosphingolipids (GSL). By hydrolyzing sialic acids from glycosphingolipids, lipids rafts are disturbed and TRPV5 is stabilized at the plasma membrane.

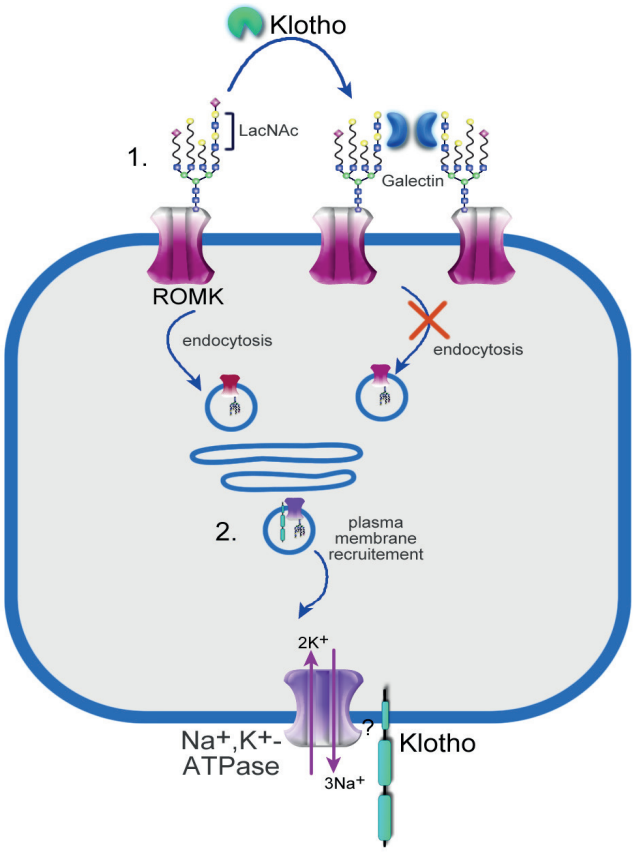

Figure 3. Klotho regulates several ion channels.
1. ROMK is stimulated by klotho in a similar manner as previously proposed for TRPV5 (Fig 1A) (54). **2.** The Na^+,K^+-ATPase channel is recruited towards the plasma membrane by klotho. It remains unknown how klotho binds this channel and which type of klotho (membrane bound or soluble) is involved in this mechanism (56).

Literature described that the membrane stabilization involves galectin-1 binding to the TRPV5 N-glycan (48). An antibody against galectin-1, but not against galectin-8, abolished klotho-dependent TRPV5 stimulation in CHO cells (48). In addition, this group isolated galectin-1 via a co-immunoprecipitation with TRPV5 after cross-linking the cell membrane (48). In contrast, our group could not detect galectin-1 expression in HEK293 cells, as explained in **chapter 3**. Therefore the expression pattern of galectin-1 in the kidney was further elucidated. Galectin-3, but not galectin-1, mRNA was enriched in isolated mouse DCT2/CNT cells. Moreover, TRPV5 co-localized with galectin-3 in the kidney, but not with galectin-1. It has been demonstrated that galectin-3 is essential for apical targeting of proteins (59) and protein stability regulation (60). Extracellular galectin-3 treatment increased TRPV5 activity only in the presence of the TRPV5 N-glycan, since the $TRPV5^{N358Q}$ mutant was not regulated. Though, galectin-3 in combination with klotho did not further increase TRPV5-mediated Ca^{2+} influx (**chapter 3**), suggesting that klotho-mediated channel stabilization does not involve galectin-3 binding. Next to the stimulating effect of extracellular klotho on TRPV5, a recent study described that intracellular klotho can also stabilize the channel on the plasma membrane (61). However, future research should determine the physiological relevance of this recent finding.

The mystery of klotho, the molecular basis for TRPV5 activation.
The concept that klotho has sialidase activity is improbable based on the data depicted in **chapter 3.** Moreover, β-glucuronidase activity is doubtful, as β-glucuronic acids are only scarcely expressed in N-glycans. It is interesting to address the question if klotho could be a lectin-like protein that binds glycans without altering the glycan structure (Fig 4A). An example of such action by klotho can be found in the FGF23-bone-kidney axis. Binding of klotho to the fibroblast growth factor receptor (FGFR) down-regulates the $1,25(OH)_2D_3$ production, as outlined in **chapter 1**. Membrane-

bound klotho converts the canonical FGFR to a specific receptor for fibroblast growth factor 23 (FGF23), enabling high-affinity binding of FGF23 and thereby inhibition of the $1,25(OH)_2D_3$ production (62). Klotho has no enzymatic activity towards the FGFR, probably the protein regulates the FGFR solely via binding (Fig 4B). It should be noted that membrane-bound klotho binds the receptor, while soluble klotho regulates TRPV5. **Chapter 3** demonstrated that simultaneous treatment with galectin-3 and klotho did not additively stimulate TRPV5 activity. This could imply that klotho and galectin-3 stimulate TRPV5 in a similar manner, indicating that klotho functions as a lectin that recognizes the TRPV5 N-glycan. One can speculate that klotho competes with regular galectins, but has a higher affinity for specific saccharide repeats. Thereby klotho can either stabilize the protein on the plasma membrane or prevent localization to clathrin-enriched regions. Both pathways will result in increased expression of the channel at the plasma membrane. Interestingly, the hypothesis of klotho being a binding protein would be in line with the homology of the protein, since residues presented in the active site of glycosidases are not conserved in klotho. Moreover, homology has been found with the lactase-like protein (21% amino acid sequence identity), a protein that lacks glycosidase activity (45). However no homology was detected with any type of lectin.

To investigate the exact mechanism via which klotho stimulates TRPV5 activity, the glycan sequence to which klotho binds needs to be determined. This can be studied via a highly sensitive glycan microarray using klotho with a tag (63). The defined glycan array available from the Consortium for Functional Glycomics (CFG) is the easiest method to use. Klotho can be tagged with NHS-activated biotin, a compound that reacts with primary amine groups in proteins. Following, klotho can be detected by binding of fluorescent streptavidin to the biotin. After determining the sequence of the glycan that binds klotho, assays can be performed to elucidate if the presence of klotho results in modification of the glycan. Future research should be performed to analyse the glycan sequence that binds klotho, and determine its activity on this glycan sequence.

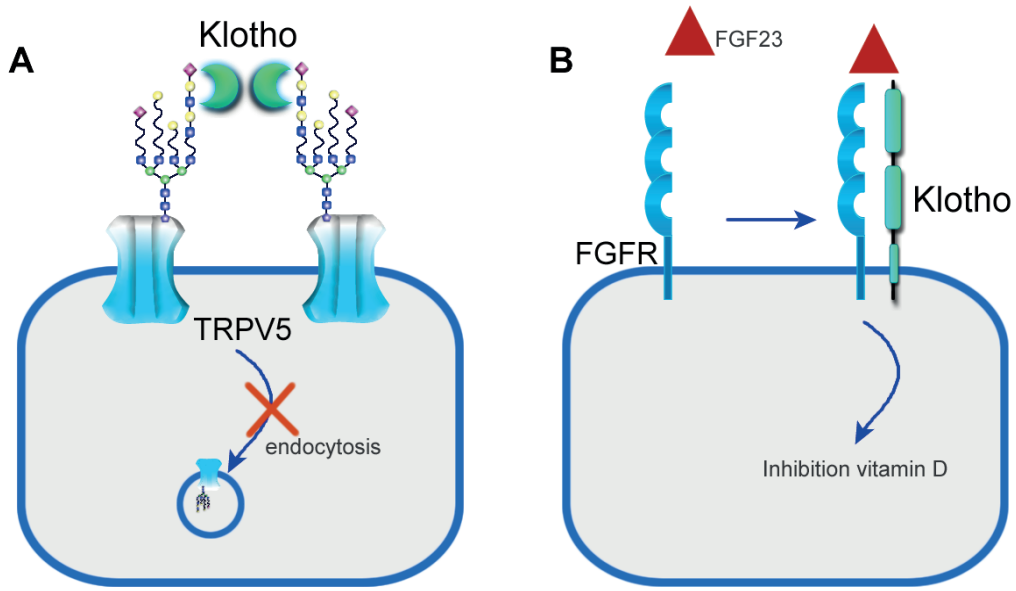

Figure 4. Klotho has no enzymatic activity.
A) One could hypothesize that klotho has only binding properties. Binding of soluble klotho will stabilize the channel at the plasma membrane, either by stabilizing the protein at the plasma membrane (as depicted) or by localizing the protein away from the clathrin-enriched regions. **B)** Klotho regulates the specificity of FGFR for FGF23, by binding to the FGFR. Full-length klotho is involved in this system (62).

β-galactosidase stimulates TRPV5 activity

Glycosidases play important roles in protein localization, stabilization and activity (2). β-galactosidase (β-gal) is a glycosidase that catalyses the hydrolysis of terminal β(1,3), β(1,4) or β(1,6) linked galactose saccharides in di- and oligosaccharides such as lactose and galactobiose, but also in glycoproteins or glycosaminoglycans (64). β-gal is mainly expressed in the lysosomes, where it is responsible for the degradation of sialylated glucoconjugates. β-gal activity from lysosomal β-D-galactosidase (active at pH 4.5) is the most extensively used biomarker for cell senescence (65-67). Many glycosidases are detected in the urine, such as β-glucosidase, β-glucuronidase and *N*-acetyl-D-glucosaminodase (NAG) (68). Since β-gal activity can be measured in the urine of humans (0.45-1.4 mU/μmol creatinin) (69), the physiological relevance of β-gal-mediated stimulation is investigated (69). Urinary β-gal, is relatively unstable at low pH values and has an optimum at neutral pH (70). Interestingly, β-gal is excreted into the pro-urine in the proximal tubule, located upstream of the DCT2/CNT where TRPV5 is expressed. **Chapter 4** demonstrated that β-gal stimulates TRPV5-mediated Ca^{2+} influx, only in the presence of the TRPV5 N-glycan. Close evaluation indicated that β(1,4)-gal activity is responsible for this effect. TIRF-M revealed that the plasma membrane expression of the channel is increased upon β(1,4)-gal treatment. In addition, isolated primary mouse DCT2/CNT cells display an increased Ca^{2+} transport upon apical β(1,4)-gal treatment. This excludes that the detected effect is due to the overexpression system used for this study. The study described in this thesis highlights a physiological regulatory mechanism of the TRPV5 N-glycan.

Deficiencies of β-gal cause human metabolic disorders with heterogeneous clinical phenotypes, such as GM1 gangliosidosis (OMIM nr. 230500) and Morquio type B disease (OMIM nr. 253010). GM1 gangliosidosis is associated with a highly vacuolated cytoplasm containing GM1 ganglioside as storage substance (71). GM1 ganglioside is a glycosphingolipid, capped with a β-galactose subunit. Neurodegeneration and skeletal abnormalities characterize GM1 patients (71). Morquio type B disease is also caused by deficiencies in β-gal, therefore the clinical lines between GM1 and Morquio disease are rather vague. Mutation of TRPV4, a TRPV5 homologue, is known to cause a pseudo-Morquio syndrome (72). Another connection between TRPV5 and β-gal can be found in diabetes mellitus patients, as illustrated in **chapter 4**. Diabetes mellitus type 1 is associated with renal Ca^{2+} wasting, although the molecular mechanism for this remains unknown. Moreover, these patients show elevated β-gal levels in blood and urine, which may represent a mechanism of compensation to prevent renal Ca^{2+} wasting (73,74).

Future research should reveal whether differences in the urinary excretion of glycosidases are linked to disturbances in the Ca^{2+} balance or other electrolyte abnormalities.

TRPV5 regulation by glycosidases

Interestingly, several similarities can be found between β-gal and klotho. Serum klotho expression and urinary β-gal activity both decline with increasing age (69,75). In addition, klotho shares 39% amino acid sequence identity with lactase-phlorizin hydrolase, a member of the β-gal family that is responsible for cleavage of lactose (76). Although β-gal and klotho both stimulate the plasma membrane expression of TRPV5, as demonstrated in **chapter 3** and **chapter 4**, klotho is not likely to possess galactosidase activity. A β-gal enzyme assay, in which the colorimetric o-nitrophenyl-β-D-galactopyranoside becomes UV-active upon cleavage into o-nitrophenol and galactose, was used to study potential β-gal activity for klotho. Lysates of klotho- and β-gal-expressing HEK293 cells were tested for β-gal activity. Activity was detected in the β-gal lysate (3.2 arbitrary units (au)), but not in the klotho lysate (0.07 au). However, it cannot be excluded that klotho needs a 'glycan signature' to exert its function, as discussed previously.

Cleavage of Gal-(β-1,4) by β(1,4)-gal, as well as treatment with other glycosidases

(**chapter 3**), can increase TRPV5 channel function. Therefore, it seems that any type of alteration to the TRPV5 N-glycan increases Ca^{2+} influx via TRPV5. Possibly, the N-glycan binds a protein that blocks the channel pore via steric hindrance, but this is not likely as the N-glycan-deficient mutant $TRPV5^{N358Q}$ has similar channel characteristics as wild type TRPV5. Removal of the TRPV5 N-glycan does not influence the open probability or the conductance of the channel as described in **chapter 4**. This implies that the N-glycan is not involved in the intrinsic function of the TRPV5 channel, and this is in accordance with the idea that the N-glycan mediates membrane expression of the channel.

Stabilization by galectins

Galectins bind specifically to LacNAc repeats, composed of repeating Gal-(β-1,4)-GlcNAc units. β(1,4)-gal will modify the end-standing LacNAc unit by hydrolysing the Gal-(β-1,4) saccharide. Since galectins are often involved in membrane stability of glycoproteins, it is likely that these proteins are involved in the glycan-mediated regulation of the TRPV5 cell surface expression. Galectin-1, -3, -7, -8 and -9 are expressed in human and mice kidney (77,78).

Galectin-1 induces anti-inflammatory cytokines and inhibits the production of pro-inflammatory cytokines (2). The protein is expressed in tubular epithelial cells, but not in the progenitor cells of the collecting duct (79). Moreover, TRPV5 does not co-localize with galectin-1 (**chapter 3**).

Galectin-3 is expressed in mice DCT2/CNT, where it co-localizes with TRPV5 as described in **chapter 3**. Moreover, extracellular galectin-3 was shown to increase the TRPV5 channel activity dependent on the TRPV5 N-glycan (**chapter 3**). Based on this finding, ablation of galectin-3 binding by β(1,4)-gal treatment would decrease the TRPV5 activity, in contrast to what is demonstrated in **chapter 4**. Interestingly, capping with sialic acids only slightly influences galectin-3 binding to LacNAc repeats, as galectin-3 does not need an end-standing LacNAc repeat for binding (80). β(1,4)-gal treatment will not modify LacNAc repeats if capped with sialic acids, therefore β(1,4)-gal treatment may not affect galectin-3 binding. Of note, galectin-3 expression in adult kidney is low and appears to be confined to the cytoplasm of collecting duct cells (81).

Galectin-7 is selectively expressed in the cilia of the kidney. Cilia are membrane protuberances that sense changes in the fluid flow (82). Here, galectin-7 plays a key role in plasma membrane stabilization of glycoproteins, involved in epithelial wound healing (77). Up until now, TRPV5 expression in cilia has not been properly investigated. Galectin-7 might be involved in TRPV5 regulation in the cilia, but, only unciliated kidney cells were used for the above-described experiments, therefore galectin-7 is probably not involved for TRPV5 regulation via klotho or β(1,4)-gal. Next, galectin-8 has a strong affinity for α2,3 sialylated Galβ(1,3)GalNAc (83), which are not cleaved by β(1,4)-gal treatment, thereby omitting a role for galectin-8 in the regulation of TRPV5 activity via β(1,4)-gal.

Galectin-9 serves a variety of functions and is mostly expressed in the lysosomal/endosomal compartments along the renal tubule (84,85). Galectin-9, in contrast to galectin-3, is highly expressed in adult kidney (78). This galectin has a high affinity for end-standing LacNac repeats in N-glycans and Frossman pentasaccharides present on apical residing glycolipids (86). The protein functions as an urate channel/transporter (87), a regulator of thymocyte-epithelial cell interactions (88), a tumor antigen (89) and a mediator of apoptosis (88). Furthermore, galectin-9 is involved in the polarization of epithelial cells and facilitates the apical sorting of proteins and lipids (85,90). Knockdown of this protein leads to loss of epithelial polarity in renal Madin-Darby Canine Kidney (MDCK) cells (90). Finally, galectin-9 binding stabilizes glycoproteins in clathrin-enriched domains, thereby increasing their endocytosis (51). Hence, removal of the Gal-(β-1,4) saccharide from the TRPV5 N-glycan may inhibit galectin-9 binding, thereby reducing endocytosis (Fig 5). It would be interesting to

investigate the effect of extracellular galectin-9 on TRPV5 plasma membrane expression.

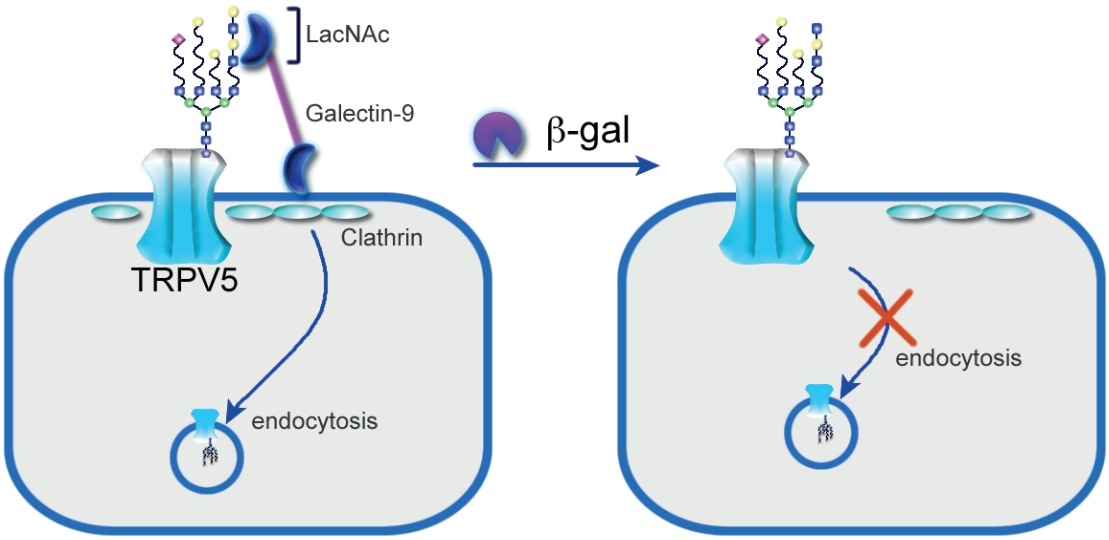

Figure 5. TRPV5 activity is stimulated by β-gal, possibly via galectin-9 interaction.
TRPV5 is endocytosed via the clathrin-dependent pathway. Galectin-9 binding to the LacNAc region will translocate TRPV5 into clathrin-enriched regions, thereby stimulating endocytosis. Upon β-gal treatment, the galectin-9 interaction is lost and the channel is located into regions with low clathrin expression, reducing endocytosis.

TRPV5 homology model

Chapter 5 outlined the construction and investigations of a TRPV5 homology model, based on the recently resolved rat TRPV1 structure (91). This structure was solved by electron cryo-microscopy, at ~ 3.4 Å resolution for the TM domains and ~ 4.8 Å resolution for the cytoplasmic domains (91). The structure of TRPV1 is solved in a close state conformation from residue leucine 111 to alanine 719 (total TRPV1 is composed of 838 amino acids), excluding a small and highly divergent region (605-626). This region was removed to increase the biochemical stability of the TRPV1 channel. With an amino acid sequence identity of 29% between rabbit TRPV5 and rat TRPV1, a rabbit TRPV5 homology structure from methionine 1 to valine 644 was modeled (total rabbit TRPV5 is composed of 729 amino acids). The amino acid sequence identity in combination with the size of the protein was sufficient to develop a valid homology model (92). The structures revealed that both TRPV1 and TRPV5 contain four-fold symmetry around the central ion pathway, which is formed by TM 5, 6 and the pore loop.

To validate the model, several aspects were highlighted as described in **chapter 5**. Previously, the N-terminal ankyrin repeat domain (ARD) of TRPV6 was elucidated by crystallization at a resolution of 1.7 Å (93). Since the ARD of TRPV5 and TRPV6 share an amino acid sequence identity of 88%, it is likely that the tertiary structures are similar. The TRPV6 ARD contains anti-parallel inner and outer α-helices, with a finger loop to link the helical layers together. The large twist between ankyrin 4 and 5 is characteristic for the ARD of TRPV6 and is also detected in the TRPV5 homology model (Fig 7A), implying that the model correctly represents the TRPV5 N-terminal domain. Next, the N-glycosylation position is expected to be located at the extracellular site of the channel, as urinary glycosidases can influence TRPV5 channel activity. In agreement, N358 is located at the extracellular side with the side chain pointing into the extracellular solvent in the homology model (Fig 7B). The glycosylation site of TRPV1 is not present in the

electron cryo-microscopy-solved structure, as it is situated in the excluded region (amino acid 604) (91). The aspartic acid (D) 542 residue, which is responsible for selective Ca^{2+} gating, is located directly above the pore, as displayed in **chapter 5** (94). However, the distance between the four D542 residues in the model is rather large to form a selectivity gate (~ 9.5 Å). The selectivity filter of the TRPV1 channel was only ~ 4.6 Å (91). On the other hand, TRPV5 displays a different selectivity filter sequence compared to TRPV1, as it has a more pronounced selectivity for Ca^{2+} over monovalent cations (95). Moreover, intracellular acidification decreases the size of the filter gate from 10.3 Å at pH 9.0 to 5.6 Å at pH 6.0, as estimated by electrophysiological analysis (96). Even though, the physiological pH varies only from 6.8 to 8.4 (63), these data suggests a noticeable flexibility of the pore. Finally, the highly conserved TRP domain, located after TM 6, is a key feature in TRP ion channels (97-99). Similar to TRPV1 (91), the TRPV5 homology model reveals that the TRP domain interacts with the loop between TM 4, TM 5 and the pre-TM 1 α-helix via hydrogen bonds. This domain is involved in phosphatidylinositol 4,5-bisphosphate (PIP_2) binding, which is shown to stimulate TRPV5 channel activity (100). Taken together, the homology model appears a reliable structure based on known structural characteristics of TRPV5. However, it should be considered that the presented structure is a model and, therefore, may not fully represent the authentic TRPV5 conformation.

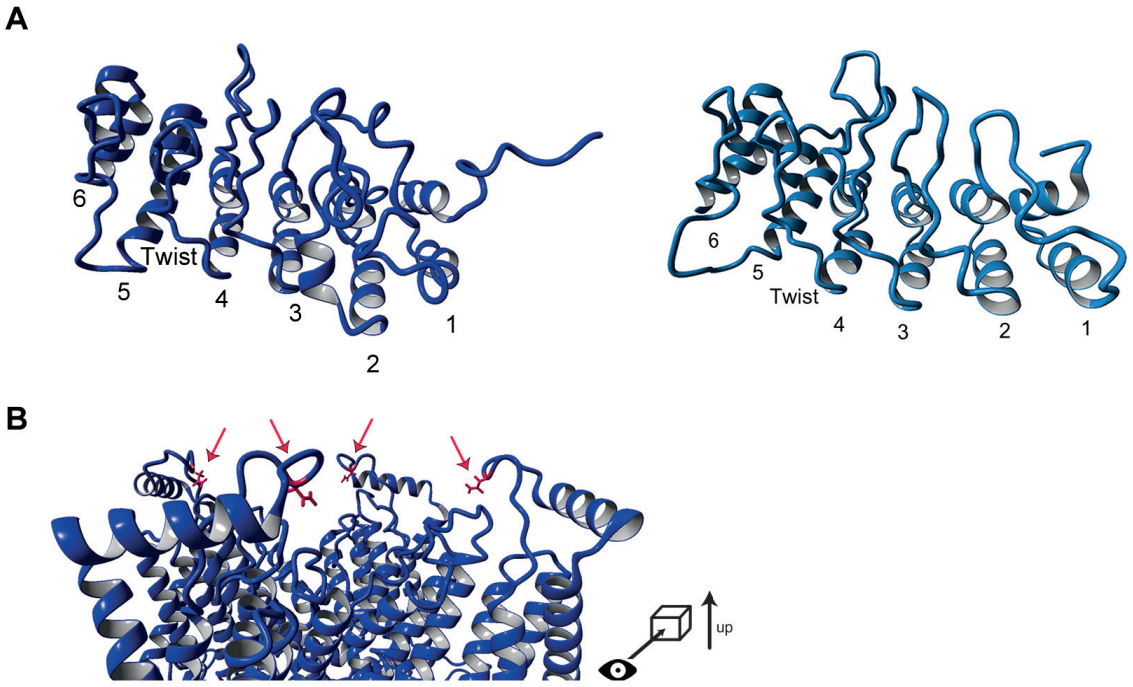

Figure 6. Key features of the TRPV5 homology model.
A) TRPV5 ARD (left) presented in the homology model is similar to the previously crystallized TRPV6 ARD (93) (right, PDB = 2RFA). Both, the model and the crystal structure, show a characteristic twist between ankyrin 4 and ankyrin 5. **B)** The TRPV5 homology model displays the N358 glycosylation sites at the top of the tetrameric channel (red), pointing towards the extracellular matrix.

TRPV5 regulation by an aromatic gate and a glycine hinge

The TRPV5 homology model improves our understanding of the channel function by studying the process of channel opening and closing. Three main gating movements are known to regulate K^+ and related ion channels; *i)* rotation of the inner pore α-helices around the pore; *ii)* kinking of the inner pore α-helix in the middle or *iii)* kinking at the

bottom of the inner pore α-helix in combination with an aromatic gate (101). Evaluation of the TRPV5 model led to the identification of the aromatic tryptophan (W) 583 residue located at the bottom of the pore mouth helix. Modification of W583 resulted in an over-active TRPV5 channel and provoked cell death as explained in **chapter 5**. This indicates that the four W583 residues together form a so-called W-gate, essential for channel function. Many prokaryotic K^+ channels are regulated by the concerted action of an aromatic gate with α-helical bending via a glycine hinge (102). Interestingly, TRPV5 contains a glycine (G579) approximately one α-helical turn above W583 (Fig 7B). **Chapter 5** delineates that mutation of the flexible glycine residue into a more restrained alanine nearly completely ablates TRPV5-mediated Ca^{2+} transport. These gating residues are highly conserved amongst species and also in the homologous TRPV6 channel. Taken together, the data suggest that TRPV5 is regulated by kinking of the pore α-helix (G579) in combination with an aromatic gate (W583) (Fig 6A). Importantly, the other TRPV family members (TRPV1-4) do not display such an aromatic residue in the pore, suggesting that they are regulated via a different mechanism.

Stimuli causing bending of the TRPV5 α-helix at the G579 position have not been elucidated. Interestingly, a conserved histidine (H) 582 residue is located in close proximity to the W-gate as described in **chapter 5**. This residue is conserved among different species and in TRPV6. Histidine residues are pH sensitive, and therefore it can be speculated that H582 causes the α-helix to bend upon pH changes. Low extracellular pH inhibits for example the proton-selective influenza virus M_2 channel via histidine residues (103). These residues are located four amino acids above the W-gate, situating the side chains of the tryptophan and histidine residues on top of each other in the 3D structure. Protonation of the histidine residue initiates bending or rotation of the tryptophan side chains, thereby closing the channel (103). Extracellular and intracellular pH changes regulate TRPV5, as acidification at either side decreases channel activity (96). In the TRPV5 model, the side chains of the W583and H582 residues are sticking in opposite directions (Fig 7C), indicating that a proton-selective influenza virus M_2 channel-like mechanism is likely not involved in channel regulation. However, a positively charged lysine (K) at position 484 is located at only ~ 7 Å distance from H582. Protonation of H582 may repel K484, causing the helix to bend (Fig 6D). In contrast, the model displays a methionine (M) 485 residue that stabilizes the H582 side chain via a hydrogen bond. The value of the hypothesis that the protonated H582 will repel the positively charged K484, causing the W583 to change position needs to be determined. This can be studied by mutation of the H582 in the positively charged arginine or in a non-charged tyrosine. Following, differences in TRPV5 activity should be studied and will indicate whether H582 is a factor influencing the W-gate. Another signaling molecule that could be involved in the TRPV5 gating mechanism is PIP_2, a membrane phospholipid that binds the positively charged TRP domain located directly below the W-gate. Binding of PIP_2 stabilizes TRPV5 in its open conformation (100). In addition, the slow Mg^{2+}-mediated TRPV5 inhibition is counteracted by PIP_2, even though activation of TRPV5 via PIP_2 is independent of Mg^{2+} (104). Interestingly, both TRPV5 and TRPV6 contain the W-gate and are stimulated by PIP_2. In contrast, TRPV1 is inhibited by PIP_2 and shows no conservation of the G-hinge and the W-gate (100). K^+ channels that display a similar type of gating, as postulated for TRPV5, are also stimulated by PIP_2 (101,105). As all channels regulated via a G-hinge and W-gate are stimulated by PIP_2, this factor might be the stimulus in this system. The importance of PIP_2 in TRPV5 gating can be studied in more detail by investigating the effect of additional PIP_2 on wild type TRPV5, $TRPV5^{G579A}$ and $TRPV5^{W583Y}$. If the

stimulating effect of exogenous PIP_2 is no longer detected on the $TRPV5^{G579A}$ and $TRPV5^{W583Y}$ mutant, it is likely that PIP_2 is involved. However, a direct connection cannot be determined via this method as PIP_2 is involved in many different processes (105).

Finally, the selectivity filter might be able to communicate with the closing gate, as described for the KcsA channel (106,107). In this system, the gate and selectivity filter are able to communicate bi-directionally, thereby regulating channel opening and closing. Future research should determine mechanistic principles underlying a possible conformational coupling.

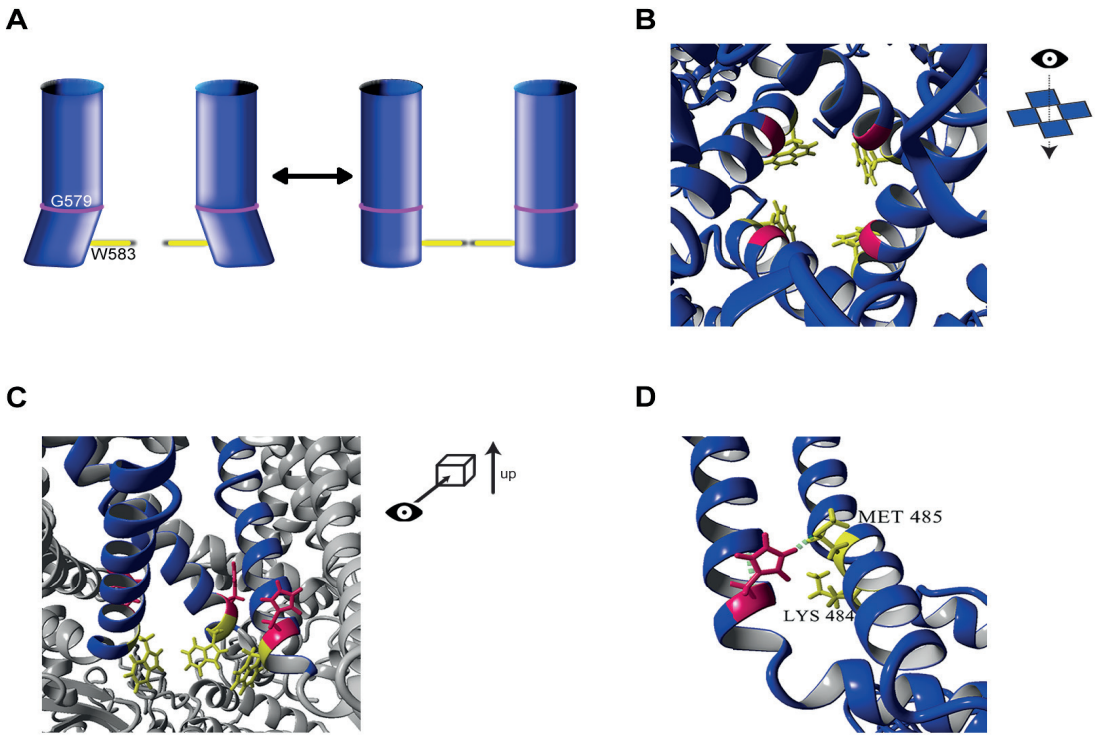

Figure 7. The TRPV5 gate is composed of a W-gate in combination with a G-hinge.
A) Schematic representation of the TRPV5 gating mechanism. The W583 residues are indicated in yellow, and the G579 bending point is indicated in pink. **B)** The flexible G579 (red) is located approximately one turn above W583, which is proposed to function as a W-gate (yellow). **C)** The W-gate (yellow) is placed at the end of TM domain 6 (blue), a H (red) residue is located directly above the gate. The sensitive H side chain is pointing towards TM domain 5. **D)** An increase in pH will result in protonation of H582 (pink), which may repel the positively charged K484 (yellow). H582 forms a hydrogen bond with M485 (yellow) of TM domain 5.

Outlook

The aim of this thesis was to investigate how glycosylation regulates the Ca^{2+} channel TRPV5. It is important that specific research methods are developed to accurately investigate this type of complex posttranslational modification. The origin of many glycosylation disorders is not determined yet. Therefore, mechanistic insights in the glycosylation processes will support the design of new diagnostical methods and eventually contribute to the development of therapeutics. Nevertheless, many questions remain to be answered. Implementing charge in BCN increases the membrane labeling specificity, but will this work for other cyclooctynes as well? This thesis provided a basis for future studies in which genetic encoding can be used to insert one of the tags on the protein, followed by metabolic incorporation of a saccharide analog to implement a different tag. Would it also be possible to develop a dual labeling system through which

we can label TRPV5 with one tag and the N-glycan with another? Next, we demonstrated that klotho stimulates the TRPV5 channel activity via the N-glycan, by stabilizing the protein at the plasma membrane. However, what is the exact enzymatic activity of klotho, if there is any? Analogously, β-gal influences TRPV5 activity by stabilizing the channel at the cell surface. Are galectins involved in this stabilization process? What is the physiological importance of β-gal in regulation of the Ca^{2+} homeostasis? Moreover, animal experiments should validate if β-gal also regulates TRPV5 activity *in vivo*. Finally, the TRPV5 homology model provides significant new insights in understanding channel regulation on the molecular level. We identified important residues in channel functioning and thereby propose a gating model composed of a W-gate and a G-hinge. However, which factors regulate this gating mechanism? Is TRPV5 a voltage-gated channel, such as the resembling K^+ channels? Future research could provide more information on the stimulus for conformational changes in the pore structure. In addition, the TRPV5 gating mechanism might be extended to TRPV6 and possibly other channels. The molecular revelations described in this thesis will contribute to further understanding of TRPV5 regulation and the Ca^{2+} handling in the human body.

References

1. Apweiler, R., Hermjakob, H., and Sharon, N. (1999) On the frequency of protein glycosylation, as deduced from analysis of the SWISS-PROT database. *Bba-Gen Subjects* **1473**, 4-8
2. Varki, A., Cummings, R. D., Esko, J. D., Freeze, H. H., Stanley, P., Bertozzi, C. R., Hart, G. W., and Etzler, M. E. (2009) Essentials of Glycobiology, 2nd edition. *Cold Spring Harbor (NY)*
3. Boons, G. J. (2010) Bioorthogonal chemical reporter methodology for visualization, isolation and analysis of glycoconjugates. *Carbohydr Chem* **36**, 152-167
4. Dimke, H., Hoenderop, J. G., and Bindels, R. J. (2011) Molecular basis of epithelial Ca^{2+} and Mg^{2+} transport: insights from the TRP channel family. *J Physiol* **589**, 1535-1542
5. Lallana, E., Riguera, R., and Fernandez-Megia, E. (2011) Reliable and Efficient Procedures for the Conjugation of Biomolecules through Huisgen Azide-Alkyne Cycloadditions. *Angew Chem* **50**, 8794-8804
6. van Geel, R., Pruijn, G. J., van Delft, F. L., and Boelens, W. C. (2012) Preventing thiol-yne addition improves the specificity of strain-promoted azide-alkyne cycloaddition. *Bioconjug Chem* **23**, 392-398
7. Beatty, K. E., Fisk, J. D., Smart, B. P., Lu, Y. Y., Szychowski, J., Hangauer, M. J., Baskin, J. M., Bertozzi, C. R., and Tirrell, D. A. (2010) Live-Cell Imaging of Cellular Proteins by a Strain-Promoted Azide-Alkyne Cycloaddition. *Chembiochem* **11**, 2092-2095
8. Debets, M. F., Van Berkel, S. S., Dommerholt, J., Dirks, A. J., Rutjes, F. P. J. T., and Van Delft, F. L. (2011) Bioconjugation with Strained Alkenes and Alkynes. *Accounts Chem Res* **44**, 805-815
9. Almaraz, R. T., Aich, U., Khanna, H. S., Tan, E., Bhattacharya, R., Shah, S., and Yarema, K. J. (2012) Metabolic oligosaccharide engineering with N-Acyl functionalized ManNAc analogs: Cytotoxicity, metabolic flux, and glycan-display considerations. *Biotechnol Bioeng* **109**, 992-1006
10. Bussink, A. P., van Swieten, P. F., Ghauharali, K., Scheij, S., van Eijk, M., Wennekes, T., van der Marel, G. A., Boot, R. G., Aerts, J. M. F. G., and Overkleeft, H. S. (2007) N-Azidoacetylmannosamine-mediated chemical tagging of gangliosides. *J Lipid Res* **48**, 1417-1421
11. Chigrinova, M., McKay, C. S., Beaulieu, L. P. B., Udachin, K. A., Beauchemin, A. M., and Pezacki, J. P. (2013) Rearrangements and addition reactions of biarylazacyclooctynones and the implications to copper-free click chemistry. *Org Biomol Chem* **11**, 3436-3441
12. Gordon, C. G., Mackey, J. L., Jewett, J. C., Sletten, E. M., Houk, K. N., and Bertozzi, C. R. (2012) Reactivity of Biarylazacyclooctynones in Copper-Free Click Chemistry. *J Am Chem Soc* **134**, 9199-9208
13. Debets, M. F., van Berkel, S. S., Schoffelen, S., Rutjes, F. P. J. T., van Hest, J. C. M., and van Delft, F. L. (2010) Aza-dibenzocyclooctynes for fast and efficient enzyme PEGylation via copper-free (3+2) cycloaddition. *Chem Commun* **46**, 97-99
14. Dommerholt, J., Schmidt, S., Temming, R., Hendriks, L. J. A., Rutjes, F. P. J. T., van Hest, J. C. M., Lefeber, D. J., Friedl, P., and van Delft, F. L. (2010) Readily Accessible Bicyclononynes for Bioorthogonal Labeling and Three-Dimensional Imaging of Living Cells. *Angew Chem Int Edit* **49**, 9422-9425
15. Fairbanks, B. D., Sims, E. A., Anseth, K. S., and Bowman, C. N. (2010) Reaction Rates and Mechanisms for Radical, Photoinitated Addition of Thiols to Alkynes, and Implications for Thiol-Yne Photopolymerizations and Click Reactions. *Macromolecules* **43**, 4113-4119
16. Kim, E. J., Kang, D. W., Leucke, H. F., Bond, M. R., Ghosh, S., Love, D. C., Ahn, J. S., Kang, D. O., and Hanover, J. A. (2013) Optimizing the selectivity of DIFO-based reagents for intracellular bioorthogonal applications. *Carbohyd Res* **377**, 18-27
17. Chang, P. V., Prescher, J. A., Sletten, E. M., Baskin, J. M., Miller, I. A., Agard, N. J., Lo, A., and Bertozzi, C. R. (2010) Copper-free click chemistry in living animals. *Proc Natl Acad Sci U S A* **107**, 1821-1826
18. Stockmann, H., Neves, A. A., Stairs, S., Ireland-Zecchini, H., Brindle, K. M., and Leeper, F. J. (2011) Development and evaluation of new cyclooctynes for cell surface glycan imaging in cancer cells. *Chem Sci* **2**, 932-936
19. Christiansen, M. N., Chik, J., Lee, L., Anugraham, M., Abrahams, J. L., and Packer, N. H. (2014) Cell surface protein glycosylation in cancer. *Proteomics* **14**, 525-546

20. Ning, X., Guo, J., Wolfert, M. A., and Boons, G. J. (2008) Visualizing metabolically labeled glycoconjugates of living cells by copper-free and fast huisgen cycloadditions. *Angew Chem* **47**, 2253-2255
21. Dommerholt, J., van Rooijen, O., Borrmann, A., Guerra, C. F., Bickelhaupt, F. M., and van Delft, F. L. (2014) Highly accelerated inverse electron-demand cycloaddition of electron-deficient azides with aliphatic cyclooctynes. *Nat Commun* **5**, 5378
22. Mbua, N. E., Flanagan-Steet, H., Johnson, S., Wolfert, M. A., Boons, G. J., and Steet, R. (2013) Abnormal accumulation and recycling of glycoproteins visualized in Niemann-Pick type C cells using the chemical reporter strategy. *P Natl Acad Sci USA* **110**, 10207-10212
23. Besanceney-Webler, C., Jiang, H., Zheng, T. Q., Feng, L., del Amo, D. S., Wang, W., Klivansky, L. M., Marlow, F. L., Liu, Y., and Wu, P. (2011) Increasing the Efficacy of Bioorthogonal Click Reactions for Bioconjugation: A Comparative Study. *Angew Chem* **50**, 8051-8056
24. Jewett, J. C., Sletten, E. M., and Bertozzi, C. R. (2010) Rapid Cu-Free Click Chemistry with Readily Synthesized Biarylazacyclooctynones. *J Am Chem Soc* **132**, 3688-3690
25. Yang, Y. L., Yang, X. M., and Verhelst, S. H. L. (2013) Comparative Analysis of Click Chemistry Mediated Activity-Based Protein Profiling in Cell Lysates. *Molecules* **18**, 12599-12608
26. van der Linden, W. A., Li, N., Hoogendoorn, S., Ruben, M., Verdoes, M., Guo, J., Boons, G. J., van der Marel, G. A., Florea, B. I., and Overkleeft, H. S. (2012) Two-step bioorthogonal activity-based proteasome profiling using copper-free click reagents: A comparative study. *Bioorgan Med Chem* **20**, 662-666
27. Ning, X. H., Guo, J., Wolfert, M. A., and Boons, G. J. (2008) Visualizing metabolically labeled glycoconjugates of living cells by copper-free and fast huisgen cycloadditions. *Angew Chem* **47**, 2253-2255
28. Poloukhtine, A. A., Mbua, N. E., Wolfert, M. A., Boons, G. J., and Popik, V. V. (2009) Selective Labeling of Living Cells by a Photo-Triggered Click Reaction. *J Am Chem Soc* **131**, 15769-15776
29. Baskin, J. M., Prescher, J. A., Laughlin, S. T., Agard, N. J., Chang, P. V., Miller, I. A., Lo, A., Codelli, J. A., and Bertozzi, C. R. (2007) Copper-free click chemistry for dynamic in vivo imaging. *P Natl Acad Sci USA* **104**, 16793-16797
30. Codelli, J. A., Baskin, J. M., Agard, N. J., and Berozzi, C. R. (2008) Second-generation difluorinated cyclooctynes for copper-free click chemistry. *J Am Chem Soc* **130**, 11486-11493
31. Sletten, E. M., and Bertozzi, C. R. (2008) A hydrophilic azacyclooctyne for Cu-free click chemistry. *Org Lett* **10**, 3097-3099
32. Lin, W., Du, Y., Zhu, Y., and Chen, X. (2014) A cis-membrane FRET-based method for protein-specific imaging of cell-surface glycans. *J Am Chem Soc* **136**, 679-687
33. Yang, Y., Lin, S. X., Lin, W., and Chen, P. R. (2014) Ligand-Assisted Dual-Site Click Labeling of EGFR on Living Cells. *ChemBioChem* **15**, 1738-1743
34. Naganathan, S., Ye, S. X., Sakmar, T. P., and Huber, T. (2013) Site-Specific Epitope Tagging of G Protein-Coupled Receptors by Bioorthogonal Modification of a Genetically Encoded Unnatural Amino Acid. *Biochemistry* **52**, 1028-1036
35. Hao, Z. Y., Song, Y. Q., Lin, S. X., Yang, M. Y., Liang, Y. J., Wang, J., and Chen, P. R. (2011) A readily synthesized cyclic pyrrolysine analogue for site-specific protein "click" labeling. *Chem Commun* **47**, 4502-4504
36. Borrmann, A., Milles, S., Plass, T., Dommerholt, J., Verkade, J. M. M., Wiessler, M., Schultz, C., van Hest, J. C. M., van Delft, F. L., and Lemke, E. A. (2012) Genetic Encoding of a Bicyclo[6.1.0]nonyne-Charged Amino Acid Enables Fast Cellular Protein Imaging by Metal-Free Ligation. *ChemBioChem* **13**, 2094-2099
37. Nikic, I., Plass, T., Schraidt, O., Szymanski, J., Briggs, J. A. G., Schultz, C., and Lemke, E. A. (2014) Minimal Tags for Rapid Dual-Color Live-Cell Labeling and Super-Resolution Microscopy. *Angew Chem* **53**, 2245-2249
38. Niederwieser, A., Spate, A. K., Nguyen, L. D., Jungst, C., Reutter, W., and Wittmann, V. (2013) Two-color glycan labeling of live cells by a combination of Diels-Alder and click chemistry. *Angew Chem* **52**, 4265-4268
39. Plass, T., Milles, S., Koehler, C., Szymanski, J., Mueller, R., Wiessler, M., Schultz, C., and Lemke, E. A. (2012) Amino Acids for Diels-Alder Reactions in Living Cells. *Angew Chem* **51**, 4166-4170
40. Agard, N. J., and Bertozzi, C. R. (2009) Chemical approaches to perturb, profile, and perceive glycans. *Acc Chem Res* **42**, 788-797
41. Kuroo, M., Matsumura, Y., Aizawa, H., Kawaguchi, H., Suga, T., Utsugi, T., Ohyama,

Y., Kurabayashi, M., Kaname, T., Kume, E., Iwasaki, H., Iida, A., Shirakilida, T., Nishikawa, S., Nagai, R., and Nabeshima, Y. (1997) Mutation of the mouse klotho gene leads to a syndrome resembling ageing. *Nature* **390**, 45-51
42. Chen, C. D., Podvin, S., Gillespie, E., Leeman, S. E., and Abraham, C. R. (2007) Insulin stimulates the cleavage and release of the extracellular domain of Klotho by ADAM10 and ADAM17. *Proc Natl Acad Sci USA* **104**, 19796-19801
43. Imura, A., Iwano, A., Tohyama, O., Tsuji, Y., Nozaki, K., Hashimoto, N., Fujimori, T., and Nabeshima, Y. (2004) Secreted Klotho protein in sera and CSF: implication for post-translational cleavage in release of Klotho protein from cell membrane. *Febs Lett* **565**, 143-147
44. Chang, Q., Hoefs, S., van der Kemp, A. W., Topala, C. N., Bindels, R. J., and Hoenderop, J. G. (2005) The beta-glucuronidase klotho hydrolyzes and activates the TRPV5 channel. *Science* **310**, 490-493
45. Ito, S., Fujimori, T., Hayashizaki, Y., and Nabeshima, Y. (2002) Identification of a novel mouse membrane-bound family 1 glycosidase-like protein, which carries an atypical active site structure. *Bba-Gene Struct Expr* **1576**, 341-345
46. Tohyama, O., Imura, A., Iwano, A., Freund, J. N., Henrissat, B., Fujimori, T., and Nabeshima, Y. (2004) Klotho is a novel beta-glucuronidase capable of hydrolyzing steroid beta-glucuronides. *J Biol Chem* **279**, 9777-9784
47. Huang, C. L. (2010) Regulation of ion channels by secreted Klotho: mechanisms and implications. *Kidney International* **77**, 855-860
48. Cha, S. K., Ortega, B., Kurosu, H., Rosenblatt, K. P., Kuro-O, M., and Huang, C. L. (2008) Removal of sialic acid involving Klotho causes cell-surface retention of TRPV5 channel via binding to galectin-1. *P Natl Acad Sci USA* **105**, 9805-9810
49. Kopitz, J., Muhl, C., Ehemann, V., Lehmann, C., and Cantz, M. (1997) Effects of cell surface ganglioside sialidase inhibition on growth control and differentiation of human neuroblastoma cells. *Eur J Cell Biol* **73**, 1-9
50. Singh, R. D., Marks, D. L., Holicky, E. L., Wheatley, C. L., Kaptzan, T., Sato, S. B., Kobayashi, T., Ling, K., and Pagano, R. E. (2010) Gangliosides and beta1-integrin are required for caveolae and membrane domains. *Traffic* **11**, 348-360
51. Torreno-Pina, J. A., Castro, B. M., Manzo, C., Buschow, S. I., Cambi, A., and Garcia-Parajo, M. F. (2014) Enhanced receptor-clathrin interactions induced by N-glycan-mediated membrane micropatterning. *P Natl Acad Sci USA* **111**, 11037-11042
52. van de Graaf, S. F. J., Rescher, U., Hoenderop, J. G. J., Verkaart, S., Bindels, R. J. M., and Gerke, V. (2008) TRPV5 is internalized via clathrin-dependent endocytosis to enter a Ca2+-controlled recycling pathway. *J Biol Chem* **283**, 4077-4086
53. Cha, S. K., Wu, T., and Huang, C. L. (2008) Protein kinase C inhibits caveolae-mediated endocytosis of TRPV5. *Am J Physiol-Renal* **294**, 1212-1221
54. Cha, S. K., Hu, M. C., Kurosu, H., Kuro-o, M., Moe, O., and Huang, C. L. (2009) Regulation of Renal Outer Medullary Potassium Channel and Renal K(+) Excretion by Klotho. *Mol Pharmacol* **76**, 38-46
55. Lu, P., Boros, S., Chang, Q., Bindels, R. J., and Hoenderop, J. G. (2008) The beta-glucuronidase klotho exclusively activates the epithelial Ca^{2+} channels TRPV5 and TRPV6. *Nephrol Dial Transpl* **23**, 3397-3402
56. Imura, A., Tsuji, Y., Murata, M., Maeda, R., Kubota, K., Iwano, A., Obuse, C., Togashi, K., Tominaga, M., Kita, N., Tomiyama, K., Iijima, J., Nabeshima, Y., Fujioka, M., Asato, R., Tanaka, S., Kojima, K., Ito, J., Nozaki, K., Hashimoto, N., Ito, T., Nishio, T., Uchiyama, T., Fujimori, T., and Nabeshima, Y. I. (2007) alpha-klotho as a regulator of calcium homeostasis. *Science* **316**, 1615-1618
57. Khuituan, P., Teerapornpuntakit, J., Wongdee, K., Suntornsaratoon, P., Konthapakdee, N., Sangsaksri, J., Sripong, C., Krishnamra, N., and Charoenphandhu, N. (2012) Fibroblast growth factor-23 abolishes 1,25-dihydroxyvitamin D-3-enhanced duodenal calcium transport in male mice. *Am J Physiol Endocrinol and Metab* **302**, 903-913
58. Sopjani, M., Alesutan, I., Dermaku-Sopjani, M., Gu, S. C., Zelenak, C., Munoz, C., Velic, A., Foller, M., Rosenblatt, K. P., Kuro-o, M., and Lang, F. (2011) Regulation of the Na+/K+ ATPase by Klotho. *Febs Lett* **585**, 1759-1764
59. Delacour, D., Greb, C., Koch, A., Salomonsson, E., Leffler, H., Le Bivic, A., and Jacob, R. (2007) Apical sorting by galectin-3-dependent glycoprotein clustering. *Traffic* **8**, 379-388
60. Wang, Y., Balan, V., Kho, D., Hogan, V., Nangia-Makker, P., and Raz, A. (2013) Galectin-3 regulates p21 stability in human prostate cancer cells. *Oncogene* **32**, 5058-5065
61. Wolf, M. T., An, S., Nie, M., Bal, M. S., and Huang, C. L. (2014) Klotho upregulates

renal calcium channel transient receptor potential vanilloid 5 (TRPV5) by intra- and extracellular N-glycosylation dependent mechanisms *J Biochem*
62. Urakawa, I., Yamazaki, Y., Shimada, T., Iijima, K., Hasegawa, H., Okawa, K., Fujita, T., Fukumoto, S., and Yamashita, T. (2006) Klotho converts canonical FGF receptor into a specific receptor for FGF23. *Nature* **444**, 770-774
63. Cha, S. K., Jabbar, W., Xie, J., and Huang, C. L. (2007) Regulation of TRPV5 single-channel activity by intracellular pH. *J Membr Biol* **220**, 79-85
64. Conzelmann, E., and Sandhoff, K. (1987) Glycolipid and Glycoprotein Degradation. *Adv Enzymol Ramb* **60**, 89-216
65. Dimri, G. P., Lee, X. H., Basile, G., Acosta, M., Scott, C., Roskelley, C., Medrano, E. E., Linskens, M., Rubelj, I., Pereirasmith, O., Peacocke, M., and Campisi, J. (1995) A Biomarker That Identifies Senescent Human-Cells in Culture and in Aging Skin in-Vivo. *P Natl Acad Sci USA* **92**, 9363-9367
66. Gary, R. K., and Kindell, S. M. (2005) Quantitative assay of senescence-associated beta-galactosidase activity in mammalian cell extracts. *Anal Biochem* **343**, 329-334
67. Lee, B. Y., Han, J. A., Im, J. S., Morrone, A., Johung, K., Goodwin, E. C., Kleijer, W. J., DiMaio, D., and Hwang, E. S. (2006) Senescence-associated beta-galactosidase is lysosomal beta-galactosidase. *Aging Cell* **5**, 187-195
68. Robinson, D., Price, R. G., and Dance, N. (1967) Rat-Urine Glycosidases and Kidney Damage. *Biochem J* **102**, 533-538
69. Xu, G., Zhu, L., Hong, J., Cao, Y., and Xia, T. (1999) Rapid colorimetric assay of urinary beta-galactosidase and N-acetyl-beta-D-glucosaminidase with Cobas Mire Auto-analyzer. *J Clin Lab Anal* **13**, 95-98
70. Delacadena, M. P., Rodriguezberrocal, J., Cabezas, J. A., and Gonzalez, N. P. (1986) Properties and Kinetics of a Neutral Beta-Galactosidase from Rabbit Kidney. *Biochimie* **68**, 251-260
71. Callahan, J. W. (1999) Molecular basis of GM1 gangliosidosis and Morquio disease, type B. Structure-function studies of lysosomal beta-galactosidase and the non-lysosomal beta-galactosidase-like protein. *Biochim Biophys Acta* **1455**, 85-103
72. Nishimura, G., Dai, J., Lausch, E., Unger, S., Megarbane, A., Kitoh, H., Kim, O. H., Cho, T. J., Bedeschi, F., Benedicenti, F., Mendoza-Londono, R., Silengo, M., Schmidt-Rimpler, M., Spranger, J., Zabel, B., Ikegawa, S., and Superti-Furga, A. (2010) Spondylo-epiphyseal dysplasia, Maroteaux type (pseudo-Morquio syndrome type 2), and parastremmatic dysplasia are caused by TRPV4 mutations. *Am J Med Genet A* **152A**, 1443-1449
73. Kohler, E., Sheth, K. J., and Good, T. A. (1979) Urinary Acidic Glycohydrolases as an Index of Kidney Damage in Juvenile Diabetes-Mellitus. *Acta Diabetol Lat* **16**, 247-255
74. Serrano, M. A., Reglero, A., Cabezas, J. A., Diez, L. C. G., Corrales, J. J., Decastro, S., and Miralles, J. M. (1983) Serum Glycosidases in Diabetes-Mellitus in Relation to the Retinopathy and to the Length of the Disease. *Clinica Chimica Acta* **132**, 23-27
75. Yamazaki, Y., Imura, A., Urakawa, I., Shimada, T., Murakami, J., Aono, Y., Hasegawa, H., Yamashita, T., Nakatani, K., Saito, Y., Okamoto, N., Kurumatani, N., Namba, N., Kitaoka, T., Ozono, K., Sakai, T., Hataya, H., Ichikawa, S., Imel, E. A., Econs, M. J., and Nabeshima, Y. (2010) Establishment of sandwich ELISA for soluble alpha-Klotho measurement: Age-dependent change of soluble alpha-Klotho levels in healthy subjects. *Biochem Biophys Res Commun* **398**, 513-518
76. Boll, W., Wagner, P., and Mantei, N. (1991) Structure of the chromosomal gene and cDNAs coding for lactase-phlorizin hydrolase in humans with adult-type hypolactasia or persistence of lactase. *Am J Hum Genet* **48**, 889-902
77. Rondanino, C., Poland, P. A., Kinlough, C. L., Li, H., Rbaibi, Y., Myerburg, M. M., Al-bataineh, M. M., Kashlan, O. B., Pastor-Soler, N. M., Hallows, K. R., Weisz, O. A., Apodaca, G., and Hughey, R. P. (2011) Galectin-7 modulates the length of the primary cilia and wound repair in polarized kidney epithelial cells. *Am J Physiol-Renal* **301**, F622-F633
78. Hughes, R. C. (2002) Galectins in kidney development. *Glycoconjugate J.* **19**, 621-629
79. Burger, A., Filsinger, S., Cooper, D. N. W., and Hansch, G. M. (1996) Expression of the 14 kDa galactose-binding protein, galectin-1, on human tubular epithelial cells. *Kidney International* **50**, 754-759
80. Ahmad, N., Gabius, H. J., Kaltner, H., Andre, S., Kuwabara, I., Liu, F. T., Oscarson, S., Norberg, T., and Brewer, C. F. (2002) Thermodynamic binding studies of cell

surface carbohydrate epitopes to galectins-1,-3, and-7: Evidence for differential binding specificities. *Can J Chem* **80**, 1096-1104
81. Winyard, P. J., Bao, Q., Hughes, R. C., and Woolf, A. S. (1997) Epithelial galectin-3 during human nephrogenesis and childhood cystic diseases. *J Am Soc Nephrol* **8**, 1647-1657
82. Huang, L. W., and Lipschutz, J. H. (2014) Cilia and Polycystic Kidney Disease, Kith and Kin. *Birth Defects Res C* **102**, 174-185
83. Carlsson, S., Oberg, C. T., Carlsson, M. C., Sundin, A., Niisson, U. J., Smith, D., Cummings, R. D., Almkvist, J., Karlsson, A., and Leffler, H. (2007) Affinity of galectin-8 and its carbohydrate recognition domains for ligands in solution and at the cell surface. *Glycobiology* **17**, 663-676
84. Wada, J., and Kanwar, Y. S. (1997) Identification and characterization of galectin-9, a novel beta-galactoside-binding mammalian lectin. *J Biol Chem* **272**, 6078-6086
85. Mo, D., Costa, S. A., Ihrke, G., Youker, R. T., Pastor-Soler, N., Hughey, R. P., and Weisz, O. A. (2012) Sialylation of N-linked glycans mediates apical delivery of endolyn in MDCK cells via a galectin-9-dependent mechanism. *Mol Biol Cell* **23**, 3636-3646
86. Nagae, M., Nishi, N., Nakamura-Tsuruta, S., Hirabayashi, J., Wakatsuki, S., and Kato, R. (2008) Structural analysis of the human galectin-9 N-terminal carbohydrate recognition domain reveals unexpected properties that differ from the mouse orthologue. *J Mol Biol* **375**, 119-135
87. Lipkowitz, M. S., Leal-Pinto, E., Cohen, B. E., and Abramson, R. G. (2002) Galectin 9 is the sugar-regulated urate transporter/channel UAT. *Glycoconjugate J.* **19**, 491-498
88. Wada, J., Ota, K., Kumar, A., Wallner, E. I., and Kanwar, Y. S. (1997) Developmental regulation, expression, and apoptotic potential of galectin-9, a beta-galactoside binding lectin. *Journal of Clinical Investigation* **99**, 2452-2461
89. Tureci, O., Schmitt, H., Fadle, N., Pfreundschuh, M., and Sahin, U. (1997) Molecular definition of a novel human galectin which is immunogenic in patients with Hodgkin's disease. *J Biol Chem* **272**, 6416-6422
90. Mishra, R., Grzybek, M., Niki, T., Hirashima, M., and Simons, K. (2010) Galectin-9 trafficking regulates apical-basal polarity in Madin-Darby canine kidney epithelial cells. *Proc Natl Acad Sci U S A* **107**, 17633-17638
91. Liao, M. F., Cao, E. H., Julius, D., and Cheng, Y. F. (2013) Structure of the TRPV1 ion channel determined by electron cryo-microscopy. *Nature* **504**, 107-112
92. Sander, C., and Schneider, R. (1991) Database of homology-derived protein structures and the structural meaning of sequence alignment. *Proteins* **9**, 56-68
93. Phelps, C. B., Huang, R. J., Lishko, P. V., Wang, R. R., and Gaudet, R. (2008) Structural analyses of the ankyrin repeat domain of TRPV6 and related TRPV ion channels. *Biochemistry* **47**, 2476-2484
94. Voets, T., Janssens, A., Droogmans, G., and Nilius, B. (2004) Outer pore architecture of a Ca2+-selective TRP channel. *J Biol Chem* **279**, 15223-15230
95. Owsianik, G., Talavera, K., Voets, T., and Nilius, B. (2006) Permeation and selectivity of TRP channels. *Annu Rev Physiol* **68**, 685-717
96. Yeh, B. I., Kim, Y. K., Jabbar, W., and Huang, C. L. (2005) Conformational changes of pore helix coupled to gating of TRPV5 by protons. *EMBO J* **24**, 3224-3234
97. Valente, P., Garcia-Sanz, N., Gomis, A., Fernandez-Carvajal, A., Fernandez-Ballester, G., Viana, F., Belmonte, C., and Ferrer-Montiel, A. (2008) Identification of molecular determinants of channel gating in the transient receptor potential box of vanilloid receptor I. *FASEB J* **22**, 3298-3309
98. Prescott, E. D., and Julius, D. (2003) A modular PIP2 binding site as a determinant of capsaicin receptor sensitivity. *Science* **300**, 1284-1288
99. Garcia-Sanz, N., Fernandez-Carvajal, A., Morenilla-Palao, C., Planells-Cases, R., Fajardo-Sanchez, E., Fernandez-Ballester, G., and Ferrer-Montiel, A. (2004) Identification of a tetramerization domain in the C terminus of the vanilloid receptor. *J Neurosci* **24**, 5307-5314
100. Rohacs, T., Lopes, C. M. B., Michailidis, I., and Logothetis, D. E. (2005) PI(4,5)P-2 regulates the activation and desensitization of TRPM8 channels through the TRP domain. *Nat Neurosci* **8**, 626-634
101. Zhou, H. X., and McCammon, J. A. (2010) The gates of ion channels and enzymes. *Trends Biochem Sci* **35**, 179-185
102. Elinder, F., Nilsson, J., and Arhem, P. (2007) On the opening of voltage-gated ion channels. *Physiol Behav* **92**, 1-7
103. Tang, Y. J., Zaitseva, F., Lamb, R. A., and Pinto, L. H. (2002) The gate of the influenza virus M-2 proton channel is formed by a single tryptophan residue. *J Biol*

Chem **277**, 39880-39886
104. Lee, J., Cha, S. K., Sun, T. J., and Huang, C. L. (2005) PIP2 activates TRPV5 and releases its inhibition by intracellular Mg^{2+}. *J Gen Physiol* **126**, 439-451
105. Suh, B. C., and Hille, B. (2005) Regulation of ion channels by phosphatidylinositol 4,5-bisphosphate. *Curr Opin Neurobiol* **15**, 370-378
106. Cuello, L. G., Jogini, V., Cortes, D. M., Pan, A. C., Gagnon, D. G., Dalmas, O., Cordero-Morales, J. F., Chakrapani, S., Roux, B., and Perozo, E. (2010) Structural basis for the coupling between activation and inactivation gates in K+ channels. *Nature* **466**, 272-U154
107. Uysal, S., Cuello, L. G., Cortes, D. M., Koide, S., Kossiakoff, A. A., and Perozo, E. (2011) Mechanism of activation gating in the full-length KcsA K+ channel. *P Natl Acad Sci USA* **108**, 11896-11899


VII

CHAPTER 7

Nederlandse samenvatting

In onderzoek worden DNA, RNA en eiwitten vaak gezien als de belangrijkste onderdelen van een cel. Deze drie bestandsdelen kunnen echter niet ten volle zorgdragen voor de totale opmaak en complexiteit van een cel. Hoewel het belang van vetten en suikers (sacchariden) vaak onderbelicht blijft, zijn deze eveneens essentieel voor het verloop van de noodzakelijke biologische processen.

Glycosylering is een proces waarbij een aantal saccharide-eenheden aan een eiwit- of vetstructuur gekoppeld worden, zoals uitvoerig beschreven in **hoofdstuk 1**. Bij meerdere gekoppelde saccharide-eenheden spreken we dan van glycanen. Deze glycanen zijn noodzakelijk voor het complexe functioneren van een cel. Het glycaan kan deze functie vervullen door op verschillende niveaus te variëren, door de samenstelling van de sacchariden, de chemische verbindingen, het type polymeer formatie (lineair of vertakt) en eventuele chemische modificaties zoals acetylering. Ongeveer 50% van alle eiwitten in het menselijk lichaam is geglycosyleerd. Een klein defect in het glycosyleringssysteem heeft vaak grote gevolgen voor het functioneren van het gehele organisme. Echter, de huidige kennis over eiwitglycosylering is beperkt in vergelijking met onze kennis over DNA en eiwitten. Een van de belangrijkste redenen hiervoor is de complexiteit van de glycanen en het gebrek aan goede detectiemethoden.

Dit proefschrift richt zich specifiek op de N-glycosylering. Dit is de koppeling van een glycaan aan het amine van het aminozuur asparagine in een eiwit. Het glycaan verzorgt bindingsplaatsen voor een scala aan eiwitten. Daarnaast kan het glycaan ingekort worden door een glycosidase, een enzym dat een specifiek saccharide van het glycaan kan verwijderen. Door deze modificatie verandert de bindingsplaats voor eiwitten en kunnen de activiteit, de membraan lokalisatie en vele andere processen van een eiwit beïnvloed worden. Het transient receptor potential vanilloid type 5 (TRPV5) is een gespecialiseerd eiwit, dat calcium (Ca^{2+}) ionen door het plasmamembraan kan transporteren, een Ca^{2+}-selectief ionkanaal. TRPV5 bevindt zich in het distale deel van de nierbuis, waar vier dezelfde TRPV5 eiwitten samen het kanaal (een tunnel) vormen, dat specifiek de Ca^{2+} ionen doorlaat. In de nier is het kanaal betrokken bij de Ca^{2+} opname vanuit de voorurine terug naar de bloedbaan. Dit gebeurt via een actief transcellulair transport, dat zorgdraagt voor de nauwe regulatie van de Ca^{2+} balans in ons lichaam. Aangezien Ca^{2+} een belangrijke rol speelt bij vele fysiologische processen, zoals de productie van hormonen, botmineralisatie en spiercontracties, is het van groot belang om een goede Ca^{2+} balans te handhaven. Verstoringen in deze balans als gevolg van een defect in TRPV5 resulteren in botafwijkingen en in verhoogde Ca^{2+} excretie via de urine. Kennis omtrent de regulatie van TRPV5, is van essentieel belang om het moleculaire mechanisme van de renale Ca^{2+} huishouding te begrijpen. De mate van Ca^{2+} transport door TRPV5 wordt bepaald door de intrinsieke activiteit van het kanaal en de hoeveelheid aanwezige kanalen op het plasmamembraan, zoals uitvoerig beschreven in **hoofdstuk 1**. Deze processen blijken gereguleerd te worden via het N-glycaan dat zich bevindt op TRPV5. Dit proefschrift levert nieuwe inzichten in de rol van het N-glycaan ten aanzien van de TRPV5 activiteit.

Om inzicht te krijgen in N-glycaan afhankelijke regulatieprocessen is de detectie van het N-glycaan essentieel. De diversiteit van glycanen maakt de ontwikkeling van goede technieken voor de detectie van het glycaan tot een moeilijke zaak. De meest gebruikte methode om glycanen te labelen is de zogenaamde azide-alkyn [2+3] cycloadditie, ook wel bekend als de klikreactie. Een erg populaire klikreactie is de spanning-gemedieerde azide-alkyn cycloadditie (SPAAC). Normaliter is een alkyn-groep recht en reageert deze alleen in de aanwezigheid van een katalysator zoals koper met een azide. In het geval

van de SPAAC is de alkyn gebogen, de buiging geeft spanning op het alkyn. Dit is gedaan door deze te plaatsen in een achtring. Dit maakt dat het alkyn reactiever is, waardoor de reactie met een azide kan plaatsvinden in afwezigheid van een katalysator. SPAAC is de reactie tussen een gebogen en dus gespannen alkyn, vaak een cyclooctyn, en een azide functionaliteit waarbij een stabiele triazool-ring gevormd wordt. Om glycanen te kunnen labelen met behulp van deze reactie worden cellen behandeld met een azide-bevattend saccharide-analogon. In dit proefschrift is ManNAz gebruikt, een analoge saccharide welke wordt opgenomen door de cel en op de positie van een eindstandig siaalzuur-saccharide wordt ingebouwd. Dit resulteert in de expositie van een azidegroep op de positie van het siaalzuur in het glycaan (Fig 1). Vervolgens vindt er een reactie plaats met een cyclooctyn, welk gebonden is aan een fluorescent label. Een van de meest gebruikte cyclooctynen is bicyclo[6.1.0]nonyne (BCN) (Fig 1). De toepassing van deze reactie en andere SPAAC reacties op cellulaire en dierlijke systemen wordt vaak bemoeilijkt door aspecifieke interacties. Aspecificiteit ontstaat in de SPAAC reactie vooral als gevolg van hydrofobe interacties en aspecifieke thiol-yn additions. Een thiol-yn additie is de reactie tussen een thiol - welk bijvoorbeeld voorkomt in het aminozuur cysteine en dus ook in veel eiwitten - en de cyclooctyn, in ons geval BCN.

Om de chemische gereedschapskist voor het biologische onderzoek naar glycanen uit te breiden zijn in **hoofstuk 2** nieuwe varianten van BCN bedacht, ontwikkeld en getest met als doel de reactiespecificiteit in cellulaire glycaan-labeling te verhogen. Hierbij zijn drie verschillende afgeleiden van het cyclooctyn BCN ontwikkeld, die ieder enigszins verschillen in chemische structuur. De eerste bevat een extra hydroxylgroep (BHM-BCN), de tweede een glutaryl-aminogroep (GA-BCN) en de derde een aminogroep (A-BCN). Deze veranderingen verhogen allen het hydrofiele karakter van het cyclooctyn. De lading van een molecuul heeft een grote invloed op het hydrofiele karakter van een stof. Verwacht wordt dat A-BCN en GA-BCN een lading, respectievelijk positief en negatief, laten zien bij neutrale pH. In vergelijking tot het al bestaande BCN lieten A-BCN en GA-BCN een verhoogde specificiteit zien in het labelen van glycanen. Toevoeging van een extra hydroxylgroep (BHM-BCN) liet daarentegen geen verbetering in de specificiteit zien. Daarnaast kon de aanwezigheid van A-BCN worden aangetoond in het Golgi-apparaat van de cel, de locatie waar glycanen aan een eiwit gebonden worden. Tot slot zijn deze nieuw ontwikkelde cyclooctynen gebruikt om TRPV5 te detecteren op het plasmamembraan. Dit onderzoek geeft aan dat een lading in het cyclooctyn de specificiteit van glycaan detectie door middel van de klikreactie kan verhogen. De belangrijkste factoren hierin zijn hoogst waarschijnlijk verminderde aspecifieke hydrofobe interacties en een daling in de hoeveelheid intracellulair cyclooctyn waardoor minder thiol-yn additions plaats kunnen vinden.

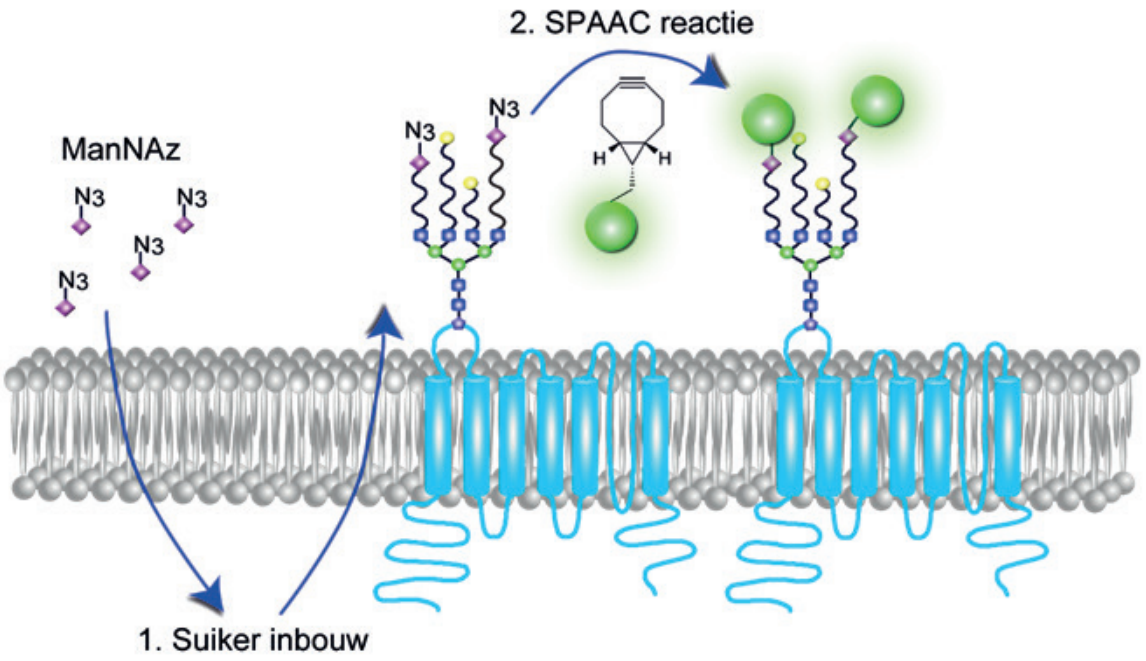

Figuur 1. De metabole incorporatie van een azido-saccharide en de SPAAC reactie met BCN. Als eerste wordt een azide-bevattend saccharide-analogon door de cel opgenomen en gebruikt voor de bouw van N-glycanen. Vervolgens wordt de azidegroep gebruikt voor de SPAAC reactie met gelabelde BCN. Middels deze techniek is het eiwit dat de gelabelde N-glycaan bevat zichtbaar op het plasmamembraan.

Er zijn verschillende enzymen en hormonen geïdentificeerd die een belangrijke rol spelen bij de Ca^{2+} balans via regulatie van TRPV5. Een van de eiwitten die specifiek aangrijpt op het N-glycaan van TRPV5 is klotho. Klotho is een antiverouderingshormoon, dat in de nieren voorkomt en vervolgens via de urine wordt uitgescheiden. Klotho stimuleert de hoeveelheid TRPV5 kanalen op het plasmamembraan, afhankelijk van de aanwezigheid van het N-glycaan. De enzymatische activiteit van klotho blijft echter onbekend. Zo is er beschreven dat klotho sialidase activiteit heeft. Dit betekent dat klotho siaalzuren van het N-glycaan kan verwijderen. Door deze verandering in saccharidesamenstelling kan er een saccharidebindend eiwit, het galectine-1, aan het TRPV5 N-glycaan binden en daarmee het kanaal op het plasmamembraan stabiliseren. Uit het onderzoek beschreven in **hoofdstuk 3** blijkt echter dat sialidase een stimulerend effect heeft op de activiteit van zowel het wild type TRPV5 kanaal als de ongeglycosyleerde TRPV5 mutant ($TRPV5^{N358Q}$). Dit impliceert dat het effect van sialidase onafhankelijk is van het TRPV5 N-glycaan. De stimulatie door sialidase is toe te schrijven aan een verminderde internalisatie van het kanaal vanuit het plasmamembraan. Deze internalisatie wordt gemedieerd door dynamische vetstructuren in het membraan, bekend als lipid rafts. Lipid rafts zijn onder andere opgebouwd uit geglycosyleerde vetten, welke een siaalzuur bevatten. Deze siaalzuren zullen ook door sialidase verwijderd worden en daarmee wordt de structuur van de dynamische lipid rafts verstoord. Deze verstoring zal de internalisatie van TRPV5 verminderen (Fig 2). Door de formatie van lipid rafts te hinderen via een chemische remmer wordt inderdaad de sialidase-gemedieerde stimulatie op de TRPV5 functie belemmerd.

Dezelfde verstoring heeft daarentegen geen effect op TRPV5 stimulatie via klotho, wat doet vermoeden dat klotho anders functioneert dan sialidase. Verder is er aangetoond, dat sialidase het siaalzuur van een geglycosyleerd modeleiwit (transferrine) kan verwijderen, terwijl klotho geen verandering geeft in de transferrine glycosylering.

Deze bevindingen leiden tot de conclusie dat sialidase TRPV5 reguleert op een N-glycaan-onafhankelijke wijze. Dit in tegenstelling tot klotho, dat het N-glycaan nodig heeft voor stimulatie van de TRPV5 functie. Verder hebben we aangetoond dat het niet waarschijnlijk is, dat galectine-1 het kanaal stabiliseert op het membraan na klotho behandeling. Galectine-3 is een ander glycaan-bindend eiwit dat zich in de nier bevindt. Dit eiwit zou de functie van galectine-1 kunnen overnemen. Behandeling met galectine-3 stimuleert inderdaad de TRPV5 activiteit. Een combinatiebehandeling met galectine-3 en klotho geeft daarentegen geen extra stimulans voor het kanaal.

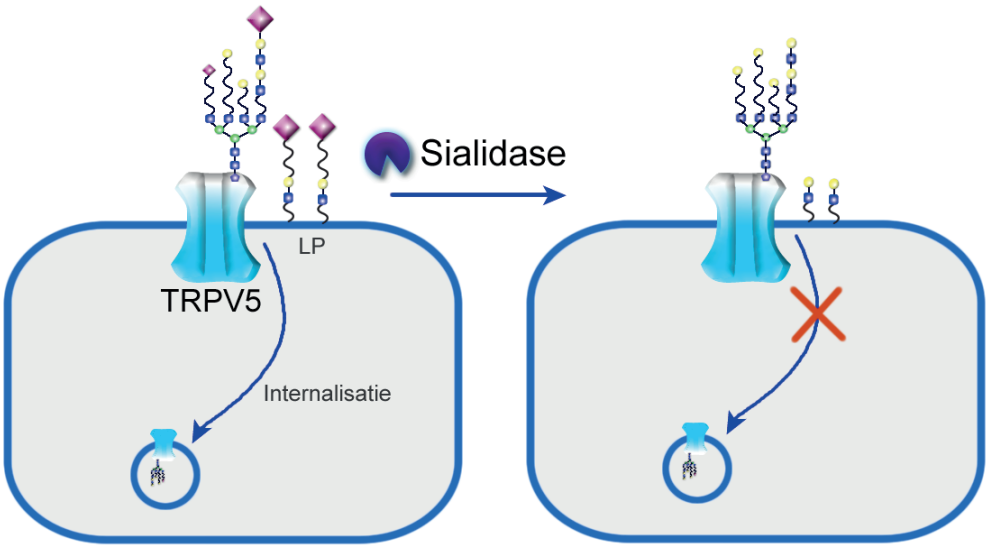

Figuur 2. Sialidase reguleert TRPV5 via geglycosyleerde vetten in de lipid rafts. Sialidase verwijdert de siaalzuren van het N-glycaan van TRPV5, maar ook van de vetten in de dynamische lipid rafts (LP). Deze dynamische vetstructuren in het plasmamembraan zijn verantwoordelijk voor de internalisatie van TRPV5. Door de siaalzuren van deze vetten te verwijderen blijft TRPV5 stabiel op het plasmamembraan. Klotho reguleert TRPV5 specifiek via het N-glycaan. Het regulatiemechanisme blijft vooralsnog onbekend.

Om de fysiologische regulatie via het TRPV5 N-glycaan verder te ontrafelen is er tevens onderzoek gedaan naar verscheidene glycosidases, welke ieder een andere saccharide van het glycaan afknippen en daarmee van invloed kunnen zijn op TRPV5. Het β-galactosidase verwijdert eindstandige β-galactose sacchariden van een glycaanstructuur en is in enzymatisch actieve vorm aanwezig in de urine. De TRPV5 kanaalactiviteit wordt gestimuleerd door β-galactosidase en dit effect was alleen zichtbaar in de aanwezigheid van het TRPV5 N-glycaan zoals beschreven in **hoofdstuk 4**. Afbraak van een specifiek β1,4-gebonden galactose door β1,4-galactosidase (β1,4-gal) stimuleert de TRPV5-gemedieerde Ca^{2+} opname door het kanaal te stabiliseren op het plasmamembraan. Gezien de aanwezigheid van actieve β-galactosidase in de urine zou dit enzym van belang kunnen zijn voor de Ca^{2+} balans. Om de fysiologische relevantie te bestuderen hebben we primaire distale nierbuiscellen geïsoleerd uit de muis. Net als in de nier zijn deze cellen gepolariseerd. Dit betekent dat ze twee verschillende kanten hebben, een apicale (voorurine) zijde waar TRPV5 aanwezig is en een basolaterale (bloed) kant. In deze cellen kan het Ca^{2+} transport ook gestimuleerd worden door behandeling met β1,4-gal vanaf de voorurine kant (apicaal). Dit impliceert dat β-galactosidase, aanwezig in de voorurine, TRPV5 kan stimuleren en daarmee invloed heeft op de Ca^{2+} balans.

Tot slot wordt in **hoofdstuk 5** een mechanisme besproken dat verantwoordelijk is voor het functioneren van het TRPV5 kanaal op moleculair niveau. Een kanaal werkt als een soort poort die kan openen en sluiten door verandering in de eiwitstructuur. Er is een model van de TRPV5 eiwitstructuur ontwikkeld aan de hand van een opgehelderde TRPV1 structuur. Gedetailleerd inzicht in de TRPV5 structuur heeft tot nieuwe bevindingen geleid. Zoals verwacht, is aan de bovenkant van het kanaal het N-glycaan gepositioneerd in het model. De porie van het kanaal, ook wel gezien als een tunnel, heeft aan de bovenkant een selectiviteitsfilter, bestaande uit vier asparaginezuren die samen ervoor zorgen dat het kanaal alleen Ca^{2+} doorlaat. Tot onze verbazing is aan het einde van de tunnel een groot aromatisch, hydrofoob aminozuur, tryptofaan, gelokaliseerd. De locatie is onverwacht, aangezien de zijketen van dit aminozuur het kanaal insteekt en de doorgang deels blokkeert. Ook energetisch gezien is dit een ongunstige positie voor het betreffend aminozuur. Vervanging van dit tryptofaan door een ander aminozuur resulteert in extreem hoge intracellulaire Ca^{2+} niveaus en daarmee gepaard gaande celdood. De intrinsieke activiteit van het kanaal blijkt sterk verhoogd, waardoor er meer Ca^{2+} ionen doorgelaten worden. Uit deze data kan worden opgemaakt, dat de tryptofaanresiduen als een soort poort aan het einde van de tunnel fungeren. Vervolgens is onderzocht wat maakt dat de tryptofaanresiduen zich verplaatsen opdat de poort zich kan openen. In de directe nabijheid van deze tryptofaan-poort blijkt een flexibel glycine gelokaliseerd. Glycine is het kleinste aminozuur en fungeert vaak als een buigpunt binnen eiwitten. Als dit glycine wordt vervangen door het meer rigide alanine, blijkt Ca^{2+} transport niet meer mogelijk. Hieruit kan geconcludeerd worden dat sluiting van het TRPV5 kanaal geregeld wordt door een glycine buigpunt in combinatie met een tryptofaan-poort.

In **hoofdstuk 6** worden de conclusies van het beschreven onderzoek op een rij gezet. Daarnaast worden er enkele mogelijkheden voor toekomstig onderzoek op het gebied van TRPV5 glycosylering beschreven. De nieuw ontwikkelde BCN derivaten worden geplaatst in het licht van de reeds bekende cyclooctynen. Tevens worden mogelijke mechanismen besproken voor de N-glycaan afhankelijke TRPV5 regulatie door klotho. Een louter bindende functie voor klotho zou een verklaring kunnen geven voor de stimulatie via klotho. Dit zou betekenen dat klotho geen enzymatische, maar uitsluitend een bindende functie heeft. Daarnaast wordt een moleculair mechanisme besproken als mogelijke verklaring voor de β1,4-gal-gemedieerde TRPV5 stimulatie. De verwijdering van β1,4-galactose zou binding van galectin-9 kunnen voorkomen, hetgeen de internalisatie van TRPV5 zou kunnen verminderen. Tot slot worden verschillende factoren belicht, die verantwoordelijk kunnen zijn voor de buiging van de eiwitstructuur middels glycine en het daarmee gepaard gaande openen en sluiten van de tryptofaan-poort.

VIII

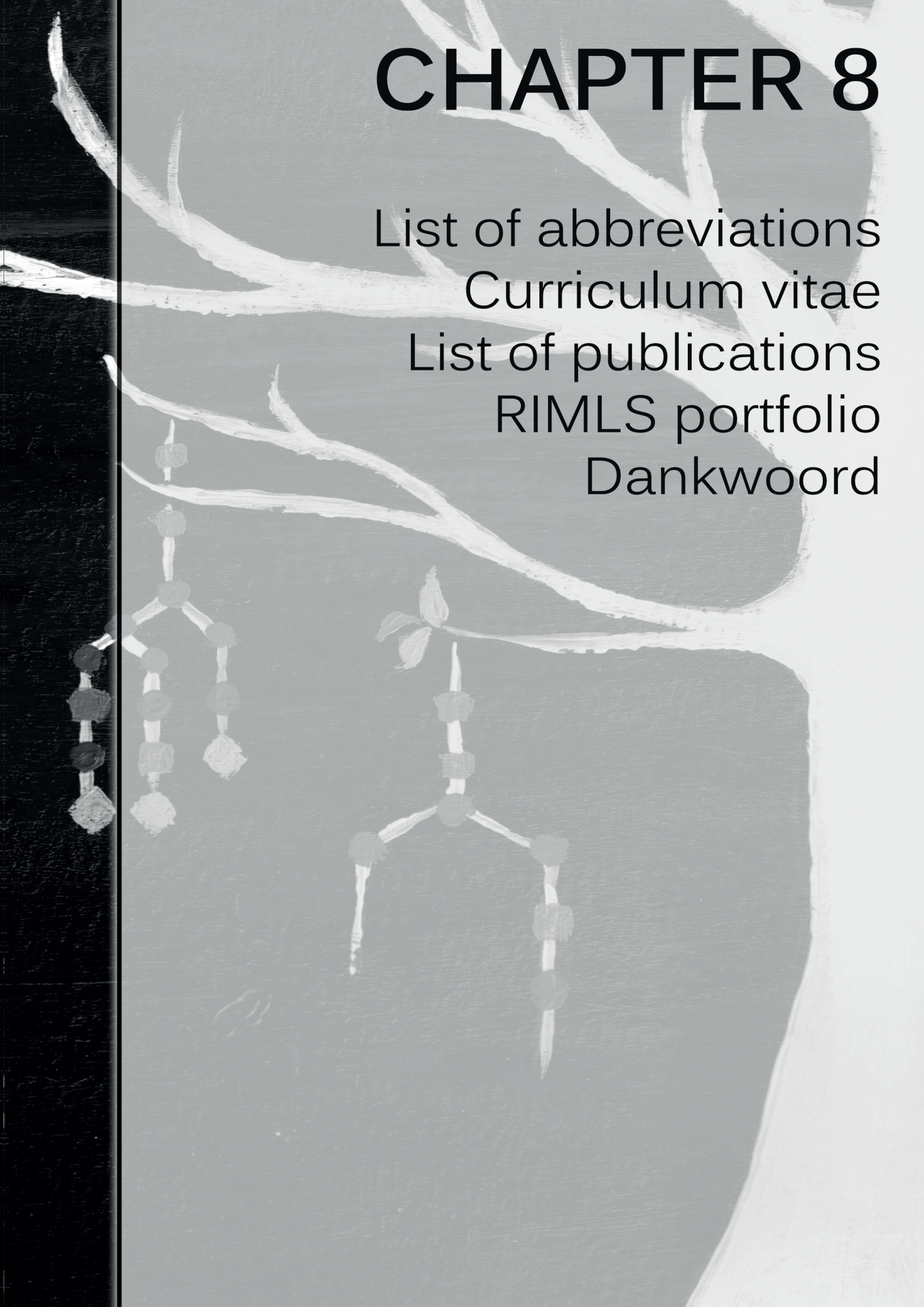

CHAPTER 8

List of abbreviations
Curriculum vitae
List of publications
RIMLS portfolio
Dankwoord

List of abbreviations

1α-OHase	25-hydroxyvitamin D_3-1α-hydroxylase
17β-E_2	17β-estradiol
1,25$(OH)_2D_3$	1,25-dihydroxy-vitamin D_3
80K-H	protein kinase C substrate 80K-H
A-BCN	amino-bicyclo[6.1.0]nonyne
ADAM	a disintegrin and metalloprotease
ANK	ankyrin
ANOVA	analysis of variance
ARD	ankyrin repeat domain
AU	arbitrary units
ß-gal	ß-galactosidase
ß(1-3)-gal	ß(1-3)-galactosidase
ß(1-4)-gal	ß(1-4)-galactosidase
BAPTA-AM	1,2-Bis(2-aminophenoxy)ethane-N,N,N′,N′-tetraacetic acid tetrakis(acetoxymethyl ester)
BARAC	bisarylazacyclooctynone
BCN	bicyclo[6.1.0]nonyne
BCRP	breast cancer resistant protein
BHM-BCN	bis(hydroxymethyl)-bicyclo[6.1.0]nonyne
BSA	bovine serum albumin
BTTAA	bis[(tert-butyltriazoyl)methyl]-[(2carboxymethyltriazoyl)methyl]amine
BTTES	tris(triazolylmethyl) amine-based ligand
$^{45}Ca^{2+}$	radioactive calcium isotope
Ca^{2+}	calcium ion
CaM	calmodulin
CaSR	calcium-sensing receptor
CD	collecting duct
CFG	consortium for functional glycomics
CHO	chinese hamster ovarian
CNT	connecting tubule
COPAS	complex object parametric analyzer and sorter
CRD	carbohydrate recognition domain
Cu	copper ion
CuAAC	copper catalyzed azide-alkyne cycloadditon
DCM	dichloromethane
DCT	distal convoluted tubule
DIBAC/DBCO	dibenzoazacyclooctyne
DIBO	dibenzocyclooctyne
DIFO	difluorocyclooctyne
DIMAC	dimethoxyazacyclooctyne
DMAP	4-dimethylaminopyridine
DMEM	dulbecco's Modified Eagle's Medium
DMF	dimethylformamide
DMP	Dess-Martin periodinane
DNA	deoxyribonucleic Acid
DTT	dithiothreitol
DVF	divalent-free
EBP	elastin/laminin-binding protein
EDEM	endoplasmic reticulum degradation-enhancing α-mannosidase like protein

EDTA	Ethylenediaminetetraacetic acid
Endo-F	endoglycosidase-F
EGF	epidermal growth factor
eGFP	enhanced green fluorescent protein
EGFR	epidermal growth factor receptor
EGTA	ethylene glycol tetraacetic acid
ER	endoplasmic reticulum
ERK1/2	extracellular signal-regulating kinase 1/2
FACS	fluorescence activated cell sorting
FGF23	fibroblast growth factor 23
FGFR	fibroblast growth factor receptor
FRET	förster resonance energy transfer
Fura-2-AM	fura-2-acetoxymethyl ester
GA-BCN	glutarylamino-bicyclo[6.1.0]nonyne
GFP	green fluorescent protein
GSDB	goat serum dilution buffer
GSL	glycosphingolipids
GST	glutathione *S*-transferases
H^+	proton
HEK293	human embryonic kidney 293
IAM	iodoacetamide
IC_{50}	half maximal inhibitory concentration
IEDDA	Diels-Alder reaction with inverse electron-demand
IEF	isoelectric focusing
IRES	interinal ribosome entry site
Kl	klotho
KO	knockout
LacNAc	*N*-acetyllactosamine
ManLev	*N*-levulinoylmannosamine
ManNAz	*N*-azidoacetyl-mannosamine
MDCK	madin darby canine kidney
MeCN	acetonitrile
Mw	molecular weight
Na^+	sodium ion
NAG	*N*-acetyl-D-glucosaminodase
NCX1	sodium-calcium exchanger
nDVF	nominally divalent-free
NeuAc	*N*-acetylneuraminic acid, sialic acid
NHERF2	sodium-hydrogen exchange regulatory cofactor 2
PBS	phosphate buffered saline
PCR	polymerase chain reaction
PDB	protein databank
PFA	paraformaldehyde
PIP_2	phosphatidylinositol 4,5-bisphosphate
PKA	protein kinase A
PKC	protein kinase C
PLC	phospholipase C
PMCA	plasma membrane calcium-ATPase
PMSF	phenylmethanesulfonylfluoride
P_o	open probability
PSS	physiological salt solution
PT	proximal tubule

PTH	parathyroid hormone
Rab11a	ras-related protein 11a
ROMK	renal outer medullary K^+
RP-HPLC	reversed-phase HPLC
RR	ruthenium red
SDS-PAGE	sodium dodecyl sulfate polyacrylamide gel electrophoresis
SEM	standard error of the mean
SGK1	serum and glucocorticoid-regulated kinase 1
SNR	signal-to-noise ratio
SPAAC	strain-promoted alkyne-azide cycloaddition
SPIEDAC	strain-promoted inverse-electron-demand Diels-Alder cycloaddition
TAL	thick ascending limb of Henle's loop
THPTA	tris(hydroxypropyltriazolyl)-methylamine
TIRF-M	total internal reflection fluorescent microscopy
TK	tissue kallikrein
TM	transmembrane segment / domain
TMDIBO	tetramethoxydibenzocyclooctyne
TRPV	transient receptor potential channel, subfamily vanilloid
tTG	tissue transglutaminase
UAA	unnatural amino acid
UMOD	uromodulin
WNK4	with-no-lysine kinase 4
WT	wild type

Curriculum vitae

Liz Leunissen werd geboren op 31 maart 1987 te Hilvarenbeek. In 2005 behaalde ze haar VWO diploma aan het Sintermeerten college te Heerlen, waarna ze Moleculaire Levenswetenschappen aan de Radboud Universiteit (RU) Nijmegen studeerde. Tijdens deze opleiding volgde zij een bachelorstage van 3 maanden op de afdeling Fysiologie van het Radboud universitair medisch centrum (RadboudUMC) onder leiding van J.B. Peng. Gedurende haar masteropleiding Moleculaire Levenswetenschappen volgde ze een stageonderzoek van 6 maanden bij de afdeling Bio-organische Chemie (RU) waar ze onder begeleiding van Dr. M.B. Hansen en Dr. D.W.P.M. Löwik onderzoek verrichtte naar een nieuw transductiesysteem waarbij eiwitten non-covalent (via een leucine zipper) worden gebonden aan cel permeabele peptiden. Op de afdeling Biofysische Chemie (RU Nijmegen) verdiepte ze zich, onder leiding van F.H.T. Nelissen en Prof. Dr. S.S. Wijmenga, in het replicatiesysteem van het hepatitis B virus. Deze stage was een samenwerkingsproject met Prof. Dr. M. Nassal van de afdeling Internal Medicine II/ Molecular Biology van het Freiburg universitair medische centrum te Duitsland, waar zij 3 maanden als onderdeel van deze stage heeft uitgevoerd. In november 2010 behaalde zij haar Msc dimploma met de toevoeging bene meritum. Ze startte in december 2010 als promovendus op de afdelingen Fysiologie (RadboudUMC) en Synthetische Organische Chemie (RU), op een door het Radboud Instituut voor Moleculaire Levenswetenschappen (RIMLS) gesubsidieerd samenwerkingsproject. Dit onderzoek heeft geleid tot de in dit proefschrift beschreven bevindingen. Tijdens haar promotieperiode begeleidde ze masterstudenten van de studies Scheikunde en Medische Biologie.

List of publications

Leunissen EH, Blanchard MG, Lavrijsen M, Bindels RJ, Hoenderop JG.
Urinary ß-galactosidase stimulates Ca^{2+} transport by stabilizing TRPV5 at the plasma membrane.
Submitted

Leunissen EH, Meuleners MH, Verkade JM, Dommerholt J, Hoenderop JG, van Delft FL.
Copper-free click with polar bicyclononyne derivatives for modulation of cellular imaging.
ChemBioChem 15: 1446-1451, 2014.

Leunissen EH, Nair AV, Büll C, Lefeber DJ, van Delft FL, Bindels RJ, Hoenderop JG.
The epithelial calcium channel TRPV5 is regulated differentially by klotho and sialidase.
J. Biol. Chem. 228: 29238-29246, 2013.

Nelissen FH, **Leunissen EH**, van de Laar L, Tessari M, Heus HA, Wijmenga SS.
Fast production of homogeneous recombinant RNA. Towards large scale production of RNA.
Nucl. Acids Res. 40: e102, 2012.

Hansen MB, Verdurmen WP, **Leunissen EH**, Minten I, van Hest JC, Brock R, Löwik DW.
A Modular and Noncovalent Transduction System for Leucine-Zipper-Tagged Proteins.
ChemBioChem 12 : 2294-2297, 2011.

Löwik DW, **Leunissen EH**, van den Heuvel M, Hansen MB, van Hest JC.
Stimulus responsive peptide based materials.
Chem. Soc. Rev. 39 : 3394-3412, 2010.

Institute for Molecular Life Sciences
Radboudumc

Name PhD student: *E.H.P. Leunissen*	PhD period: *01-12-2010 – 01-12-2014*
Departments: *Physiology and Synthetic Organic Chemistry*	Promotor: *Prof. Dr. Joost G.J. Hoenderop.*
Research School: *Nijmegen Centre for Molecular Life Sciences*	Co-promotor(s): *Dr. Floris L. van Delft, Dr. Jenny van der Wijst*

	Year(s)	ECTS
TRAINING ACTIVITIES		
a) Courses & Workshops		
- RIMLS Graduate Course	2011	3
- Radiation Safety course – Level 5B	2011	1.75
- Glycobiology Course	2012	3.5
- Imaging Workshop	2012	0.2
- Employment Outside Academia Course	2014	1.75
b) Seminars & lectures^		
- RIMLS Seminars	2011-2014	2.4
- RIMLS Technical Forums	2011-2014	0.8
- RIMLS in the Spotlight/Radboud Research Rounds	2011-2014	0.6
- Glycobiology meeting	2011-2014	1.1
c) (Inter)national Symposia & congresses^		
- RIMLS New Frontiers#	2011	1
- RIMLS PhD retreat#,*	2011-2014	3
- NIGRAM Meeting	2012	0.25
- RIMLS New Frontiers#	2013	1
- IBR symposium Barcelona#	2013	1.25
- RIMLS New Frontiers	2014	0.5
- EMBO Chemical biology*	2014	1.5
d) Other		
- Review scientific publication	2011-2014	0.2
- NCMLS Affairs*	2011	0.25
- Glycobiology meeting*	2012	0.25
- Organization Technical Forum	2013	0.5
TEACHING ACTIVITIES		
e) Students		
- Supervision Mandy Meuleners	2011-2012	3.5
- Supervision Dennis Dean	2014	2
TOTAL		30.3

Oral and poster presentations with a * and # after the name, respectively.

VIII

Dankwoord

Eindelijk is het dan zover, na iets meer dan vier jaar hard doorwerken ligt het er dan toch, het proefschrift. Uiteraard heb ik dit niet alleen gedaan en wil ik graag iedereen bedanken die in meer of mindere mate heeft bijgedragen aan de totstandkoming van dit proefschrift. Tijdens het schrijven van het dankwoord bleek dit een hele rij te zijn en ik hoop dus ook dat ik niemand ben vergeten. Ik heb veel geleerd over het beoefenen van onderzoek tijdens deze vier jaren, maar misschien nog meer over het leven in het algemeen.

Allereerst wil ik mijn promotoren en copromotor bedanken, Joost Hoenderop, Floris van Delft en Jenny van der Wijst. Jullie hebben het mogelijk gemaakt dat ik dit onderzoek kon doen en ik heb veel van jullie geleerd.

Joost, als mijn directe begeleider heb je mij van dichtbij meegemaakt. Van jou heb ik veel geleerd over het schrijven van papers en de gang van zaken binnen het onderzoek. Dankzij jouw hulp is het mogelijk geweest om dit proefschrift in deze hoedanigheid te maken, bedankt! Ik wens je heel veel succes in de toekomst!

Floris, bedankt voor je wetenschappelijke input en begeleiding tijdens deze periode. Je zat altijd vol ideeën en ik vind jouw enthousiasme over het onderzoek bewonderenswaardig. Ik waardeer je enorme kennis over Organisch Chemie. Ik wil je het allerbeste toewensen voor de toekomst en met SynAffix!

Jenny, als laatste toegevoegd aan mijn lijst met promotoren. In de laatste maanden heb je mij ontzettend geholpen met het schrijven van dit proefschrift. Daarnaast heb je ook nog hard meegedacht en gewerkt aan hoofdstuk 5, bedankt voor je waardevolle suggesties. Ik wens je alle succes met je onderzoek carrière, en wie weet ooit als professor...

Tijdens mijn 4-jarig traject heb ik zowel op de afdeling Fysiologie als op de afdeling Organische Chemie gewerkt. Ik wil dus ook graag mensen bedanken van beide afdelingen. Te beginnen met de afdeling Fysiologie, waar ik uiteindelijk de meeste tijd heb doorgebracht.

René Bindels, als hoofd van het RIMLS ben je een druk bezette man. Desondanks heb je nog steeds tijd om je met het reilen en zeilen van afdeling bezig te houden, dat vind ik heel knap. Bedankt voor het meedenken met mijn onderzoek.

Ellen, jou zal ik het meeste missen. De jaren met jou in de unit waren gezellig en jij was degene die mij weer op wist te beuren wanneer het iets minder goed ging. Je grappige zelfbedachte liedjes en vrolijke ‘goedemorgen collega’s’ op de vroege ochtend werden altijd goed ontvangen. Ik heb veel geleerd van jouw visie op verschillende aspecten in het onderzoek en in het leven. Het is dan ook voor mij niet meer dan logisch dat jij op deze belangrijke dag naast me zal staan. Nog even en dan ben jij ook aan de beurt!

Sjoerd, onze eeuwige optimist. Bedankt voor je wetenschappelijke en strategische input tijdens de afgelopen vier jaar. Ze waren heel waardevol voor mij en ik heb er een hoop van geleerd. Jouw onverbeterlijke enthousiasme is erg belangrijk voor het lab. Gelukkig wist je toch tijd vrij te maken om me te wijzen op mijn interessante woordkeuze, misschien toch een beetje jaloers op mijn uitgebreide woordenschat?

Wilco, je kwam ons kleine Ca^{2+}-groepje, helaas maar tijdelijk, aanvullen als post-doc. Je was een gezellige en nuchtere unit-genoot, dat kon ik erg waarderen. Je sarcasme en nuchtere kijk op het leven zette mij bij tijd en wijle weer met twee benen op de grond.

Ik weet zeker dat we je aan het zingen hadden gekregen als we nog een jaartje de tijd hadden gehad. Veel geluk met de kleine!

Anke, bedankt voor de adviezen en de gezelligheid op het lab. Ik weet zeker dat het je goed zal gaan in de toekomst!

Eline, ik bewonder je kritische blik op het onderzoek. Met vragen kon ik altijd bij jou terecht en ik waardeer je eerlijkheid. Ik wens je heel veel succes als klinisch chemicus.

Mark, bedankt voor je luisterend oor. Jouw kalme karakter binnen deze hectische afdeling heb ik altijd als prettig ervaren. Jij bent er bijna, nog even doorbijten!

Maxime, thank you for your wise advices and support with the papers. I liked working with you and I believe you are one of the best researchers I know.

Lauriane, it was nice to work with you at the lab. I am sorry I did not improve my French more, but it was too difficult. I wish you all the best for the future!

Femke, **AnneMiete** en **Marla**, bedankt voor jullie hulp met de verschillende experimenten. **Femke**, het was altijd gezellig tijdens de pauzes en ik wens jou veel geluk toe met de kleine. **AnneMiete**, jij was de hoeder van het lab. Ik heb jou inbreng gemist de laatste jaren. **Marla**, jouw grappige verhalen waren vaak een welkome afleiding. Ik wens je veel succes in de toekomst!

Kukiat, I loved working with you on the lab as you were always calm and relaxed. Moreover, you were the only one who appreciated my singing. Thank you and good luck at Harvard!

Irene, voor jou geen exotische bestelling meer. Ondanks dat niet iedereen altijd even blij is als er weer iets gedaan moet worden (ik), zien we uiteindelijk allemaal in dat jij van onschatbare waarde bent voor het lab. Bedankt.

Naast het werken op het fysiologie lab heb ik met geweldige mensen mogen samenwerken op het Organisch Chemische lab. Ik wil graag allereerst alle mensen in vleugel 1 bedanken, jullie waren behulpzaam en vriendelijk. Ik heb me altijd welkom gevoeld, en jullie hebben mijn talloze (en soms nutteloze) vragen altijd met geduld beantwoord. Dit vind ik heel bijzonder en is iets om trots op te zijn, jullie zijn een top afdeling(en)!

Olumide, I would like to thank you for your guidance at the Organic Chemistry department in the beginning. You are a wonderful person and I enjoyed our discussions. I wish you all the best for the future!

Jorge, bedankt voor je hulp met het BCN manuscript! Daarnaast wil ik graag heel **SynAffix** bedanken voor hun gezelligheid en ondersteuning. Ik heb ontelbaar veel vragen gesteld, en jullie waren altijd bereid om mij hiermee te helpen. Bedankt!

Jan, dankjewel voor je hulp en uitleg wanneer ik het even niet meer kon volgen!

Lab 03.118 bedankt voor de gezelligheid (thanks for the nice time) en in het bijzonder wil ik graag **Willem-Jan Karstens** bedanken voor zijn wetenschappelijke raad.

Daarnaast wil ik nog mijn studenten bedanken voor hun hulp bij het onderzoek **Mandy** en **Dennis**. Mandy, de publicatie die uit jou onderzoek volgde was niet meer dan verdiend. Dennis, ook al liep het project wat moeilijk, het was fijn om met jou samen te werken.

Ook wil ik graag **Dr. Dirk Lefeber** bedanken voor zijn adviezen. Naast de waardevolle wetenschappelijke input die jij mij gaf, was jij ook een goede mentor.

Tot slot wil ik graag mijn familie, de familie Gommans en al mijn vrienden bedanken. De vriendengroep uit **Nijmegen**, de meiden van **Sintermeerten**, **Joyce** en de groep uit **Grubbenvorst** bedanken voor hun gezelligheid en steun tijdens de afgelopen jaren. Deze lijst is te lang om op te noemen, maar ik wil speciaal mijn familie en Jos bedanken.

Te beginnen met mijn zussen, die tevens ook mijn beste vriendinnen zijn. **Nina** en **Lotte**, bedankt voor jullie onvoorwaardelijk vertrouwen, liefde en gezelligheid. Het was fijn om te weten dat jullie altijd achter me stonden, ik altijd mocht bellen en ik (af en toe) mocht klagen over de gang van zaken. Jullie hielden mij met beide benen op de grond en hielpen mij er regelmatig aan herinneren dat er ook andere dingen in het leven zijn dan promotieonderzoek. Natuurlijk hebben ook de “ex-buitenlanders” bijgedragen hieraan, **Pim** en **Armand**! Bedankt voor jullie gezelligheid en adviezen tijdens deze periode. Armand, ik ben heel blij met de mooie voorkant! Tijdens mijn promotie zijn er nog twee mensen bijgekomen die ik wil toevoegen aan dit rijtje, **Lara** en **Sam**. Jullie hielpen mij herinneren aan de belangrijke dingen in het leven en het is natuurlijk altijd leuk om jullie vrolijke gezichtjes te zien. En we verwelkomen van harte mijn nieuwe neefje **Roan**.

Lieve **Mam** en **Pap**, ongeacht wat er is, jullie staan altijd voor me klaar. Dankzij jullie hulp, steun en liefde heb ik het tot hier gebracht. De gezellige avonden, goede adviezen en rustgevende weekendjes in het zonnige zuiden waren belangrijke momenten voor mij in deze hectische periode. Bedankt voor de geweldige ouders die jullie zijn en jullie oneindige vertrouwen in mij.

Lieve **Jos**, bedankt voor alles. Als ik alle elementen apart ging benoemen had ik nog wel twee pagina’s nodig. We weten beide dat ik hier zonder jou nooit had gestaan. Dankjewel voor je support, liefde en vooral je eeuwige geduld. Ik kijk uit naar de nieuwe avonturen die we samen gaan beleven, want ik weet, met jou naast mij komt alles altijd goed.

Veel liefs,

Liz

VIII